THÈSE DE DOCTORAT DE L'UNIVERSITÉ PARIS VI

Spécialité :
Chimie et Physico-chimie des Polymères

Présentée par
Nicolas MARTIN

Pour obtenir le grade de
DOCTEUR de l'UNIVERSITÉ PARIS VI

Sujet de la thèse :

Colloidal stability and folding of antibodies in the presence of chaperone-like poly(acrylate) derivatives – role of hydrophobic and electrostatic interactions

Soutenue le 24 octobre 2014 devant le jury composé de :

Mme Françoise Winnik	Présidente
Mme Fouzia Boulmedais	Rapportrice
M. Renko De Vries	Rapporteur
M Didier Boquet	Examinateur
M. Alain Fradet	Invité
M. Christophe Tribet	Directeur de thèse

Il arrive souvent que lorsque nous pensons
faire une expérience sur les autres,
nous en faisons une sur nous-mêmes.

Oscar Wilde, *Le portrait de Dorian Gray*

Le Pompier
Vous voulez que je vous raconte des anecdotes ?

M^me Smith
Oh, bien-sûr, vous êtes charmant.

M. Smith, M^me Martin, M. Martin
Oui, oui, des anecdotes, bravo !

[...]

Le Pompier
Je parle de choses que j'ai expérimentées moi-même.
La nature, rien que la nature. Pas les livres.

M. Martin
C'est exact, la vérité ne se trouve d'ailleurs
pas dans les livres, mais dans la vie.

Eugène Ionesco, *La cantatrice chauve*

A Nonna et à Mémée

Remerciements

Ma thèse touche à sa fin, voici donc venu le traditionnel exercice de la page des remerciements sans lesquels ce manuscrit ne saurait être complet.

Mes plus chaleureux remerciements vont à Christophe Tribet pour avoir encadré ce travail de recherche. Christophe, je souhaite t'exprimer ma plus profonde reconnaissance pour la confiance que tu m'as accordée durant ces trois ans, ton enthousiasme à toute épreuve, ta disponibilité sans faille (jusque dans les dernières relectures attentives de ce manuscrit), la liberté d'action que tu m'as laissée et tes encouragements souvent teintés d'humour. Je tiens ici à saluer tes qualités d'encadrant, tant humaines que scientifiques, auxquelles j'ai été extrêmement sensible. Les nombreuses discussions toujours instructives que nous avons eues, ton regard critique et tes conseils avisés ont pour moi été source d'inspiration, et seront, j'en suis certain, d'une aide précieuse pour mon parcours futur. Je te remercie enfin pour les moyens que tu as mis à ma disposition, que ce soit dans mon travail quotidien au laboratoire ou pour me permettre de partir au Canada et de participer à plusieurs conférences internationales. Pour cela, et pour tout le reste, merci!

Les travaux réalisés au cours de cette thèse on été effectués au laboratoire PASTEUR (UMR 8640), au Département de Chimie de l'École Normale Supérieure à Paris. Je remercie Ludovic Jullien de m'y avoir accueilli. J'ai pu bénéficier de conditions de travail tout à fait stimulantes au sein de l'unité et d'une autonomie qui m'ont permis de mûrir scientifiquement.

Je tiens à remercier Fouzia Boulmedais et Renko de Vries pour avoir accepté de juger ce travail de recherche. Je remercie également Françoise Winnik et Didier Boquet pour leur participation à mon jury de thèse, ainsi que Christine Ménager en sa qualité de présidente du jury.

Ce travail expérimental n'aurait pas été le même sans le concours d'un grand nombre de collaborateurs. Je remercie toutes les personnes qui ont apporté leur pierre, petite ou grande, à l'édifice :

- Françoise Winnik pour les échanges fructueux sur nos projets communs et pour m'avoir accueilli pendant un mois au sein de son laboratoire à l'Université de Montréal, ainsi que tous les membres de son groupe, notamment Ma Dewang avec qui j'ai étroitement collaboré pour les travaux sur les IgG, Adeline Laffont pour la SPR et Jean-Richard Bullet pour la synthèse de polymères;
- Didier Boquet et Amaury Herbet du CEA à Saclay pour nos discussions enrichissantes sur les aspects biologiques de ce travail, pour les mesures d'activité et pour les quelques jours/nuits passés ensemble à SOLEIL, ainsi que Narciso Costa, pour m'avoir régulièrement approvisionné en fragments d'anticorps, et Céline Ortega

pour m'avoir initié aux protocoles de renaturation;
- Frank Wien pour les mesures de SRCD à SOLEIL;
- Fabien Ferrage pour la RMN ^{15}N-$^{-1}$H, et Cyril Charlier;
- Damien Laage pour la modélisation;
- Fabrice Giusti et Jean-Luc Popot, pour les mesures de SEC à l'IBPC;
- Guylaine Ducouret et Nicolas Sanson du laboratoire SIMM à l'ESPCI pour la viscosimétrie et l'ultracentrifugation respectivement;
- Ilias Iliopoulos et Sophie Norvez du laboratoire MMC à l'ESPCI pour le dichroïsme circulaire;
- Thomas Le Saux pour la FCS;
- Emmanuelle Marie pour la synthèse d'agents RAFT et la GPC;
- Renaud Respaud et Marie-Claude Viaud de l'Université François Rabelais à Tours pour l'accès aux anticorps monoclonaux thérapeutiques.

Je remercie également les enseignants que j'ai cotoyé durant ces trois années et qui ont contribué, si ce n'est à ce travail scientifique, du moins à ma formation doctorale, entre autres: Hélène Monin-Soyer, Jean-Bernard Baudin, Nicolas Lévy, Gilles Wallez, Dominique Hourdet, Clotilde Policar, Damien Baigl. Je tenais aussi à remercier Anne Halloppé pour son aide logistique, toujours dynamique et efficace.

Enfin, je remercie tous les membres du pôle Chimie BioPhysique pour les moments que nous avons partagé, que ce soit repas ou discussions, avec une pensée particulière pour mes compagnons de fortune (d'infortune ?): Louise (et sa motivation sans faille pour la piscine, "qui fait travailler tous les muscles!"), Geoffrey (et ses gâteaux et autres mets délicats – ou pas ! – qu'il nous a cuisinés), Fabrice (pour son humour et "son" Tariquet qui nous a conduit à 3 dans un certain lit "king size"!), Quentin (le seul vrai courageux face à l'épreuve du karaoké), Jérôme (pour l'organisation des afterworks "binouze"), Alexandra (qui nous a suivi dans nos soirées).

Je remercie aussi Flore qui a su me remotiver à un moment crucial de la rédaction, et Maxime qui m'a soutenu (supporté ?) et que j'ai embêté jusqu'aux tous derniers instants de cette aventure.

Je m'arrête là, et remercierai les autres lorsque j'aurai remporté un Oscar.

List of abbreviations

β-CD	β-cyclodextrin
p-NPA)	*para*-nitrophenylacetate
ADA	anti-drug antibody
ADC	antibody-drug conjugate
APBS	adaptative Poisson-Boltzmann solver
BLAST	basic local alignment search tool
BSA	bovine serum albumin
CAB	bovine carbonic anhydrase
CD	circular dichroism
CDR	complementarity-determining region
CHESG	cholesterol group-bearing enzymatically synthesized glycogen
CHO	Chinese hamster ovary
CHP	cholesterol hydrophobically-modified pullulan
cmc	critical micellar concentration
CS	citrate synthase
CSA	(1R)-(−)-10-camphorsulfonic acid
CZE	capillary zone electrophoresis
DCC	N, N'-dicyclohexyl-carbodiimide
DLS	dynamic light scattering
DMSO	dimethyl sulfoxide
DSC	differential scanning calorimetry
DSSP	dictionary of protein secondary structure
DTT	dithiothreitol
ESG	enzymatically synthesized glycogen
ETBR	endothelin receptor B
FCS	fluorescence correlation spectroscopy
FITC	fluoresceine isothiocyanate
FRET	Förster resonance energy transfer
GMO	genetically-modified organism
GndCl	guanidinium chloride
GPC	gel permeation chromatography
hAMHR-II	human anti-Mullerian hormone type II receptor
HSQC	heteronuclear single quantum coherence
IB	inclusion body
IgG	immunoglobulin G

IPTG	isopropyl β-D-1-thiogalactopyranoside
ITC	isothermal titration calorimetry
kDa	kilo Dalton
LCST	lower critical solution temperature
mAb	monoclonal antibody
MeO	mesityl oxide
MFI	mean fluorescence intensity
NMP	*N*-methyl-pyrrolidone
NMR	nuclear magnetic resonance
PAA	poly(acrylic acid) and poly(sodium acrylate)
PAAm	poly(allylamine)
PDMS	poly(dimethylsiloxane)
PEAMA	poly(*N*, *N*-diethylaminoethyl methacrylate)
PEG	poly(ethylene glycol
pI	isoelectric point
PLA	poly(lactide)
PLGA	poly(L-glutamic acid)
PLL	poly(L-lysine)
PM	photomultiplier
PMA	poly(methacrylate)
PNIPAM	Poly(*N*-isopropylacrylamide)
PPO	poly(propylene oxide)
PrP	prion protein
PrP^{Sc}	prion protein in the Scrapie form
PSS	poly(styrene sulfonate)
PVA	poly(vinyl alcohol)
SANS	small angle neutron scattering
scFv	single-chain Fv fragment
SEC	size exclusion chromatography
SLS	static light scattering
SRCD	synchrotron-radiation circular dichroism
TMAO	trimethylamine *N*-oxide
WT	wild-type

Contents

List of abbreviations **vii**

General Introduction **1**

I Proteins in solution: from folding and stability issues to the design of synthetic chaperones **3**

1 Protein folding and stability: to aggregate or not to aggregate? **5**
1.1 Preamble: about the development of therapeutic antibodies and practical issues 7
1.2 Basic mechanisms leading to *in vitro* protein aggregation 14
1.3 Conventional strategies to limit *in vitro* protein aggregation 20

2 Towards the design of polymer-based and colloidal artificial chaperones **25**
2.1 *In vivo* folding and aggregation: role and mode of action of natural chaperones 27
2.2 *En route* to the design of artificial chaperones 29
2.3 Amphiphilic polyelectrolyte as promising artificial chaperones: protein binding, influence on conformational stability and on aggregation of proteins 44
2.4 Our project: study of model poly(sodium acrylate) derivatives as artificial chaperones for antibodies and their derivatives 54

II Chemical refolding of proteins in the presence of amphiphilic polyelectrolytes **59**

3 Renaturation of a model enzyme with amphiphilic poly(acrylate) chaperones **61**
3.1 Bovine carbonic anhydrase B: a model enzyme to study aggregation during refolding 63
3.2 Keeping CAB soluble with poly(acrylate) derivatives 66
3.3 Polymers allow recovery of a native-like and active protein 72
3.4 Conclusion: discussion on the role of Coulomb and hydrophobic associations 81

4 Chemical refolding of scFv fragments with poly(acrylate) derivatives 83
4.1 Preamble: structure, use and folding of scFv 85
4.2 Size of scFv during refolding 94
4.3 Do polymers affect the secondary structure of scFv? 101
4.4 Conclusive remarks and perspectives 113

III Amphiphilic polyelectrolytes for the stabilization of IgG 115

5 Stabilization of IgG during thermal stress in the presence of poly(acrylate) derivatives 117
5.1 Motivation to study IgG stability 119
5.2 IgG:polymer complexes at room temperature 120
5.3 Evidence of association between polymers and heat-stressed IgG 129
5.4 Impact of poly(acrylate) derivatives on IgG aggregation upon thermal stress 135
5.5 Conclusion 142

Conclusion and perspectives 145

A Materials and methods 147

B Experimental techniques 157

C Supplementary data on CAB refolding assisted with PAA derivatives 173

D Supplementary data on scFv refolding assisted with PAA derivatives 181

E Supplementary data on thermally-induced IgG aggregation in the presence of PAA derivatives 193

Bibliography 207

List of Figures 235

List of Tables 241

Abstract 243

General Introduction

Since the 1980s, recombinant proteins have become routinely used in biotechnology, medicine and research. Antibodies are in particular highly versatile and promising tools in the therapeutic and diagnosis fields. However, with the development of therapeutic proteins come concerns about their physical instability in solution: unfolding and aggregation are ubiquitous pitfalls in protein production, storage and administration. Multi-domain proteins, such as antibodies or their bio-engineered artificial fragments are particularly prone to aggregation. Accordingly, there is a strong demand for additives and/or procedures aimed at controlling *in vitro* the aggregation propensity of recombinant proteins and enhancing renaturation yields. Within this scope, chemists have been greatly inspired by molecular chaperones, namely proteins that are naturally expressed *in cellulo* to guide new-born proteins or stress-unfolded ones towards their native conformation while avoiding off-pathway aggregation. Reproducing the most remarkable properties of natural chaperones, such as their specific association with partly-folded conformers and the controlled release of the latter into bulk solution, is highly desirable. But at the moment no generic additive that would ensure high renaturation yields – notably of artificially engineered antibody fragments – has been designed.

Owing to their capacity to bind and release proteins under an appropriate stimulus, amphiphilic polyelectrolytes are envisioned to provide a suitable environment for protein folding, ideally capturing partly-folded conformers (ensuring confinement or increasing their solubility under the form of complexes), while allowing proper folding towards the native structure. These macromolecular additives can indeed bind to hydrophobic and/or charged patches on proteins, which impacts both the colloidal and conformational stabilities of the latter. Since they develop differential hydrophobic association and electrostatic interactions with the polypeptide chains according to their degree of unfolding, amphiphilic polyelectrolytes affect the conformation of proteins and should control complex association/folding/unfolding/dissociation schemes. It remains unclear in the literature whether the main driving force of colloidal stabilisation relies on shielding hydrophobic attraction or on the sequestration (immobilization) of transiently unstable conformers.

The work described in the present manuscript aims at rationalizing the general features required for a macromolecular additive to be a generic and efficient aggregation suppressor (and renaturation enhancer). To unravel the contributions of electrostatic and hydrophobic interactions to the chaperone-like activity of polymers, we studied a set of hydrophobized poly(sodium acrylate) (PAA) derivatives mixed with a model enzyme, scFv fragments of antibodies, and IgGs. Protein's conformation, size and degree of aggregation,

and formation of complexes in solution with PAA chains were characterized mainly by light and fluorescence correlation spectroscopies, circular dichroism, calorimetry, and activity assays. Chapter 1 introduces the origin of the physical instability of (therapeutic) multi-domain proteins, as well as conventional strategies developed to circumvent these aggregation issues. Chapter 2 describes the state of the art on artificial chaperone systems. Results are divided into three chapters focusing on increasingly complex protein structures. As a proof of concept, Chapter 3 investigates the use of PAA derivatives to stabilize a well-characterized model enzyme, bovine carbonic anhydrase B (CAB), during refolding from the urea-denatured state. Chapter 4 extends the use of PAA additives to the handling of two-domain antibody single-chain Fv (scFv) fragments during chemical refolding. Chapter 5 is dedicated to the stabilization against aggregation of full-length polyclonal immunoglobulins G (IgG), which is here assessed in heat-stress conditions.

Part I

Proteins in solution: from folding and stability issues to the design of synthetic chaperones

Chapter 1

Protein folding and stability: to aggregate or not to aggregate?

Antibodies are versatile tools for the treatment of several diseases and constitute nowadays the fastest growing class of human drugs. Yet, aggregation of antibodies during both production and post-production stages gives rise to undesired side-effects (immunogenicity of aggregates, toxicity) that currently restrain progress in the field.

This first introductory chapter is focused on the basic mechanisms that are at the origin of protein aggregation. A particular attention is paid to proteins of therapeutic interest, notably antibodies. The chapter also describes some of the main conventional strategies adopted to prevent aggregation, both during storage under potentially stressful conditions and during refolding procedures. Motivations of the work and the necessity to find other stabilising approaches are introduced.

Contents

1.1 Preamble: about the development of therapeutic antibodies and practical issues 7

1.1.1 Antibody-based therapies 7

1.1.2 A practical bottleneck: aggregation of therapeutic proteins . . 12

1.2 Basic mechanisms leading to *in vitro* protein aggregation . 14

1.2.1 Native aggregation 15

1.2.2 Aggregation as a result of conformational instability (non-native aggregation) 15

1.2.3 Competition between folding, misfolding and aggregation during renaturation 17

1.3 Conventional strategies to limit *in vitro* protein aggregation 20

1.3.1 Optimisation of protein concentration and incubation time in renaturation buffers 21

1.3.2 Reversible immobilization on chromatography columns 21

1.3.3 Formulation-based strategies (use of additives) 22

1.3.4 Conclusion 24

1.1 Preamble: about the development of therapeutic antibodies and practical issues

Since the end of the 1990s, the downward trend of therapeutic innovation has become apparent [1, 2]. Costs associated to the production of new drugs soar and leave no room for improvisation. The numerous patent expiries of blockbusters drugs in the forthcoming years contributes to fierce competition of generic drugs, sold on average 60% cheaper than their branded equivalents. Harsher regulatory requirements, in particular in terms of innocuousness, and scandals in the pharmaceutical industry also fuel the increase of production costs of drugs. Accordingly, pharmaceutical groups tend to progressively abandon the research of drugs based on proprietary molecule libraries and chemical modifications, and turn now to the rational design of biomolecules. Whereas chemistry and search for "lead" small molecules (screening) was at the center of developments in the 1980s, by 2004 some 50% of the projects underway in drug companies were based on biotechnology [survey of the USA Biotechnology Industry Organization], a trend that was boosted by the allowance to patent genes and genetically-modified organisms (GMO) since the early 1980s. More personalized treatments are in the pipeline, seeking at rapid diagnosis of a disease (through the identification of specific biological markers) and subsequent prescription of the best suited treatment for a given patient. The word "theranostic" has been used to describe this coupling between therapy and diagnosis. Vaccines, hormones, enzymes or antibodies are highly versatile (bioengineerable) and promising tools in this context: these drugs are designated as "biopharmaceuticals" or "biologics", namely drugs derived from biological sources.

Among therapeutic proteins, antibodies play an increasingly important role in the treatment of viral infections (including HIV) [3], autoimmune disorders [4], cancers [5–7] and several other human diseases [8]. This preamble aims to introduce some of the milestones that marked out the development of these biopharmaceuticals, as well as give some economic considerations and issues that currently restrain progress in the field. We will particularly justify the need to control protein folding and stability.

1.1.1 Antibody-based therapies

More than a century has passed since the discovery of agents – that were soon to be called "antibodies" – capable of conferring immunity against diseases such as diphtheria that were until then incurable. Nowadays, antibodies are routinely used to treat cancer and other scourges of modern society. Motivations for the use of antibodies can be found in their structure and biological role.

1.1.1.1 Antibody structure and biological role: an overview

Antibodies are glycoproteins (*i.e.* proteins that contain oligosaccharides chains covalently attached to the polypeptide backbone) belonging to the superfamily of "immunoglobulins" (Ig). All proteins of this family share a structural motif called "immunoglobulin domain" [9], which structure will be analysed more in detail in Chapter 4 and Chapter 5. In a simplistic view, several Ig domains assemble (through non-covalent interactions and disulfide bridges) to form one antibody molecule that adopts a distorted "Y" shape (see Figure 1.1). In mammals, antibodies are classified into five main classes, referred to as "isotypes" (IgG, IgA, IgM, IgE and IgD). Each class has a distinct structure and biological activity but they all possess the common "Y"-shaped element [9].

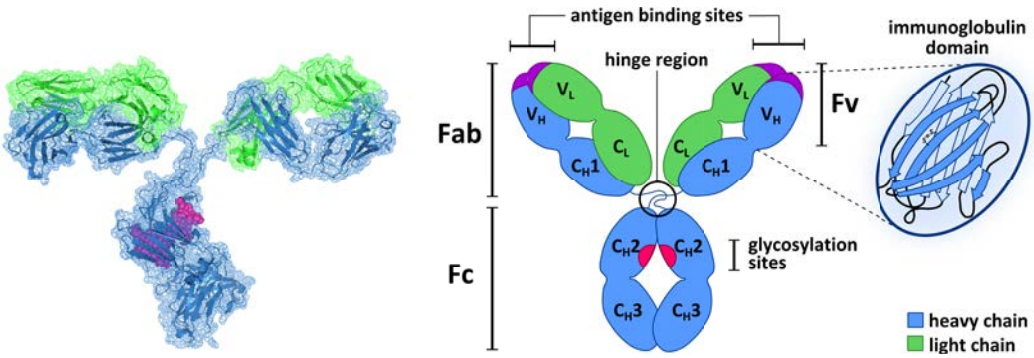


Figure 1.1: The structure of immunoglobulins G. Left: three-dimensional structure of a crystallized IgG molecule from the Protein Data Bank (PDB entry: 1IGT). Right: schematic representation of the IgG structure.

Immunoglobulins G (IgG) constitute the most abundant isotype found in normal human serum (accounting for $\sim$ 70-85% of seric antibodies) [8, 10]. These proteins of *ca.* 150 kDa molecular weight consist of a heterotetramer of two identical light chains ($M_W \sim 25$ kDa) and two identical heavy chains ($M_W \sim 50$ kDa) held together by disulfide bridges (Figure 1.1) [11]. Each IgG heavy chain contains a variable domain (V_H) and three conserved domains (C_H1, C_H2 and C_H3), while an IgG light chain is composed of a single variable domain (V_L) and a single constant domain (C_L) [9]. Enzymatic cleavage can be used to separate the two identical Fab arms of the "Y"-shaped protein (fragment antigen-binding) from the Fc fragment (fragment crystallizable) [12]. These three fragments are connected via the hinge region that confers a certain flexibility to IgG. The two antigen-binding sites (or paratopes) are located at the very ends of each arm of the "Y"-shaped molecule (N-terminal domains, purple regions in Figure 1.1), and contain particularly diverse strands of amino acids that form 6 hypervariable loops, also called complementarity-determining regions (CDR), which confers a high specificity to each IgG.

IgG are involved in the protection of organisms against pathogens or toxins by neutralizing them and inducing their elimination. Lymphocyte B (or B-cells) are able to produce a seemingly unlimited number of IgG that can be highly specific for a given antigen recognized as foreign by the organism. IgG can function by different modes of action, as schematically illustrated on Figure 1.2. Upon binding to cell receptors, IgG can in particular recruit proteins from the complement system, phagocytes and cytotoxic cells (schematically recruited and activated via the Fc region), which eventually leads to the destruction (lysis or phagocyosis) of the targeted element. A detailed mechanism of action of IgG is beyond the scope of this introduction and can be found in several reviews [4, 7].

Antibody-based therapies aim to eliminate or neutralize pathogens or diseased cells. Upon administration, therapeutic antibodies are expected to specifically bind to their target – which is, in $\sim$ 70% of cases, a surface protein (membrane receptors, glycoproteins, adhesion molecules or viral capsid proteins for instance) – subsequently inducing the elimination of the addressed element, without affecting healthy tissues (see Figure 1.3).

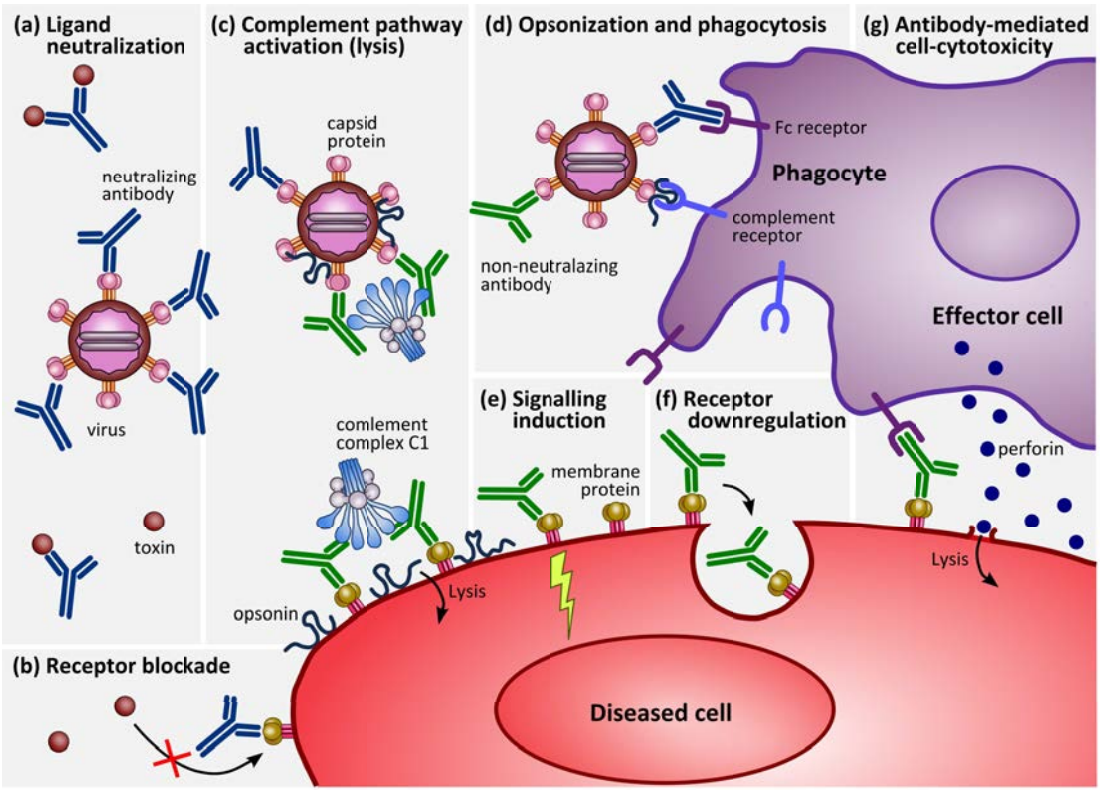


Figure 1.2: Schematic illustration of the main biological roles of IgG. (a) Ligand neutralization: IgG bind a toxin or a virus thus preventing it from activating their cognate cell receptors and penetrating cells. (b) Receptor blockade: IgG act as antagonists by inhibiting a cell receptor. (c) Complement pathway activation: IgG activate complement-mediated lysis and opsonization. (d) Opsonization and phagocytosis: the pathogen is digested by phagocytes that are recruited by IgG (via the Fc fragment) and opsonins. (e) Signalling induction: IgG induce cascade reactions (active signals) that alter cellular fates. (f) Receptor downregulation: binding of cell surface receptors by IgG result in their internalization (thus limit the receptors that can be activated). (g) Antibody-mediated cell cytotoxicity: effector cells recruited by IgG secrete proteins that contributes to the lysis of the cell.

1.1.1.2 Historical and economical considerations

The development of therapeutic antibodies has been greatly facilitated when production of monodisperse monoclonal antibodies (mAbs), *i.e.* antibodies targeted against one specific antigen, became possible, after the work of Köhler and Milstein who, back in the 1970s, developed methods for the isolation of monoclonal antibodies [13].

Advances in genetic engineering and molecular biology in the 1990s made available humanization of mAbs, paving the way to their use as specifically targeted therapeutic agents in humans (see Timeline on Figure 1.6) [14, 15]. Problems of anti-antibodies immune responses were partly solved with the use of chimeric antibodies [16] (murine variable part and human constant region), then humanized antibodies [17] (murine amino acids of the variable region replaced by human residues, except in the hypervariable regions [18, 19]) and eventually fully human antibodies. Therapeutic antibodies are

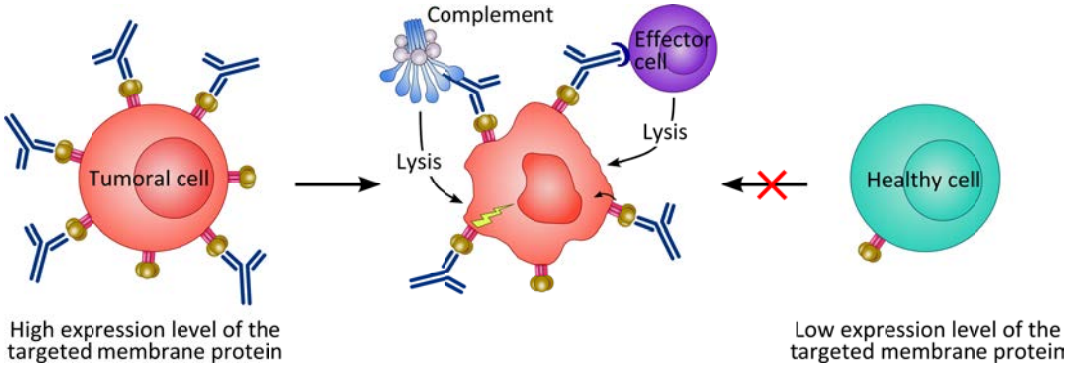


Figure 1.3: Schematic illustration of the advantages of using antibody-based therapies in cancer. Tumoral cells often over-express a membrane protein compared to healthy cells. Unlike most of conventional chemical drugs, IgG will hence target specifically the diseased cells and induce their elimination, with minimal side-effects on healthy tissues (targeted therapy).

nowadays used routinely in the treatment of severe diseases: more than 40 therapeutic antibodies and their derivatives have been approved by the FDA in the past 25 years and 338 are currently in clinical trials [2013 PhRMA report on biologics in development].

Therapeutic mAbs now constitute the fastest growing class of human drugs [20]. Soon after their regulatory approval, antibody products have already reached breathtaking sales: Humira, for instance, has now become the first worldwide best-selling drug (> $10 billion worldwide sales in 2013) only 12 years after its commercialization [Medscape]. As an illustration, Figure 1.4 plots the worldwide sales of the top 10 best-selling drugs in 2013. Seven of these drugs are biopharmaceuticals, six of which are antibody-based products. These top six antibodies account for a total annual sale in excess of $48 billion, which represents *ca.* 8% of the global market for pharmaceuticals. Due to the almost infinite combinations of sequences that can be designed, financial investments will certainly continue at high rate in the upcoming years. The global market of recombinant antibodies is expected to growth by more than 12% in 2013-2017 [Reuters].

1.1.1.3 Other formats: antibody-drug conjugates and antibody fragments

Most therapeutic mAbs today appear not to be sufficiently potent to be efficient on their own and are hence often used in combination with conventional chemical drugs ("drug cocktail") [21]. For cancer therapy, efforts are now more and more directed towards the coupling of cytotoxic drugs onto monoclonal antibodies, with the aim of increasing tumour selectivity and efficacy of chemical drugs with minimal side effects on healthy tissues. These chemically-modified antibodies have been termed antibody-drug conjugates (ADC). By now, two ADC have already gained regulatory approval from the FDA (for a recent review, see Chari *et al.* [21]).

Other antibody formats are also largely being developed. In the past few years, the variety of antibody structures has indeed been widely extended. Advances in recombinant DNA technology has enabled the design of fusion proteins (such as protein-Fc fusions, called immunoadhesins) and fragments of antibodies that have been further assembled to obtain very diverse nano-constructs. Figure 1.5 lists some of the already existing antibody-based constructs. Amongst them, single-chain Fv fragments (scFvs) have

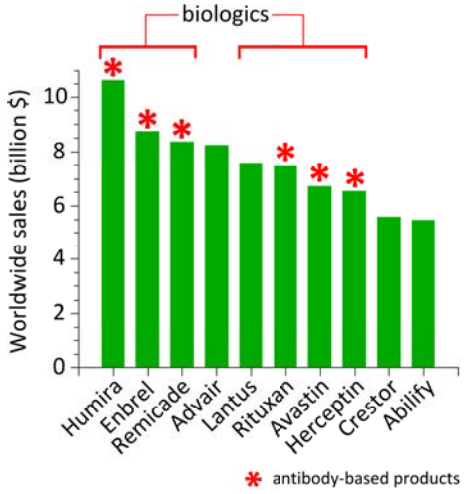


Figure 1.4: Top 10 best-selling drugs in 2013 (in terms of worldwide sales).

become interesting building blocks of antibody fragments. These artificial constructs are made of the variable regions of the heavy and light chains of an IgG that have been linked together via a peptide linker, thus retain the high specificity and affinity of antibodies and can multimerize depending on the chain length of the peptide linker to form dimeric, trimeric or tetrameric forms, conferring at will multi-specificity to the constructs.

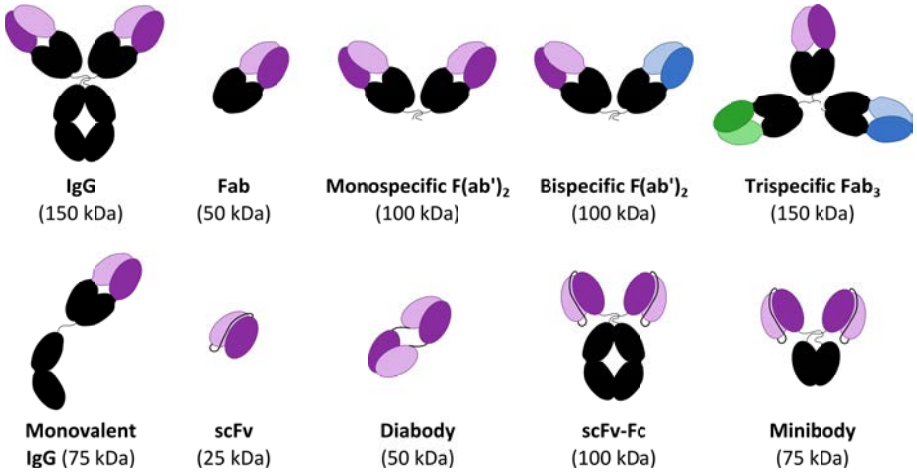


Figure 1.5: A selection of engineered antibody fragments.

Antibody fragments offer advantages over complete IgG. Their smaller size in particular increases their diffusion rate into tissues, as well as their clearance rate, making these tools interesting markers of tumoral tissues for *in vivo* imaging (fragments coupled with fluorescent reporters or radio-isotopes). Chapter 4 will focus on scFvs currently developed for therapeutic imaging. A complete review of antibody fragments in development is beyond the scope of this introduction. The interested reader shall find more details in reviews [22], [23] and [24].

1.1.2 A practical bottleneck: aggregation of therapeutic proteins

1.1.2.1 Origin of antibody aggregation

Therapeutic mAbs – as well as their fragments and other therapeutic proteins – face practical issues that hamper their present development. One of the main bottlenecks is undoubtedly their *in vitro* aggregation, which is an ubiquitous hurdle during biopharmaceuticals' expression and purification, storage, shipping and administration.

Aggregation can manifest upon production of recombinant proteins
Recombinant proteins over-expressed in bacteria are hardly produced under their native form but tend to be expressed into *in cellulo* insoluble aggregates called inclusion bodies (IBs) [25]. Albeit usually highly homogeneous, which may facilitate protein purification, inclusion bodies are often regarded as a bottleneck since refolding procedures are needed, after solubilization of the IBs, to obtain active proteins. Frequently used chaotropic agents to solubilize IBs include denaturants, such as urea and guanidinium chloride (GndCl), that break intra- and inter-molecular interactions, but also ionic detergents (such as sodium dodecylsulfate) [26]. Reductants may also be added to disperse aggregates of proteins containing disulfide briges. Refolding of IBs is not a straightforward process, and often requires many steps of handling (exchange of buffer conditions, addition and removal of additives, immobilisation/release of the protein which is both time-consuming and expensive) [25]. In addition, it may lead to the formation of insoluble protein aggregates, in particular when working with artificial antibody fragments that have not been screened to optimize their solubility.

Aggregation can manifest upon post-production treatments
In order to gain regulatory approval, mAbs need to be purified after production. These purification treatments involve several steps, typically including protein A chromatography (for capture of the product and removal of impurities), viral inactivation (performed at low pH of 3-4), cation/anion exchange chromatography as well as ultra-filtration (to sterilize the samples). Because of the far-from-physiological conditions used, all this steps are critical for IgG aggregation.

Aggregation can manifest upon long-term storage/shipping/administration
As opposed to common chemical (molecular) drugs, that are only subjected to potential chemical degradation upon storage, therapeutic proteins also face physical degradation issues. Environmental stresses (temperature excursions, pH changes, agitation, freeze/thaw, adsorption to air-liquid or solid-liquid interfaces, shear, light exposure...) easily lead to the formation of protein aggregates because of partial unfolding (see details in Section 1.2). In addition, because of the relatively high dose required for efficacy, formulations tend to be prepared at high concentrations (typically 10-50 $mg.mL^{-1}$) which further enhances self-association.

1.1.2.2 Side-effects of aggregation of therapeutic proteins

Aggregates must be avoided in therapeutic formulations. First of all, aggregates often exhibit a lower activity than the monomeric protein, therefore requiring multiple injection at a higher dose to reach the correct dose for treatment efficacy. Second, from a practical point of view, aggregates are associated to increased production costs, since they require

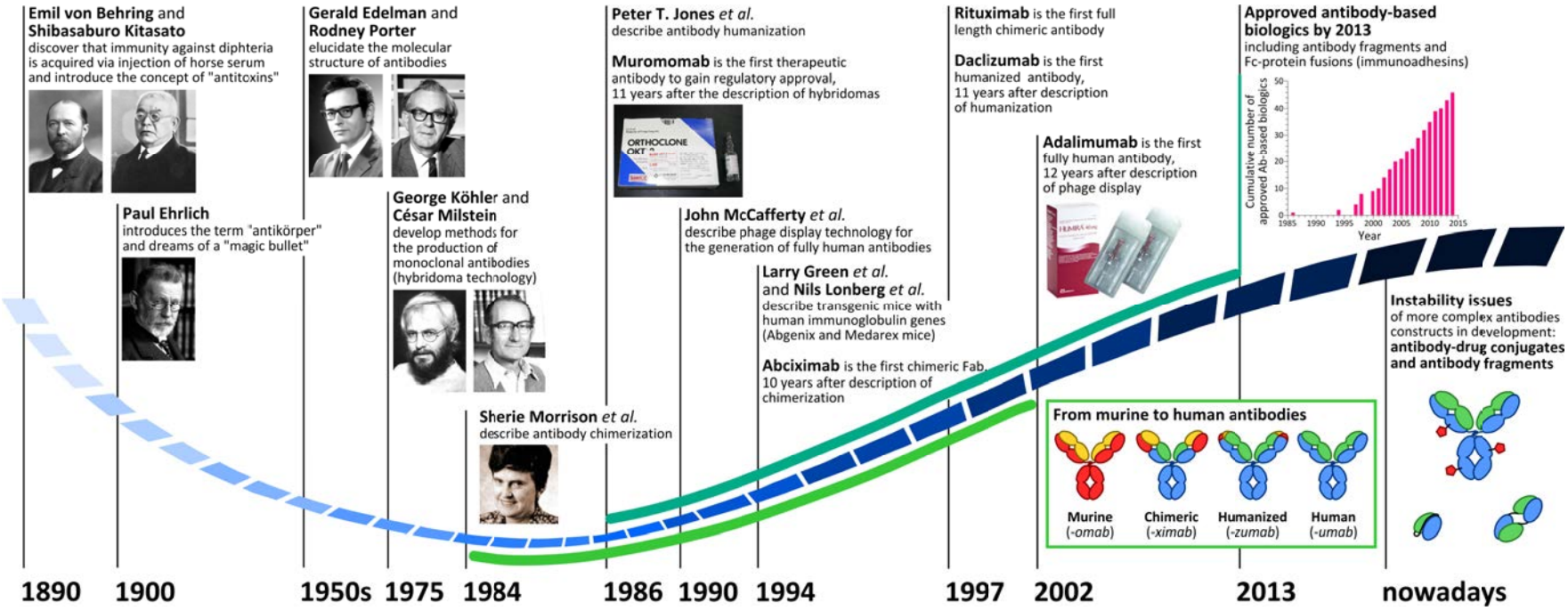


Figure 1.6: The development of therapeutic antibodies.

more purification steps and expensive optimization of formulations (based on trial-and-error approaches). Third, aggregates have been shown to cause both toxicity and immune responses upon administration to patients [27–31], which mainly manifests through the formation of binding or neutralizing antibodies (anti-drug antibodies, ADA) that can also decrease the activity of the therapeutic protein.

The ability of protein aggregates to elicit unwanted immune responses against the monomeric form of the protein of interest has been known for more than half a century, but little is known about the particularities that make protein aggregates potent inducers of the immune system. It has been shown that, depending on the size, structure, amount or solubility, not all aggregates are immunogenic [32]. According to current knowledge, high-order multimeric protein aggregates containing native-like molecules with repetitive epitope presentation seem to be the most immunogenic type of aggregates.

Overall, aggregation of therapeutic proteins fosters decreased production yields (*i.e.* increased associated costs), loss of activity and is a key factor in causing adverse events associated with immunogenicity in the clinic. To avoid formation of aggregates, it is hence crucial to control the stability of IgG and to understand what the origin of such aggregation is. We will see in the next section that the presence of partially folded (resp. unfolded) protein intermediates generated during refolding steps (resp. under environmental stresses) is critical in the formation of aggregates.

1.2 Basic mechanisms leading to *in vitro* protein aggregation

In this section, we will focus on inter-protein interactions and discuss the origin of protein aggregation. We will limit ourselves to *in vitro* protein aggregation, which is the main purpose of this thesis.

In an attempt to standardize the still debatable definition, it has been proposed that aggregates be defined as any protein species in non-native states and which size is at least twice as that of the native protein (dimers, trimers..., that maintain a native-like structure therefore would not fall under this definition of aggregates) [32].

Table 1.1: Classification of protein aggregates proposed by Narhi *et al.* [33]

Category	Classification
Size	<100 nm, 100-1000 nm (submicrometer), 1-100 μm, >100 μm
Reversibility	Reversible, irreversible, dissociable, dissociable under physiological conditions, dissociable under defined conditions
Secondary/tertiary structure	Native, partially unfolded, unfolded, inherently disordered, amyloid
Covalent modification	Cross-linked, reducible cross-link, non-reducible cross-link, intramolecular modification, oxidation, deamidation, no modification
Morphology	Number of monomeric subunits, aspect ratio, surface roughness, internal morphology, optical properties, translucent, heterogeneous

However, aggregation is commonly used as a vague term, encompassing protein assemblies that can differ in size, involve non-covalent or covalent linkages, be ordered or disordered, soluble or not, and whose formation can be reversible or not [34]. Accordingly, Narhi *et al.* recently suggested a standardized classification of aggregates based on five categories: size, reversibility of formation, conformation, chemical modification and morphology (see Table 1.1) [33]. In this approach, quantitative values are notably used to refer to size of aggregates instead of the widely found vague terms (such as visible/subvisible or soluble/insoluble).

In the following, we choose arbitrarily to classify aggregates according to their size, regardless of the reversibility of their formation, covalent modifications, or the preservation of a native-like structure in such objects. Accordingly, we will refer to "small-sized", <100 nm, multi-protein objects as "oligomers", whilst larger objects will be termed "aggregates".

Aggregation of proteins may be the result of a combination of several factors, including chemical degradation (hydrolysis, deamidation, oxidation or isomerization), chemical linkages (*e.g.* inter-molecular disulfide bond formation/exchange), potential self-association of native proteins (depending on the physico-chemical characteristics of the protein, that can be altered through chemical degradation) and partial unfolding [32, 35]. The different origin of protein aggregation are discussed in the following.

1.2.1 Native aggregation

Self-association of native proteins under particular pH and/or ionic strength conditions (*e.g.* salting-out processes, protein crystallization) without unfolding as been denoted as "native aggregation". In native aggregation processes, globular proteins are considered as densely-packed, rigid, colloid-like objects that stick to each other without unfolding. It is often governed practically by thermodynamics of phase separation and will not be discussed in detail here (for reviews, see [36, 37]).

Formulations of therapeutic antibodies typically try to avoid self-association through fine adjustment of salt type, ionic strength and pH conditions. In some cases, native aggregation can be reversible. However, native self-association is often accompanied by formation of insoluble aggregates [38, 39]. Irreversibility is particularly likely in the case of artificial proteins, such as antibody-fragments, that present in their natively-folded state unnatural, mostly hydrophobic, solvent-exposed interfaces prone to inter-chain association (the example of scFv fragments will be discussed in Chapter 4).

1.2.2 Aggregation as a result of conformational instability (non-native aggregation)

Protein non-native aggregation results from the (partial) loss of native protein structure [40]. Since the native structure of a globular protein is based on weak intra-molecular interactions (hydrogen bonds, Van der Waals interactions, hydrophobic association, electrostatic interactions, and in some cases additional contributions of aromatic pairing, covalent disulfide bridges or metal binding), it is not rigid, but rather fluctuates around the time-averaged native structure to different extents depending on the environmental conditions. To rationalize non-native aggregation, it is crucial to quantify the thermodynamic (conformational) stability of the protein of interest, to be able to predict whether it will readily unfold under stressful conditions or not.

1.2.2.1 Definition of the conformational stability of globular proteins

The conformational stability of globular proteins is conveniently quantified in terms of the magnitude of a free energy ΔG [41]. In the context of protein folding, ΔG is the difference in Gibbs energy between the folded native conformation (F) and the unfolded states (U), under the hypothesis of a rapid, reversible (*e.g.* no aggregation), cooperative and two-state folding process [42]:

$$F \rightleftharpoons U$$

$$\Delta G = G_U - G_F = \Delta H - T\Delta S = -RT \ln K_{eq} \tag{1.1}$$

where ΔH and ΔS are the enthalpy and the entropy changes respectively, and K_{eq} is the equilibrium constant.

This reversible, two-state equilibrium hypothesis is the easiest model to describe protein folding/unfolding. Albeit applicable to small globular proteins, this mechanism obviously does not cover the great diversity of folding/unfolding equilibria (additional complexities are accounted by the introduction in the model of intermediate folding states, creating a network of dynamic equilibria). It offers yet the advantage of laying the foundations to understand and define the protein's thermodynamic stability. In practice, conformational stability is assessed through different experiments, mostly equilibrium studies of denaturant- or thermally-unfolded/folded proteins. It has been experimentally noted that most of globular proteins are only marginally stable, with typical values of ΔG falling within a narrow range between – 5 and – 15 kcal.mol^{-1} (compared to $\sim$ 30 – 100 kcal.mol^{-1} for a single covalent bond) [42]. This marginal stability has been suggested to represent an evolutionary advantage since it increases the ability of proteins to acquire new functions, due to protein conformational plasticity [43, 44]. However, marginal stability is also at the origin of non-native aggregation (aggregation upon partial protein unfolding).

1.2.2.2 Basic mechanism of non-native aggregation

The poor thermodynamic stability of globular proteins as well as their potential complex structure (several domains for IgG, post-translational modifications, S-S bonds, bio-engineering/mutations of sequences of recombinant proteins) make them particularly sensitive to partial unfolding under environmental stresses. For instance, antibodies have been shown to aggregate after partial unfolding under pH changes [38, 39, 45, 46], temperature excursions [47–51], chemical modifications [52], adsoprtion to air-liquid [53] and solid-liquid interfaces, high protein concentration, shaking [54], shear or lyophilization [55].

Significant evidence suggests that the loss of native structure, even when it is partial, paves the way for aggregation [32, 40]. This is because partly unfolded intermediates expose on their surface non polar residues that are buried in the core of native proteins and have higher flexibility relative to the folded states [32, 56]. Large hydrophobic patches present at the water interface drive inter-protein association and the formation of protein oligomers and/or aggregates. Most non-native aggregation processes may be described by a universal Lumry-Eyring extended model [57] which involves the formation of an aggregating-prone non-native conformer, followed by reversible oligomer formation then nucleation of reversible or irreversible aggregates and growth towards larger aggregates. Mechanistic details fall outside the scope of this discussion and can be found in several articles [39, 39, 58, 59]. Since non-native aggregation is generally

constrained by the availability of a high concentration of partly-unfolded intermediates and the absence of forces opposing inter-molecular contacts, the protein charge (and charge anisotropy) should not be neglected in this process. Charge can indeed modulate the repulsive/attractive inter-protein interactions and impact the conformational stability of proteins [60–63]. Sahin *et al.* showed that variations of pH and ionic strength conditions could lead to different aggregation pathways for IgG antibodies [46], which was attributed to electrostatic interactions and non-uniform surface-charge distributions.

The marginal thermodynamic stability of proteins (conformational instability) is accordingly one of the main causes of aggregation. Due to possible inter-protein covalent linkages upon unfolding, and re-arrangement of secondary structures (with a marked increase of β-sheet content observed in many protein aggregates [64]) non-native aggregation is most of the time irreversible in physiological conditions (even though the reversibility does depend on the stage of the aggregation process and on the size of the aggregates [65]).

1.2.3 Competition between folding, misfolding and aggregation during renaturation

Protein aggregation is frequently encountered as a major unproductive off-pathway of protein folding. The simple folding/unfolding equilibrium model has to be amended accordingly (see Figure 1.7): non-native folding routes (misfolding) leading to thermodynamically favoured protein aggregation may compete with productive on-pathways. Misfolding refers to metastable (kinetically trapped) protein states that have developed non-native secondary and tertiary structures. Because they tend to expose hydrophobic residues, misfolded states as well as off-pathway but also on-pathway folding intermediates (which may possess partly formed secondary structures but not yet tertiary contacts) are highly prone to aggregation, particularly when they represent major kinetic traps in the folding pathway. Studies on protein folding are important to rationalize the folding rates of proteins and aggregation of partly-folded intermediate states.

1.2.3.1 Basic principles of protein folding

Observation of folding intermediates caught in the act of folding have become the key since the 1970s to unravel how an unfolded polypeptide chain finds its native structure [67–70]. Several models have been proposed and are detailed elsewhere [71]. Advances in both spatial and temporal high-resolution experimental techniques as well as protein engineering and molecular dynamics simulation methods have suggested since then that three key factors determine the folding of many globular proteins:

– hydrophobicity. Following the influential 1959 paper by Kauzmann [72], it has been suggested from the 1980s that the hydrophobic effect (that favours the clustering and burial of hydrophobic residues from the surrounding water molecules [73]) could be the dominant factor to protein folding[1] [67, 77]. According to this model, hydrophobic residues are progressively buried in the core of the protein

[1] The debate remains yet open. There are claims in favour of the predominance of hydrophilic forces, namely interactions resulting from short-ranged hydrogen bonds with water and solvation effects (water molecule bridging between two or more hydrophilic side chains) [74]; or of the major role of hydrogen bonds within the polypeptide backbone [75]. Interestingly, a recent article reports for the first time a protein that has a water-filled core, unlike most proteins which have hydrophobic inner surfaces that exclude water [76], suggesting that the hydrophobic effect may in some cases not be the driving force of protein folding.

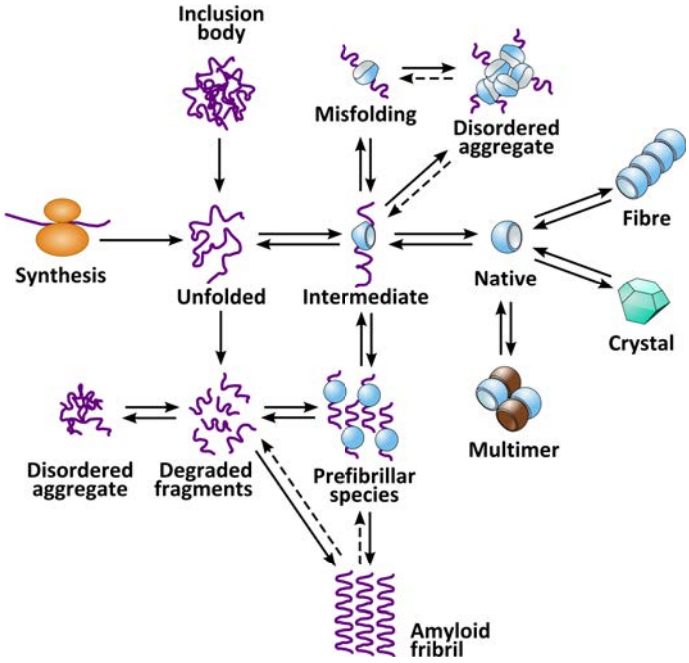


Figure 1.7: A unified view of some of the types of structure that can be formed by polypeptide chains during folding, adapted from Dobson *et al.* [66].

during folding (hydrophobic collapse). Macromolecular compaction is simultaneous to the formation of secondary structures [78] that tend to optimize the intramolecular hydrogen bonding network (see Figure 1.8). The predominance of the hydrophobic association is supported, *inter alia*, by the observation that sequences that only retain their correct polar/non-polar patterning fold to their expected native state[2] [80].

– cooperativity. The formation of tertiary contacts between partly-formed secondary structures as well as cooperativity of multiple weak intra-protein interactions participate to the stabilization of the native structure [42, 81].
– some key residues. A protein can possess specific residues which mutation can influence the folding rate and intermediate states. Their presence is essential for the correct folding to occur.

Since they tend to expose hydrophobic residues to solvent molecules, folding intermediates, such as the *molten globule* states (namely compact intermediates having most of the native secondary structures but lacking the proper tertiary contacts) are prone to aggregation, in particular if they constitute kinetic traps of folding.

1.2.3.2 Folding and aggregation of multi-domain proteins

Folding of single-domain globular proteins with 100 residues or less is usually under complete thermodynamic control, with a folding rate that has been experimentally observed to fall within the microseconds to tens of seconds range [82]: these small proteins

[2]Other authors found an upper limit of *ca.* 200 residues on the length of proteins for which hydrophobic collapse and non-polar/polar residue segregation would suffice, without further natural selection, to give realistic (biological) folding time-scales [79].

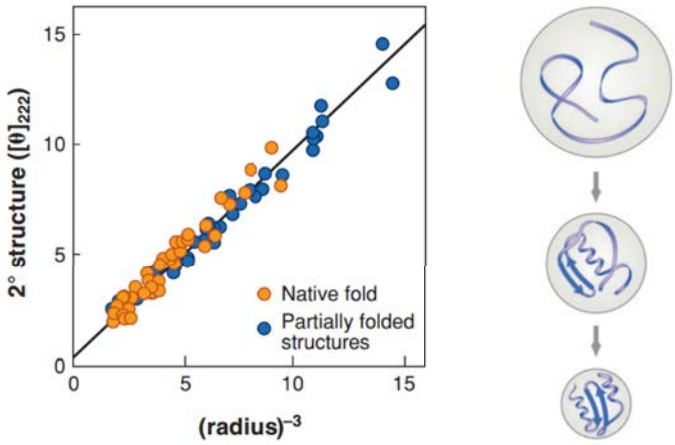


Figure 1.8: Schematic view of protein folding: compactness correlates with and stabilizes the secondary structures (adapted from [77]).

can find their most stable fold without the complication of highly populated (kinetically-trapped) intermediates. On the opposite, for proteins with more than 100 residues (*i.e.* most of therapeutic proteins), one or more intermediates have experimentally been shown to be significantly populated during folding[3] [82]. Overall, most of experimental results can be interpreted in terms of equilibria between two or more states (folded, unfolded, intermediates), each of them being characterized by temperature- and solvation-dependent thermodynamic constants [42, 75, 83]. This average view allows the use of the transition state theory with a simple activation barrier between the folding intermediates to interpret the kinetic relaxation towards the most stable state. But kinetically-trapped intermediates readily tend to be involved in the formation of aggregates.

With folding of large proteins, that account for more than 70% of eukariotic proteins – and approximately 40-65% of prokariotic proteins [84–86], come also questions about the involvement of distinct domains. Large globular proteins, such as antibodies that constitute the core of this thesis, are composed of multiple domains of relatively compact structure, a domain being defined as a "structural, functional and evolutionary component of proteins, which can often be expressed as a single unit" [87]. The size of domains has been shown to range from about 20-40 to 400 amino acids [88].

Owing to the difficulty to express a soluble form of an artificial individual domain, most studies have focused on the folding of naturally-occurring single-domain proteins, with the underlying assumption that these principles would be applicable to larger proteins if one considers that a protein domain is an autonomous folding unit. However, the independent folding hypothesis is now challenged and research efforts tend to understand whether or not neighbouring domains affect each other's folding and stability. Understanding the folding and conformational stability of multi-domain proteins is of paramount importance to be able to predict and control their aggregation propensity during *in vitro* renaturation procedures.

Some general comments can be deduced from the handful of studies that have concentrated on these questions so far. The key factor that determines if connected domains fold cooperatively is the surface area of the interface between them [90–92]: neighbouring

[3]There is still a debate about the role of such intermediates, whether they constitute traps that slow down the folding process or whether they assist the protein to find its native structure.

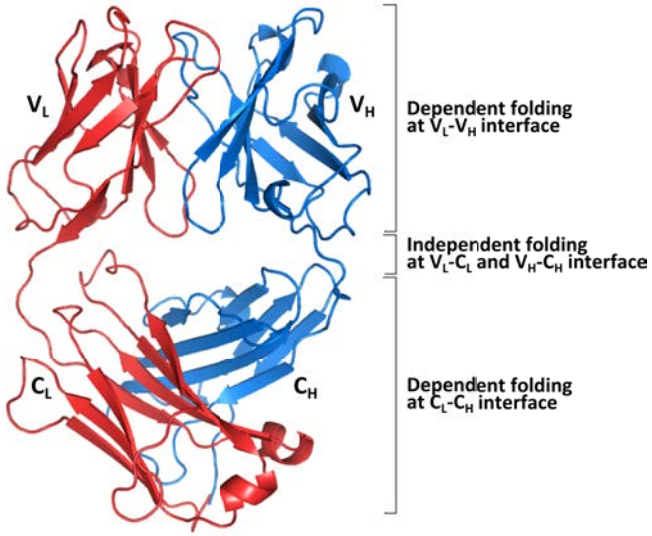


Figure 1.9: Domain interface and folding dependency in multi-domain proteins. The Fab fragment (PBD code 1nbv) illustrates the general relationship between folding dependency and domain interface. The light (L) and heavy (H) chains are coloured in red and blue, respectively. In the folding studies, the constant (C) and variable (V) domains from light and heavy chains were covalently linked either by a disulfide bridge or an artificial linker [89]. The results from the folding experiments showed that inter-chain V_L-V_H and C_L-C_H domain interfaces lead to mutual stabilization, whereas direct intra-chain interactions in V_L-C_L and V_H-C_H interfaces have no influence on each other's folding. Structural analysis showed that in domain interfaces where folding dependency exists the interfaces are large (∼1,800 Å^2) and tightly packed (local atomic density ∼40). However, when the folding of domains is independent (2) the domain interface is small (∼400 Å^2) and loosely packed (LD∼18). Adapted from [90].

domains which interface is small and rather flexible tend to fold independently (with some exceptions to the rule), unlike domains that share densely packed, hydrophobic interfaces. In the latter case, domains stabilize each other from a thermodynamic point of view and hence fold cooperatively. The length and flexibility of the linker are also contributing factors to the stabilization or destabilization of tethered domains [91–93]. Studies on antibody Fab fragments support these observations: loose and distant interactions between the variable and the constant light chains domains (V_L and C_L) do not affect the stability of either domain, whereas dense inter-chain interactions between the $V_L - V_H$ and the $C_L - C_H$ domains contribute to stability of the folded structure and on the folding cooperativity [89] (see Figure 1.9). More insights into folding of two-domain scFv fragments will be given in Chapter 4.

1.3 Conventional strategies to limit *in vitro* protein aggregation

Sequence tailoring through *in silico* prediction of aggregation-prone regions [94–96], as well as bio-engineered point mutations [97], are commonly used to design stable structures, namely structures with increased thermodynamic and colloidal stability.

Another approach consists of covalent attachment of a hydrophilic polypeptide (such as an intrinsically disordered peptide [98]) or a poly(ethylene glycol) (PEG) chain [99–103] that aim at increasing the protein solubility. But these strategies cannot be utilized for all sequences, for instances when working with peculiar therapeutic proteins which sequence cannot suffer mutations or covalent grafting (that can be deleterious for bio-activity). In this section, we will focus on strategies that rely on modification of the experimental conditions and buffers instead of alteration of the protein's intrinsic sequence or covalent attachment of solubilizing tags. We will highlight some commonly encountered approaches to prevent or reduce *in vitro* protein aggregation during refolding procedures or to stabilize the native structure during storage.

1.3.1 Optimisation of protein concentration and incubation time in renaturation buffers

Because aggregation results from an intermolecular association, it is highly protein concentration dependent. One of the easiest way to reduce the probability of aggregation during renaturation or storage is to use lower protein concentration. It has been suggested that optimal renaturation yields of can be expected if the protein concentration is in the range of about 10-50 $\mu g.L^{-1}$ [26, 104, 105]. However, these low concentrations require large volumes of refolding buffer, which is associated to increased production costs, and may lead to poor protein recovery in case of protein adsorption on surfaces. In addition, high protein concentrations are often needed for applications, such as protein crystallization or therapeutic treatments (typical concentrations higher than 1 $g.L^{-1}$), which necessitates further re-concentration steps that may be critical for aggregation.

Gradual dilution/dialysis into successive solutions of decreasing denaturant concentration enables to control incubation times at critical transition steps during renaturation, such as the collapse of unfolded coils into a globular state that exposes less hydrophobic residues to the solvent [26]. Provided that the lag-time between each change of the solution composition is optimized, this procedure should allow proteins to reach equilibrium conformation and to fold while preventing the accumulation of aggregation-prone intermediates. This sequential manipulation can be achieved by one-step or step-wise dialysis or simple mixing with compositon-buffering solutions [106].

1.3.2 Reversible immobilization on chromatography columns

Reversible immobilization of proteins on chromatography columns is the most drastic way to avoid aggregation during refolding procedures [106]. Here, proteins are reversibly attached to a solid matrix, through non-covalent bonds, classically involving complexation of nickel ion with a histidine-tag added at one end of the polypeptide chain. The column is then eluted with the refolding buffer, which makes the protein to fold without aggregating. The folded protein is subsequently detached from the column and recovered.

Attachment on a solid substrate may yet interfere with the correct folding of the protein, either because of steric constraints due to the matrix or because of multiple anchoring points of the protein on the substrate. It can be advantageous to work in slightly dissociating conditions, where protein is allowed to fluctuate between bound and unbound states. Even then, one of the major limitations of immobilization is the small amount of protein manipulated.

1.3.3 Formulation-based strategies (use of additives)

Chemical additives are commonly added either during refolding procedures or in storage formulations. Two types of additives can be schematically distinguished: additives that stabilize the native state from a conformational point of view (*i.e.* limit unfolding) and additives that reduce intermolecular attractions (*i.e.* aggregation) [107]. Both mechanisms are not mutually exclusive: rather, additives that stabilize the native structure also decrease its solubility because both effects derive from the same driving force: the solvation of the peptide chain by the additive.

1.3.3.1 Additives stabilizing the native conformation

Back in the 1980s, Yancey *et al.* developed the concept of osmolyte [108, 109], namely naturally organic solutes found in cells that participate to the stability of the native conformation of proteins. Osmolytes are also commonly referred to as cosmotropic agents, as opposed to chaotropic agents (urea, GndCl, detergents) that break intra-protein interactions (and are preferentially bound to the protein surface). They include sugars, polyols, particular amino acids, such as glycine or alanine, or trimethylamine *N*-oxide (TMAO). Experimental studies show that these additives are preferentially excluded from the hydration shell of proteins (see Figure 1.10): the protein is said to be preferentially hydrated, namely its hydration shell mostly contains water molecules [110].

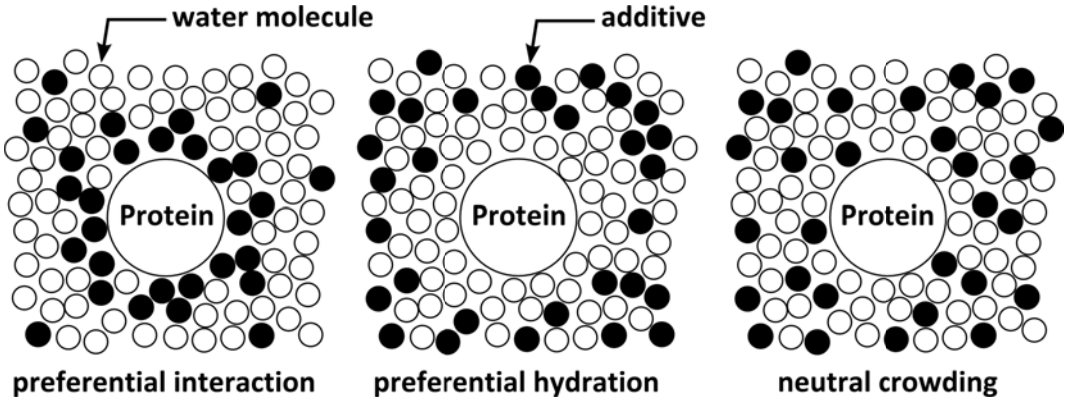


Figure 1.10: Schematic view of preferential interaction, preferential hydration and neutral crowding. Adapted from [110].

The presence of osmolytes induces an increase in the dissolution free energy of the protein. If preferential hydration remains similar upon unfolding of the polypeptide, the exclusion zone becomes more extended (increased surface exposed to the solvent), so that unfolding is disfavoured. Different models have been developed to predict protein stabilisation in the presence of osmolytes [111–113]. Overall, it has been suggested that osmolytes develop balanced interactions between the polypeptide backbone and side-chains [111] with additional contributions to conformational stability resulting from steric exclusion or increase of water surface tension [110]. However, in order to be effective, these additives need to be added at high concentrations, typically above *ca.* 1 mol.L^{-1}.

1.3.3.2 Additives preventing aggregation

Beyond the optimisation of the storage/refolding buffer conditions (in terms of pH and ionic strength) to limit inter-protein attraction (for instance, by working at pH values far from the isoelectric point of the protein of interest), additives that limit aggregation are commonly added. They include surfactants and amino acids, notably L-arginine.

Surfactants

Surfactants are largely used to limit protein aggregation. As opposed to ionic surfactants, which often exhibit a denaturing effect on proteins, neutral ones do not usually destabilize the structure of proteins (from a conformational point a view). They are yet able to limit inter-protein association by interacting with partly-folded intermediates [114]. In the case of bovine carbonic anhydrase (CAB), it was established that micellisation of surfactants is not required to obtain improved renaturation yields. The major limitation of surfactants, however, is that they can be scarcely removed from the refolded protein solution [26].

Amino acids: the peculiar role of L-arginine

Amongst all amino acid that have been tested with regard to their ability to suppress protein aggregation, L-arginine is the most efficient, even though L-lysine and L-proline also appeared to have some positive effect [107, 115, 116]. L-arginine is the most basic naturally-occurring amino acid (pI of about 10.8). It is a derivative of the denaturing agent guanidine and has been used extensively to prevent aggregation of recombinant proteins during their *in vitro* refolding. Several studies have been carried out to unravel the molecular mechanisms of suppression of aggregation. In particular, it has been observed that:

- L-arginine usually becomes more effective as a co-solvent, namely at concentrations in the molar range [115],
- unlike denaturants, the thermodynamic stability of the native state is generally not affected by L-arginine, which only reduces aggregation [117, 118]
- L-arginine is preferentially excluded from the solvation sphere of proteins, even though after careful revision the sign and magnitude of preferential interaction appears to depend on both the protein and the concentration of additive [119],
- L-arginine increases the solubility of aromatic compounds and amino acids (notably L-tyrosine and L-tryptophan) [120],
- the surface tension of aqueous solutions of L-arginine increases with increasing concentration [121],
- the aggregation suppression ability of L-arginine strongly depends on the counter-ion (anion) used, and follows the order of the empirical Hofmeister series [122],
- chirality does not play a role, *i.e.* D-arginine is as effective as the natural enantiomer [115].

Owing to the negligible effect of L-arginine on the conformational stability of the native state of proteins, it has been suggested that this additive solely affects the kinetics of protein aggregation. The purely kinetic model proposed by Baynes *et al.* [123] is based on the assumption that L-arginine interacts with the protein surface with the same strength as water molecules, acting as a so-called neutral crowder (see Figure 1.10). Due to its bigger size than solvent molecules, it is sterically excluded from inter-protein space when proteins come into vicinity, which leads to unfavoured protein attraction.

The increased surface tension of water in the presence of L-arginine is however incompatible with suppression of aggregation, since higher surface tension tends to favour the de-solvation of proteins and their attraction to limit the water-exposed surface. Accordingly, it as been argued that specific interactions between L-arginine and the protein must play a role. Some studies suggest that L-arginine develops direct interactions with aromatic amino acid residues, either through its guanidino moiety or by forming clusters exhibiting a methylene-based hydrophobic surface [124]. Dynamic clusters of L-arginine cations have recently been identified at the surface of proteins by molecular simulations and have been suggested to have an impact on protein thermodynamic stability [125]. Recently, an equimolar mixture of L-arginine and L-glutamic acid was shown to induced a compaction of unstructured loops [126]. However, the molecular origin of the arginine effects on protein aggregation is still controversial and the comprehensive mechanism of its action remains elusive.

1.3.4 Conclusion

Albeit efficient, the strategies presented so far to control and reduce protein aggregation suffer from several limitations: sequence mutation is protein-dependent and can lead to loss of activity, so as covalent attachment of a hydrophilic polymer, while reversible immobilization on chromatography columns limit the quantities of protein that can be refolded. The addition of molecular additives is also fraught with difficulties. For instance, formulations of therapeutic proteins have to be finely tailored, which participate to the increased cost of the final product. Moreover, owing to the variability of folding processes from one protein to another, costly and time-consuming trial-and-error approaches are necessary to find the best refolding conditions (additives, concentration, temperature, incubation-times...) for a given protein (experiment design). In this context, the development of a generic tool to assist protein folding and avoid aggregation is highly desirable. We will see in the next chapter how Nature can inspire chemists to find alternative strategies.

Chapter 2

Towards the design of polymer-based and colloidal artificial chaperones

Protein aggregation is an ubiquitous phenomenon, not only *in vitro* but also in the highly crowded cellular environment. Cells have developed sophisticated quality-control mechanisms that help newly synthesised chains of amino acids to escape misfolding and dead-end aggregation. Tools found within the cell include protein machineries, the chaperones, able to guide protein folding, to catalyse it, to unfold misfolded structures and even to untangle protein aggregates.

We will see in this chapter how Nature inspired chemists to design artificial chaperones sharing some characteristics with their biological counterparts. Several strategies have been developed to sequester partly-folded proteins, hence preventing unproductive intermolecular contacts, and favouring correct refolding upon controlled release. Unlike naturally-occurring molecular chaperones that bind proteins with high affinity and through hydrophobic association, artificial chaperones usually interact with proteins by non-specific, weak binding, that combines hydrophobic association and Coulomb interaction (and, in some examples, with a predominant Coulomb attraction).

Amphiphilic polyelectrolytes are good candidates as aggregation-suppressor since they combine i/ hydrophobic moieties that are expected to bind to partly-folded protein intermediates (shielding the exposed hydrophobic residues from contact with water, in competition with inter-protein hydrophobic aggregation) and ii/ long-range electrostatic as well as steric repulsions brought by the charges in the polyelectrolyte chain that help to achieve colloidal stabilization. As discussed in this chapter, they provide simple, low-cost and generic tools for the recovery of activity of unstable proteins in various contexts of interest to biotechnologies.

Contents

2.1 *In vivo* folding and aggregation: role and mode of action of natural chaperones 27

2.1.1 Protein aggregation *in cellulo* 27

2.1.2 The molecular chaperone concept 27

2.1.3 Chaperonins: the GroEL/GroES example 28

2.2 *En route* to the design of artificial chaperones 29

2.2.1 Basic concept of an artificial chaperone 29

2.2.2 Synthetic chaperones based on hydrophobic (self-)association . 30

2.2.3 Electrostatic-mediated aggregation-suppression and protein refolding 40

2.2.4 Conclusions 43

2.3 Amphiphilic polyelectrolyte as promising artificial chaperones: protein binding, influence on conformational stability and on aggregation of proteins 44

2.3.1 Interactions between native proteins and (amphiphilic) polyelectrolytes: driving forces 44

2.3.2 Impact of (amphiphilic) polyelectrolytes on the conformational stability and aggregation of proteins 47

2.4 Our project: study of model poly(sodium acrylate) derivatives as artificial chaperones for antibodies and their derivatives 54

2.4.1 Problematic 54

2.4.2 Potential application 55

2.4.3 Aim of this work: a study of mixed model polymers:model protein solutions subjected to chemical or heat stress 55

2.1 *In vivo* folding and aggregation: role and mode of action of natural chaperones

2.1.1 Protein aggregation *in cellulo*

In cell, the nascent linear amino acid sequence emerging from ribosomes must fold into a stable three-dimensional structure to gain functional activity (at least for globular proteins). Albeit often rapid and spontaneous in dilute *in vitro* conditions for small proteins, folding is much more challenging in the crowded cytosol, especially for large proteins (>100 residues, ∼90% of proteins in a cell) for which kinetically-trapped intermediates seem to be the rule [127].

Folding intermediates exhibit partial secondary structures as well as extended hydrophobic patches that favour unproductive intermolecular contacts. Correct folding appears all the more difficult when one realize that cooperative *in vivo* folding can only take place when a full protein domain (∼50-300 amino-acids) has been synthesized: nascent chains are hence exposed in aggregating-prone partially-folded states for relatively long periods of time (typically ∼15-75 seconds for a 300-residue protein) [128–130]. It is also reported that the chance to aggregate should be enhanced by the close proximity of nascent polypeptides in polyribosome complexes [131] and by excluded volume effects resulting from crowding (300-400 $g.L^{-1}$ of proteins and other macromolecules in *E. Coli*) [132].

Aggregation of non-native proteins is not limited to *de novo* protein synthesis but can also occur under conditions of stress. Many proteins are marginally stable in their physiological environment (*e.g.* when conformational flexibility is required for protein functionality). Minor environmental stresses can disrupt the native structure and favour the exposure of hydrophobic residues and therefore aggregation [133].

Controlling and preventing aggregation during both *de novo* protein folding and under environmental stress is of paramount importance since *in vivo* protein aggregates often result in diseases, especially when amyloid fibrils are formed [134]. Cells have thus evolved elaborate quality-control strategies aimed at preventing the accumulation of aggregation-prone incorrectly-folded proteins. Part of these strategies rely on "housekeeping" roles of complex cell metabolisms, such as degradation of misfolded proteins (via the ubiquitin-proteasome and autophagy systems) [135] or on their accumulation and sequestration into specific compartments (such as inclusion bodies in bacteria) [136]. Assisting the structuration of proteins is the role of chaperones, which is essential particularly for multi-domain proteins, that constitute *ca.* 90% of the proteins found in cells, and are hardly foldable *in vitro* by spontaneous convergence toward the thermodynamically-stable state.

2.1.2 The molecular chaperone concept

The cellular machinery actually uses a "chaperone" arsenal and the input of metabolic energy to assist folding of newly-synthesized proteins. Molecular chaperones have been defined as any protein which interacts, stabilizes or helps another protein to acquire its functionally active conformation without being present in its final structure [130, 133, 137, 138]. They may not accelerate folding reaction, but rather increase the chance of entering productive folding pathways.

Although they are constitutively expressed, many chaperones are up-regulated under stress conditions (such as heat), in which the concentration of aggregation-prone misfolded protein increases. For that reason, they have been called heat-shock proteins (Hsp).

Several classes of chaperones have been identified and are usually classified according to their molecular weight (Hsp40, Hsp60, Hsp70, Hsp90, Hsp100 and the small Hsps) [133]. Their common role include suppression of aggregation through sequestration of intermediates as well as stabilization/destabilization of partially structured intermediates that enables proteins to avoid kinetic traps and (re)enter in productive folding pathways. In addition, some chaperones act as enzymes capable of accelerating the folding process of proteins by catalysing the rate-limiting steps (such as the *cis-trans* isomerisation of the proline residues and disulfide bonds formation and exchange), while others are capable of untangling large and otherwise irreversible aggregates [139, 140].

The recognition of substrate proteins by chaperones is an open question. Chaperones generally recognize structural features common to partly-folded intermediates, namely exposed hydrophobic residues and/or accessible disordered backbone regions that are buried in the native conformation. Many chaperones have been shown to possess intrinsically disordered regions that help them to discriminate between unfolded proteins and partly-folded intermediates [141]. A recent study shows that the loss of structure of certain regions of a chaperone is required for it to gain its function, namely to be able to associate with partially structured intermediates [142]. Overall, the recognition of substrate proteins by chaperones seems to be non-specific, meaning here a sequence-independent capacity to bind and accommodate a wide range of substrates, but with high affinities in the nM to μM range [143, 144].

In several cases (Hsp60, Hsp70), the binding of partly-folded or misfolded "client" proteins and their release once they have been refolded proceed from highly regulated cyclic conformational changes in the chaperones (with displacements of 20-30 kDa domains over distances of 2-5 nm and rotations of up to 100° [139, 140]) that are under the control of adenosine triphosphate hydrolysis (energy input) and cofactor proteins. Some chaperones (small Hsps, Hsp47) act *in vitro* independently of ATP, but it is under debate whether they play in cell a significant role in renaturation or participate mainly to keep "client" proteins in soluble (sequestred) state, "buffering" the concentration of misfolded proteins in cell until chaperonins capture and refold them. Chemists have been particularly inspired by the chaperonin system (described below), *i.e.* the idea of activatable trapping/release cycles.

2.1.3 Chaperonins: the GroEL/GroES example

Chaperonins are large chaperones characterized by a conserved double-ring structure forming a central cavity. The most characterized group of chaperonin is the GroEL/GroES system found in *E. Coli*. By a complex binding and release process involving ATP, ADP and the co-chaperone GroES (Figure 2.1), the *trans* ring of the GroEL unit is able to capture a misfolded protein through multiple hydrophobic contacts (with typical nanomolar affinities [144]), to isolate it from the cytoplasm and to enable its aggregation-free folding for *ca.* 10 seconds (corresponding to the time necessary for the hydrolysis of the 7 ATP in the *cis* ring). The protein is then released in the milieu (and potentially recaptured if not yet correctly folded after the allowed 10 seconds). Most of the proteins taken in charge by the GroEL/GroES system have sizes comprised between 20 and 60 kDa and leave GroEL with half-lives ranging from 15 seconds to several minutes [145].

Energy-transfer between chaperonins and client proteins is debated. Mechanisms may involve i/ a passive regulation of the sequestration times and/or ii/ an active up-hill escort giving access to protein conformers of higher free energy levels. Speaking for point i/, the ATP-dependant hydrophilic/hydrophobic switch in the GroEL cavity has been shown to

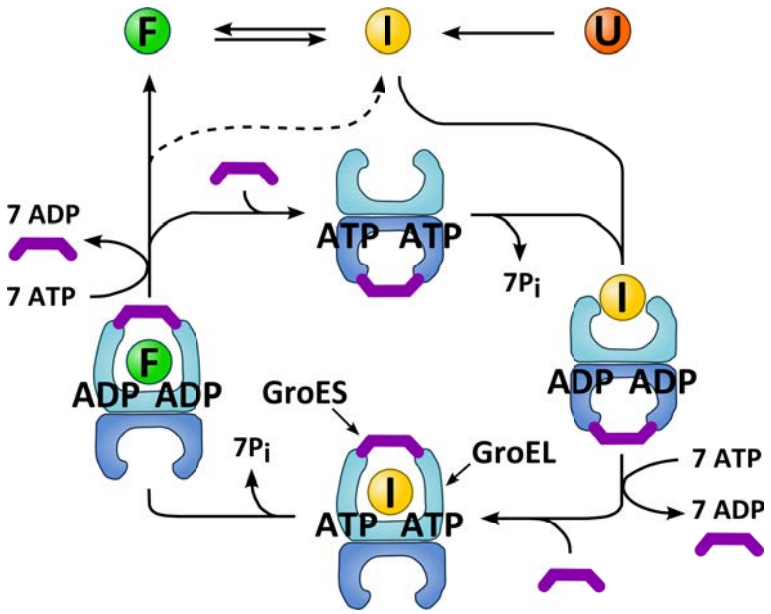


Figure 2.1: Working cycle of the GroEL/GroES chaperonin system. Misfolded proteins (denoted "I" for intermediates) are captured by multiple hydrophobic interactions with the *trans* region of the asymmetrical GroEL subunit, which is closely followed by the binding of 7 ATP molecules and the GroES co-chaperone unit. As a consequence, the substrate is displaced into the central ring cavity and causes the dissociation of 7 ADP molecules and of the GroES unit in the former *cis* region. Binding of GroES on top of the *trans* ring induces a massive rotation and upward movement of residues forming the GroEL unit, resulting in enlargement of the cavity and switch from its former hydrophobic inner surface to a hydrophilic one. The protein is allowed to fold for 10 s, after which the hydrolysis of the 7 ATP in ADP leads to the detachment of the GroES subunit and the release of the folded protein.

fasten the binding of client proteins (regulation of the *on* rate) and to alleviate rebinding of the released proteins with no significant effect on the *off* release rate. It is now recognized that the GroEL/GroES chaperonin also regulates refolding by changes in the size of the cavity, suggesting in line with point ii/ that stretching forces apply on the entrapped polypeptide [146] and that composition variation of the inner surface from hydrophobic to hydrophilic is coupled with conformation stabilisation [147]. Increasing number of studies report on active unfolding of kinetically-trapped intermediates (unfoldase activity) [146, 148] or on preventing their formation (smoothing of the folding energy landscape) [149]. In eukarya, the less-characterized TRiC complex seems to play a similar role.

2.2 *En route* to the design of artificial chaperones

2.2.1 Basic concept of an artificial chaperone

Controlling the *in vitro* aggregation propensity of proteins with purely synthetic tools is highly desirable: it would allow efficient *in vitro* refolding of recombinant proteins, with positive economic impacts for biotechnological and industrial applications, and would

also enable the preservation of stable monomeric therapeutic proteins upon long-term storage. Besides, in the context of the emergence of synthetic biology, the promising cell-free protein synthesis techniques could benefit from artificial chaperones to rescue misfolded proteins.

Molecular chaperones have inspired chemists to design artificial systems with similar properties, namely i/ prevention of aggregation of partly-folded/unfolded intermediates and ii/ destabilization of the misfolded structures so that kinetically-trapped intermediates can go back on productive folding routes.

In this biomimetic approach, artificially-designed chaperones should develop non-specific (meaning sequence-independent) interactions with misfolded or partly-folded proteins, so as to be able to accommodate a wide range of substrates just like their biological counterparts. They should also specifically associate with partly-structured intermediates while releasing the natively-folded state (reversible association). The design of an artificial chaperone should thereby encompass protection against protein aggregation and differential affinity for the partly-structured and folded proteins. In the following, some of the main systems developed in the literature either to assist protein folding from a chemically-denatured state or to prevent protein aggregation under an external denaturing condition (such as heat stress) are reviewed. Two kinds of strategies are adopted, namely improving colloidal stability or improving conformational stability. Strategies based on colloidal stability aim at increasing the solubility of protein intermediates; the ones seeking to affect the conformation of proteins generally aim at increased thermodynamic stability of the native state compared to unfolded/misfolded ones to limit unfolding under external stresses. In both cases, the underlying idea is to prevent protein aggregation by decreasing the concentration of free (unbound) aggregation-prone conformers in the solution (and then rely on spontaneous refolding upon releasing partially-unfolded structures).

2.2.2 Synthetic chaperones based on hydrophobic (self-)association

2.2.2.1 First attempts: spontaneous folding with surfactants, liposomes or dendrimers

The firsts refolding studies of globular proteins in the presence of aggregation-suppressors date back to the mid 1980s. Until then, dialysis of very dilute protein solutions was used conventionally to improve *in vivo* renaturation yields. Influenced by the well-characterized GroEL/GroES chaperonin system, Tandon and Horowitz proposed for the first time the use of surfactants above their critical micellar concentration (cmc) (already employed at that time to stabilize highly hydrophobic membrane proteins) to preserve the folding intermediates in a non-aggregated state [150, 151]. Association of partly-folded intermediates with micelles of surfactants was shown to dramatically improve the refolding yields, most-likely because of reduced aggregation resulting from the shielding of the exposed aggregation-prone hydrophobic residues at the surfaces of intermediate folding states (enhanced solubility of intermediate states) [152].

Based on similar principles, liposomes have been successfully used to assist protein refolding [152]. Membrane fluidity was reported as a the most important criterion for the chaperone-like activity of liposomes [153–155]. It has been proposed that dynamic motions of lipids and fluctuations of lipid density induce packing defects, resulting in local exposure of hydrophobic regions on the lipid membrane and binding of partly-folded protein intermediates [155, 156]. Interactions between intermediates and liposomes

were shown to be weakened upon rigidification of the lipid membrane by addition of cholesterol [157]. It has been hypothesized that membrane fluidity facilitates the folding of intermediates without blocking proteins in a misfolded state [156].

The surface charge density of liposomes is also as an important factor to modulate their interaction with partly-structured intermediates [155, 156]. Experimentally, when an adequate amount of negatively-charged lipids was added to lipid membranes, the renaturation of basic lysozyme was improved, which was attributed to the rapid sequestration of positively-charged lysozyme intermediates by negatively-charged liposomes at the early stage of refolding. An appropriate balance between hydrophobic and electrostatic interactions had to be found to efficiently prevent aggregation while allowing the protein to fold to its native structure without being trapped in misfolded states [155]. Practical developments of liposome-based renaturation have emerged: immobilization of liposomes in gel matrix and balancing hydrophobic and Coulomb interactions facilitate recovery of folded proteins by elution and spontaneous detachment in gel columns (immobilized liposome chromatography) [156, 158].

Dubey *et al.* reported improved renaturation yields of lipases and amylases in the presence of dendrons and dendrimers [159]. They showed that these additives shifted the thermal unfolding of proteins towards higher temperatures (stabilization of the folded state) and inhibited protein aggregation upon heating. By comparing the effect of charged or neutral (hydrophobic) dendrons/dendrimers, they found that the best performance was achieved with uncharged hydrophobic additives and with the dendrimer of the largest size tried, which was attributed to the need of multipoint hydrophobic associations with partly-folded conformers in order to get efficient protection.

In the systems presented so far, no active release step is envisioned. The protein is thought to passively detach from surfactants, liposomes or dendrimers once it has adopted its native structure. Accordingly, interactions between proteins and host additives have to be carefully adjusted in a way that the binding affinity decreases when the protein reaches its natively-folded structure, otherwise complete folding may not be achieved, especially in conditions of elevated concentrations of surfactants or charged lipids due to their denaturing properties.

2.2.2.2 The two-step strategy of Rozema and Gellman

To cope with the question of controlled release, Rozema and Gellman proposed to trigger the release of the folded protein by the sequential use of a solubilization agent (surfactant) and a competitor for association with this agent (cyclodextrin) (Figure 2.2) [160]. In the first capture step, unfolded proteins are trapped by host surfactants (at concentrations above or close to their critical micellar concentration), presumably under the form of hydrophobic assemblies. Sequestration by surfactants helps to maintain the misfolded structures in a non-aggregated state, but it generally disfavours the native conformation (surfactants act as denaturants). The next step (called stripping) is a gradual decrease of the activity of surfactant by addition of cyclodextrins that act as competitor guests and form complexes with surfactants. Proteins are thus detached from surfactants and gradually allowed to fold. The term "artificial chaperone" was first coined in 1995 to name this two-step strategy. It has been successfully used to assist refolding of various denaturant-unfolded proteins, such as carbonic bovine anhydrase or lysozyme [161–163].

From a practical point of view, a last step of purification is required to recover a cyclodextrin- and surfactant-free protein. This could be performed by extensive

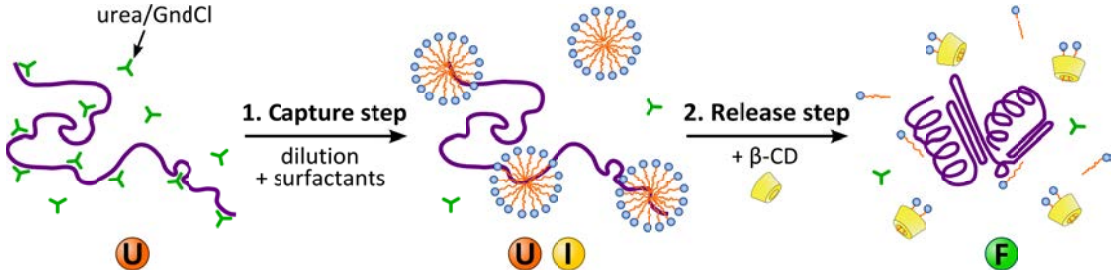


Figure 2.2: Artificial chaperone system developed by Rozema and Gellman [160]. i/ Capture step: upon dilution of the unfolded protein into a surfactant-containing renaturation buffer, the protein is maintained in a soluble state though hydrophobic association with surfactants. ii/ Release step: addition of β-cyclodextrin triggers the stripping of surfactants and the subsequent folding of the protein. U: unfolded, I: intermediate, F: folded.

dialysis. Another possibility is to immobilize β-CD on solid supports. Yazdanparast *et al.* developed an insoluble β-CD-rich copolymer acting as a refolding resin that allowed to reach *ca.* 75% of activity recovery using 5 mg of the copolymer per 0.0343 mg of CAB [164]. Separation of the β-CD/surfactants complexes from the refolded protein solution can also be achieved with CDs conjugated on magnetic nanoparticles [165], gathered by an external magnetic field, or by the use of CD-functionnalized polymer chains that are readily precipitated from aqueous solutions in mild conditions, *e.g.* thermo-responsive PNIPAM [166], that becomes insoluble at T > 32°C.

2.2.2.3 Polymer-based self-assembled nanogels

Inspired by the principle of artificial chaperone of Rozema and Gellman, Akiyoshi and co-workers took advantage of the use of cyclodextrin to modulate the hydrophobic self-association of amphiphilic polysaccharides that showed high affinity for partly-folded proteins under their self-assembled form (nanogels).

Hydrophobized pullulan nanogels

Akiyoshi and collaborators first developed cholesterol-functionnalized pullulans (CHP) that self-assemble in water to form nanogels of about 30 nm in diameter (the cholesterol groups associate into micro-domains that act as physical cross-linkers). CHP nanogels were shown to spontaneously trap heat-denatured [167–169], chemically-denatured [170, 171] or newborn proteins synthesized by cell-free synthesis [172, 173], most-likely through hydrogen bonds with the saccharide moieties [174].

Interestingly, most of the native proteins tested did not associate with the CHP nanogels, making the binding specific to partially-unfolded or unfolded proteins. In agreement with the tight binding of non-native conformers, association displaced the folding equilibrium toward unfolding: in aqueous solutions, the secondary structure of α-chymotrypsin [175] or bovine serum albumin [176] were shown to be altered upon complexation with cholesterol-functionnalized pullulan nanogels. The sequestered proteins were protected against intermolecular contacts in a partly-unfolded state.

The release and folding of proteins is triggered by the addition of an excess of cyclodextrins that causes the dissociation of the nanogels due to competitive complexation

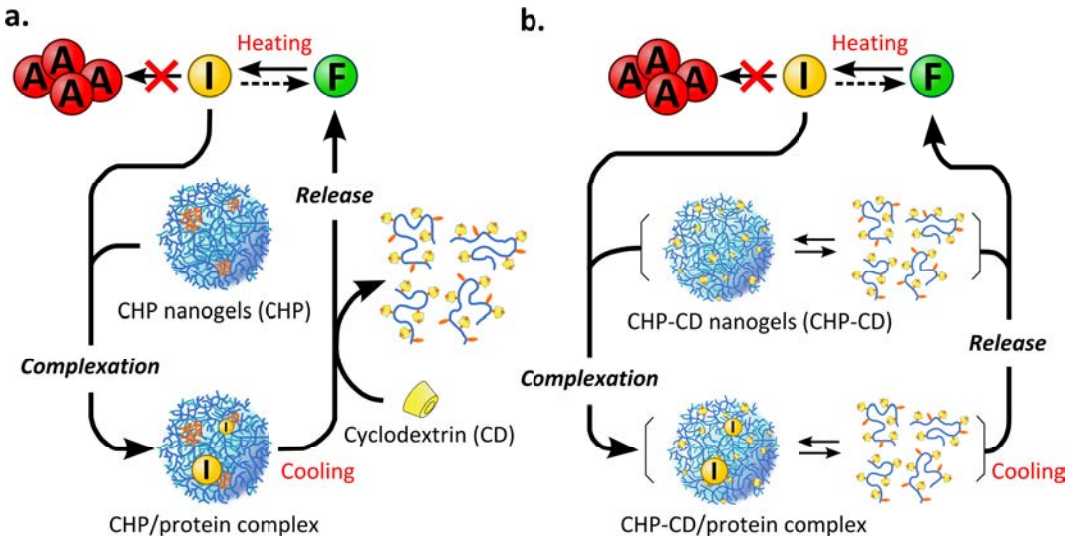


Figure 2.3: Hydrophobically-modified pullulan nanogels developed by Akiyoshi and coll. a. Two-step system: unfolded proteins are first captured by cholesterol-functionnalized pullulan nanogels, then the addition of cyclodextrin disrupts the nanogel 3D structure, which triggers the release of the folded protein. b. One-step system: A mixture of pullulan nanogels and cyclodextrin is used to modulate the hydrophobic (self-)association of pullulans and binding of (unfolded) proteins. It also ensures the spontaneous release of folded proteins. Adapted from [168].

of the cholesterol moieties (as schematically depicted on Figure 2.3a). Refolding efficiency of acid-denatured GFP were increased by *ca.* 15% compared to spontaneous refolding, a value that was comparable to that obtained with the natural GroEL/GroES system [171]. The sequential capture and release of proteins, which is technically not without difficulties (addition/withdrawal of cyclodextrin), could also be converted into a one-pot system by directly using an appropriate mixture of CHP nanogels and cyclodextrins (see Figure 2.3b). However, the dynamic equilibrium between the structured nanogels and the flexible free polymer chains led to a substantially lower refolding efficiency than the two-step system [168].

Enzymatically synthesized glycogen nanogel

Another system developed by Akiyoshi and co-workers involves the use of enzymatically synthesized glycogen (ESG), a monodisperse spherical hyperbranched nanoparticle. Grafting of cholesterol groups on ESG led to self-assembly into nanogels of *ca.* 35 nm in diameter, containing a few cholesterol group-bearing ESG (CHESG) molecules [177].

The sequential addition to protein solutions of CHESG nanogels and cyclodextrins was shown to be efficient in protecting heat-denatured proteins against aggregation and allowed them to refold to their native structure (upon cooling). Interestingly, the simultaneous use of the two additives showed similar efficiency, presumably because the three-dimensional structure of the ESG particles was retained, even if the nanogel was disrupted. A single ESG particle provided a suitable confined space to accommodate denatured proteins (see Figure 2.4).

By using an appropriate ratio of the two additives, it is possible to control the

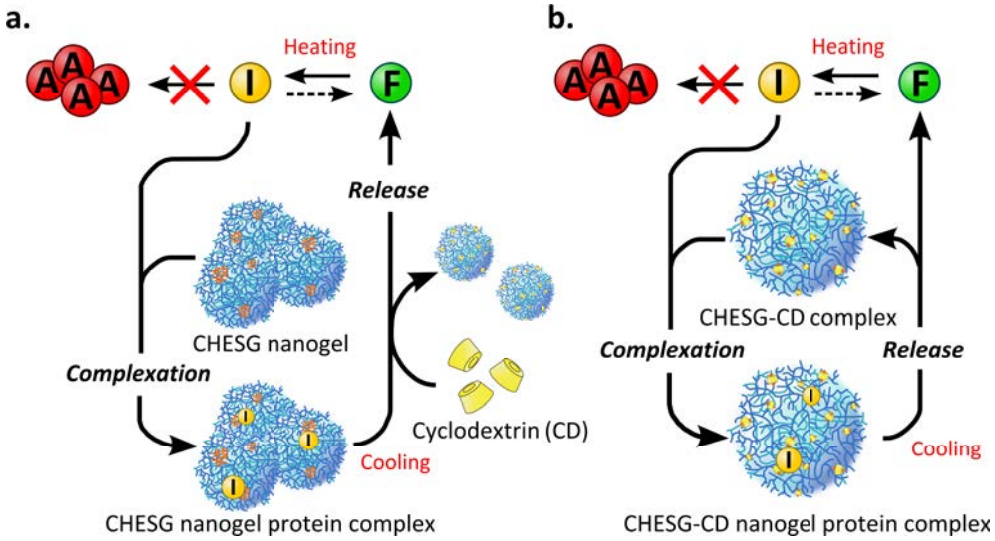


Figure 2.4: Hydrophobically-modified enzymatically synthesized glycogen (ESG) developed by Akiyoshi and coll. a. Two-step system: unfolded proteins are first entrapped in cholesterol-bearing ESG nanogels (CHESG), then the addition of cyclodextrin (CD) disrupts the hydrophobic associations, which releases the folded proteins. b. One-step system: a mixture of CHESG and CD is used to assist protein refolding; the nanogel assembly is disrupted but the ESG building block retains its 3D structure and is able to efficiently entrap heat-unfolded proteins and release them upon cooling. Adapted from [177].

binding affinity for a given protein, depending on the structure of the latter (partly-folded or folded). This balance is required to achieve sequestration of the partly-folded intermediates but still allow the release of the native protein.

Photo-responsive nanogels

Akiyioshi and collaborators also developed photo-responsive nanogels composed of self-assembled spiropyrane-bearing pullulan chains [178]. Spiropyrane groups were used as (hydrophobic) "stickers" driving the self-assembly of polymer chains instead of cholesteryl groups. Under exposure to UV light, spiropyrane undergo a photo-induced isomerization into the hydrophylic/charged merocyanine form. The authors showed that decreasing the hydrophobicity of the nanogels by photoisomerization resulted in the release of citrate synthase (CS). This is the first report that exploits photo-responsive polymer-based systems to photo-release entrapped proteins.

2.2.2.4 Thermo-responsive polymer systems

In water, thermo-responsive polymers undergo a reversible transition, above a lower critical solution temperature (LCST), from a soluble coil conformation to a less hydrated, collapsed state that exhibits increased hydrophobicity. In this regard, increasing the temperature above the LCST changes markedly the polymer hydrophobic/hydrophilic balance, which may be beneficial to design synthetic chaperones with adjustable affinity for proteins. Triggering the hydrophobicity of polymers by external additive-free stimulus, such as temperature, enables to cycle a sample between conditions of high (protein

capture) and low (protein release) affinities, which is difficult to achieve with molecular competitor guests. Another advantage of thermo-responsive polymers is the possibility to precipitate them out from the refolded protein solution by gentle heating of the mixture above the LCST while remaining below the protein's denaturation temperature.

Poly(*N*-isopropylacrylamide)

Poly(*N*-isopropylacrylamide) (PNIPAM) has been extensively studied for its thermo-responsive behaviour. Its LCST of about 32°C is close to the temperature of the human body, which makes it a promising polymer for drug delivery or tissue engineering applications. PNIPAM has been used to help refolding of chemically-denatured proteins. Below its LCST, PNIPAM was shown to bind to partly-folded intermediates of β-lactamase [179], carbonic anhydrase [180] and lysozyme [181, 182], presumably via hydrophobic interaction (and possibly hydrogen bonds), thus preventing aggregation. Lu *et. al.* showed in addition that the refolding yield of lysozyme and CAB could be enhanced in the presence of PNIPAM by using a temperature sweep, starting above the polymer critical temperature and ending below (see the case of CAB on Figure 2.5) [183]. The gradual/controlled decrease of polymer association with partially folded intermediates (formed upon dilution in water of urea-unfolded proteins) was suggested by light scattering size measurements, and eventually yielded a high degree of renaturation [183]. Dynamic simulation confirmed that decreasing the polymer hydrophobicity during the folding process could result in an optimized free-energy landscape that enhances both the folding yield and kinetics [184].

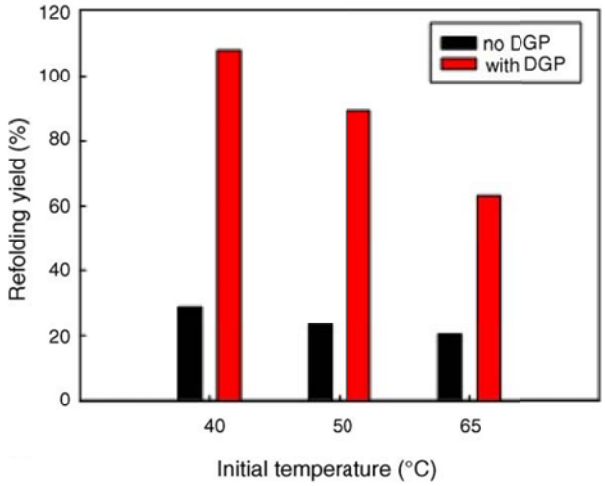


Figure 2.5: Protein refolding in a temperature sweep in the presence of a thermo-sensitive polymer. Refolding is performed by the quick dilution of denatured CAB in the refolding buffer with and without dextran-grafted PNIPAM (DGP). The temperature of the refolding system decreased linearly from the initial temperature (40, 50, 65°C) to 10°C in 30 min. After incubation for 24 h at 10°C, the activity of protein was measured. The initial CAB concentration was 6 mg.mL^{-1}. The final protein concentration was 1 mg.mL^{-1}. From [183].

The molecular weight of PNIPAM has a significant influence on polymer-assisted refolding (of lysozyme from the urea-denatured state) [181]: high molecular weight PNIPAM (47,000 g.mol^{-1}) was shown to sequester partly-folded/misfolded intermediates with poor release of the folded structure, while low molecular weight PNIPAM (4,000

g.mol^{-1}) did not prevent protein-protein hydrophobic association (aggregation). An optimal chain length (18,000 g.mol^{-1}) allowed high renaturation yield. Polydispersity is thus an issue for application. Because of the sensitivity to chain length, the use of conventional macromolecular synthesis (yielding polydisperse linear or cross-linked PNIPAM chains) may imply several pitfalls: for instance, poor control over the chain length leading to fluctuations of activity recovery due to earlier formation of polymer aggregates with longer polymers or chain-length-dependent slow kinetics of swelling/deswelling of cross-linked architectures. To avoid these problems, Ge *et al.* developed well-defined hairy particles consisting of a PNIPAM brush grafted on a polystyrene core (by using the "grafting from" approach to obtain elevated chain densities) [185]. Particles with a thick brush layer were good refolding enhancers, although the refolding kinetics was slowed down compared to refolding in the absence of particles. The particles could be removed easily by heating and centrifugation after refolding. Another mean to put LCST polymers into practical systems is proposed by Cui *et al.* who developed millimetre-sized particles of cross-linked PNIPAM hydrogel with tailored porosity (to entrap unfolded bovine prethrombin-2 via hydrophobic association and allow slow recovery of the native protein) [186].

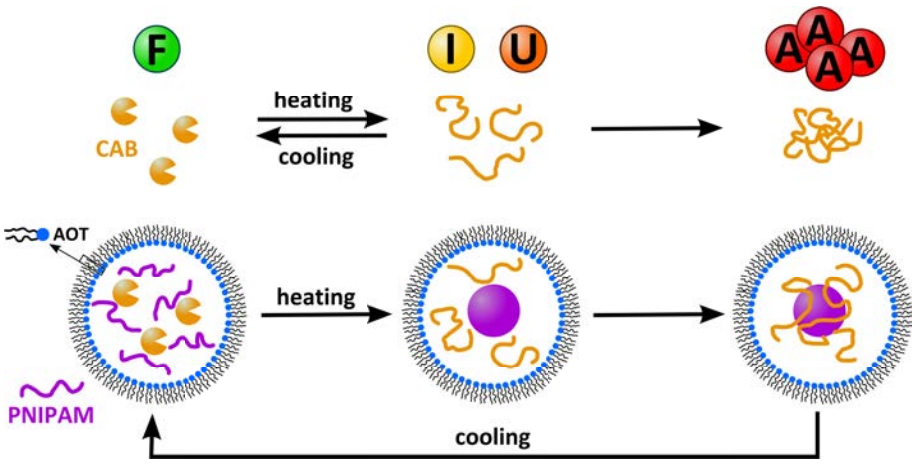


Figure 2.6: Schematic illustration of protecting CAB against heat inactivation by PNIPAM in microemulsion developed by Tao *et al.* (F: folded, I: intermediates, U: unfolded, A: aggregate, AOT: dioctylsulfosuccinate). Adapted from [187].

Formation of large insoluble PNIPAM aggregates in bulk aqueous solution limits its ability to assist protein refolding, as illustrated in Figure 2.7. Tao *et al.* showed that diblock copolymers of PNIPAM and hydrophilic polymers, such as poly(ethylene glycol) (PEG), also appeared hardly effective in preventing thermally-induced CAB aggregation, because the hydrophobic NIPAM segments were sequestered in the core of PEG-decorated micelles upon heating and were not accessible to partly-unfolded intermediates (see Figure 2.7) [187]. The authors thus suggested to confine CAB and PNIPAM chains into a reverse microemulsion to avoid the formation of large aggregates of PNIPAM (Figure 2.6 and 2.7). In confined droplets, CAB was hypothesized to adsorb onto the nanometre-sized PNIPAM aggregates that were formed, with both high specific surface and high hydrophobicity, which led to a strong increase of renaturation yield.

Following the same goal to avoid formation of large polymer aggregates, Shi and collaborators recently designed mixed shell polymeric micelles with a poly(lactide) (PLA)

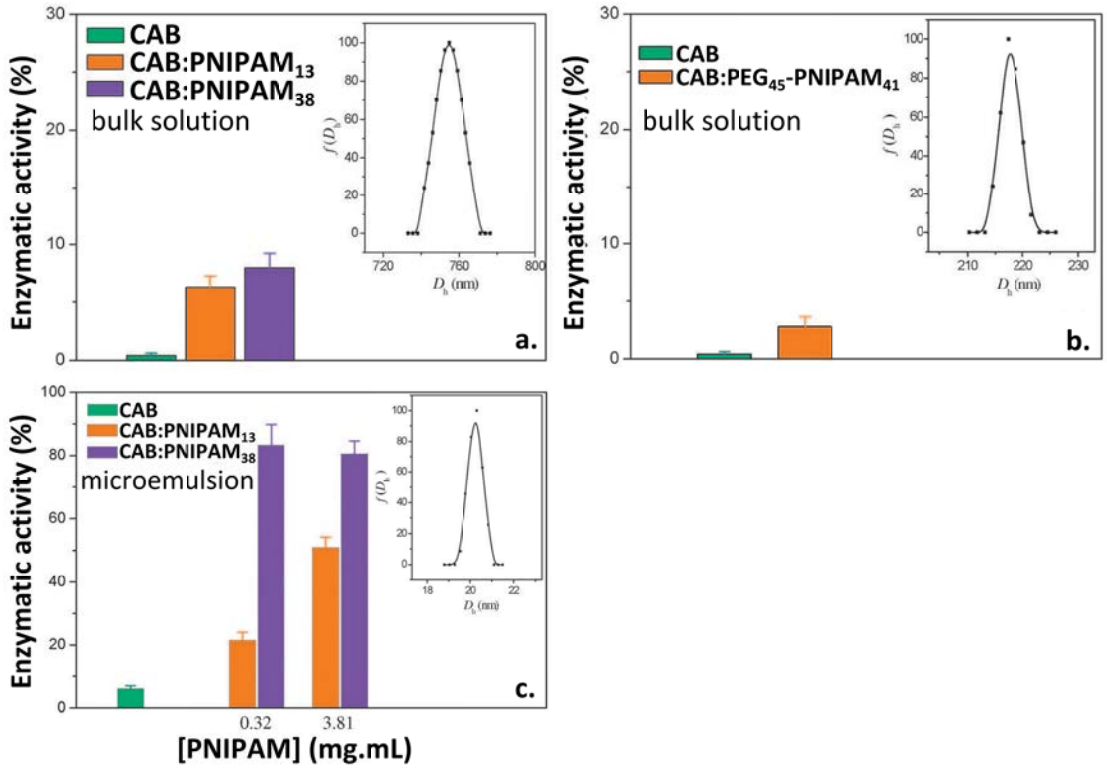


Figure 2.7: Comparison of CAB activity recovery in the presence of PNIPAM or PNIPAM-PEG copolymer in bulk solution or PNIPAM confined in microemulsion droplets. a. Residual enzymatic activity of free CAB and CAB with PNIPAM in phosphate buffer saline (PBS) after heat treatment. The concentration of CAB was 0.016 mg.mL^{-1} and those of $PNIPAM_{13}$ and $PNIPAM_{38}$ were both 0.32 mg.mL^{-1}. The inset shows the hydrodynamic diameter distributions of $PNIPAM_{38}$ aggregates formed in PBS at 70°C. b. Residual enzymatic activity of free CAB and CAB with PEG_{45}-*b*-$PNIPAM_{41}$ in PBS after heat treatment. The concentrations of CAB and PEG_{45}-*b*-$PNIPAM_{41}$ were 0.016 and 0.51 mg.mL^{-1}, respectively. The inset shows hydrodynamic diameter distributions of PEG_{45}-*b*-$PNIPAM_{41}$ micelles formed in PBS at 70°C. c. Residual enzymatic activity of CAB and CAB with PNIPAM in a microemulsion after heat treatment. The concentration of CAB was 0.016 mg.mL^{-1}. The inset shows the hydrodynamic diameter distributions of $PNIPAM_{13}$ in the microemulsion droplets ($[PNIPAM_{13}]$ = 3.81 mg.mL^{-1}) at 70°C. From [187].

core and a shell composed of both PEG and PNIPAM chains (see Figure 2.8) [188]. Increasing the temperature above the LCST of PNIPAM resulted in the collapse of the PNIPAM chains, while extended PEG chains still ensured the solubility of the micelles ("patchy" particle). Heat-unfolded CAB was shown by dynamic light scattering and transmission electron microscopy to be sequestered by hydrophobic patches of collapsed PNIPAM and could be reversibly released and refolded upon cooling. An ideal PEG:PNIPAM weight ratio of 1:6 was needed to prevent polymeric micelles from self-aggregating upon heating while ensuring proper capture of CAB intermediates. Moreover, the higher the concentration of micelles in the mixture, the higher the recovered enzyme activity during the refolding procedure (up to a micelle:protein weight ratio of 10:1).

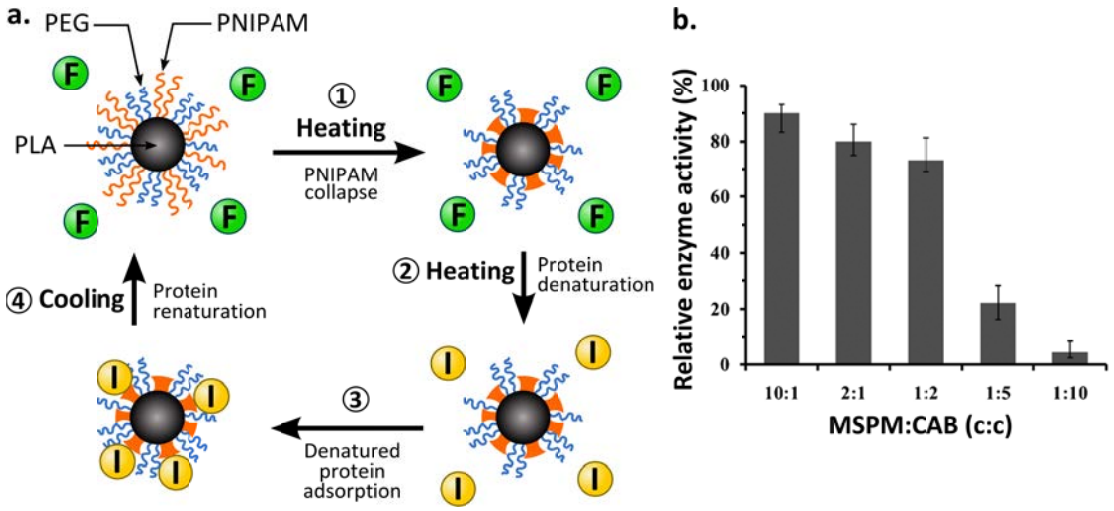


Figure 2.8: Stabilization and refolding of the heat-denatured proteins assisted by thermo-responsive mixed shell polymeric micelles (MSPMs). a. Schematic illustration of the protection mechanism (F: folded, I: intermediate, A: aggregate). b. Influence of the concentration of the MSPMs on the enzymatic activity recovery of thermally denatured CAB (17 μg.mL^{-1}). Adapted from [188].

Poly(ethylene glycol) and poly(propylene glycol)

PEG is an hydrophilic polymer that has also been used to assist protein-refolding. For instance, Wang and co-workers showed that PEG could enhance the activity recovery of CAB by binding to the molten globule intermediate – a state showing ordered secondary structures altogether with exposed hydrophobic surfaces –, hence preventing self-association and aggregation [189–191]. Influence of parameters such as PEG concentration and molecular weight was investigated: while short PEG oligomers ($M_W <$ 600 g.mol^{-1} did not prevent CAB aggregation during refolding, longer PEG chains (typically 600 g.mol^{-1} $< M_W <$ 8,000 g.mol^{-1}) ensured almost complete activity recovery at polymer:protein molar ratio as low as 2 mol/mol.

PPO-PEG thermo-responsive diblock copolymers were shown to increase CAB activity recovery and decrease protein aggregation during refolding from GndCl-unfolded CAB at temperatures where the copolymer chains form hydrophobic assemblies with diameters of a few nm [192, 193]. The chaperone-like activity could be modulated (up to 100% activity recovery after refolding) depending on the chain length of the less polar PPO block, as well as the polymer concentration and the temperature.

PEG was also used to prevent thermally-induced lysozyme aggregation: Tomita *et al.* showed that high concentrations of short PEG chains (M_W = 1,000 g.mol^{-1}, ∼100 mg.mL^{-1}) inhibited intermolecular collisions of thermally-unfolded proteins, which resulted in the inhibition of disulfide exchange and therefore of irreversible protein aggregation [194].

Kinbara and co-workers recently showed that the topology of PEG was an important parameter to get efficient inhibition of protein aggregation upon thermal stress [195, 196]. When aqueous solutions of lysozyme were heated to 90°C in the presence of structured, cyclic PEG (added at a weight ratio of 10 to 50), protein aggregation was not detected to the naked eye (in the presence of the same amount of linear PEG, macroscopic

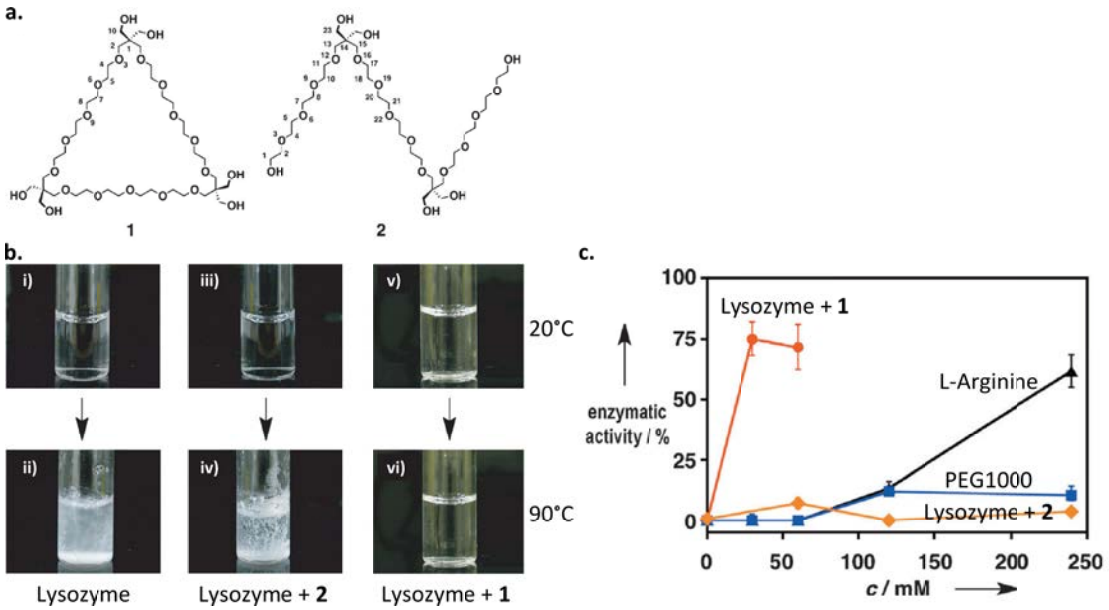


Figure 2.9: Suppression of protein aggregation by cyclic PEG developed by Kinbara and coll. [195]. a. Molecular structures of structured monodisperse PEGs **1** and **2**. b. Photographs of lysozyme in PBS (3.0 mg.mL^{-1}) at 20°C (top) and 90°C (bottom). i) and ii) no additive, iii) and iv) with **2** (30 mg.mL^{-1}), and v) and vi) with **1** (30 mg.mL^{-1}). c. Enzymatic activity of lysozyme (3.0 mg.mL^{-1} = 0.21 mM) after heating (98°C, 30 min) with different concentrations of additives, as indicated.

aggregates formed in solutions, see Figure 2.9b). Strikingly, millimolar concentration of cyclic PEG was enough to obtain *ca.* 80% of lysozyme enzymatic activity recovery after cooling down to room temperature, instead of about 0-5% activity recovery when linear PEG was used (Figure 2.9c). The peculiar efficiency of cyclic PEG was ascribed to the *gauche*-to-*anti* conformational change of the ethylene oxide units upon heating above 60°C. A similar transition occurs in linear PEG, but at a temperature markedly higher (> 80°C). This transition decreases the polarity inside the polymer ring, compared to the room temperature "all-*gauche*" conformation, which is hypothesized to trigger hydrophobic association of cyclic PEG with partially unfolded lysozyme. The formation of complexes was shown to stabilize ordered secondary structures in the heated protein solutions, which was conjectured to be at the origin of the prevention of aggregation. For cyclic PEG to be an efficient aggregation suppressor, the denaturation temperature of the protein had to be above the dehydration temperature of the polymer [196].

Nanoparticles of hydrophobized poly(vinyl alcohol)

Cavalieri *et al.* developed nanoparticles of hydrophobically-modified poly(vinyl alcohol) (PVA) that exhibited a chaperone-like activity for heat-denatured CAB. Upon heating, the unfolded protein was captured by thermally exposed hydrophobic domains on the surface of the nanoparticles, which prevented aggregation of protein intermediates (see Figure 2.10). Upon cooling, the affinity of the nanoparticles for the protein decreased, which should have led to the spontaneous release of the folded protein. However, addition of β-cyclodextrin was still necessary here to complex methacryloyl groups of PVA and trigger the release of native proteins.

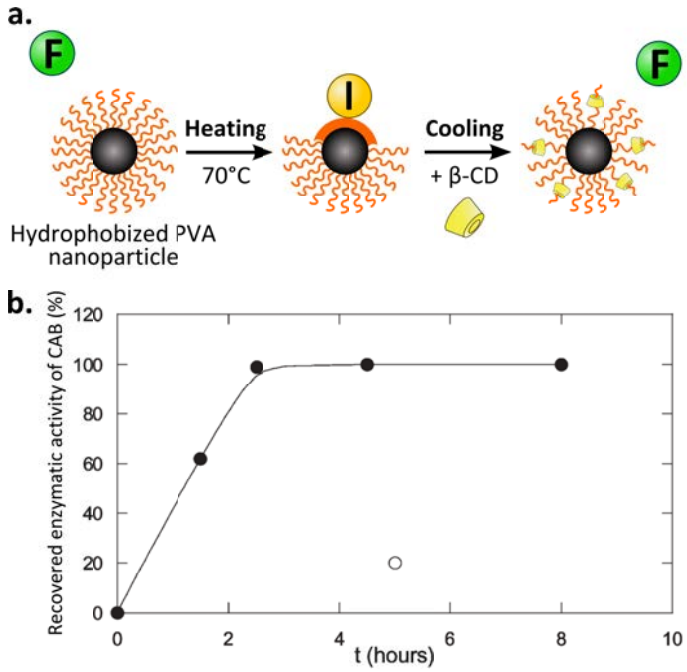


Figure 2.10: Nanoparticles of hydrophobized poly(vinyl alcohol) to suppress heat-induced protein aggregation. a. Mechanism of nanoparticle-induced refolding of CAB (F: folded, I: intermediates). b. Recovery of enzyme activity of complexed CAB in the presence of (full symbols) or without (empty symbols) β-CD. [CAB] = 2 mM; [hydrophobized-PVA] = 0.06 mg.ml^{-1}. Adapted from [197].

2.2.3 Electrostatic-mediated aggregation-suppression and protein refolding

Recent experiments ruled out the supremacy of hydrophobic association in the protection of proteins against aggregation. Electrostatic interactions are shown in a few studies to be highly efficient in assisting protein refolding, which finally points to the major importance of protein immobilization independently of the physical origin of the (non-covalent) attachment to "aggregation suppressor" systems.

2.2.3.1 Immobilization at the surface of charged particles

Inspired by the two-step protein folding strategy developed by Rozema and Gellman, Rotello and collaborators proposed to capture partly-folded intermediates by electrostatic interaction with charged residues [198]. They successfully designed negatively-charged, functionnalized gold nanoparticles that were shown to be efficient hosts for refolding intermediates of basic proteins (pI above 8.5) at low ionic strength (5 mM phosphate buffer pH 7.4).

Functionnalization of nanoparticles allowed to control the surface charge density, with typical zeta potentials of –45 mV. Electrostatic interactions with the positively-charged residues of basic proteins ensure sequestration and immobilization, preventing deleterious hydrophobic interprotein interactions. The partially-refolded proteins adsorbed on the nanoparticles can be gradually released from the host (and then allowed to refold) by shielding electrostatic attractions via the increase of the ionic strength of the solution

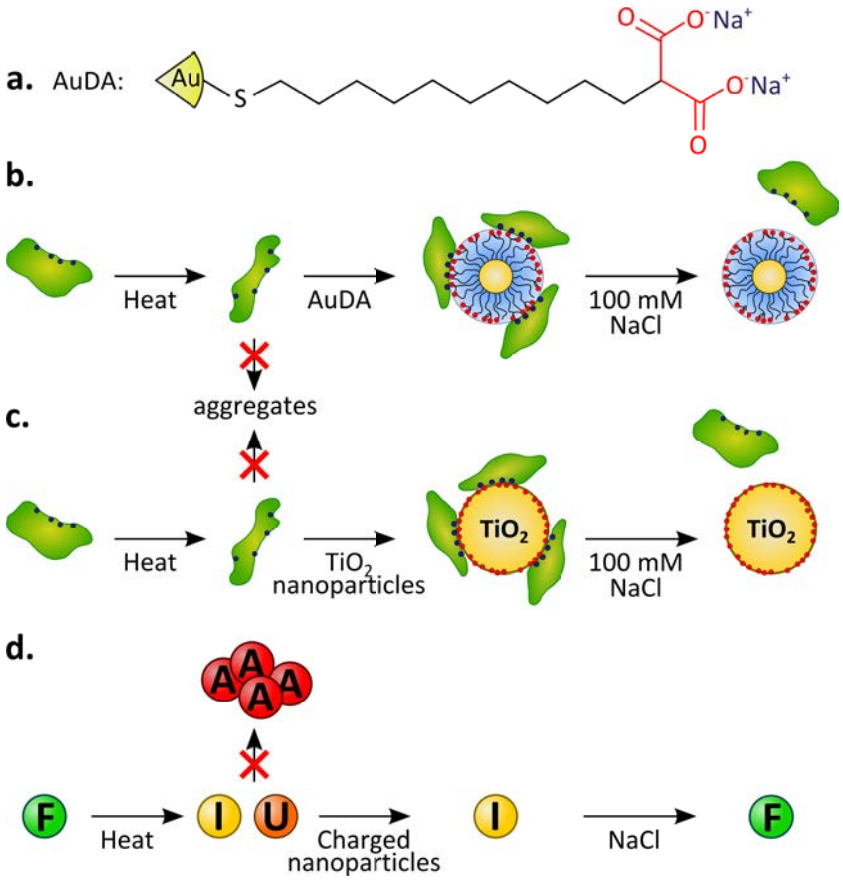


Figure 2.11: Protein refolding assisted by negatively-charged nanoparticles. a. Schematic representation of the structure of the AuDA (2 nm gold core functionnalized by 2-(10-mercaptodecyl)malonic acid)). b. Thermal denaturation followed by nanoparticle-mediated refolding of proteins adapted from Rotello and coll. [198]. The red dots on the particle represent negative charges whereas the blue dots on the protein represent positive charges. c. TiO_2 nanoparticles as synthetic chaperones, adapted from [199]. d. Schematic illustration of the state of the protein during heat-treatment and refolding in the presence of negatively-charged nanoparticles (F: folded, I: intermediates, U: unfolded).

(Figure 2.11, 100% activity recovery compared to the initial non-denatured sample). This is one of the first study on an artificial chaperone that is predominantly based on controlled electrostatic interactions with proteins.

The work by Rotello and colleagues was extended to unmodified titanium dioxide nanoparticles by Raghava *et al.* of similar zeta potential (about –36 mV) [199]. These 60 nm-diameter, negatively-charged nanoparticles were shown to behave like the functionnalized gold particles and bind electrostatically to α-chymotrypsin, papain or RNase. All these model enzymes have a pI above 7.0, so they were positively-charged at the working pH of 7.4. This resulted in adsorption of the enzymes (characterized by the decrease of the zeta potential to –17 mV, altogether with the progressive increase of the size of the objects up to a plateau at *ca.* 450 nm of diameter in the case of α-chymotrypsin). Addition of salt to increase the ionic strength was used as the stripping step (Figure 2.11) and led to activity recoveries close to 100%. Interestingly, the secondary structure of

proteins bound to the particles was hardly different after heat-treatment from that of the native state (it depended on the protein), and the activity of the bound proteins remained about 75%, therefore suggesting that preservation of the native folding of surface-bound proteins is possible. Strikingly, binding of acidic proteins (pI < 7.0), such as GFP (pI ~ 5.0) or lipase (pI ~ 6.0), to TiO_2 nanoparticles was not possible, confirming the importance of electrostatic interactions. Such proteins hence aggregated when subjected to thermal treatment and activity could not be recovered.

2.2.3.2 Protein refolding in confined, charged nanospaces

Inorganic mesoporous materials

Zeolites (nanoporous materials with channel sizes of 0.3-3 nm) and mesoporous materials (with pore sizes ranging from 2 to 50 nm) were shown to be able to entrap unfolded proteins and assist refolding upon controlled release in the buffered solution [200–202]. Mesoporous channels in particular can be easily tailored to accommodate individual denaturant-unfolded proteins thereby preventing deleterious intermolecular contacts during refolding.

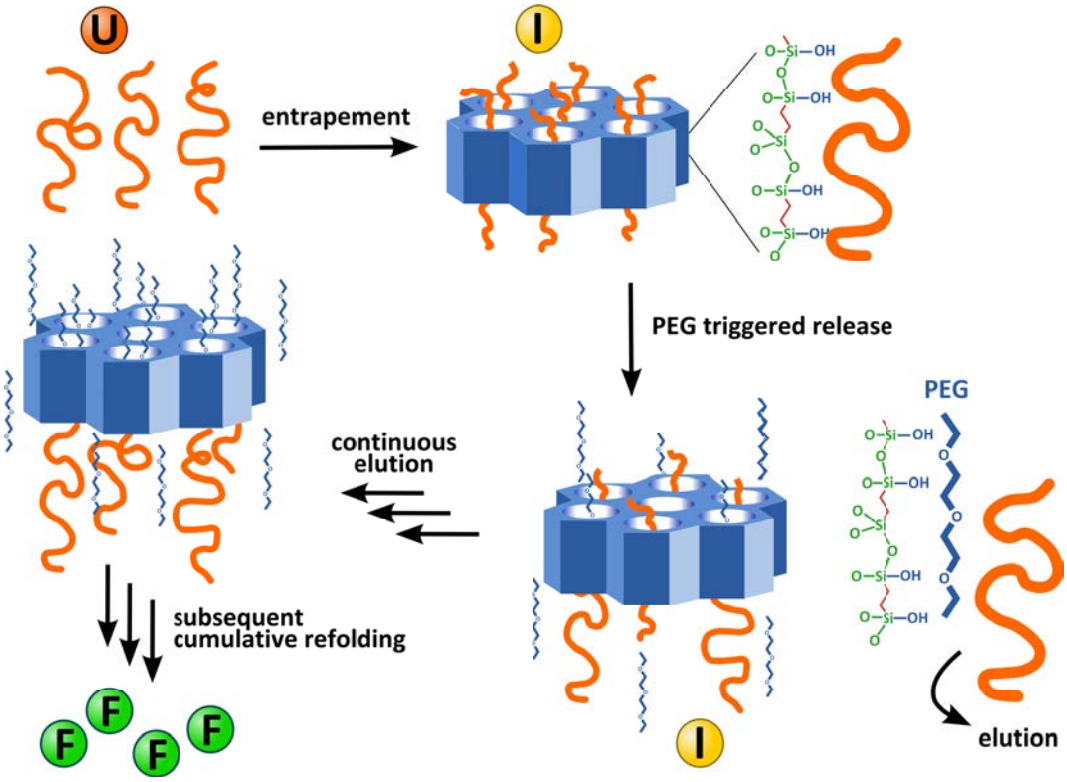


Figure 2.12: Protein refolding assisted by periodic mesoporous organosilicas. Adapted from [200].

In the work reported by Wang *at al.* [200], lysozyme was entrapped in mesoporous materials through electrostatic interactions between its positively-charged residues and the negatively-charged silica-based surface of the mesoporous channels, in conjunction with hydrophobic association between ethylene groups present in the pores and exposed hydrophobic surfaces of the protein (capture step, see Figure 2.12). Upon addition of an

excess of polyethylene glycol (PEG) of appropriate molecular weight as competitor guest, the proteins could be gradually released and fold to their native state.

It is known that native protein are prone to adsorb on silica-based surfaces, including mesoporous ones [203], where they generally undergo irreversible structural changes. In the work of Wang *et al.*, the surface charge density of the mesoporous material had to be finely tailored in order to ensure proper release of the adsorbed unfolded lysozyme, as well as to limit adsorption of the refolded protein. In particular, highly charged pure siliceous mesoporous channels did not allow the release of lysozyme, presumably because of the strong electrostatic surface interaction they can develop. The periodic mesoporous organosilicas developed by Wang *et al.* exhibited a lower density of silanol groups on the surface due to the presence of organic groups. Even then, protein recovery only reached ∼20%, most-likely because the release of adsorbed proteins was not efficient. Similarly, in the case of zeolites, surfactants were necessary, in conjunction to PEG, to disrupt the strong associations between proteins and the surface of the material (to reach ∼30% release) [201].

Self-assembled nanotube hydrogels

Other examples of refolding in confined nanospaces include the work of Kameta and collaborators [204], in which they exploited the self-assembly of rationally designed amphiphilic monomers to entrap unfolded proteins in nanometer-sized channels. The encapsulation was primarily based on electrostatic interactions between positively-charged moieties in the inner surface of nanotubes and negatively-charged residues on unfolded proteins, with enhanced loading when hydrophobic groups were added on the inner surface of the pores.

As for mesoporous materials, confinement prevented aggregation and provided additionally a higher conformational stability to encapsulated native proteins against heat- or denaturant-induced unfolding [204]. The release step and thereby refolding of proteins was here achieved by slight increase of the pH that altered the surface charges of the nanotubes and allowed the recovery of up to 71% of proteins.

2.2.4 Conclusions

A large variety of systems is finally reported to share characteristic features of artificial chaperones. Behind their apparent heterogeneous design, a few common principles emerge as the minimal requisites. Protection of proteins, which basically comes down to prevention of aggregation under stressful conditions, is achieved upon interaction with any colloidal object (particles, polymer coils or gels, assemblies of amphiphilic molecules) provided that:

- non-covalent interactions allow the capture or immobilization of the protein of interest, that may be under the form of unfolded or partly-folded conformers,
- controlled release is occurring over an appropriate time lapse, which maintains a low concentration of free (unbound) unstable intermediates in the solution, while allowing the refolding of freshly released protein chains.

Prevalence of hydrophobic association shall thus be questioned. The need for providing an hydrophobic interface to non-polar residues exposed to contact with water appears vastly overrated, even though amphiphilic colloids are quite successful protective agents. Up to now, most of the studies have relied on hydrophobic (self-)associations to assist protein refolding. The few reported cases that were predominantly based on electrostatic-mediated interactions with chaperones required a fine control over the charge density

(presumably to escape irreversible adsorption on charged surfaces). But this suggests that sequestration/release schemes in/on host additives is the true objective, regardless of details about the nature of interactions.

The capture and release can be controlled by external parameters (competitive associations, variation of environmental conditions such as pH, T, ionic strength) or can occur spontaneously from dynamic equilibrium between free and bound partners. The latter (stripping-free) case involves highly dynamic (transient) complexation with conformers of the protein that are unstable if they are not complexed. The affinity of artificial chaperones and life-time of complexes with unstable protein conformers are thus key issues. Interestingly, the physico-chemical properties of polyelectrolytes can be easily tailored (by synthesis of copolymers) to achieve optimal attractive/repulsive balance with a target protein, and control inter-complexes repulsions (*e.g.* coulombic repulsions preventing aggregation) while allowing dissociation of the thermodynamically stable native structure. Polyelectrolyte-based systems may thus advantageously combine all of the features of artificial chaperones, namely confinement, immobilization and enhanced protein solubility, providing that relationships are established between polymer:protein association and the architecture or composition of polymer chains.

2.3 Amphiphilic polyelectrolyte as promising artificial chaperones: protein binding, influence on conformational stability and on aggregation of proteins

A polyelectrolyte is defined as any macromolecule that carries a non-zero fraction of ionizable monomers. As discussed hereafter, the binding affinity of hydrophobically-modified polyelectrolytes for proteins and the resulting structures can be easily adjusted through modulation of the charge density along the backbone, the ratio of hydrophilic and hydrophobic moieties, as well as their nature, or the length of the polymer chains. The design of polyelectrolytes to that purpose has however not attracted much attention. But since the pioneering studies of Morawetz and Hugues [205], a large body of literature has reported on association between native globular proteins and polyelectrolytes (or hydrophobically-modified polyelectrolytes) in water, from which we extracted in this section the results shedding some light on the relevant parameters affecting protein binding and folding/unfolding equilibrium.

2.3.1 Interactions between native proteins and (amphiphilic) polyelectrolytes: driving forces

A wide range of experimental techniques has been used to characterize complexes between proteins and polyelectrolytes (reviewed in [206, 207]). Complexation was found to be dependent on the charge density and degree of ionization of the polymer chain [208–212] and on its hydrophobicity [211, 213–216], the degree of polymerization [217], the chain stiffness [210, 218, 219], the composition of the mixture, the isoelectric point of the protein and its charge anisotropy [220, 221] as well as the pH and ionic strength of the solution [206, 219, 222–230] (that respectively modulate the protein surface charge and the range of electrostatic interactions). In many cases, the detailed insight into the molecular recognition is not available, even though it is now recognized that both the hydrophobicity and the electric charge of the two partners are the most important parameters for their association [231]. These interactions are briefly discussed here. The

reader is referred to several reviews for detailed data on protein:amphiphilic polyelectrolyte complexes [206, 207, 219, 222, 223, 231, 232].

2.3.1.1 Coulomb interaction and entropy of the counterions

The solvent-accessible surface of native globular proteins is mostly polar and exhibits both positive and negative charges. For most, if not all, proteins, the charges are not distributed at random over the surface, but constitute patches of unlike-charges. If the size and charge density of these patches are high enough, the counterions will be localized in the vicinity of the patches (a quantitative analysis can be found in [222]). At low salt regime, where the local concentration of counterions bound to the charged patches is higher than the salt concentration in bulk, polyelectrolytes are strongly attracted onto patches of charge opposite to their own charge. Coulomb association with a polyelectrolyte chain releases the confined monovalent counterions in the bulk solution, which corresponds to an increase of the entropy of the system (see Figure 2.13) [222, 233]. In this process, the configurational and translational entropy loss for the confined segments of the polymer chain is negligible when sufficiently long polymer chains are used [234]. Examples of endothermic complexation are reported (see Figure 2.13) [233, 235], confirming that the net entropy gain constitutes the driving force of association. The counterion release effect is more marked if dense brushes or nanogels of polyelectrolytes are used instead of linear chains [236]. In this case, owing to the high local concentration of polymer chains, the polymer counterions are also condensed inside the brushes or gels. Binding to a protein thereby results in the release of counterions from both the polymer and the protein, which strongly drives the complex formation [233].

Experimental studies, as well as theoretical models, show that complexation of proteins by polyelectrolytes can also occur on the "wrong side" of the isoelectric point, namely when the net charge of the protein and that of the polyelectrolyte are of same sign [219, 220, 223, 225]. Two theoretical frameworks have been used to explain this phenomenon: i/ at extremely low salt concentration regime, the polyelectrolyte:protein attractive interactions are dominated by the charge regulation mechanism [237–240], namely the property of a protein to modulate its surface charge as it approaches a charged object [241]; ii/ at moderate and high ionic strengths, the "charge patch" mechanism prevails [206, 207, 225], *i.e.* protein anisotropy may lead to the existence of surface patches having a charge opposite to the protein's net charge. If the charge density of these patches is high enough, long-range ion-ion repulsion can be overcome by ion-dipole and tight local Coulomb attractive interactions.

Electrostatic-based complexation between proteins and polyelectrolytes usually results in cooperatively-formed soluble species composed of several polymer chains and several proteins (or protein oligomers, see Figure 2.14). Their radius depends on pH, ionic strength and composition of the mixture [231]. Extensive studies by Dubin [206–208, 220, 242–246], Schaaf [235], de Vries [219, 247] and collaborators showed that these soluble complexes formed at a certain pH_c value between highly-charged polyelectrolytes and proteins can undergo macroscopic phase separation upon charge neutralization at a critical pH_ϕ value through coacervation and/or precipitation, in consistency with theoretical predictions. Precipitation or coacervation phenomena have been used to purify mixtures of proteins carrying different net charges (or with peculiar charge anisotropy) [248], including mixtures of monoclonal antibodies [249–251], or to form self-assembled structures [252]. Interestingly, Kurinomaru *et al.* recently developed a precipitation-redissolution method for concentration of therapeutic proteins (antibodies, hormones or enzymes) based

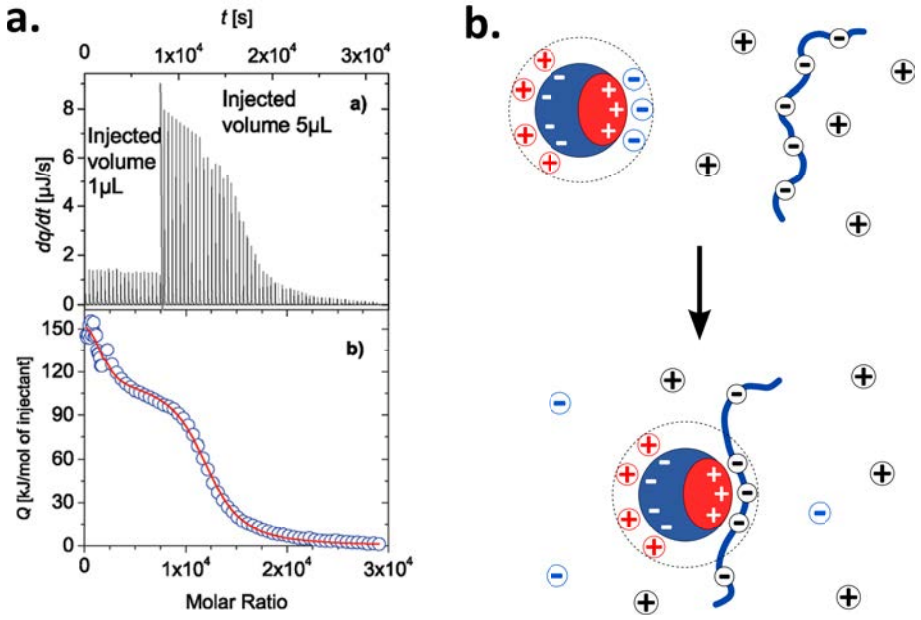


Figure 2.13: Release of counterions upon complexation between proteins and polyelectrolytes. a. ITC data for the adsorption of β-lactoglobulin onto spherical polyelectrolyte brushes in MES buffer at pH 6.1 and an ionic strength of 5 mM. The upper panel shows the raw data of the ITC. The integrated heats of each injection (circles) are shown in the lower panel together with the fit of the two sets of independent binding sites model (red line). From [233] b. Sequestration of proteins by polyelectrolytes. A positively charged patch on a protein can replace the counterions of negatively charged polymer brush, despite the fact that the overall charge of the protein is negative. The counterions from the surface of the protein are released into the bulk of the solution. The increase in entropy upon counterion release is the main driving force for protein complexation. Adapted from [233]

on complexation with polyelectrolytes at low ionic strength [253]: depending on their isoelectric point, proteins were precipitated by addition of poly(L-lysine) (PLL) or poly(L-glutamic acid) (PLGA) at a protein:polymer weight ratio in the range 1:0.05 to 1:0.3 (formation of insoluble complexes), then complexes were re-dissolved by addition of 150 mM NaCl. The released proteins were shown to recover both their native secondary structure and their activity.

2.3.1.2 Hydrophobic association

Hydrophobic association between globular proteins and hydrophobically-modified polyelectrolytes can contribute to an enhanced stability of the complexes, depending on the surface hydrophobicity of the protein (as long as the protein does not unfold). Serum albumins and β-lactoglobulin have been shown to have an effective hydrophobicity significantly higher than other proteins and have been accordingly often used to characterize hydrophobic association with hydrophobically-modified polyelectrolytes.

It was observed that hydrophobic association can predominate in the formation of soluble complexes when both the protein and polymer carry the same net charge, and when influence of patches on the protein surface is negligible (as in the case of hydrophobically-

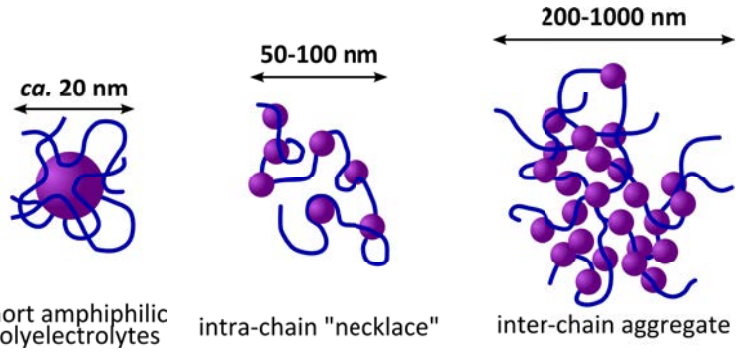


Figure 2.14: Schematic illustration of the different types of protein:amphiphilic polyelectrolytes complexes: with short amphiphilic polyelectrolytes, complexes tend to be composed of a single protein surrounded by several polymer chains; with long amphiphilic polyelectrolytes, complexes generally comprise one single polymer chain and several proteins (intra-chain "necklace"), while inter-chain aggregates are formed essentially in the case of Coulombic complexation of polyelectrolyte and protein. Adapted from [231].

modified poly(acrylic acid) and serum albumins at pH > pI [216, 231, 254]). Hydrophobic association are usually inferred from indirect observations, for instance anti-cooperativity of association or increasing affinity when the ionic strength increases [213, 215, 216, 231].

Depending on the polymer chain length, different type of soluble complexes are formed (see Figure 2.14) [231]: i/ with long polymers, complexes generally comprise one single polymer chain and several proteins, with an apparent radius close to that of the free polymer chain ("necklace"), ii/ with short polymers, complexes tend to be composed of a single protein surrounded by several polymer chains, as in the case of amphipols and integral membrane proteins [255, 256]. At high concentrations ([polymer] $\sim C^*$), polymers can be interconnected by the proteins and induce the physical gelation of the system [231, 257, 258]. Such gels are visco-elastic and flow like a liquid if the stress is maintained for hours, which confirms the transient (labile) nature of connectivity.

Amphipols, *i.e.* short hydrophobically-modified polyelectrolyte-based copolymers, keep soluble highly amphiphilic insoluble integral membrane proteins as dilution resistant, monomeric and almost monodisperse soluble complexes, via hydrophobic association between the polymer and the protein transmembrane region. Electrostatic repulsion presumably improves solubility [255, 259–262]. Although non-covalent, binding of amphipols was for long considered to be almost irreversible in usual dilution conditions, but it was shown finally that bound polymers can be displaced by excess free amphipols or by detergents, as observed by isothermal titration calorimetry (ITC) and Förster resonance energy transfer (FRET) measurements [261, 263]. The labile nature of bonds formed between the proteins and polymer chains is thus the general rule in hydrophobic association with proteins.

2.3.2 Impact of (amphiphilic) polyelectrolytes on the conformational stability and aggregation of proteins

Since hydrophobic intra-protein association stabilises the collapsed structure of globular protein (with additional contributions of intra-molecular electrostatic interactions and hydrogen bonding), complexation with amphiphilic polyelectrolytes could compete with

folding and disrupt, if too strong, the native folding. A destabilized native conformation does not however necessarily lead to aggregation. Formation of highly charged complexes is indeed expected to increase colloidal stability. In the absence of obvious instability in water (no aggregation), only a handful of studies have considered the influence of polyelectrolytes on the thermodynamic stability of proteins. Most of them have focused on single-domain proteins, and on conditions where the two partners carry opposite charges. Under these conditions, complexes are formed with the native protein, prior to protein unfolding by an external stress (*e.g.* upon heating). This section reviews the influence of (amphiphilic) polyelectrolytes on the conformation of proteins and on their colloidal stability under denaturing conditions.

2.3.2.1 Structure and activity of proteins in complexes with amphiphilic polyelectrolytes in water

In aqueous buffers (no denaturant, no surfactants), association between (amphiphilic) polyelectrolytes and proteins often does not affect the native-like secondary structure, and the activity can be preserved, as reported in various studies on polyanions/proteins mixtures, either when polymers and proteins carry opposite net charges [217, 264, 265] or near the proteins' pI [266, 267]. Absence of deleterious effect on structure was also observed with hydrophobized polyanions in complexes with negatively-charged BSA [254]. Protein structure and activity was shown to be preserved in polyelectrolyte multilayers, for a wide range of enzymes or other proteins [268–272], including cell growth factors [273, 274] or antibodies [275].

However, preservation of the native structure is not a general rule: for instance, insulin was denatured by complexation with poly(diallyldimethylammonium chloride) [267]. Strong association conditions between polyelectrolytes and proteins can result in the loss of the native structure of the protein, in consistency with data on enzyme immobilization that indicate that proteins often exhibit less activity in immobilized form. Schwinté *et al.* showed that the secondary structure of proteins (cationic BSA or anionic lysozyme) was altered when adsorbed into a polyelectrolyte brush only when polymers were carrying charges of opposite sign than that of the protein [276].

Similarly, SANS measurements by Cousin *et al.* showed that when excess poly(styrene sulfonate) (PSS) was added to a lysozyme solution, the internal structure of the protein changed [277]. It was observed that after an initial strong electrostatic binding (long-range attraction), lysozyme was progressively unfolded through short-range hydrophobic association with the polymer. Gao *et al.* showed that copolymers of alkenes and maleic acid [214] or sulfamate carboxylate [278] could result in a decreased activity and loss of secondary structure of lysozyme, in particular with the more hydrophobic copolymers (stronger association). NaCl could be used to release the enzyme from the complexes, which regenerated the protein native structure and activity.

Shiraki, Nagasaki and co-workers found that copolymers of a cationic polyamine, poly(*N*, *N*-diethylaminoethyl methacrylate) (PEAMA), and PEG interacted with lysozyme under physiological conditions, which resulted in the inactivation of the enzyme activity without alteration of the protein secondary structure (a specific association with the active site was hypothesized) [279, 280]. Activity could be restored by addition of a polyanion that sequestered the polycation (see Figure 2.15). To the best of our knowledge, this is the first report that shows that "wrong side" interactions, *i.e.* interactions between a polymer and a protein that carry the same charge, may be exploited to control enzyme activity. The sequential use of the polycationic copolymer and a

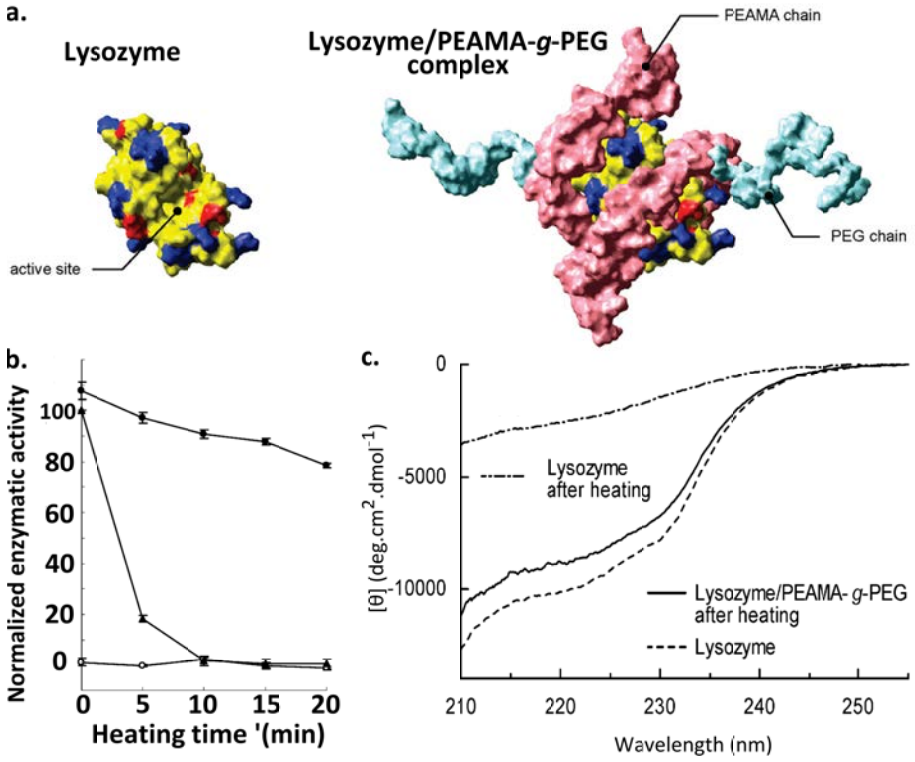


Figure 2.15: Interaction between lysozyme and PAEMA-*g*-PEG. a. Molecular models of lysozyme and lysozyme/PEAMA-*g*-PEG complex. b. Changes in the enzymatic activity of lysozyme and the lysozyme/PEAMA-g-PEG complex as a function of the heating time: (black trianlge) lysozyme with heating, (black circle) lysozyme/PEAMA-g-PEG complex with heating, and (empty circle) lysozyme/PEAMA-g-PEG complex with heating followed by the addition of PAA. The concentrations of lysozyme, PEAMA-g-PEG, and PAA were 0.5, 10, and 10 mg.mL^{-1}, respectively. Heat treatment was carried out at 98°C for 20 min, and then measurements were carried out at room temperature and pH 7.0. c. CD spectra of lysozyme, lysozyme after heating, and the lysozyme/PEAMA-g-PEG complex after heating at 98°C for 20 min. From [279].

polyanion was further implemented to control the activity of other cationic enzymes, namely ribonuclease A [281, 282], and less surprisingly of anionic ones, such as α-amylase or β-galactosidase [283]. Anionic poly(sodium acrylate) was also shown to be a generic noncompetitive inhibitor for cationic enzymes activity with no or little changes in the secondary structure of proteins upon association [284]. The structure of trypsin, the most hydrophobic enzyme used in the study, was yet affected by PAA, presumably because of a stronger non-covalent association with the polymer. Opposite cases of hyperactivation of enzymes in the presence of cationic of polyanionic polymers were reported when using charged substrates [285]. Kinetics studies showed that polyelectrolytes led to a decrease in the Michaelis constant in the case of α-chymotrypsin, indicating that the hyperactivation of the enzyme by polyelectrolytes was related to increased affinity of α-chymotrypsin for the substrate.

2.3.2.2 Conformational stability of proteins sequestered by polyelectrolytes

Preservation of native structure in water happens when the complexation of native and non-native protein conformers does not markedly displace the folding equilibrium, which corresponds in most reported studies to date to a large predominance of the native globular form. Differential association with native and non-native states is however expected to shift this equilibrium, and the impact of polyelectrolyte can be observed in condition of marginal stability of the native state (high T or in the presence of denaturing agents in solutions). Izumrudov and colleagues focused on interactions between polyanions (poly(acrylic acid), poly(methacrylic acid), poly(styrene sulfonate)) and basic (cationic) enzymes. They showed that complexation with polyanions does not impair the activity of the native enzyme but lowers the unfolding temperature in water, as measured by differential scanning calorimetry (see Figure 2.16). This clearly points to the destabilization of the native structure, especially when short polymer chains were used (which was tentatively attributed to their ability to penetrate "deep" into the protein [217, 265], but may also reflect end-group contributions). Interestingly, addition of NaCl or of a cationic polymer to the protein:polyanion mixtures restores the unfolding temperature of the free protein, confirming the predominant electrostatic origin of the destabilization. The hydrophobicity of the polyanions was shown to further increase the destabilization of enzymes [209, 217].

Antalik and co-workers identified two major parameters in the complexation of proteins with polyanions, namely the basicity of the proteins and the hydrophobicity of the polyanions [211, 286]. The magnitude of decrease of the unfolding enthalpy in mixed protein:polymer solutions was shown to correlate with the isoelectric point of the protein and hydrophobicity of the polyanion, as illustrated on Figure 2.16: at fixed pH and ionic strength, the effect of polyanions increased with increasing pI (namely when the net positive charge of proteins became higher) and was more pronounced when more hydrophobic polymers were used (*e.g.* Nafion, which contains long uncharged segments, and poly(4-styrene-sulfonate), which contains aromatic moieties), due to the additional noncoulombic interaction.

Wittemann and co-workers studied mixtures of polyelectrolyte brushes and proteins. They showed that adsorption of proteins into these brushes resulted in the decrease of their unfolding temperature (of about 10°C in the case of ribonuclease A) [287].

In urea solutions, CD measurements performed by Sun *et al.* showed that the chemically-induced unfolding transition of cytochrome c was systematically shifted to lower denaturant concentrations in the presence of poly(sodium acrylate) (PAA) and hydrophobically-modified PAA copolymers, namely polyanions destabilized the protein (see Figure 2.17) [288]. Up to a 3-fold decrease of ΔG^{H_2O} was observed in the presence of polyelectrolytes, while hydrophobically-modified neutral hydrophilic polymers did not affect the unfolding energy. Azobenzene-based copolymers were used to modulate *in situ* the hydrophobicity of polymers (apolar, dark-adapted *trans* isomers of azobenzene side groups are turned into polar, UV-adapted *cis* form). Polarity switch under UV irradiation had no impact on the thermodynamic stability of the protein (see Figure 2.17). On the contrary, UV-induced ionization of hydroxyl-azobenzene moieties on neutral hydrophilic polymers (photo-ionization) resulted in the destabilization of cytochrome c, pointing to the importance of Coulomb interaction for the control of protein folding. These results suggest that intermolecular Coulomb interactions between polyanions and cytochrome c compete with protein intra-protein interactions, *i.e.* weaken the native contacts between residues and favour unfolding.

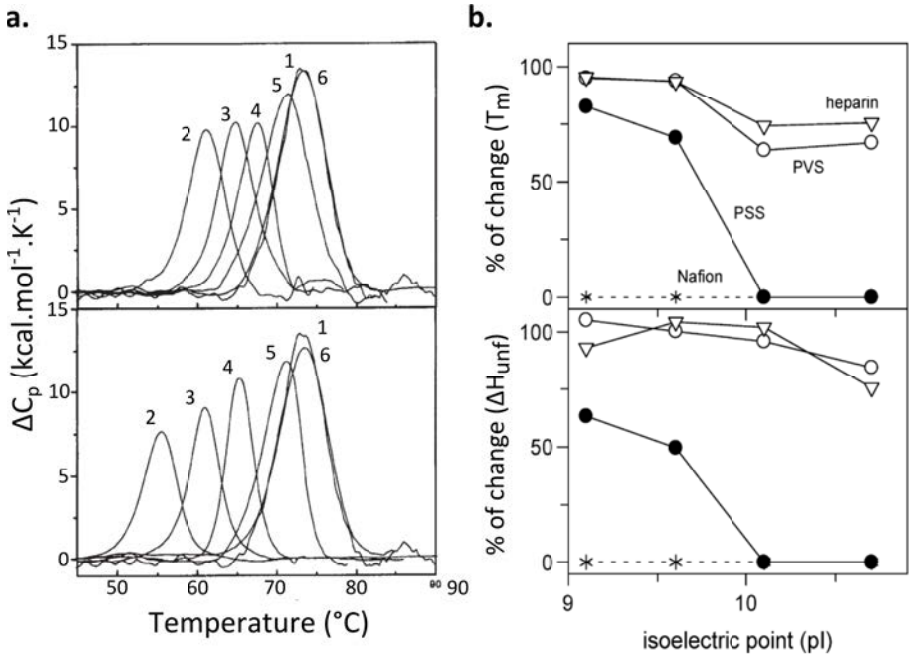


Figure 2.16: Destabilization of proteins upon association with polyelectrolytes. a. Temperature dependence of partial heat capacity ΔC_p of free lysozyme (curve 1) and lysozyme in the presence of (top) sodium poly(methacrylate) (PMA, $\bar{DP}$ = 1830) and (bottom) poly(sodium acrylate) (PAA, $\bar{DP}$ = 2400) respectively, containing different NaCl concentration: 40 mM (curve 2), 100 mM (curve 3), 200 mM (curve 4), 300 mM (curve 5), and 600 mM (curve 6). From [265]. b. Dependence of temperatures of thermal transition T_m and calorimetric enthalpies ΔH_{unf} of protein:polyanion complexes vs. isoelectric points of the proteins expressed in percentile change calculated as the ratio of the obtained parameter of the protein in the presence of polyanion and in its absence (100% means no contribution of the polyanion). From [211].

2.3.2.3 Aggregation propensity of proteins in the presence of amphiphilic polyelectrolytes

The formation of soluble complexes between proteins and (amphiphilic) polyelectrolytes can result in inhibition of protein aggregation, due to electrostatic repulsion between the highly-charged complexes.

In their studies on basic proteins:polyanions mixtures, Izumrudov and co-workers showed that enzymes were protected against irreversible thermal-induced aggregation when bound to synthetic polyanions [209], in particular when long polymer chains of high charge density were used, with an additional stabilization as the hydrophobicity of polyanions increased [217, 289]. The same effect was observed with polycations when the pH was above the isoelectric point of the protein [290]. Schwinté *et al.* also showed that protein:polyelectrolyte complexation resulted in prevention of protein aggregation at ambient temperature, while heat-induced aggregation was or not suppressed depending on the strength of electrostatic interactions between polyelectrolytes and proteins [276].

Dubin and collaborators extended the investigations to pH conditions in vicinity of the isoelectric point of proteins. They showed that negatively-charged glycosaminoglycans, notably heparin, could inhibit or reverse the aggregation of native BSA, β-lactoglobulin

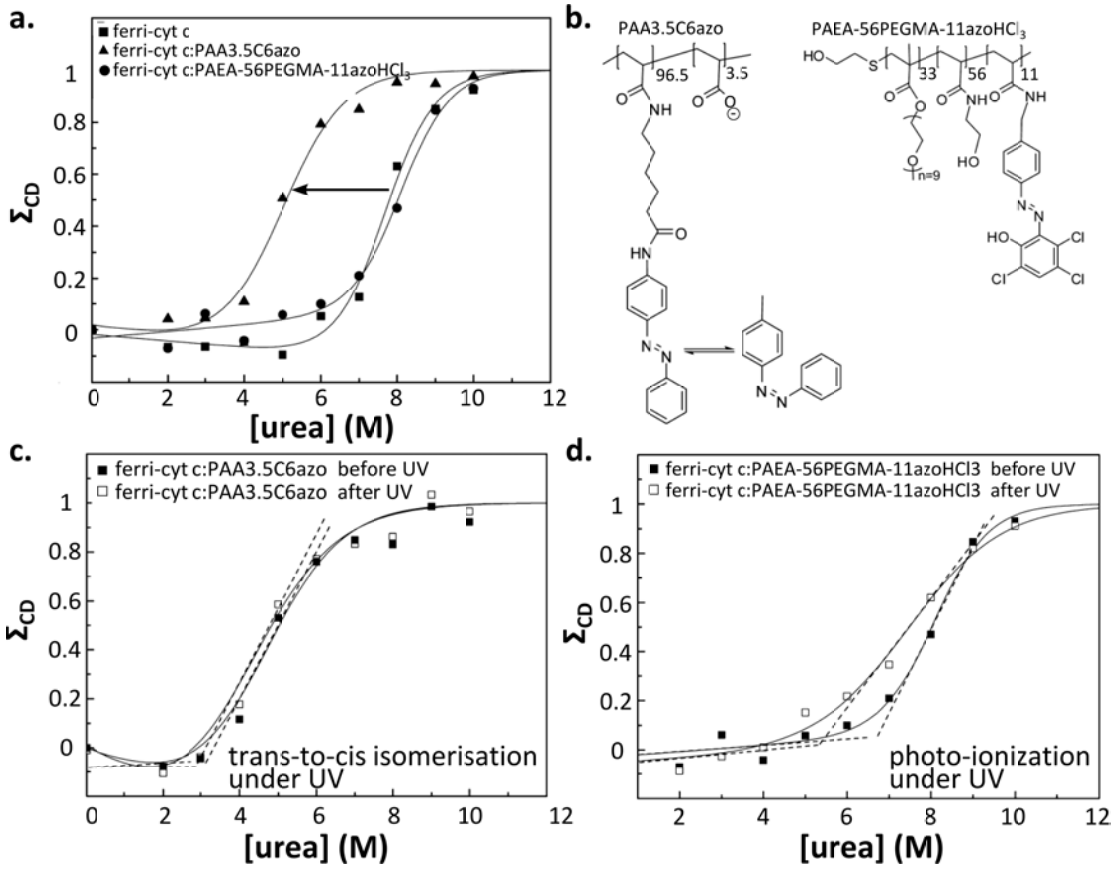


Figure 2.17: Effect of azobenzene-bearing copolymers on the urea-induced unfolding of ferri-cytochrome c. a. Fraction of unfolded protein (CD measurements) in the absence of presence of polymers. PAA-3.5C6azo (negatively-charged) destabilises the protein (shift to lower [urea]), unlike PAEA-56PEGMA-11azoHCl$_3$ (neutral). b. Chemical structure of the polymers. c. Effect of PAA-3.5C6azo on the urea-induced unfolding of ferri-cyt c before and after exposure to UV (switch of polarity). d. Effect of PAEA-56PEGMA-11azoHCl$_3$ on the urea-induced unfolding of ferri-cyt c before and after exposure to UV (photo-induced ionization). Adapted from [288].

or Zn-insulin at ambient temperature and at pH close to the isoelectric point of the proteins [291, 292]. The effect could be extended to suppression of heat-induced protein aggregation [292]. Chung *et al.* similarly found that dextran-sulfate prevented BSA aggregation upon heat-induced partial unfolding only at pH close to the protein's pI [293].

Unexpectedly, Shiraki, Nagasaki and co-workers found that copolymers of poly(N,N-diethylaminoethyl methacrylate) and PEG improved the thermal stability of cationic lysozyme under physiological conditions, resulting in a good activity recovery (up to 80%) after thermal treatment and after addition of poly(sodium acrylate) to sequester the polycation (see Figure 2.15) [279, 280]. This is the first report on stabilization against heat-stress by association with polyelectrolytes on the "wrong side" of the pI. The PEG segment was shown however to play a crucial role in the preservation of soluble complexes: a polycationic chain with no PEG indeed induced irreversible aggregation and denaturation of enzymes (see Figure 2.18) [283].

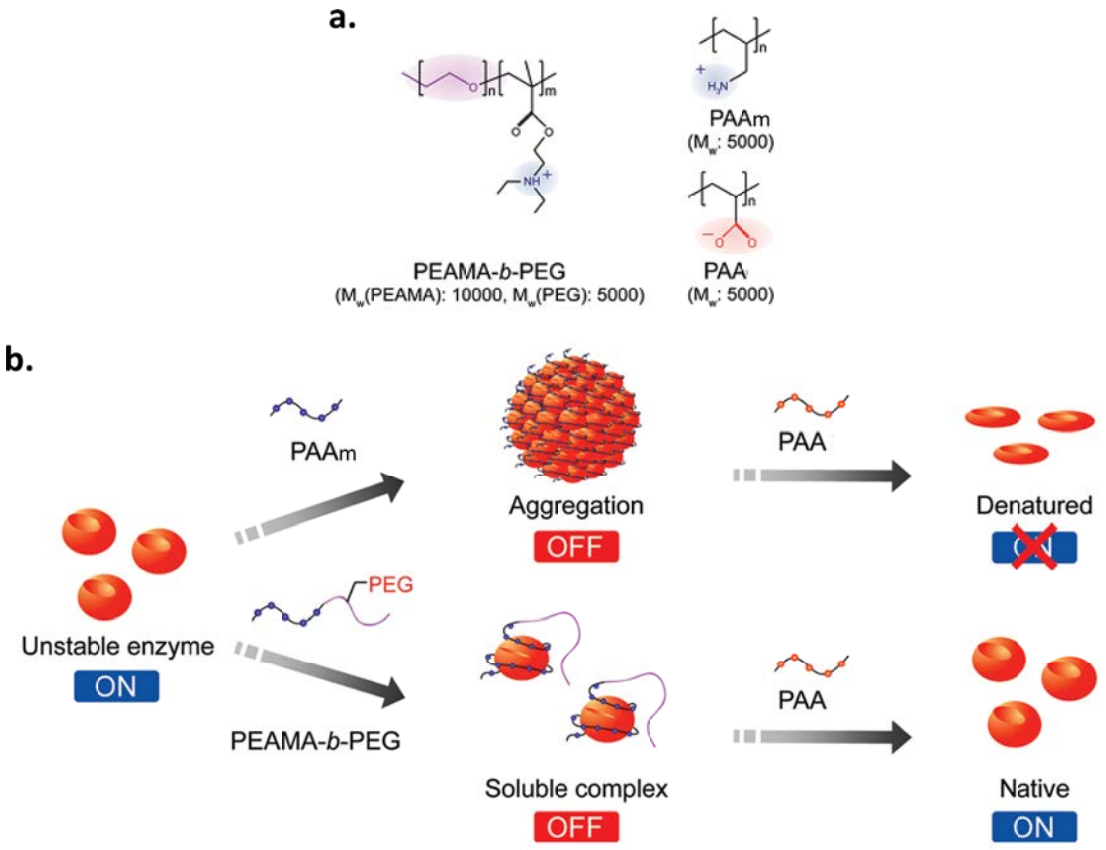


Figure 2.18: Switching for enzyme activity by PEGylated polycations. a. Chemical structures of polymers used by Kurinomaru*et al.* (PAAm: poly(allylamine), PAA:poly(acrylic acid)). b. Schematic illustration of improved complementary polymer pair system to control enzyme aggregation propensity and activity. Adapted from [283].

Other studies report on the increased protein aggregation propensity in the presence of polyelectrolytes. Mounsey *et al.* found that chitosan significantly increased aggregation of β-lactoglobulin in the pH range 5.5-7.0, while aggregation was suppressed at pH 4.0 [294]. Polyelectrolytes have also been observed to increase protein fibrillation: negatively-charged nucleic acids and glycosaminoglycans were shown to favour the fibrillogenesis of various amyloidogenic proteins including human lysozyme [295], α-synuclein [296], tau [297], gelsolin [298], transthyretin [299] and Aβ40 peptide [300]. Electrostatic association of heparin to lysozyme was suggested to bring in vicinity cationic proteins, which were therefore more prone to aggregation (higher local concentration) [295]. On the other hand, in the case of tau protein, polyanions were shown to specifically bind to critical positive charges, mostly involved in β-forming motifs, thereby stabilizing regions that are crucial for aggregation and promoting the formation of fibrils [301].

Interestingly, polyelectrolytes could also inhibit fibril formation. For instance, poly(4-vinylstyrenesulfonate) was shown to bind to the Aβ40 peptide, mainly through hydrophobic association, which resulted in the stabilization of the peptide [302]. Here, the hydrophobicity of the polyelectrolyte was identified as essential to prevent the formation of amyloid fibrils, supposedly because it trapped the peptide in an unfolded state that could not form β-structures. Taluja and Bae also found that electrostatic association

between PEG-poly(histidine) and insulin could reduce the fibrillation rate at pH 5.5 through an increased protein solubility [303]. Gold nanoparticles coated with polyelectrolyte multilayers were reported to inhibit amyloidogenesis of prion protein both *in vivo* and *in vitro* [304].

2.3.2.4 Protein refolding assisted by amphiphilic polyelectrolytes

Protein refolding assisted by polyelectrolytes has scarcely been investigated. A few studies report on the refolding of thermally- or urea-denatured proteins in the presence of synthetic polyelectrolytes (*e.g.* Eudragit S-100, a methyl methacrylate polymer [305–307] or a copolymer of methacrylic and acrylic acids [308]) and naturally occurring ones (such as alginate [309–312] or chitosan [313, 314]). The selective binding of denatured proteins to polyelectrolytes, either hydrophobic or hydrophilic ones, was shown to promote protein refolding to the native, active conformation, most-likely because of minimization of aggregation. Purification could be undertaken simultaneously by affinity precipitation of protein:polyelectrolytes complexes (either via a change in pH for Eudragit or addition of calcium ions for alginate), then release of the folded protein from the polymer precipitate (for instance by addition of NaCl).

Amphipols were also applied to the refolding of detergent-denatured integral membrane proteins [315, 316], as well as cell-free membrane protein synthesis [317]. Hydrophobic associations to the partially-folded proteins were expected, and shown *in vitro*, to increase the solubility of the refolding intermediates, without preventing native-like folding. The charged polymers were however not compatible with an application in cell-free expression systems because of interfering interactions with the rich mix of proteins present in cell extracts.

2.3.2.5 In summary

To sum up, it is unclear whether general rules can be made explicit out of the available studies. Polyelectrolyte:protein Coulomb association could compete with inter-protein (presumably hydrophobic) attraction in several examples of heat-stressed mixtures, but formation of complexes may also stabilize/favour aggregation-prone conformers and gather in close proximity unstable proteins (multiprotein complexes) which favours aggregation. To unravel this apparent complexity, in-depth investigation should be carried out, aiming at a correlation between colloidal stability (aggregation rates) with conformational stability, binding site(s), affinity, or dynamics of complexation. To our knowledge, this data is not available in literature.

2.4 Our project: study of model poly(sodium acrylate) derivatives as artificial chaperones for antibodies and their derivatives

2.4.1 Problematic

Studies on the effect of protein association with amphiphilic polyelectrolytes have been mostly restrained so far to conditions where soluble complexes already formed between the native protein and the polymer, namely in strong interacting conditions, *e.g.* when the two partners bear opposite net charge and/or at relatively low ionic strength. Single-domain globular protein models have been almost exclusively used. However, many

therapeutic proteins, such as antibodies, comprise several domains which complicates the refolding procedures and makes them very sensitive to stress-triggered irreversible aggregation.

On the route to design amphiphilic polyelectrolyte-based artificial chaperones for proteins of therapeutic interest, unanswered questions abound. A few are listed below:

- Is association of the native protein with polyelectrolytes necessary to get protection against stress-induced (*e.g.* heat-induced) aggregation?
- Instead, can complexation of proteins with polyelectrolyte derivatives result from protein (partial) unfolding?
- If so, what is the driving force of association with partly-unfolded intermediates? Can we achieve selective binding to partially unfolded proteins?
- In this case, is protection against aggregation still achieved or does the bound (unfolded) conformers enter faster into oligomerization processes?
- Can we control the typical stoichiometries of complexes formed with partly-unfolded intermediates (*e.g.* at 1:1 mol/mol, the chance for oligomerization shall be reduced)?
- Can hydrophobically-modified polyelectrolytes also be of help in assisting protein refolding from a chemically denatured state? And at which step of the refolding does complexation/dissociation occur?
- Do interactions with polymers perturb inter-domain association in multidomain proteins?
- Is there any benefits of using external stimuli (pH, ionic strength, light) to modulate the interactions between proteins and polymers, so as to release proteins with high temporal resolution, or can we rely on spontaneous binding of non-native states/dissociation of the native one?

2.4.2 Potential application

Protein aggregation is one of the main bottlenecks that restrain the development of therapeutic antibodies and antibody fragments. The use of molecular additives in formulations is severely restricted in biomedical practices, because of toxicity issues, need to precisely adjust concentrations depending on the protein, and high amounts usually required to achieve obvious gains (molar concentration), saying nothing about the high cost of implementation of complex procedures of handling solutions, and operating purification, dilution, concentration in sterile conditions.

A major breakthrough would be to find a generic additive that could be used at (low) fixed stoichiometric ratio to limit, if not prevent, aggregation of antibodies during storage and/or stressful conditions that occur during the whole renaturation and purification procedures. The use of amphiphilic polyelectrolytes for enhancing antibody solubility and avoiding aggregation has not yet been implemented. Study of model polymers is thus desirable to assess the potential relevance of Coulomb and hydrophobic interactions in antibody stabilisation.

2.4.3 Aim of this work: a study of mixed model polymers:model protein solutions subjected to chemical or heat stress

To unravel the contributions of electrostatic and hydrophobic interactions to chaperone-like activity of polymers, we studied a set of hydrophobized poly(sodium acrylate)(PAA) derivatives (see Figure 2.19), mixed with model proteins in conditions were their native structure was disrupted.

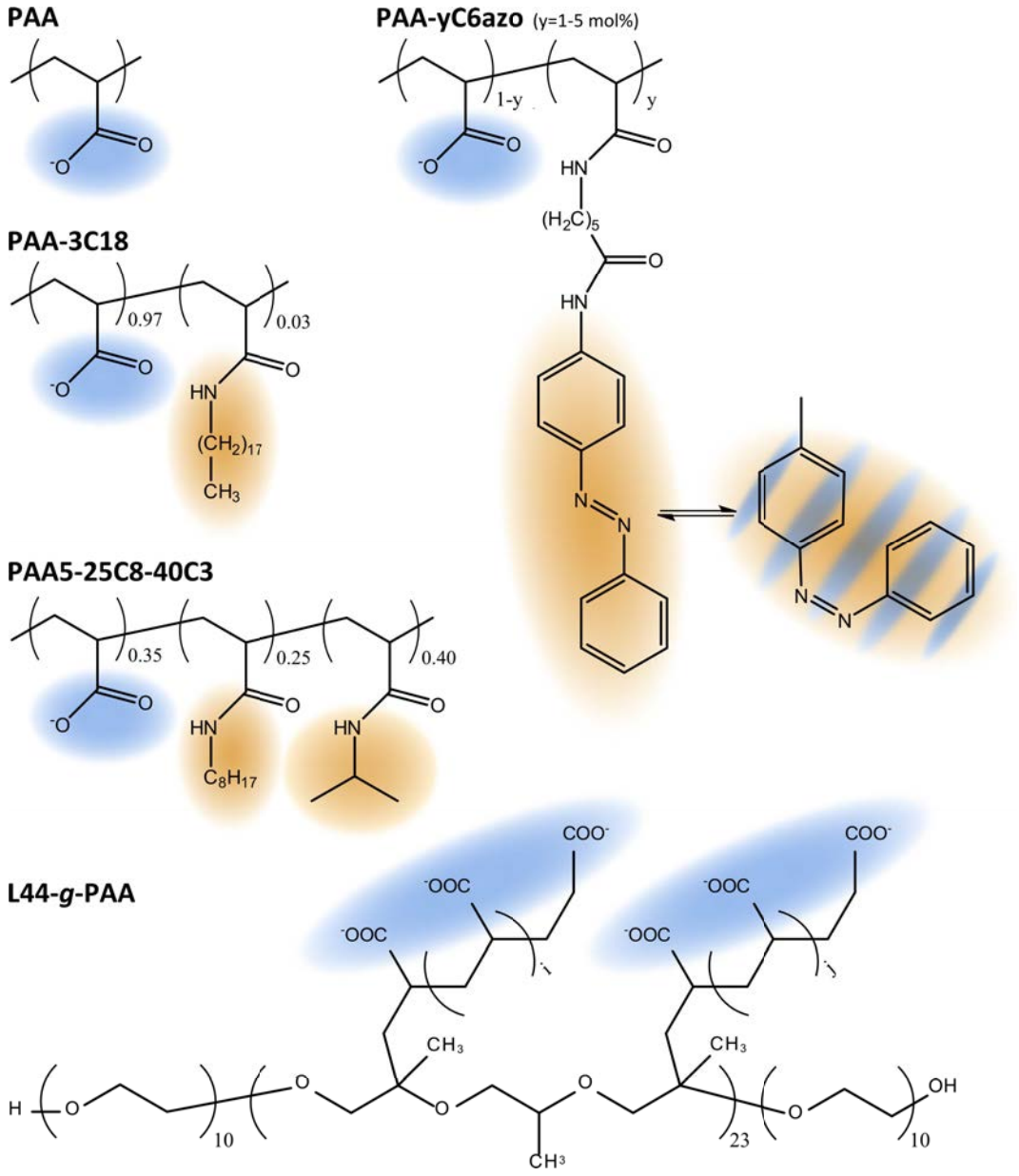


Figure 2.19: Chemical structures of the polymers used in the thesis. All polymers but L44-*g*-PAA are composed of a negatively-charge poly(sodium acrylate) (PAA) backbone (in blue) that has been modified to contain a few mol% of hydrophobic moieties (in orange), including photoswitchable azobenzene ones. L44-*g*-PAA result from the grafting of short PAA chains onto a PEG-PPO-PEG triblock polymer.

In the following, the hydrophobically-modified PAA derivatives are referred to according to the systematic nomenclature:

$$\text{PAA}n\text{-}x\text{C}m$$

where n refers to the nominal average molecular weight of the poly(acrylic acid) backbone (in kg.mol^{-1}), x is the grafting ratio (in mol %) of hydrophobic moieties, containing m

carbon atoms (C18, C8 and C3 refer respectively to *n*-octadecyl, *n*-octyl and isopropyl chains).

It is worth noting that one of the polymers, conventionally called "Amphipol A8-35" in the literature, is here referred to as PAA5-25C8-40C3 to keep with homogeneous nomenclature. In addition, we assessed the efficiency of a PAA-grafted pluronic copolymer, L44-*g*-PAA, developed by SupraTech Pharma Inc. (a Canadian company) and which has gained approval from the FDA to be used in therapeutic formulations. Appendix A details some of the physico-chemical characteristics of the different PAA derivatives used in the study, as well as some synthetic steps used to modified the parent chain.

The objective of this thesis is threefold:

- to assess whether partly-folded intermediates can be selectively complexed by polymers, and if general trends emerge to control selectivity (which favourable environmental conditions, buffer, T, which predominant nature of the polymer:protein interactions – Coulomb, hydrophobic, combined...),
- to show that the release of native proteins can be achieved by modulation of Coulomb and/or hydrophobic attractions (that for practical purposes, can ideally occur not far from usual protein concentrations, buffer compositions, and ambient T),
- to estimate if one shall expect high impact of interaction with polymers on the refolding pathway, the structure or solubility of intermediate species (*i.e.* to compare the step-by-step refolding of proteins in the presence or not of polymer derivatives and estimate whether intermediate stages are composed of soluble or kinetically stabilized species).

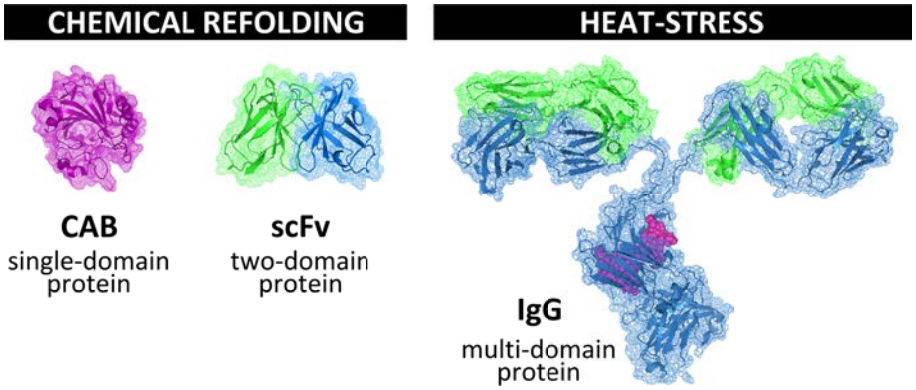


Figure 2.20: Structure of the model proteins of increasing complexity used in the thesis. We will either study the stability upon chemical refolding (CAB, scFv) or under heat-stress (IgG). CAB: bovine carbonic anhydrase B, scFv: single-chain Fv fragment, IgG: immunoglobulin G.

The manuscript is divided into three chapters focusing on increasingly complex protein structures (see Figure 2.20). As a proof of concept, Chapter 3 investigates the use of PAA derivatives to stabilize a well-characterized model enzyme, bovine carbonic anhydrase B (CAB), during refolding from the urea-denatured state. Chapter 4 extends the use of PAA additives to the handling of single-chain Fv fragments (scFv) during chemical refolding. Chapter 5 is dedicated to the stabilization against aggregation of full-length polyclonal immunoglobulins G (IgG), which is here assessed in heat-stress conditions.

Part II

Chemical refolding of proteins in the presence of amphiphilic polyelectrolytes

Chapter 3

Renaturation of a model enzyme with amphiphilic poly(acrylate) chaperones

In this chapter, we describe the refolding and renaturation of urea-denatured bovine carbonic anhydrase B (CAB) – a well-characterized, aggregation-prone, monodomain enzyme – performed in the presence of amphiphilic poly(acrylate) copolymers, PAA150 and PAA150-3C18, or photo-responsive PAA bearing azobenzene moieties that enable *in situ* control of hydrophobic interactions. We show that all these copolymers exhibit a remarkable protective effect against aggregation in water of urea-unfolded CAB, and most of them (but not the octadecyl-modified one) enhance the regain of activity.

The CAB:polymer association and the influence of mixed complexes on CAB conformation are assessed before and during renaturation by circular dichroism (CD), light scattering and fluorescence correlation spectroscopy (FCS). The hydrophobic azobenzene groups undergo *trans*-to-*cis* photoisomerisation under UV light, resulting in *in situ* (photo)dissociation of protein:polymer complexes, which offers an additional control parameter to investigate the role of binding with biomacromolecules.

It is concluded that Coulomb association of CAB (here above or close to its pI) with the polyanionic chains contributes to a significant part of the stabilization of the protein and is compatible with (hours-long) release of native CAB in solution (*i.e.* spontaneous, "stripping-free" renaturation). Hydrophobic binding, often presented in the literature as the major driving force of both aggregation and binding to artificial chaperones, has an obvious impact on the association of CAB with polymers and on the conformational stability of the enzyme, but it appears difficult to achieve balanced hydrophobic association. The more efficient mean to enhance renaturation is accordingly to tailor Coulomb attraction with or without contribution of hydrophobic interactions.

Contents

3.1 Bovine carbonic anhydrase B: a model enzyme to study aggregation during refolding 63

3.1.1 Structural features of bovine carbonic anhydrase B and *in vitro* folding mechanism 63

3.1.2 Refolding protocol in the presence of polymers 64

3.2 Keeping CAB soluble with poly(acrylate) derivatives 66

3.2.1 Evidence for the preservation of solubility 66

3.2.2 Evidence for CAB:polymer association and variation of the size of associates during renaturation (light scattering study) 67

3.2.3 Measurement of sizes by fluorescence correlation spectroscopy during refolding 70

3.2.4 Conclusion from solubility, light scattering and FCS studies . . 72

3.3 Polymers allow recovery of a native-like and active protein 72

3.3.1 Secondary structure recovery monitored by circular dichroism . 72

3.3.2 Activity recovery 76

3.4 Conclusion: discussion on the role of Coulomb and hydrophobic associations 81

3.1 Bovine carbonic anhydrase B: a model enzyme to study aggregation during refolding

3.1.1 Structural features of bovine carbonic anhydrase B and *in vitro* folding mechanism

Bovine carbonic anhydrase B (CAB) is a single-domain metalloprotein of 259 residues. The zinc-containing active site catalyses the hydration of carbon dioxide and contributes thereby to maintain the acid-base homoeostasis in the organism. It also catalyses the hydrolysis of esters [318–320], a property that is used to monitor CAB activity. The crystalline structure of CAB shown on Figure 3.1 contains *ca.* 15% of α-helices and about 30% of β-sheets [321].

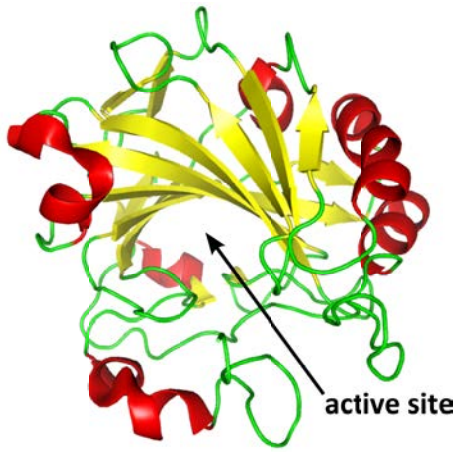


Figure 3.1: 3D structure of CAB, with emphasised α-helices (red) and β-sheets (yellow).

CAB has been widely studied [322]. In particular, it has been shown to fold through a sequential mechanism involving the formation of a pre-molten globule state (a compact structure with substantial amount of fluctuating secondary structure) having a diameter of ∼6.3 nm, followed by the formation of a molten globule state (possessing a stable secondary structure as well as solvent-accessible hydrophobic clusters) having a diameter of ∼5.3 nm [78, 323–328]. Half-times of 0.03 s and 140 s have been reported for the formation of the pre-molten and molten globule respectively [327]. The overall folding process is limited by the *trans*-to-*cis* isomerisation of the 18 proline residues of CAB: half-times of 10 to 12 minutes have been reported for the regain of the enzymatic activity [329].

CAB has also been shown to aggregate when it is refolded by direct dilution in a refolding buffer from its urea- or GndCl-denatured state [161, 330, 331]. More precisely, it has been shown that it is the molten globular state of CAB that can result in aggregated species [326, 330, 332], while other intermediate states that are unfolded to a greater extent are not aggregation-prone [332]. This enzyme is hence a good and simple model to test the effect of additives and renaturation procedures on the prevention of protein aggregation [322].

Owing to its well characterized folding mechanism, CAB has been used to assess the efficiency of diverse additives on the improvement of renaturation yields. The usual palette of osmolytes was extended to include macromolecules or self-assemblies, such as

micelles of surfactants [160, 161], self-assemblies of amphiphilic polymers [168, 170, 177] or stimuli-responsive polymers [183, 187, 188, 193, 197]. Additives are commonly tested for their influence on the aggregation propensity of CAB either during refolding from a chemically-denatured state or during an external stress (usually heat), as well as for their effect on activity recovery. We are here interested in the refolding or urea-denatured CAB in the presence of PAA derivatives.

3.1.2 Refolding protocol in the presence of polymers

A conventional renaturation procedure starts with the protein solubilized in denaturant (*e.g.* urea:water solutions) and reaches step-by-step a purely aqueous buffer condition. The aggregation of urea-unfolded CAB and renaturation yield are highly sensitive to the renaturation protocol (concentration of CAB, temperature, incubation times, etc.). With the aim of testing the efficiency of polymer additives, we resorted to a protocol that maximized aggregation (and minimized activity recovery) of CAB in the absence of additive. To ensure complete unfolding of the protein, CAB was prepared in 10M urea 24 hours prior to the experiment and was heated at 70°C for 6 minutes just before starting the renaturation procedure (see Figure 3.2). Unfolded CAB was then diluted at once (40 to 800 fold) in buffer with no urea. This protocol was applied by Hanson and Gellman who showed that these conditions, namely i/ heating the unfolded CAB solution and ii/ dilution down to a residual urea concentration below 0.04M urea, maximized aggregation of CAB in the absence of surfactants [161].

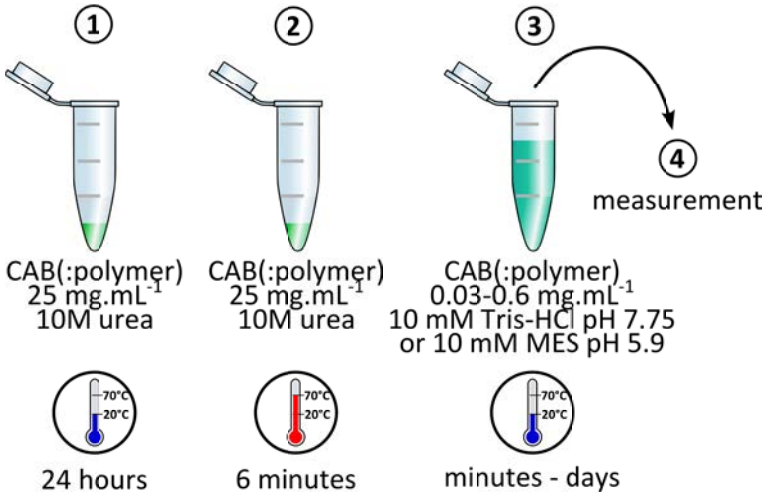


Figure 3.2: Renaturation protocol of urea-denatured CAB supplemented or not with polymers. 1. A 25 mg.mL^{-1} unfolded CAB solution is prepared by dissolving freeze-dried CAB powder in 10M urea, then this stock solution is incubated for 24 hours (for renaturation without polymers) or added to a few mg of freeze-dried polymer powder to reach a polymer concentration of 25 mg.mL^{-1} (1:1 wt/wt ratio) and incubated for 24 hours. 2. Prior to the dilution into the refolding buffer, the urea-unfolded CAB(:polymer) solution is heated at 70°C for 6 minutes. 3. The heated mixture is diluted at once in renaturation buffer at time defined as t=0 in order to reach a final concentration in the range 0.03-0.6 mg.mL^{-1} and is incubated for various amount of time before measurements (4).

Several procedures can be adopted for the renaturation of CAB in the presence of polymers: in particular, the latter can be added either in the refolding buffer or in the urea-denatured protein stock solution (*i.e.* before dilution in the polymer-free refolding buffer). Unpublished studies previously carried out in the group [Ph.D. J. Ruchmann] showed that poly(acrylate) derivatives did not improve the renaturation yield of CAB when added in the refolding buffer, presumably because the protein aggregates faster than it can bind to (dilute) polymer chains. The presence of high concentrations of polymer in the urea-denatured preparation of CAB is expected to favour protein-polymer interactions. Accordingly, we decided to use the refolding procedure illustrated on Figure 3.2: a 10M urea CAB:polymer mixture at 25 mg.mL^{-1} (1:1 wt/wt ratio) is incubated for 24 hours, then heated for 6 minutes at 70°C just before being diluted (at t= 0) into the renaturation buffer, free from additives, to reach the desired concentration (typically 0.6, 0.1 or 0.03 mg.mL^{-1} depending of the experiment).

CAB properties and CAB:polymer association can then be studied as a function of the initial polymer:CAB weight ratio, composition of the renaturation buffer and incubation time in the buffer. Two different buffers are used: either 10 mM Tris-HCl pH 7.75 (conventionally used in the literature) or 10 mM MES pH 5.9. The idea is to modulate the surface charge of the protein, which pI is about 5.85, and monitor the consequences on the interaction with the poly(acrylate) derivatives. At pH 7.75, the net charge of the protein is negative, while it is close to zero at pH 5.9 (in these conditions, native CAB was soluble at the working concentrations, namely less than 0.6 mg.mL^{-1}, *i.e.* 20 µM or less).

Taking advantage of photo-responsive polymers

In addition to PAA150 and PAA150-3C18, tested for their ability to limit CAB aggregation during refolding, we herein developed PAA-based derivatives bearing photo-responsive azobenzene groups (see Figure 2.19 in Chapter 2). Interestingly, the azobenzene moieties can undergo a conformational change depending on the illumination conditions: in the dark, or under blue-light illumination, azobenzene groups are mainly in their stable *trans* state and are hence apolar; under UV-irradiation, however, they switch to the *cis* conformation, and then acquire a dipolar moment of 3.1 Debyes, which decreases their hydrophobicity. In addition, the terminal phenyl group of the azobenzene moieties comes closer to the backbone in the *cis* state, so is less accessible to interact with proteins. Accordingly, it is possible to assess the importance of hydrophobic interaction during renaturation.

A few studies report that cis-trans isomerisation of azobenzene modulate the interaction with native proteins in water. In systems based on azobenzene-containing surfactants, Lee and collaborators reported that hydrophobic association with CAB could be modulated by exposure to light [323]: under their apolar *trans* form, surfactants were shown to favour unfolding and activity loss of CAB [323] whereas 40% of the enzyme activity was preserved under UV-light, providing a photo-control of enzyme activity.

Using azobenzene-containing PAA, previous studies in the group showed that the *cis-trans* isomerization and hydophobic assembly were effectively controlled *in situ* by exposure to UV light [333] and could modulate association with native bovine serum albumin [334] or cytochrome c [288]. All these reported effects were ascribed to higher hydrophobic interactions between the blue-adapted (*trans*) azobenzene isomer compared to the UV-adapted (*cis*) one. With PAA150-*m*C6azo, we herein want to decipher the importance of photo-switch of polarity (hydrophobicity) on the aggregation propensity

of CAB during refolding and therefore on renaturation yields.

3.2 Keeping CAB soluble with poly(acrylate) derivatives

3.2.1 Evidence for the preservation of solubility

In the absence of polymers, aggregates that are visible to the naked eye were formed upon dilution of urea-unfolded CAB into the renaturation buffers. Micrometer large aggregates sedimented rapidly at pH 5.9 or remained in suspension at pH 7.75 (see pictures on Figure 3.3). No aggregates were seen by eye in the presence of polymers (see the case of PAA150 on Figure 3.3[1]).

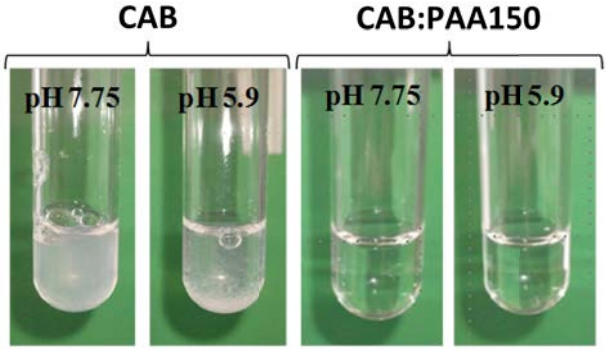


Figure 3.3: Visual aspect of 5h-old solutions in renaturation buffers of urea-denatured CAB or mixed urea-denatured CAB:PAA150 (either in 10 mM Tris-HCl pH 7.75 or 10 mM MES pH 5.9).

To quantify the protection against CAB aggregation, the concentration of CAB in solution was measured by UV-visible spectroscopy at 280 nm before and after ultracentrifugation for 10 minutes at 200,000×g. Ultracentrifugation eliminates aggregates larger than *ca.* 100 nm, so that only relatively small species remain in the supernatant. By comparing the concentration before and after ultracentrifugation, one can estimate the amount of soluble protein, S (either under the form of monomer, complexes or small oligomers), via the relationship:

$$S = 100 \cdot \frac{[\text{CAB}]_{\text{after ultracentrifugation}}}{[\text{CAB}]_{\text{before ultracentrifugation}}} \tag{3.1}$$

Solubility values obtained after 5 hours of refolding in the presence or not of polymers, at both pHs, are reported in Table 3.1. As can be seen, solubilities above $\sim 80\%$ in the presence of PAA150 or PAA150-3C18 clearly contrast with the poor solubilities obtained for CAB alone, typically below 25%. These robust observations indicate that protection against aggregation was achieved in mixed CAB:polymers solutions at 1:1 wt/wt ratio.

[1]Similar pictures were obtained for PAA150-3C18 or PAA150-3C6azo added at 1:1 weight ratio compared to urea-unfolded CAB prior to dilution in buffer (not shown).

Table 3.1: Solubility after 5 hours of incubation of 25 mg.mL^{-1} 10M urea-denatured CAB diluted 40× at time zero (to reach an incubation concentration of 0.6 mg.mL^{-1}) in aqueous renaturation buffers (either 10 mM Tris-HCl pH 7.75 or 10 mM MES pH 5.95) in the absence or presence of polymers (added at 1:1 wt/wt ratio).

	pH 7.75	pH 5.9
no additive	19–25	19
1/ STS, 2/ Me-β-CD[a]	67	nd
PAA150	87	92
PAA150-3C18	92	83

[a] The line quoted STS, Me-β-CD corresponds to the procedure of renaturation with sodium tetradecylsulfate surfactant as implemented by Hanson and coll. [161]
nd: not determined

3.2.2 Evidence for CAB:polymer association and variation of the size of associates during renaturation (light scattering study)

The intensity scattered at the angle of 90°by urea-denatured CAB:polymer mixtures diluted in refolding buffers is indicative of the evolution of aggregates during renaturation. Solutions of urea-denatured CAB that were diluted (0.6 mg.mL^{-1} final concentration) into renaturation buffers led to an abrupt jump in scattered intensity (more than 100 fold the intensity scattered by native CAB at the same concentration, see Figure 3.4)[2]. Interestingly, the intensity scattered by diluted CAB:polymer mixtures was significantly lower, and was either constant or decreased with incubation time (Figure 3.5) confirming that CAB:polymer dispersions were stable or evolved toward the formation of smaller objects.

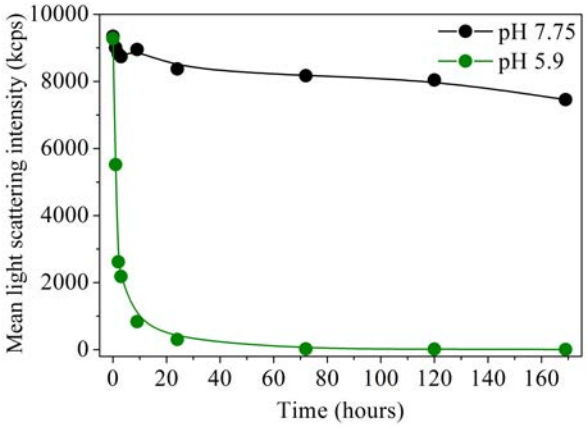


Figure 3.4: Time-dependence of the light scattering intensity of solutions of 10M urea-denatured CAB (25 mg.mL^{-1}) diluted to 0.6 mg.mL^{-1} into renaturation buffer (either 10 mM Tris-HCl pH 7.75 or 10 mM MES pH 5.9).

[2]N.B.: The drop of intensity at hours-long incubation time in Figure 3.4 (CAB alone) is not representative at pH 5.9 of the average contribution of CAB because the micrometer-large aggregates formed in these conditions sedimented and escaped the illuminated region in the scattering cell.

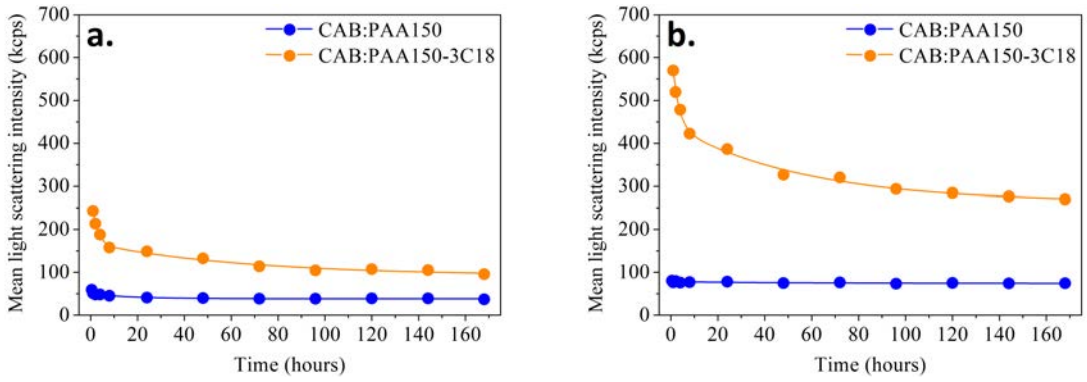


Figure 3.5: Time-dependence of the light intensity scattered after 40× dilution at time zero of a urea-denatured mixed CAB:polymer solution (1:1 wt/wt ratio) into the renaturation buffer at pH 7.75 (a.) or pH 5.9 (b.). Final protein concentration in the refolding buffer: 0.6 mg.mL^{-1}. The lines are guides to the eye.

In CAB:PAA150 mixtures (1:1 wt/wt), the light scattering intensity was constant over a week (Figure 3.5). It was almost equal to the sum of the intensity scattered by mixtures of native CAB with PAA150 (see the normalized intensity values close to 1 at t=168h in Table 3.3). Intensity scattered by solutions prepared from unfolded CAB:PAA150-3C18 mixture was initially up to 5-fold higher than that measured in native CAB:PAA150 solution, but it decreased slowly over a few days. After a week of incubation, the scattered intensities coincided with the intensity of the corresponding native CAB:PAA150-3C18 mixture (Table 3.3). It is important to point here that the scattering by mixed native CAB:polymers contained in several cases a significant contribution from complexes. We thus observed a gradual convergence of the scattering by urea-unfolded CAB:polymer mixtures toward the intensities scattered by complexes of native CAB with polymers.

Scattering by mixtures of native CAB and polymers, CAB or polymer alone (at the same concentration) were indeed indicative of the formation of native CAB:polymer complexes (data reported in Table 3.2). The presence of complexes is detected when the scattering by mixed native CAB:polymer is significantly above the sum of intensities scattered by solutions of CAB alone and polymer alone. This situation clearly occurred in all mixtures prepared at pH 5.9, and in CAB:PAA150-3C18 at pH 7.75. Within experimental errors (due to scattering by dust in weakly scattering CAB solutions) PAA150 at pH 7.75 (0.6 mg.mL^{-1}) did not bind to CAB. An increase of the order of uncertainty suggests minor formation of complexes with PAA150-3C6azo at pH 7.75.

The apparent hydrodynamic radius of the scattering species was determined by dynamic light scattering measurements. Refolding in the presence of polymers produced dispersions of objects of $R_h \sim$ 20-40 nm that were dominant in term of the fraction of collected intensity (Table 3.3). The radii of PAA150 (about 12-13 nm) and PAA150-3C18 (about 40 nm) measured by DLS are in the same range as the radius of objects present in the diluted urea-unfolded CAB:polymer solutions, which suggests the stabilization of CAB under the form of associates with one or few polymer chains.

In the case of light-responsive polymers, the scattering intensity depended on the isomerization of azobenzene side groups (Figure 3.6). Data indicate that exposure to UV light (which switches the chain in a more polar predominantly *cis* form) triggered the dissociation of complexes with CAB during renaturation (and also in native CAB:polymer solutions, see Table 3.2). When they were kept in the dark (*trans* isomer of the azobenzene

Table 3.2: Scattered intensity (kcps) by native CAB and polymer solutions and native CAB:polymer mixtures at pH 7.75 and pH 5.9 ([CAB] = [polymer] = 0.6 mg.mL^{-1}). Errors are ± 2 kcps.

	pH 7.75		pH 5.9	
	no CAB	CAB	no CAB	CAB
no additive	–	10	–	11
PAA150	25	29	13	76
PAA150-3C18	38	64	39	263
PAA150-3C6azo dark	20	38	12	62
PAA150-3C6azo UV	16	32	9	42

Table 3.3: Characteristic features determined by light scattering measurements of mixed urea-denatured CAB:polymer solutions (1:1 wt/wt ratio), diluted to 0.6 mg.mL^{-1} in 10 mM Tris-HCl pH 7.75 or 10 mM MES pH 5.9 and incubated for one week (t=168h).

Additive	Intensity at t=168h (kcps)		Normalized intensity[a]		R_h at t=168h (nm)	
	pH 7.75	pH 5.9	pH 7.75	pH 5.9	pH 7.75	pH 5.9
PAA150	39	74	1.34	0.98	28.6	22.6
PAA150-3C18	107	276	1.67	1.05	41.6	38.1
PAA150-3C6azo dark	47	62	1.24	1.00	155	48.5
PAA150-3C6azo UV	34	44	1.06	1.05	nd	nd

[a] The normalized intensity is the raw scattered intensity divided by the intensity scattered by mixed native CAB:polymer solutions at the same concentrations.

groups) mixtures of urea-unfolded CAB:PAA150-3C6azo showed an initial high scattering that gradually decreased as in other CAB:polymer systems (Figure 3.6). When UV light (365 nm, 1 mW.cm^{-2}) was shone on the solutions during incubation in the refolding buffer, the intensity dropped down more rapidly just after exposure to light (decrease by ∼30% compared to samples kept in the dark (Figure 3.6). Photo-induced intensity drop occurred in either refolding buffers at pH 5.9 or 7.75, and at short time (2 hours which is at a time of incomplete renaturation, see below) or longer time (24 hours) of incubation. The UV-triggered decrease of scattered intensity indicates that complexes between the polymer and CAB were dissociated upon *trans* to *cis* isomerization of the azobenzene side groups, presumably because of a weakening of hydrophobic association (the *cis* isomer is more polar than the *trans* one). The scattered intensity of samples subjected to UV light then re-incubated in the dark for a few hours reached again a higher value, similar to that of samples kept in the dark for the whole refolding (not shown). *In situ* variation of hydrophobic association has accordingly a significant impact on the capture/release of the protein.

It is worth noting that signals measured in the presence of hydrophobically-grafted polymers evolved rapidly during the first day, and slowly but continuously over one week, suggesting that complexes re-organize on time-scales that are far longer than

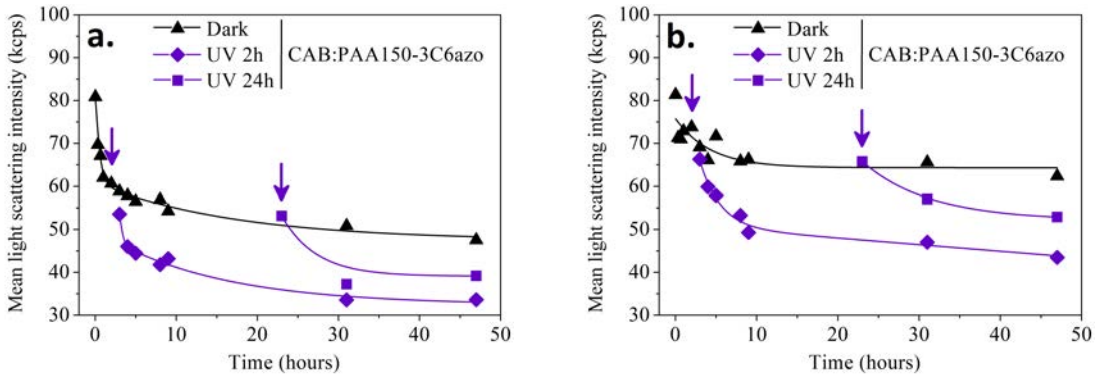


Figure 3.6: Time-dependence of the light intensity scattered after 40× dilution at time zero of a urea-denatured mixed CAB:PAA150-3C6azo solution (1:1 wt/wt ratio) into the renaturation buffer at pH 7.75 (a.) or pH 5.9 (b.). "Dark" refers to samples kept in the dark during the experiment, "UV 2h" (resp. "UV 24h") refers to samples irradiated with UV light after 2 hours (resp. 24 hours) of incubation in the dark (arrows mark the beginning of UV irradiation). Final protein concentration in the refolding buffer: 0.6 $mg.mL^{-1}$. The lines are guides to the eye.

the typical characteristic refolding time of CAB alone (half time of *ca.* 10-12 minutes from literature, and 2-3 hours from our measurements of activity recovery, see next section). Slow kinetics of renaturation has already been reported in the presence of detergents and has been attributed to long time-scales equilibration (days to months) in protein:surfactant systems [335].

3.2.3 Measurement of sizes by fluorescence correlation spectroscopy during refolding

Fluorescence correlation spectroscopy (FCS) measurements were performed to characterize the presence (and hydrodynamic radii) of complexes at higher dilutions, that are below the sensitivity limit of light scattering (see details on the technique in Appendix B). As opposed to other techniques that enable to determine the radius and fractions of protein:polymer associates (such as light scattering, NMR, SEC), FCS is the only one to combine selectivity (detection of fluorescently-labelled entities), high sensitivity (µM range) with no perturbation of equilibrium (no separation). Size measurements by FCS are indeed specific to CAB-containing objects, as only fluorescently-labelled CAB (FITC-CAB, 0.01 $mg.mL^{-1}$, see Appendix A for the labelling procedure) emits a signal. Unlabelled polymers, since they are not fluorescent, are invisible, except when bound to at least one FITC-CAB molecule. Apparent radii are thus a translation (using the Stokes-Einstein relationship) of the rate of diffusion of CAB-containing species (CAB monomers, oligomers, aggregates, or complexes with polymer chains). The final concentration of 0.01 $mg.mL^{-1}$ in FCS measurements was the highest one that did not saturate our detector.

Complexes with native or non-native CAB (prior to refolding)
The hydrodynamic radius of native CAB alone (no polymer) was measured below 3 nm (Table 3.4), which is close to values reported in the literature [330, 336]. Within

Table 3.4: Hydrodynamic radius R_h of native or 10M urea-denatured FITC-CAB measured by FCS in the absence or presence of polymers at 1:1 wt/wt ratio. Protein concentration: 0.01 mg.mL^{-1}).

	pH 7.75	pH 5.9	10M urea
CAB	2.3 ± 0.2	2.9 ± 0.3	3.2 ± 0.6
CAB:PAA150	2.1 ± 0.2	2.7 ± 0.4	2.9 ± 0.7
CAB:PAA150-3C18	2.7 ± 0.6	3.1 ± 0.2 106 ± 2	2.5 ± 0.6

experimental uncertainties, the same R_h was recorded in mixed native CAB:polymer solutions at pH 7.75. Neither PAA150 nor PAA150-3C18 interacted with native CAB at pH 7.75 and 0.01 mg.mL^{-1} concentration conditions. At pH 5.9, larger species were detected when the hydrophobically-modified PAA150-3C18 was used (R_h = 106 nm), pointing thus to formation of complexes of native CAB with PAA150-3C18. In 10M urea, the radius of CAB in the absence of polymer was slightly increased to 3.2 nm, as expected due to unfolding of the protein. In the presence of polymers, R_h remained close to that of CAB alone regardless of the polymer, pointing out that polymers at 0.01 mg.mL^{-1} did not associate with the unfolded protein in 10M urea.

To sum up, measurements on native or unfolded CAB:polymer mixtures globally indicate that polymers do not associate with native CAB nor 10M urea-unfolded CAB, except in the one case of PAA150-3C18 at pH close to the protein's pI (pH 5.9). CAB:PAA150 complexes detected by light scattering at pH 5.9 (CAB at 0.6 mg.mL^{-1}, see Section 3.2.2) are likely dissociated by the dilution.

Complexes during refolding

Similar size measurements carried out during refolding of urea-denatured FITC-CAB[3] point to a lack of complexes with PAA150 and presence of complexes with PAA150-3C18 (Figure 3.7). In the absence of polymer, and regardless of pH and incubation time, the measured radius was ∼2-3 nm, a size close to values of native CAB, which means that no aggregation was observed (Figure 3.7). A higher dilution compared to experimental conditions used for light scattering measurements and the covalent attachment of FITC presumably favour a higher solubility and better dispersion of the protein alone. Protein concentration is notably known to play an important role in CAB aggregation (for instance, partially folded intermediates do not form aggregates in 2M guanidinium chloride when the protein concentration does not exceed 0.3 mg.mL^{-1} [332, 337]).

Fluorescent objects larger than CAB monomers were present only in urea-denatured CAB:PAA150-3C18 mixed system. Since we showed that the polymers at the same concentration did not bind to urea-denatured CAB neither to native CAB (see Table 3.4), notably at pH 7.75, this result demonstrates a selective interaction of PAA150-3C18 with conformers of CAB formed during refolding.

[3]10M urea-denatured FITC-CAB:polymer at 1.35 mg.mL^{-1} brought to 70°C for 6 minutes, then subjected to 135 fold dilution in refolding buffer following to reach 0.01 mg.mL^{-1} and incubated at room temperature.

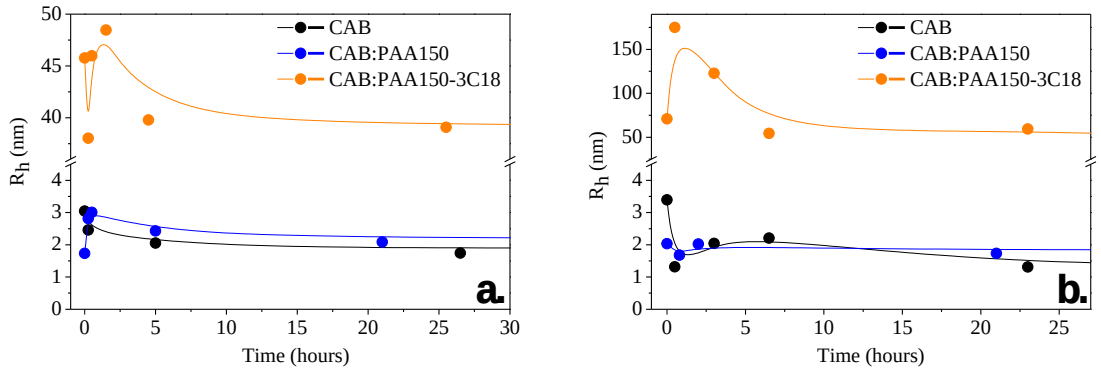


Figure 3.7: Time-dependence of the hydrodynamic radius measured by FCS in solutions of urea-denatured FITC-CAB during refolding in 10 mM Tris-HCl pH 7.75 (a.) or 10 mM MES pH 5.9 (b.) in the absence or presence (1:1 wt/wt ratio) of polymers. Dilution factor of 135 of the 10M urea solution in aqueous buffers, reaching a final protein concentration of 0.01 mg.mL^{-1}. The lines are guides to the eye.

3.2.4 Conclusion from solubility, light scattering and FCS studies

In conclusion, estimations of the size of dispersed species formed in CAB:polymer, and urea-unfolded CAB:polymer solutions show that all polymer can form complexes with partly-folded conformers of CAB at pH 5.9 (close to the protein's pI) and concentration of *ca.* 1 mg.mL^{-1}. This association increases the solubility of intermediate folding states of CAB formed during renaturation (avoiding aggregation). At pH 7.75 the association appears weaker, and requires the presence of hydrophobic side group to stabilize a detectable fraction of complexes. Dilution to 0.01 mg.mL^{-1} is also sufficient to dissociate the complexes (except with PAA150-3C18). In most cases, the complexes appear marginally stable.

From size measurements, we know that CAB is released in solution as small objects (3 nm radius) with a size comparable to the size of monomers. This does not however give any information about the structure (folding) of these soluble species. Study of the recovery of native-like protein structure and regain of activity is the purpose of the next section.

3.3 Polymers allow recovery of a native-like and active protein

3.3.1 Secondary structure recovery monitored by circular dichroism

The secondary structure of CAB (either at pH 7.75 or pH 5.9) in the presence or not of polymers can be determined by circular dichroism (CD). As references, CD spectra of native CAB mixed or not with polymers were measured and are shown in Figure 3.8. The spectrum of native CAB alone was consistent with a predominant β-sheet structure (broad minimum between 210 and 220 nm). The content of secondary structures was estimated using the yet unpublished deconvolution software BestSel developed by Micsonai *et al.* [338] (see Appendix B for details). Calculations gave values very close to the expected ones (see Table 3.5). No modifications were observed when PAA150 was added at 1:1

wt/wt ratio at either pH 5.9 or 7.75 (Figure 3.8 and Table 3.5).

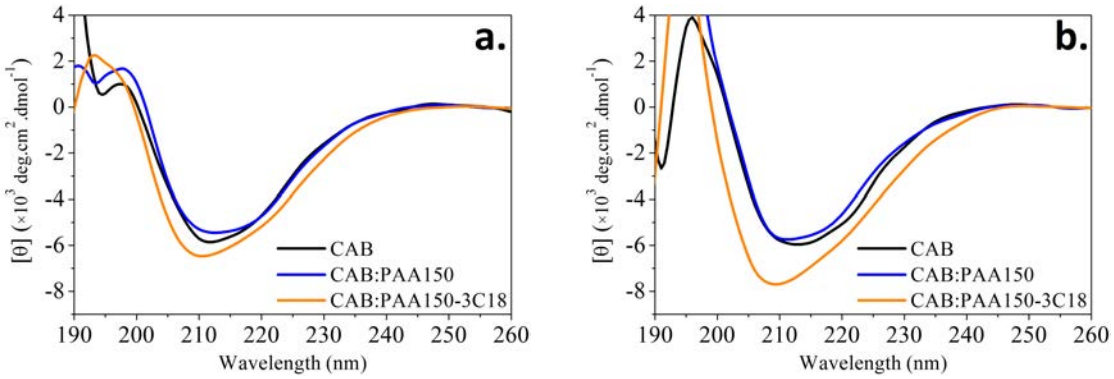


Figure 3.8: Far-UV CD spectra of native CAB (0.1 mg.mL^{-1}) at pH 7.75 (a.) or pH 5.9 (b.) in the absence or presence of polymers (added at 1:1 wt/wt ratio).

Table 3.5: Secondary structure content of native CAB in the presence or not of polymers (1:1 wt/wt ratio) at pH 7.75 or pH 5.9 obtained from the BestSel analysis ([CAB] = [polymer] = 0.1 mg.mL^{-1}).

Polymer	pH 7.75				pH 5.9			
	α-helix	β-sheet[a]	Turn	Coil	α-helix	β-sheet[a]	Turn	Coil
No polymer	11	34	12	42	11	39	11	39
PAA150	9	37	13	42	13	37	12	38
PAA150-3C18	15	30	13	41	17	24	14	41

[a] "β-sheet" refers to anti-parallel β-sheet structures, parallel β-sheets are not shown (it is the complement to 100% of the sum of secondary structures shown in the table)
nd: not determined

PAA150-3C18 affected the CD spectrum of CAB and induced an increase in the α-helix content to the detriment of β-sheet structural elements. This suggests that hydrophobic association with CAB destabilizes the native folding, a trend that is reinforced at pH 5.9, namely in conditions where the net charge of CAB is lower (making interaction with the polyanion chain less repulsive). Accordingly, CD measurements confirm that the complexation of native CAB by PAA150-3C18 involves both hydrophobic and electrostatic interactions. The same experiment carried out in the presence of PAA150-3C6azo (in the dark) showed no sign of perturbation of secondary structure [Ph.D. J. Ruchmann, unpublished results]. A specific association may thus develop between the long alkyle C18 chains and CAB.

When the protein was unfolded in 10M urea, the CD spectrum showed the characteristic shape of an unfolded polypeptide with a marked minimum at *ca.* 200 nm (Figure 3.9). PAA150 and PAA150-3C6azo did not affect the CD spectrum of unfolded CAB, while PAA150-3C18 had some influence, notably the minimum at 200 nm was not as pronounced and a shoulder appeared at 220 nm. Accordingly, the C18-modified PAA derivative interacts with the unfolded protein in urea.

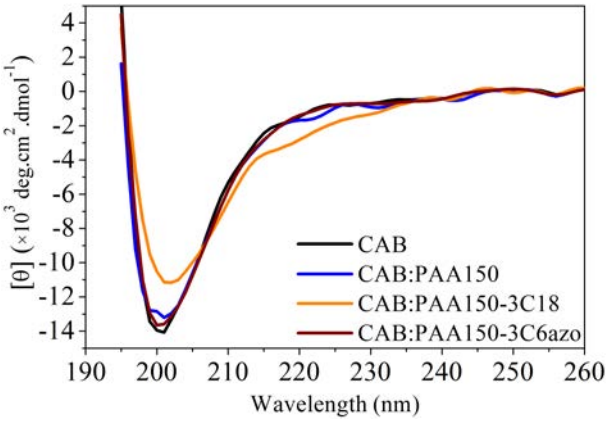


Figure 3.9: Far-UV CD spectra of 10M urea-unfolded CAB (0.1 mg.mL^{-1}) in the absence or presence of polymers (added at 1:1 wt/wt ratio).

To estimate the degree of refolding of CAB in the presence of poly(acrylate) derivatives, we recorded CD spectra at increasing incubation times after a 250 fold dilution of urea-unfolded CAB (25 mg.mL^{-1}, with or with no polymer) into aqueous refolding buffers (see Figure 3.11, same renaturation condition as for light scattering experiments discussed above). According to Hanson, refolding in the presence of a residual urea concentration of 0.04M is expected to be similar to that occurring in water [161].

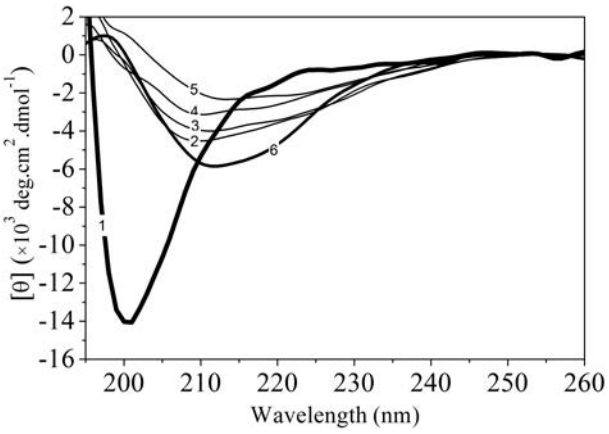


Figure 3.10: Time-dependence of far-UV CD spectra of urea-unfolded CAB during refolding in the absence of polymers. The protein, initially at 25 mg.mL^{-1} in 10M urea is diluted at time zero in aqueous buffer (10 mM Tris-HCl pH 7.75) to reach a final concentration of 0.1 mg.mL^{-1}. 1: 10M urea-denatured CAB, 2: t=0, 3: t=1h, 4: t=24h, 5: t= 168h, 6: native CAB.

In the absence of polymers, measurements could not be carried out at pH 5.9 because of the rapid aggregation of the protein resulting in high turbidity (see above). At pH 7.75, the refolding procedure without PAA additives yielded less turbid (but still turbid) solutions. In these polymer-free conditions, the CD signal gradually diminished during incubation and ellipticity was always smaller than the one measured for native CAB (Figure 3.10), which is likely due to the gradual aggregation of a fraction of the protein.

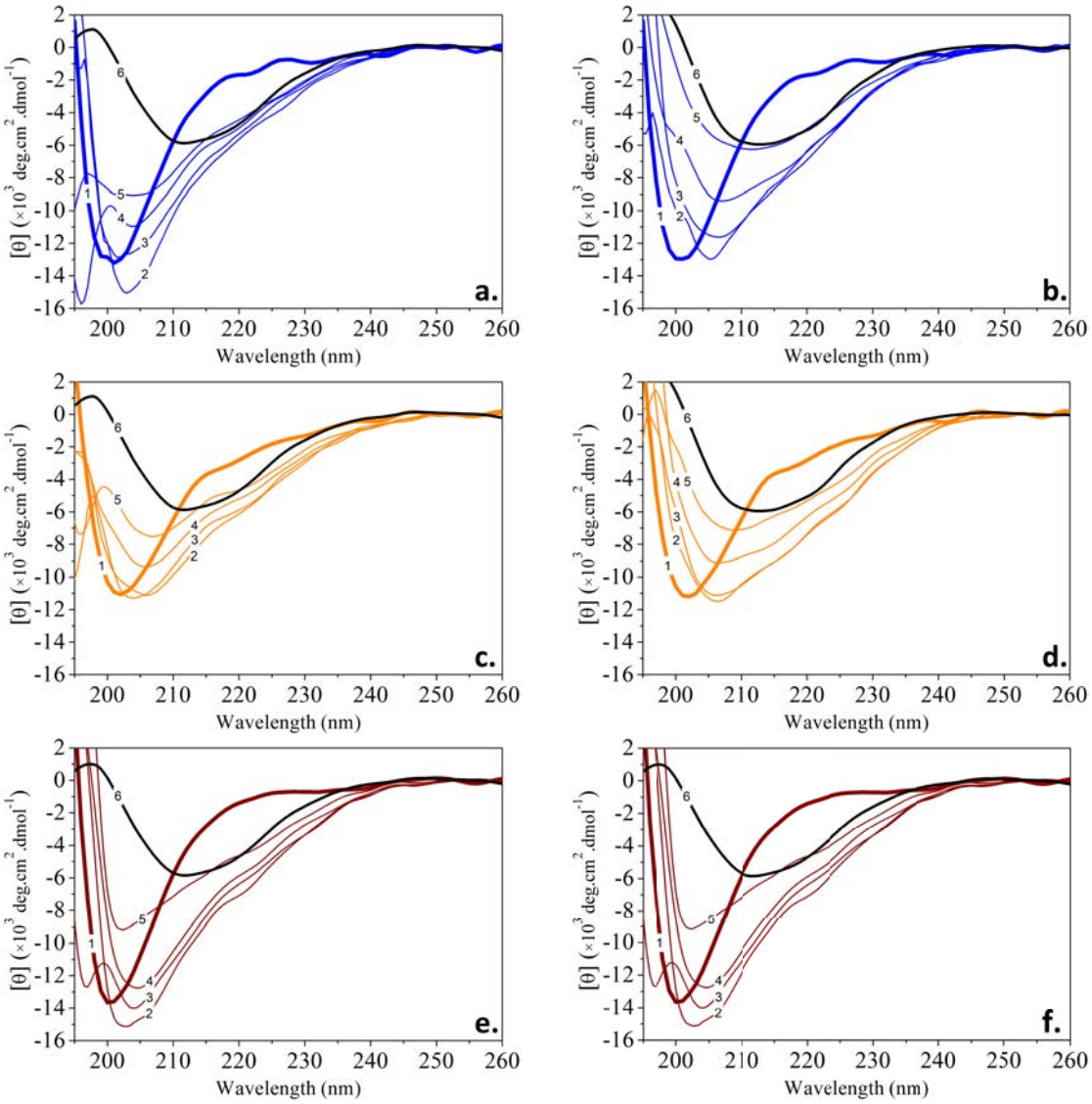


Figure 3.11: Time-dependence of far-UV CD spectra of CAB during refolding in the presence of PAA150 (a., b.), PAA150-3C18 (b., d.) or PAA150-3C6azo in the dark (e., f.) at 1:1 wt/wt ratio, either at pH 7.75 (a., c., e.) or pH 5.9 (b., d., f.). The protein, initially at 25 mg.mL^{-1} in 10M urea with polymer is diluted at time zero in aqueous buffer (10 mM Tris-HCl pH 7.75 or 10 mM MES pH 5.9) to reach a final concentration of 0.1 mg.mL^{-1}. 1: 10M urea-denatured CAB:polymer mixture, 2: t=0, 3: t=1h, 4: t=24h, 5: t= 168h, 6: native CAB.

Interestingly, the spectrum observed at time "t=0" (in practice ∼2 minutes after dilution), was the closest one to that of native CAB, within the time series, suggesting a rapid folding of the protein (in consistency with the reported half-times of folding for CAB alone).

In the presence of PAA150 or PAA150-3C18, CD spectra during the refolding procedure (Figure 3.11) indicate that the secondary structure gradually evolved for days. At pH 7.75, days-long incubation was not sufficient to recover the CD spectrum of native

CAB, suggesting that a fraction of CAB stayed trapped in misfolded states. This may occur either because of oligomerization (objects of radii < 40 nm were detected by DLS and FCS, see above) or due to association with polymers. After a week of incubation with PAA150 at pH 5.9 spectra closely resembled that of the native CAB, indicating that the recovery of the secondary structure is possible but slow. With PAA150-3C18, the CD spectrum at time 7 days approached – but was never identical to – the one of native CAB (note that the reference "native" spectrum corresponds here to a solution of native CAB without polymer). It seemed to reach though the spectrum of native CAB mixed with PAA150-3C18.

In addition, the refolding rate depended on the nature of polymer and of pH. At pH 7.75, the ellipticity increased faster in the presence of PAA150 than in the presence of PAA150-3C18 (between t=0 and t=1h). A single minimum at 205 nm was observed in spectra with PAA150, whereas a marked shoulder was visible at 220 nm in the presence of the hydrophobically-modified PAA150-3C18. It is also noticeable that the minimum value of the mean residue ellipticity at time quoted t=0 (in practice at *ca.* 2 minutes after dilution) was lower in the presence of PAA150 than with PAA150-3C18. These results suggest that different folding intermediates are contributing to the spectra according to the hydrophobic or hydrophilic nature of the polymer. Similar comments apply to the data at pH 5.9, even if the difference between the two polymers was less pronounced in this case. At pH 5.9, the shoulder at 220 nm was observed irrespective of the nature of polymer. The CD signature at pH 5.9 in mixed CAB:PAA150 solution resembled that observed in mixed CAB:PAA150-3C18 solutions at pH 7.75.

Interestingly, refolding in the presence of PAA150-3C6azo was analogous to that obtained in the presence of PAA bearing no hydrophobic side groups. At pH 7.75, similar shapes of CD spectra were obtained all along the refolding, and a similar refolding kinetics was observed, with a fast increase of the ellipticity between t=0 and t=1h.

The long refolding kinetics observed here when compared to CAB alone suggest that the rate-limiting step is not the same with and without polymers. As there is little reason for the variation of proline isomerisation kinetics, we propose that association/dissociation of CAB onto polymer chain control the slow rate of folding. The similarly days-long variation of the size of CAB:polymer complexes speaks in favour of this hypothesis.

In conclusion, results from CD highlight the importance of both Coulomb and hydrophobic interactions on a controlled recovery of native-like secondary structure, and suggest that binding on amphiphilic copolymers can significantly perturb the equilibrium folding (including in urea) and may not be favourable to native-like structure recovery (additional CD and fluorescence data on equilibirum unfolding of CAB in urea:water solutions confirms that polymers, including PAA150, decrease the conformational stability of the enzyme, see Appendix C).

3.3.2 Activity recovery

3.3.2.1 Time of renaturation

CAB is known to catalyse the hydrolysis of *para*-nitrophenylacetate (*p*-NPA into *para*-nitrophenol and ethanoic acid [320]. *p*-nitrophenol is yellow, unlike the reactant, which is colourless. UV-visible spectroscopy can thus be used to determine the rate of the hydrolysis, by measurement of the increase of absorbance at 400 nm, $A_{400\text{ nm}}$ [320]. The slope of the $A_{400\text{ nm}}$ time-variation, p, is related to the enzymatic activity, T, via the formula:

$$T = \frac{p - p_{autolysis}}{p_{native} - p_{autolysis}} \tag{3.2}$$

where p is the initial slope of the 400 nm absorbance time-variation for the studied sample, $p_{autolysis}$ is the slope obtained in the absence of protein (due to the spontaneous hydrolysis of p-NPA) and p_{native} is the slope for the native protein alone.

To assess the recovery of the native state, we measured the rate of hydrolysis of *para*-nitrophenylacetate (p-NPA) at fixed concentration of CAB (0.03 mg.mL^{-1}) and pH 7.75. The same refolding protocol as described above was used (10M urea-unfolded 25 mg.mL^{-1} CAB solution, supplemented or not with polymers at 1:1 wt/wt ratio, diluted at t=0 to 0.6 mg.mL^{-1} or 0.03 mg.mL^{-1} in 10 mM Tris-HCl pH 7.75 or 10 mM MES pH 5.9). Since the enzymatic activity of CAB is strongly dependent on pH and the protein is completely inactive at pH 5.9 [320], samples renaturated at pH 5.9 were diluted to 0.03 mg.mL^{-1} in a 50 mM Tris-HCl pH 7.75 buffer prior to activity measurements. The measured rates were normalized by the rate obtained with a fresh aqueous solution of native CAB (prepared in buffer and without urea) to obtain the % activity recovered.

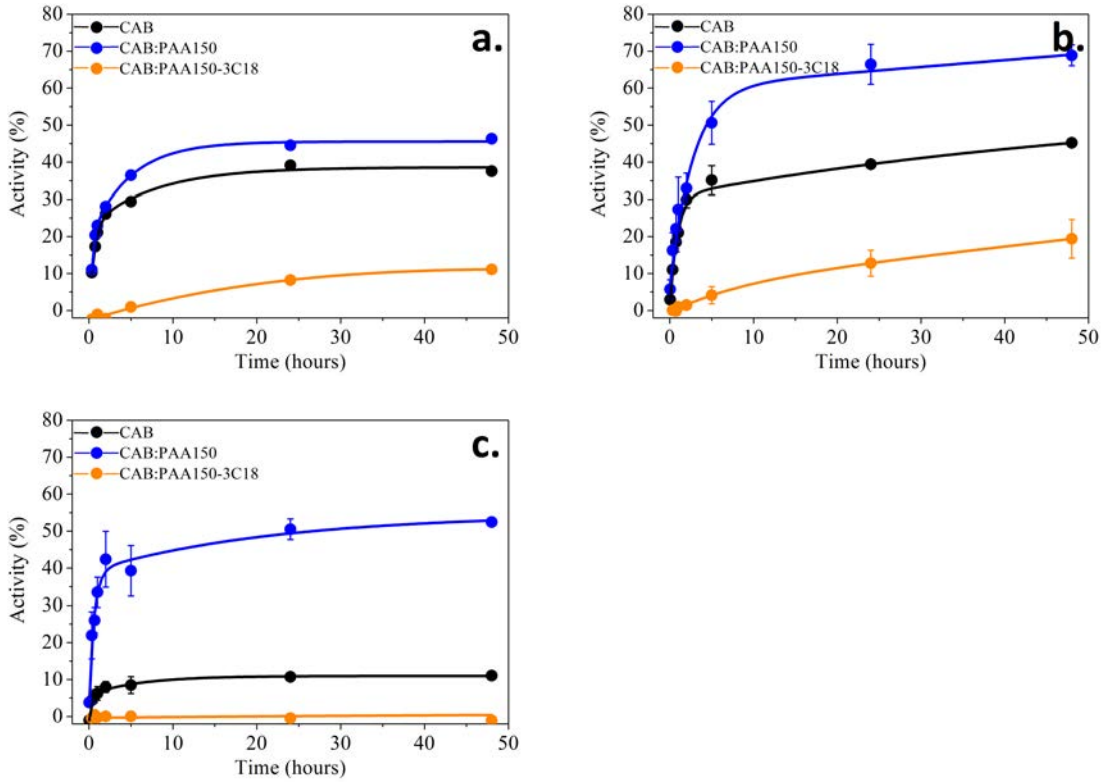


Figure 3.12: Time-dependence of enzyme activity recovery in mixed urea-denatured CAB:polymer (1:1 wt/wt) solutions after incubation at 0.03 mg.mL^{-1} (a.) or 0.6 mg.mL^{-1} (b.) in 10 mM Tris buffer 10 mM pH 7.75 or (C) at 0.6 mg.mL^{-1} in 10 mM MES pH 5.9. Reference measurement in the absence of polymers is quoted "CAB" in the figures. At time zero, the 25 mg.mL^{-1} CAB in 10M urea, with or with no polymer, is diluted in the renaturation buffer. Lines are guides to the eye.

The activity gradually increased with increasing incubation time in renaturation buffers, and reached a pseudo-plateau at incubation times > 5 hours. In the absence of polymers, the recovery at time 5 hours was typically ∼30% (pH 7.75) or ∼10% (pH

5.9). Similarly low degrees of recovery were reached when incubations were performed in the presence of polymers at low concentration (0.03 mg.mL^{-1}). In contrast, incubation with PAA150 at higher concentration (0.6 mg.mL^{-1}) clearly improved the renaturation yield, though similar shape of the regain of activity as a function of time are observed. Better activity recovery with PAA150 at higher concentration ($\sim$ 1 mg.mL^{-1}) is a robust indication of the protective role of the polymer that is more efficient than limiting inter-protein contacts by simple dilution. At lower concentration, CAB:polymer association is presumable weakened and the polymer no longer has an impact on the renaturation yield of the enzyme.

3.3.2.2 Influence of polymer/protein weight ratio

To assess the effect of CAB:polymer ratio, we fixed somewhat arbitrarily the incubation time at 5 hours, and the protein concentration during incubation at 0.6 mg.mL^{-1}, corresponding to conditions that ensured significant regain of activity when it occurred. The regain of activity depended on the PAA150/CAB weight ratio (Figure 3.13). The activity increased gradually with increasing the amount of PAA150 up to a threshold polymer/CAB ratio of *ca.* 1, indicating that the 1:1 wt/wt ratio used all along the present study was close to optimal composition to enhance the renaturation. (N.B.: no improvement was obtained at 4:1 wt/wt ratio, not shown).

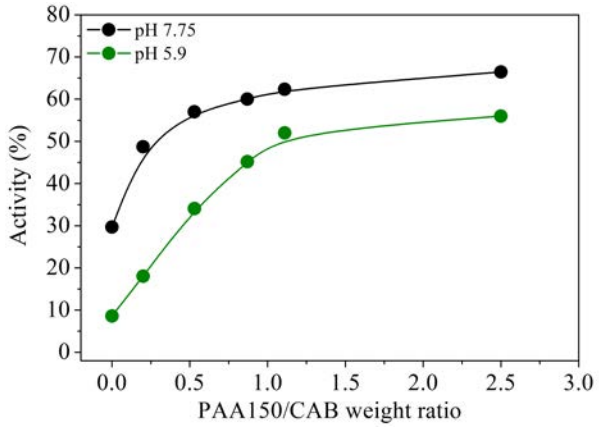


Figure 3.13: Dependence of enzyme activity on PAA150/CAB weight ratio after a 5-hours long renaturation of urea-denatured CAB (0.6 mg.mL^{-1}). The polymer is added in the 10M urea-denatured CAB solution prior to dilution at time zero of the protein in renaturation buffer (either 10 mM Tris-HCl pH 7.75 or 10 mM MES pH 5.9). The lines are guides to the eye.

3.3.2.3 Role of the hydrophobicity of the polymers

To compare the efficiency of copolymers carrying different hydrophobic side groups (aliphatic C18 or azobenzene), we fixed the composition of mixed CAB:polymer solutions (1:1 wt/wt ratio, 25 mg.mL^{-1} in 10M urea) and incubation conditions (dilution to 0.6 mg.mL^{-1}, incubation for 5 hours). The degree of activity recovery spanning a range between 4% and 60% in Table 3.6 points to the importance of polymer structure. Using PAA150 yielded a similar recovery as the reference surfactant-based procedure (STS and

cyclodextrine from Hanson and Gellman [161]). But at variance with renaturation in the presence of surfactants, no stripping step (*i.e.* sequestration of STS in cyclodextrin) was needed in the presence of PAA150. This indicates that either CAB is active under the form of complexes with the polymer chains or CAB:PAA complexes spontaneously dissociate (see size measurements above: no bound CAB are present at days-long incubation time).

Table 3.6: Enzymatic activity after 5 hours of incubation of 25 mg.mL^{-1} 10M urea-denatured CAB diluted 40× at time zero (0.6 mg.mL^{-1}) in aqueous renaturation buffers (either 10 mM Tris-HCl pH 7.75 or 10 mM MES pH 5.9) in the absence or presence of polymers (added at 1:1 wt/wt ratio).

	pH 7.75	pH 5.9
no additive	30	7-16
1/ STS, 2/ MeβCD[a]	63	nd
PAA150	58	52–56
PAA150-3C18	4–7	1–7
PAA150-1C6azo	31	nd
PAA150-3C6azo	52	nd
PAA150-5C6azo	30	nd

[a] The line quoted STS, MeβCD corresponds to the procedure of renaturation with sodium tetradecylsulfate surfactant as implemented by Hanson and coll. [161]
nd: not determined

In the presence of PAA150-3C18, activity was systematically lower than in the absence of polymer, suggesting that associations with this amphiphilic polymer hampered a correct folding or competed with the substrate for binding on the active site. Measurements on CAB freshly dissolved in aqueous buffer (no urea) in the presence of PAA150-3C18 indicated that this polymer affects the enzyme activity upon interaction with the native protein (a 17% decrease of activity is observed, see Table 3.7). This is consistent with the alteration of secondary structure observed by CD in the presence of this polymer (*vide supra*, Figure 3.8). The lack of activity recovery is thus attributed to interactions developed by PAA150-3C18 with both the unfolded and partially folded forms of CAB.

Table 3.7: Enzymatic activity of 0.03 mg.mL^{-1} native CAB in the presence of polymers (CAB:polymer 1:1 wt/wt ratio), normalized to the activity of native CAB without polymer. Errors: ±2%.

Additive	Enzymatic activity (%)
PAA150	100
PAA150-3C18	83
PAA150-3C6azo	100

In contrast, the presence of hydrophobic azobenzene groups (1-5 mol%) is not detrimental to activity recovery. In mixed CAB:PAA150-3C6azo solutions, the regain of enzyme activity was comparable to that reached in CAB:PAA150 solutions. The low degree of renaturation in the presence of PAA150-3C18 may therefore not be a general

consequence of hydrophobic binding.

3.3.2.4 Light-responsive hydrophobic groups

To assess the importance of hydrophobic interaction in mixed CAB:PAA150-3C6azo solutions, we studied the effect of *trans*-to-*cis* isomerization on the degree of renaturation. UV-light (exposure at 365 ± 10 nm, 1 mW.cm^{-2}) was shone during renaturation, at times 2 hours or 24 hours after dilution in the renaturation buffer (either pH 7.75 or pH 5.9). These conditions ensured a rapid photoisomerization of the azobenzene moieties (*ca.* 2 minutes). The degree of renaturation after shinning UV light on solutions did not markedly deviate the kinetics of activity recovery compared to that observed in mixed CAB:PAA150-3C6azo solution that were kept in the dark (variations of the order of 5%, close to experimental uncertainty, see Figure 3.14).

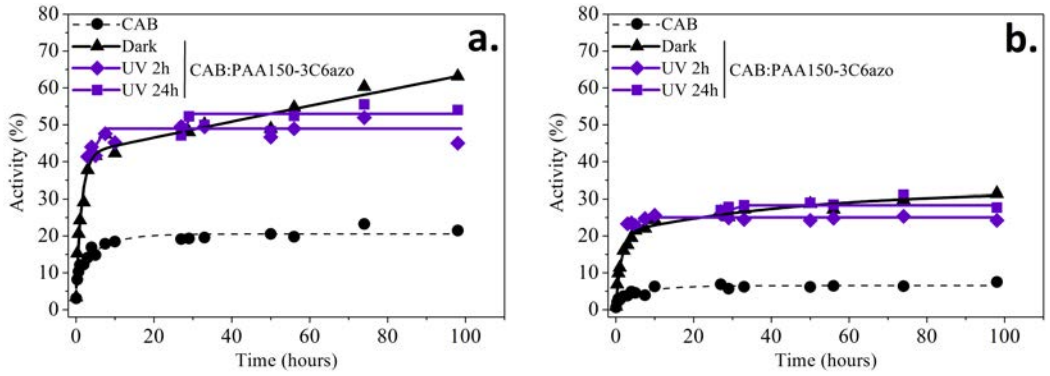


Figure 3.14: Activity recovery of urea-denatured CAB in the presence of PAA150-3C6azo (CAB:polymer 1:1 wt/wt) in the dark or after UV-light irradiation (that started at time 2 hours or 24 hours). CAB (25 mg.mL^{-1}) in 10M urea was abruptly diluted to 0.6 mg.mL^{-1} in aqueous buffers, either 10 mM Tris-HCl pH 7.75 (left) or 10 mM MES pH 5.9 (right). The lines are guides to the eye.

At long times, samples submitted to UV light showed however systematically a lower activity than the dark-adapted ones, and no drift of activity with incubation time could be observed in UV-treated samples (which differs from the slow but measurable increase in dark-adapted ones). Immediately after exposure to UV, one notice that the activity increased to values slightly above the reference activity of dark-kept sample. Recalling that UV-exposure dissociate CAB:polymer complexes (see Section 3.2.2), it is concluded that photo-release of CAB from complexes with the polymer is accompanied by a weak refolding and stops further renaturation. The azobenzene groups are nevertheless compatible with activity recovery, in contrast to C18 side groups, and they may be of practical interest to help the formation of protective complexes if the experimental conditions shield the favourable Coulomb interactions with the PAA chain (such as higher ionic strength conditions).

3.4 Conclusion: discussion on the role of Coulomb and hydrophobic associations

The results of the present study provide a clear indication that poly(acrylate) derivatives prevent massive aggregation of CAB by forming complexes with CAB refolding intermediates, while polymer chains do not associate with, or have a low affinity for, the native and the unfolded protein. Interestingly, a predominant Coulomb interaction (with PAA150) is sufficient to achieve high yield of renaturation. In this case, prevention of aggregation during folding is likely due to the formation of complexes between the polyanionic PAA and quasi neutral CAB (pH 5.9) or positively-charged patches on anionic CAB (pH 7.75, see Figure 3.15). At variance with surfactant-based renaturation, no stripping step (*i.e.* the removal of protein-bound additives) is needed, which confirms that Coulomb binding is weak and dynamic. In the present experimental conditions the concentration of protein and PAA150 chains are close to their binding affinity (FCS measurements evidenced the absence of complexes in 0.01 mg.mL^{-1} solutions). Marginal stability of complexes is probably playing a role in spontaneous (stripping-free) renaturation.

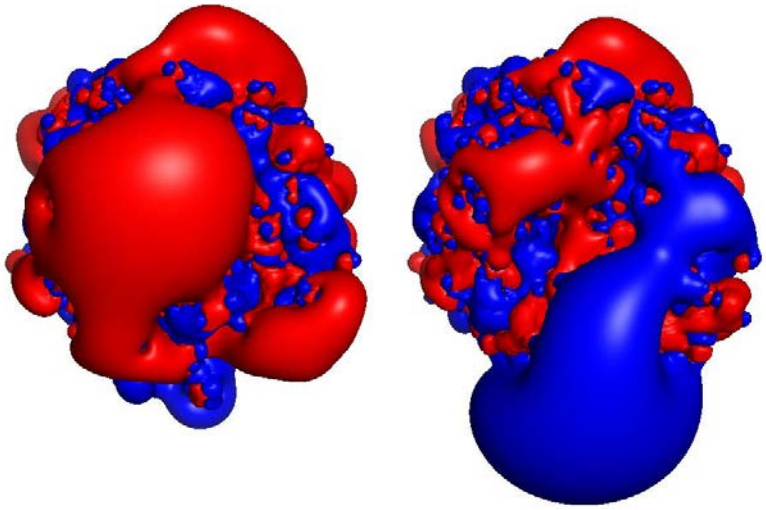


Figure 3.15: Electrostatic surface isocontour (±1kT/e) of CAB at 10 mM and pH 7.75 (left) or pH 5.9 (right). Dense positive regions (in blue) are observed at the lowest pH, while diffuse positively-charged patches are exhibited at pH 7.75.

With PAA150-3C18 or azobenzene-modified PAA150-3C6azo, an additional hydrophobic interaction increases the stability of complexes between CAB and polymers. Association with PAA150-3C18 is for instance detected by light scattering and by FCS at the lowest concentration studied. The present study suggests however that hydrophobic association does not favour renaturation. First, interaction with the octadecyl-modified chains affects the conformation of the protein (even in 10M urea) and alters the intermediate CD spectra measured during refolding, yielding to poor activity recovery. Second, when more balanced conditions of hydrophobic binding were achieved (*trans*-to-*cis* photoswitch of azobenzene groups in mixed CAB:PAA150-3C6azo solution), photo-controlled dissociation of CAB:polymer complexes had no marked contribution to the final yield of renaturation.

We conclude that balanced, photo-controlled hydrophobic association enables one to dissociate on demand hydrophobic complexes but is a marginal contributor to CAB renaturation, whereas strong hydrophobic association (PAA150-3C18) hampers renaturation and may trap the protein in an inactive state. A significant fraction of activity recovery with PAA derivatives shall thus be ascribed to slow, hours long, "self-stripping" of labile complexes with an important role of Coulomb interaction.

High renaturation yields in the presence of polymers are finally ascribed to the protection of CAB refolding intermediates against aggregation (colloidal stabilisation) that occurs massively in the absence of PAA150. In practice, we notice the low amount of polymer that is required to form protective complexes. It is another essential advantage of the complexes with polymers. In comparison to osmolytes that are typically used at molar concentration, we found that 1:1 polymer:CAB weight ratio (*i.e.* about 1:5 polymer:CAB mol/mol stoichiometry) brings an efficient protection, which corresponds to polymer used at *ca.* micromolar concentration of chains. Compared to surfactants, practical advantages of polymers include that they may be tailored to escape the need for stripping and they may be immobilized on solid support. If it can be generalized to other proteins of interest, such as manipulation of poorly stable biotherapeutics with low (hopefully non toxic) amount of additives, the principle of refolding-compatible colloidal stabilization by polyanions should find a broad range of applications (*e.g.* bioimaging and diagnostic).

Chapter 4

Chemical refolding of scFv fragmentswith poly(acrylate) derivatives

In the extending repertoire of antibody-like proteins, single-chain variable Fv fragments (scFv) are the simplest (because the smallest) fragments that retain the antigen-binding activity of its parent antibody. Their small size compared to full-length antibody is an advantage for several therapeutic or diagnostic applications. scFv are particularly well suited for *in vivo* tissue imaging (because of their high diffusivity into tissues and rapid clearance). Yet, scFv are artificially-designed proteins, which creates associated drawbacks. Expression of these artificial proteins in prokaryotes often yield inclusion bodies, thus requiring solubilization and refolding procedures. Misfolded forms and possibly the native one are easily prone to irreversible aggregation. Chemical additives conventionally added during the renaturation (urea, osmolytes) avoid the instability issues of scFv but they are efficient only at high (molar) concentrations, which hampers direct *in vivo* administration and may bias *in vitro* activity assays. In addition, as for several multi-domain proteins, the folding mechanism of scFv is complex and highly cooperative, and renaturation requires multiple steps for proper control of redox and concentration conditions, which is costly and time consuming.

In this chapter, we show that low concentrations (μM) of macromolecular additives can provide a general help for stabilizing scFv against aggregation during renaturation. We study the impact of low amounts (typically 1:1 weight ratio with the protein) of poly(sodium acrylate) derivatives on the conformation of scFv (by synchrotron-radiation circular dichroism, SCRCD) refolded from urea solutions. Aggregation and/or complexation with polymers is monitored by fluorescence correlation spectroscopy (FCS). We demonstrate that polymers preserve monomer (or oligomeric) forms of scFv during refolding, affect the folding pathway, while being compatible with conformational recovery of native-like secondary structure in aqueous environment.

Contents

4.1 Preamble: structure, use and folding of scFv 85

4.1.1 Structure of scFv fragments 85

4.1.2 scFv: an interesting format for *in vivo* tissue imaging 86

4.1.3 Stability and folding mechanism of scFv 88

4.1.4 The reference refolding protocol: role of L-arginine to prevent aggregation 93

4.2 Size of scFv during refolding 94

4.2.1 Variation of size in the absence of polymer 95

4.2.2 Do polymers limit aggregation of scFv? 97

4.3 Do polymers affect the secondary structure of scFv? 101

4.3.1 Secondary structure in water (no urea) at the end of renaturation 101

4.3.2 Folding transition: a semi-quantitative analysis 103

4.3.3 Tryptophan intrinsic fluorescence as a complement to CD study 109

4.3.4 NMR to unravel the local scFv:polymer contacts: preliminary results 110

4.4 Conclusive remarks and perspectives 113

4.1 Preamble: structure, use and folding of scFv

The use of monoclonal antibodies (mAbs) has been extended since the 1980s to *in vivo* tissue imaging. Owing to their specificity for their target, mAbs indeed allow the selective labelling of tissues, for instance tumours, with the underlying possibility to evaluate the immunotargeting efficiency of a given antibody and its half-life in the organism. The final goal is to identify metastatic tissues hardly detectable by other approaches [339]: immunolabelling indeed enables *in vivo* diagnosis and/or provides surgical assistance by allowing surgeons to visualize micro-tumours invisible to the naked eyes (the latter approach is developed by the French company SurgiMab).

However, in the context of immunoimaging, full-length IgG are not well suited because of their large size that prevents efficient penetration of tumours and results in hours- to days-long renal clearance that constraint the time between successive observations. Smaller antibody fragments are a promising alternative to full-length antibodies. For diagnostic as well as therapeutic applications, controlled labelling (fluorophores, radiolabels, drugs) is essential, and semi-artificial antibody-like formats have the advantage of being easier to tailor for a controlled coupling with a label of interest. Among them, single-chain Fv fragments (scFv) represent the simplest construct and are extensively studied as a two-domain model of the active site of antibody. This section describes the structure and properties of the scFv format in relation to practical issues (that refrain the development of scFv-based applications) and motivations of studying scFv:polymer mixed systems.

4.1.1 Structure of scFv fragments

The Fv fragment (fragment variable) of a monoclonal antibody is the smallest unit that retains the antigen-binding activity. It is composed of two immunoglobulin (Ig) domains, namely the variable part of the light (V_L) and heavy (V_H) chains, each possessing a highly conserved intra-domain disulfide bridge (see Figure 4.1). For practical applications and retention of activity, it is fundamental that the two domains remain associated at high dilution (the reported K_D values for a Fv fragment span from 10^{-9} to 10^{-6} M [340, 341]). To bias the V_H-V_L association-dissociation equilibrium towards the dimer assembly, the two domains can be covalently paired off, via a flexible peptide linker to form a single-chain Fv fragment (scFv) of $\sim$ 30 kDa molecular weight (Figure 4.1). The loss of translational freedom plays in favour of the association of the two domains [341], which becomes in general independent on dilution.

The length and amino acid composition of the linker are key elements to ensure proper V_L-V_H association and thus retention of an intact antigen-binding site. The linker has to be 3.5 nm in length (15-20 residues) and must contain stretches of hydrophilic glycine (G) and serine (S) sequences for flexibility (with potential addition of charged residues such as glutamate (Q) and lysine (K) to enhance solubility and prevent intercalation of the linker between the tethered domains during refolding) [342–345]. Shorter linkers (5 residues) make it sterically impossible to form monomers and have been used to obtain multimers, such as diabodies [346].

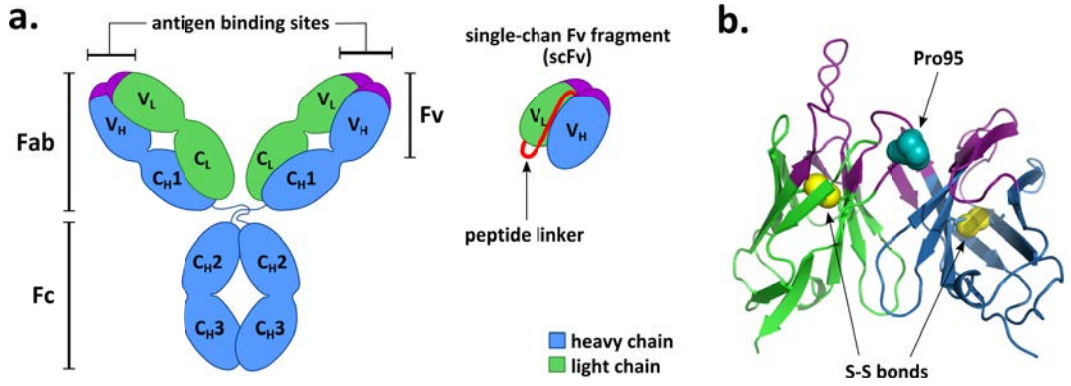


Figure 4.1: The structure of scFv. a. Schematic illustration of the scFv fragment and its context in the parent monoclonal antibody. The V_H (blue) and V_L (green) domains are joined together via a peptide linker (red); the antigen-binding site (purple) is preserved. b. Three-dimensional structure of a scFv fragment, scFv Rendomab B1 (from the corresponding crystallized Fab fragment). Each domain has highly-conserved disulfide bridges (yellow). Proline 95 (cyan) on the V_L domain is a key residue in the folding process and assembly of the two domains.

4.1.2 scFv: an interesting format for *in vivo* tissue imaging

4.1.2.1 Advantages of the scFv format for *in vivo* imaging

ScFv fragments retain the intact antigen-binding site while their smaller size compared to the parent full-length monoclonal antibody offers several advantages for therapeutic and diagnosis purposes [22, 344, 345]. They notably present a better tumour penetration [347, 348], can be fused to cytotoxic proteins or coupled to radionuclides or drugs to obtain efficient localization while their lower retention times in healthy tissues reduces their cytotoxicity [349]. In addition, their activity and production does not require post-translational glycosylation steps that can result in heterogeneity when it comes to full-length monoclonal IgG samples.

For therapeutic use, the rapid blood clearance (typically a few hours) of scFv fragments is a severe limitation since high local drug doses are often required for efficiency [22]. The lack of Fc region constitutes another major drawback, since it prevents the complement pathway activation and the recruitment of effector cells, making thus other formats better candidates than scFv. In contrast, the rapid elimination of scFv fragments from the body via kidney filtration, as well as the absence of the Fc region, are highly desirable features when it comes to *in vivo* diagnostic applications [344, 345]. They indeed result in lower immunogenicity and minimize exposure of healthy tissues to potentially cytotoxic radionuclides. scFv can easily be coupled to fluorophores, radionuclei, quantum dots or nanoparticles and therefore provide a non-invasive tool to visualize the location and distribution of a specific target.

In vivo imaging requires an optimal balance between tissue penetration and pharmacokinetics properties. Studies have shown that the optimal tumour-targeting fragments are diabodies (of $\sim$ 55 kDa molecular weight), rather than scFvs, because they combine high tissue penetration, target retention, good affinity (due to the bivalency) and fast enough blood clearance not to affect healthy tissues [344, 346]. However, scFv fragments are simpler (two domains) proteins, that can be useful models to decipher the origin

of instability in solutions, the aggregation mechanism, and folding issues found in such constructs. From the basic research point of view, scFv fragments offer tremendous advantages that make them the best suited candidates as models of antibody fragments [341]: i/ they are the smallest fragments that retain antigen-binding affinity, making it easy to read out the functionality of the folded protein; ii/ a lot of crystal structures of Fv fragments have been solved (mostly as part of easily crystallizable Fab fragments); iii/ the V_L and V_H domains can be expressed and studied separately, enabling a quantification of the contribution of the domain interactions and the linker peptide to stability, as well as an understanding of the molecular mechanisms of folding/unfolding.

4.1.2.2 The CEA's project: *in vivo* tissue imaging

The team of Didier Boquet at CEA Saclay is developing antibody-based fragments for the *in vivo* imaging of tissues, with special attention on diabodies and scFv fragments as simpler model to optimize labelling steps and refolding procedures. Several labelling strategies are being developed, such as coupling onto amines or thiols (possibly on solid matrix), or use of chelating tags.

Three different scFv fragments are used in the following:

- scFv Sha 31 is a murine fragment that recognizes the prion protein involved in the propagation of transmissible spongiform encephalopathies, which are neurodegenerative diseases. The naturally-occurring prion protein (PrP) is innocuous, but contamination with the misfolded form of the protein, PrP^{Sc} (prion protein in the Scrapie form) results in the misfolding of normal PrP and subsequent formation of insoluble fibrils that eventually leads to cellular apoptosis [350]. Sha 31 is an anti-PrP antibody that binds to the naturally-occurring PrP and presumably prevents it to interact with the PrP^{Sc} form. ScFv Sha 31 constitutes a simple model to optimize labelling procedures, it allows facile activity monitoring by ELISA assays because the fragment recognizes a peptide sequence with no particular 3D structure (that can hence be easily immobilized on multi-well plates).
- scFv 12G4 is directed against the human anti-Mullerian hormone type II receptor (hAMHR-II) that is over-expressed in malignant cancers of the genital area, and is thereby a relevant target for immunotherapy and immunolabelling of epithelial ovarian cancer. Ortega *et al.* recently described refolding protocols to produce large amounts of functional diabodies 12G4 [351].
- scFv Rendomab B1 targets the endothelin B receptor (ETBR), which is a G protein-coupled receptor that binds human endothelin peptides. ETBR is over-expressed in various diseases, notably cardiovascular diseases and tumors. The full-length anti-ETBR antibody Rendomab B1 has been recently generated and characterized by our partners at CEA Saclay [352] (see also Section E.1.2 in Chapter 5). They are now developing the corresponding fragments, diabodies and scFv, to improve pharmacokinetcis properties for *in vivo* immunoimaging.

Overall, the three fragments share common features, namely the same linker peptide made of 4 repeats of the (GSSS) stretch, a similar three-dimensional structure and some highly conserved residues (see below the sequence alignment in Figure 4.6) and a similar predicted isoelectric point (in the range 8.2-9, see Appendix D). Our study is mainly based on scFv Rendomab B1, the best characterized and which 3D structure is available (from the corresponding Fab fragment that has been crystallized).

ScFv fragments have been successfully expressed in a variety of hosts, including bacteria, yeast and plants [341]. The system that has been retained at CEA is the

cytoplasmic expression in *Escherichia Coli*. It allows the facile and rapid production of large amounts of fragment (see the expression protocol in Appendix A), but because the proteins comes in inclusion bodies, it necessitates a renaturation step to obtain the native (active) protein.

4.1.3 Stability and folding mechanism of scFv

4.1.3.1 Thermodynamic (conformational) stability of scFv fragments and folding mechanisms

The folding and conformational stability of recombinant scFv fragments have been extensively studied by Plückthun and collaborators in the 1990s (for a review, see [341]). Some general features can be derived from these seminal experiments.

Unlike single-domain globular proteins that usually follow a two-state reversible folding/unfolding equilibrium, unfolding transition of scFv is generally broad and involves several intermediate states [341]. In rare extreme cases, unfolding of each domain is largely independent and the unfolding scheme can be divided in two separated two-state transitions. Usually, however, a quantitative determination of unfolding energy is not possible, but comparison of the transition mid-points provides a rough idea of relative stabilities.

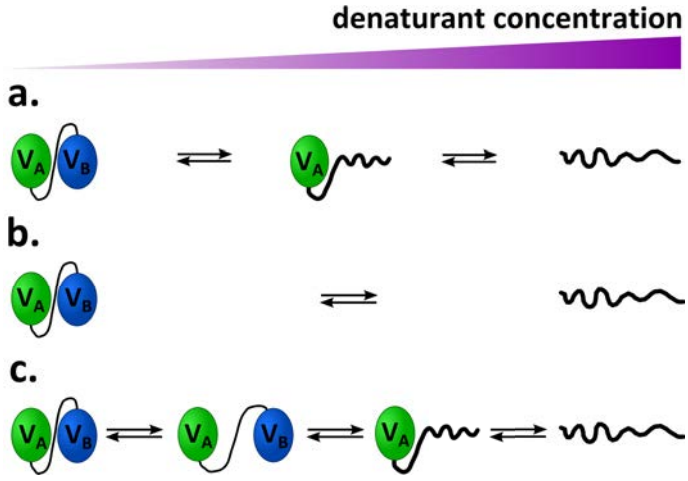


Figure 4.2: Possible equilibrium unfolding schemes of scFv fragments. a. Sequential unfolding: the more stable domain (V_A) unfolds after the less stable one (V_B). b. Simultaneous unfolding can occur when the stabilities of the two domains are of similar magnitude. c. Sequential unfolding initiated by the disruption of the V_A-V_B interface.

Studies of separate domains and of the corresponding scFv have revealed that the stability of the scFv fragment depends on the intrinsic stability of both domains but also on the stability of the V_L-V_H hydrophobic interface (contact zone ranging from 583 to 874 A^2 in size [353]). The latter has been called "extrinsic stability" by Wörn *et al.* (as opposed to the intrinsic domain stability) [341, 354]. The folding free energy contains the important contribution of intra-domain disulfide bonds (that has been estimated to be in the range 4-6 $kcal.mol^{-1}$ [355–357]). Both the intrinsic stability of domains and the stability of the V_L-V_H interface may be limiting for the overall stability of the scFv fragment, meaning that the first step towards denaturation may be the unfolding of

domains – either simultaneously (if the intrinsic stabilities of both domains are similar) or sequentially (if one domain is much more stable than the other) – or it may be the disruption of the V_L-V_H interface [341] (see Figure 4.2). In either cases, the scFv loses its antigen-binding activity.

For a detailed mechanism of folding, the reader is referred to the work of Plückthun and co-workers [341, 358–362]. It has been shown that the two domains can interact early in the folding pathway, and lead to a kinetically trapped intermediate [359, 362]. Even then, the rate-limiting step of the overall folding reaction has been shown to be dominated by the slow *trans*-to-*cis* isomerization of a highly conserved proline residue on the V_L domain (see Figure 4.1) [361].

4.1.3.2 Possible origins of insolubility and aggregation

ScFv fragments as most of multi-domain proteins can form kinetically-trapped intermediates responsible for unproductive side-reactions, notably aggregation. More specific to scFv instability are correctly folded conformations that are still prone to aggregation. The poor stability of the V_L-V_H interface has been suggested to be the main cause of irreversible aggregation: transient dissociation of the two domains indeed exposes hydrophobic patches that favour aggregation [341]. The most widely used strategy to keep this interface buried inside the protein core is to engineer an inter-domain disulfide bridge [363], but other point mutations of interface residues can also be beneficial [341]. A second reason for insolubility in scFv constructs is that the two variable domains have lost the possibility to interact with the surface of the constant domains. In natural sequences of Fv fragments, residues at the interface between variable/constant moieties are mainly hydrophobic (see Figure 4.3). These residues become solvent-exposed in scFv and may contribute to aggregation. Mutations of these key residues by polar amino acids have been shown to reduce the aggregation propensity [97].

Other studies point to the role of surface charges in the aggregation of scFv. Hugo *et al.* suggested in particular that the charge distribution at the surface of scFv as well as the total charge are important factors for the formation of charged patches critical for aggregation [364]. They showed that mutations aimed at adding or removing charges on the surface of scFv fragments did not alter the antigen-binding kinetics and affinity of model fragments but significantly affected their half-life in periplasmic extracts. Lower half-lives were tentatively attributed to aggregation through charge patches.

4.1.3.3 Electrostatic modelling reveals the existence of positively-charged patches

Electrostatic modelling can be used to identify local charge patches on the surface of scFv fragments. Identifying positively-charged patches is particularly interesting because they can constitute regions of preferential interaction with PAA derivatives. We evidenced in the previous chapter that Coulomb attractions can be the predominant origin of the association of poly(sodium acrylate) derivatives with proteins. A reasonable assumption is that positively-charged domains at the surface of the protein drive these attractive interactions with the polyanions. In an attempt to assess the plausibility of this hypothesis, and whether a general efficacy (non specific to a few scFv) of poly(acrylates) can be expected, the surface potential of scFv Rendomab B1 was scrutinised and compared to that of other scFv.

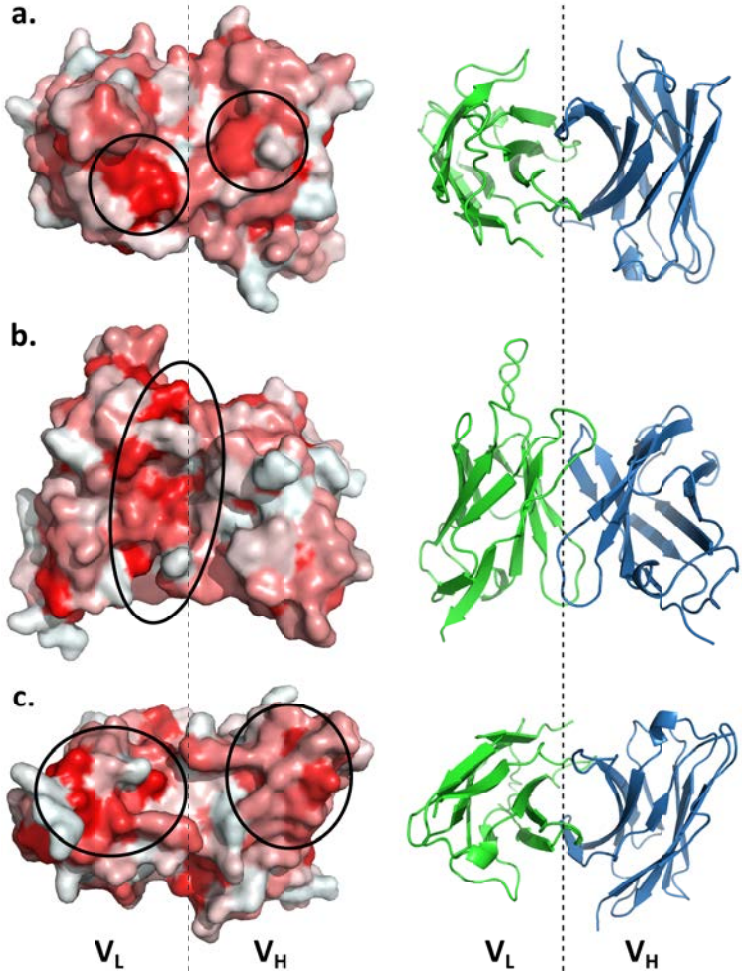


Figure 4.3: Exposed hydrophobicity on the scFv Rendomab B1 surface (in red). a. Top view. The hydrophobic patches highlighted in the antigen-binding site depend on the specific sequence of the hypervariable loops. b. Front view. Conserved hydrophobic regions are observed at the V_L-V_H interface. c. Bottom view. The former variable/constant domain interface exposes conserved hydrophobic patches.

Identification of two positively-charged patches on the scFv surface

The PDB file (3D coordinates of all atoms) of scFv Rendomab B1 was obtained by truncation of the structure of the corresponding crystallized Fab fragment (that had been determined at CEA Saclay). The software, tools and parameters used to calculate the electrostatic surface potential from the PDB file are given in detail in Appendix A. The cartoon view of the 3D structure of the fragment, as well as the corresponding surface potential calculated at pH 8 and a ionic strength of 100 mM are given in Figure 4.4 (cut-off of $\pm$ 3 kT/e). By varying the potential cut-off, two major positively-charged domains could be identified, one on each domain of the fragment. The positive patch on the V_H domain is located at the C-terminal end of the fragment, while the positive patch on the V_L domain is more distal to the antigen-binding regions. Figure 4.4 also shows the positively-charged patches identified with the Patch Finder Plus on-line program (at 150 mM ionic strength, pH 7.4), originally developed to find the largest continuous

positive patch on protein surfaces [365] (see Appendix A for details). In consistency with the surface potential previously calculated, this approach emphasized the same two positively-charged patches. The V_L patch appeared to be more extended than the V_H patch.

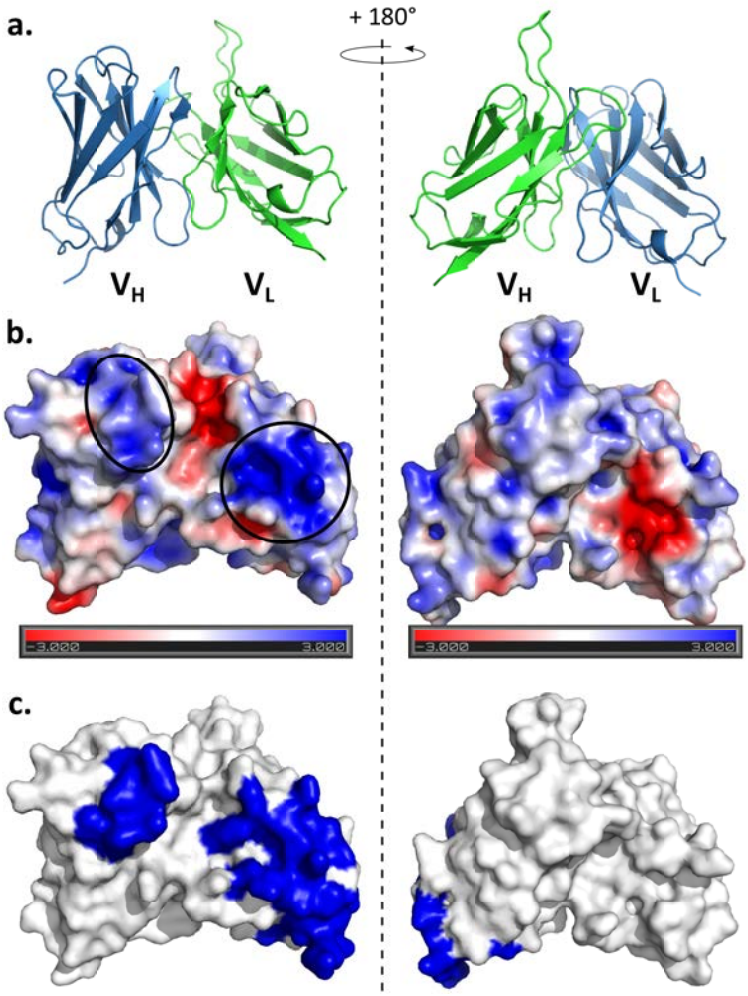


Figure 4.4: Electrostatic surface potential of scFv Rendomab B1. a. Cartoon sketch of the 3D structure. b. Electrostatic surface potential calculated via the APBS tool at 100 mM, pH 8. The potential cut-off was set to ± 3 kT/e. The two main positively-charged patches are highlighted. c. Largest positively-charged patches found by the Patch Finder Plus on-line server at 150 mM, pH 7.4.

Electrostatic potential calculations at different pH (and constant ionic strength of 100 mM) or different ionic strengths (but fixed pH 8) showed that increasing the pH or the ionic strength decreased the size and density of both positively-charged patches (see Appendix D). The V_H patch appeared to be more affected by variations of pH or ionic strength than the V_L patch. The latter remained relatively highly charged and extended even at pH 10 or I = 300 mM.

A more detailed view of the residues involved in the two positive patches is presented in Figure 4.5:

– residues involved in the V_H positive patch are mainly polar but not basic amino

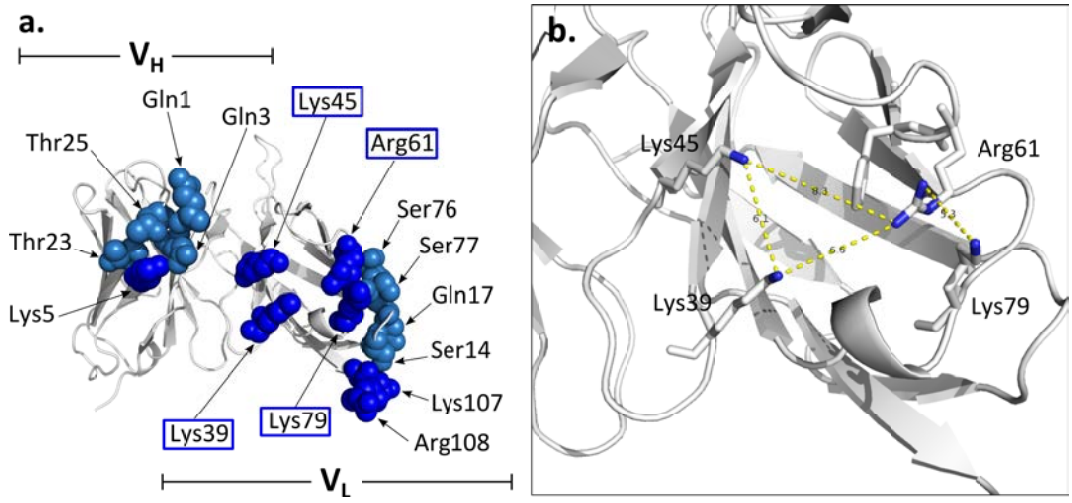


Figure 4.5: Residues involved in the positively-charged patches on the scFv Rendomab B1 surface. a. Dark blue: positively-charged residues (Lys, Arg); light blue: polar residues (Ser, Thr, Gln). b. Detail of the positive patch on the V_L domain, formed of 3 Lys and 1 Arg.

acids (threonine and glutamine), except one lysine. This may explain why this patch appeared weakly charged and "resisted" less to environment variations (increase of pH or ionic strength).

– residues involved in the V_L positive patch are mainly basic amino acids (lysine and arginine), even though one can also see polar residues (serine, threonine and glutamine). Four basic residues (3 lysine and 1 arginine) are particularly close in space (the distance between them ranges from 5.3 to 8.3 Å) and form a dense positively-charged patch.

Overall, the densely positively-charged patch on the V_L domain could be an interaction domain with polyanions.

Are these patches conserved amongst all scFv fragments?

By using the on-line AbYsis database [Andrew C.R. Martin's bioinformatics group, University College London], which contains hundreds of thousands of antibody sequences, we found that 15 negative charges were highly conserved in scFv sequences (present in more than 50% of sequences, see Table 4.1). These charges are indicated by arrows in Figure 4.6 for the sequences of the three scFv used in this thesis (the sequence alignment was performed with the Basic Local Alignment Search Tool (BLAST)). The 4 charges identified in the positive patch at the surface of the V_L domain of scFv Rendomab B1 are also indicated (circled). Three of them corresponded to conserved charges. Even though they are not adjacent to each other in the primary sequence, these charges gather at the surface of the fragment once folded. It is therefore assumed that if these charges are present in the sequence of a given scFv, the positive patch should also be formed on the surface of the fragment. Three (resp. two) of these charges were found in the sequence of scFv 12G4 (resp. scFv Sha 31). Accordingly, part of the V_L positive patch found in scFv Rendomab B1 is most-likely conserved (formed by the three positive charges that are conserved). scFv Sha 31 may constitute an exception (with only two positive charges

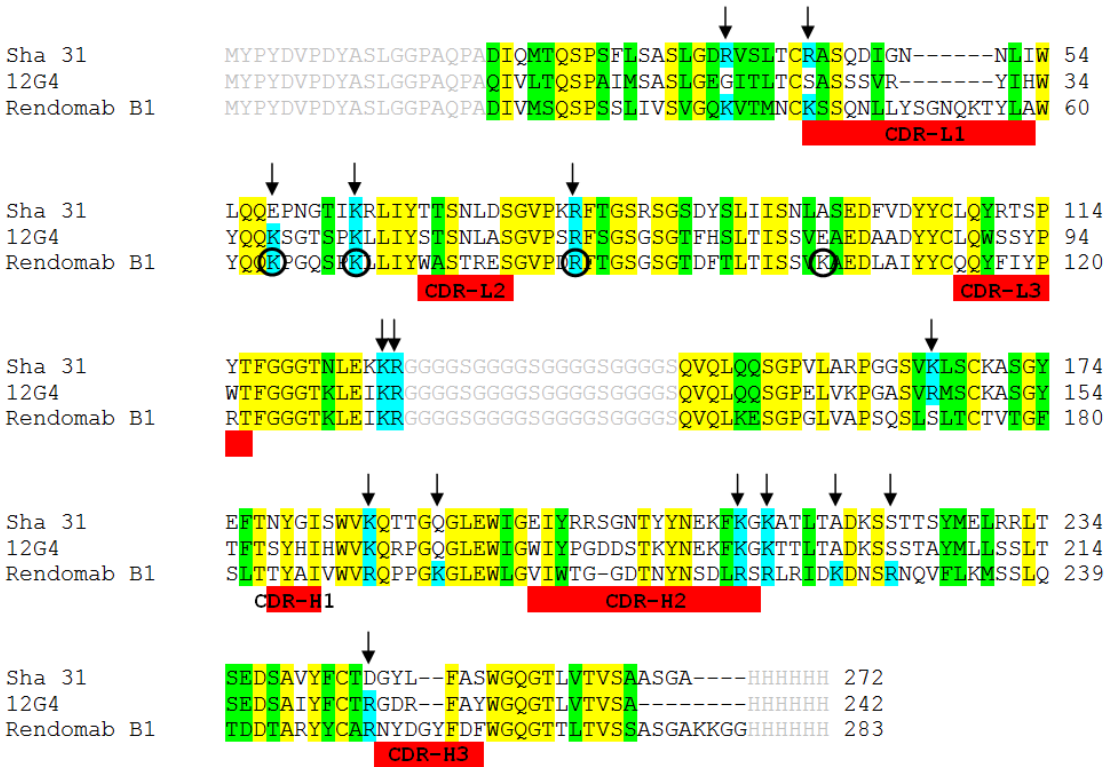


Figure 4.6: Sequence alignment of scFv Sha 31, 12G4 and Rendomab B1. Yellow: conserved residues among all three fragments; green: residues of similar properties (scoring>0.5 in the Gonnet PAM250 matrix [366]); blue: positively-charged residues (lysine or arginine) in position of conserved positive charges; circled: residues involved in the positively-charged patch identified on the V_L of scFv Rendomab B1; red: complementary-determining regions (according to the Kabat numbering).

conserved) rather than the rule. In the case of this particular fragment, one can notice that residues 65 (arginine) and 79 (lysine), which are positively-charged, are adjacent in the sequence to residues 64 (lysine) and 80 (arginine) that are part of the V_L positive patch on scFv Rendomab B1. Accordingly, they may participate in this case to reinforce the charge density of the two-charge-based positive patch.

Overall, the positively-charged patch identified on the V_L domain of scFv Rendomab B1 is supported by three conserved positive charges and may be a general feature of scFv fragments. It could constitute a preferential region of interaction with polyanions.

4.1.4 The reference refolding protocol: role of L-arginine to prevent aggregation

Rational design or evolutionary approaches for stability engineering of scFv fragments have been widely used [341], but they are highly sequence-dependent and have to be optimized for each particular scFv. Another non-specific (sequence-independent) conventional approach affording to renature unstable scFv relies on supplementation of the solutions by additives that enhance the solubility or the stability of folded polypeptides (L-arginine [116, 367, 368] and surfactants [369, 370] are the most widely used to date).

Table 4.1: List and occurrence of highly conserved charged residues on scFv fragments. Residues are identified with their Kabat numbering as well as their corresponding position in the sequence (given in the case of scFv Rendomab B1, positions for the other two fragments can be read on Figure 4.6.

V_H domain			V_L domain		
Kabat numbering	Position	Occurrence (%)	Kabat numbering	Position	Occurrence (%)
H19	172	72	L18	37	55
H38	191	99	L24	43	55
H43	196	75	L39	64	80
H64	217	78	L45	70	76
H66	219	95	L61	86	98
H71	224	57	L107	132	66
H75	228	53	L108	133	61
H94	250	83			

The refolding protocol of scFv fragments used in this thesis has been optimized in this conventional way by the team of D. Boquet in CEA and is inspired from years-long efforts by the work of Tsumoto and collaborators [116, 367, 368, 370]. The optimized renaturation protocol involves stepwise decrease of denaturant concentration (either urea or guanidinium chloride) with control of redox properties (glutathione concentration) at several steps and supplementation of L-arginine, as illustrated on Figure 4.7. This is achieved by a multi-step dialysis of solutions of chemically unfolded scFv at a typical concentration of 15 µM (*ca.* 0.45 $mg.mL^{-1}$) against buffers. This procedure allows to reach equilibrium in the different denaturant buffers [106] which is supposed to avoid the formation of kinetically-trapped aggregation-prone conformers. The control of redox potential ensures dynamic equilibration of intra-domain disulfide bonds and prevents irreversible inter-domain bridging. L-arginine is added at 0.4M as a stabilizing additive that in principle does not destabilize the native state, but increases its solubility (the mechanism remains yet unclear, see Chapter 1) [116].

Refolding in the presence of polymers is performed on a denaturant-unfolded scFv stock solution that has been supplemented with polymers at a weight ratio higher than (or equal to) 1 compared to the protein. Addition of the PAA derivatives in the urea-unfolded solution aims at favouring the interactions between the fragment and the polymers all along the stepwise dialysis refolding procedure. When polymers are present, L-arginine is not added, but the redox potential is still controlled in the last steps of refolding thanks to addition of glutathione. A final dialysis step against buffer with no urea allows to collect the refolded scFv in the presence of polymers.

4.2 Size of scFv during refolding

We used fluorescence correlation spectroscopy (FCS) to assess the monomer vs. aggregate status of scFv along the renaturation pathway. The advantages of measurements of the hydrodynamic radius by FCS (compared to light scattering or SEC) are described in Chapter 3 and Appendix B. Fluorescent (FITC-labelled) scFv was prepared by

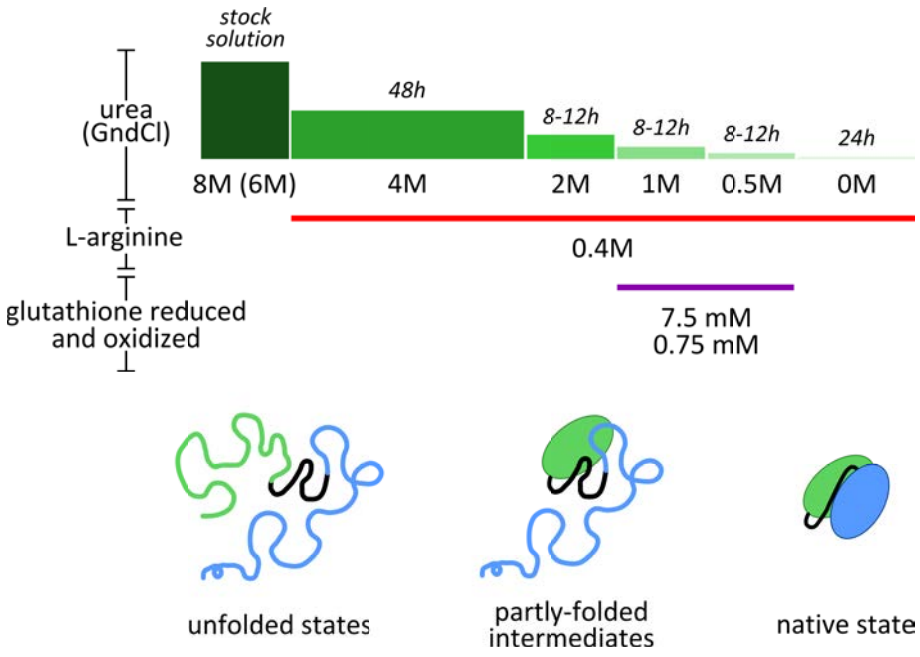


Figure 4.7: Optimized refolding protocol of scFv fragments. Urea (or guanidinium chloride) is gradually removed from the stock solution of purified scFv fragments via multi-step dialysis. L-arginine is added to prevent aggregation of partly-folded intermediates and of the native state. Reduced and oxidized glutathione is introduced in the lasts steps of refolding to ensure native formation of intra-domain disulfide bonds and prevent inter-domain bridging.

conventional coupling (in 8M urea) of amine-reactive fluorescein (see Appendix A). Calibration was performed with fluorescein at each dialysis step, notably to avoid artefacts due to index refraction mismatch (that can affect the size of the confocal volume) in buffers of high urea concentration (see Appendix B for details). In addition to radii, we fitted the average aggregation number, N_{agg}, defined as the number of FITC-scFv per object observed in the excited volume (as discussed in Appendix B). Measurements were performed here on the scFv Sha 31, which was originally used as model to optimize labelling with FITC at CEA and was readily available at the beginning of our study.

4.2.1 Variation of size in the absence of polymer

Measurements in the absence of polymers were aimed at evidencing critical steps in the reference refolding protocol. One expects to determine the moment when scFv undergo intra-chain collapse, or aggregation at threshold concentration(s) of denaturant, with or without L-arginine. To assess the impact of initial conformation of scFv, experiments were performed using urea as denaturant, or guanidinium chloride (GndCl) that is known to solubilize and unfold proteins more efficiently. Figure 4.8 shows the evolution of the FCS-measured average hydrodynamic radius as a function of the denaturant concentration with or without added L-arginine, as well as the corresponding aggregation numbers. The hydrodynamic radii were fitted from a unimodal model of the autocorrelation function (via Equation B.2 in Appendix B. Similar averaged radii could be obtained by taking the

mean of the distribution given by the MEMFCS algorithm (see Appendix B for details).

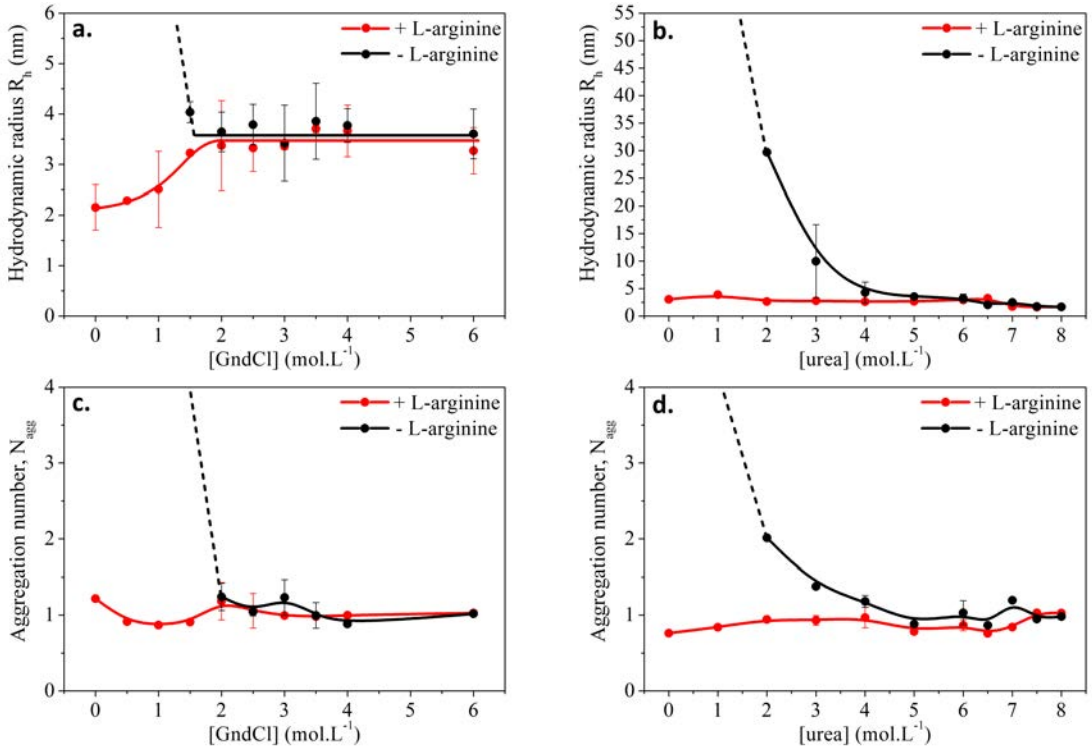


Figure 4.8: Variation upon dialysis at decreasing GndCl (a., c.) or urea (b., d.) concentration (refolding) of the hydrodynamic radius (R_h) and aggregation number of FITC-scFv (N_{agg}, defined as the averaged number of FITC-scFv molecules per fluorescent object in solution) measured by FCS. [scFv] = 0.1 mg.mL^{-1}.

In the reference refolding protocols (with L-arginine, data in red in Figure 4.8), R_h remained lower than 4 nm down to 0M denaturant concentration with typical values ranging from 2 to 3.5 nm. In particular, no oligomerization and no aggregation were observed (N_{agg} remained constant around 1). In the case of GndCl, the decrease in R_h from *ca.* 3.4 nm to 2.1 nm in the range 0-1.5 M GndCl can be tentatively attributed to the collapse transition of FITC-scFv into a more compact globule. Such a collapse is not observed in urea .

In experiments without L-arginine (black data in Figure 4.8), the situation is quite different. R_h remained almost constant down to 1.5M GndCl (resp. 4M urea), then an abrupt increase in size was observed at lower denaturant concentration (vertical dotted line in Figure 4.8). Eventually, while approaching the purely aqueous conditions, the fluorescence signal displayed strong bursts of intensity making it impossible to determine the size of the aggregates (see typical traces of fluorescence intensity in Appendix D). In urea, aggregation was more progressive (formation of oligomers), as indicated by the gradual increase of R_h between 4 and 2M urea. Surprisingly, N_{agg} increased more gradually than the radius: for instance, the hydrodynamic radius measured at 2M urea was *ca.* 30 nm but the associated N_{agg} value only reached 2, instead of a higher value expected from the measured hydrodynamic radius. Care must be taken here when interpreting the N_{agg} values since it is extracted from the collected intensity. Normalization of fluorescence

intensity with fluorescein is systematically performed, but other factors may contribute to a poor signal/noise ratio (such as quenching or change in FITC quantum yield during folding/aggregation).

Comparison of the reference protocols (with L-arginine) and the control experiments (without L-arginine) shows that addition of 0.4M of L-arginine is indispensable to prevent aggregation of FITC-scFv during refolding in both denaturants. At this high concentration, L-arginine plays the role of a buffer: in the reference protocol, pH was thus turned basic at the step of addition of L-arginine (pH 10 instead of pH 8) which can have undesirable effects on *in vitro* activity assays (particularly for assays on live cells, highly sensitive to the buffer pH). We performed experiments by adjusting the pH of the arginine-containing buffer to 8 (at the end of the renaturation procedure), which resulted in the aggregation of the fragment (not shown). Removal of L-arginine at the end (last dialysis step) of the refolding protocol also led to aggregation of the folded scFv, presumably because the folded fragment exposes surface hydrophobic residues (*vide supra*). Therefore, to avoid the use of L-arginine, one has to consider alternative protecting agents.

4.2.2 Do polymers limit aggregation of scFv?

Similar size measurements were performed in the presence of poly(sodium acrylate) (PAA) derivatives (added in the stock solution of unfolded FITC-scFv, at the very beginning of the renaturation protocol) and in the absence of L-arginine. From comparison of sizes measured in the presence or absence of polymers, it is expected to identify the moment when polymers associate to the FITC-scFv fragments (long polymers were used to facilitate the detection of the onset of complexation).

4.2.2.1 Importance of electrostatic interactions

A fixed scFv:polymer weight ratio of 1:5 was used to compare the various protein:polymer mixtures. As illustrated on Figure 4.9, polymers did not associate with FITC-scFv fragment in GndCl: R_h and N_{agg} remained small, with typical values similar to that of the free FITC-scFv. This is confirmed by the mono-modal distribution given by the MEMFCS algorithm (see Appendix D). In addition, aggregation of FITC-scFv was not prevented: brutal increase of the size was observed below 1.5M GndCl, together with strong bursts of fluorescence intensity.

This contrasts with the formation of small species ($R_h < 50$ nm) when the refolding was performed in urea. More precisely, in the case of FITC-scFv:PAA150, R_h started to increase below 2M urea, the concentration threshold that also corresponds to conditions of aggregation of FITC-scFv alone in urea. Hydrophobically-modified PAA150-3C18 interacted with unfolded FITC-scFv (in 8M urea), since R_h values of *ca.* 14 nm were measured at $N_{agg} = 1$ (the hydrodynamic radius of one polymer chain was $\sim 16.1 \pm 2.7$ nm for PAA150-3C18, as independently measured on a rhodamine-labelled polymer). A further increase to 27 nm was observed at 0M urea, but no massive aggregation occurred. In the case of FITC-scFv:PAA5-25C8-40C3, no complexes were formed with the unfolded fragments (R_h of about 4 nm down to 3M urea), but the hydrodynamic radius increased at 2M urea before reaching a plateau at 11 nm down to 0M urea. No bursts of fluorescence intensity were detected, confirming the absence of large entities (see Appendix D). It is worth noting that the given hydrodynamic radii correspond to average values: in practice,

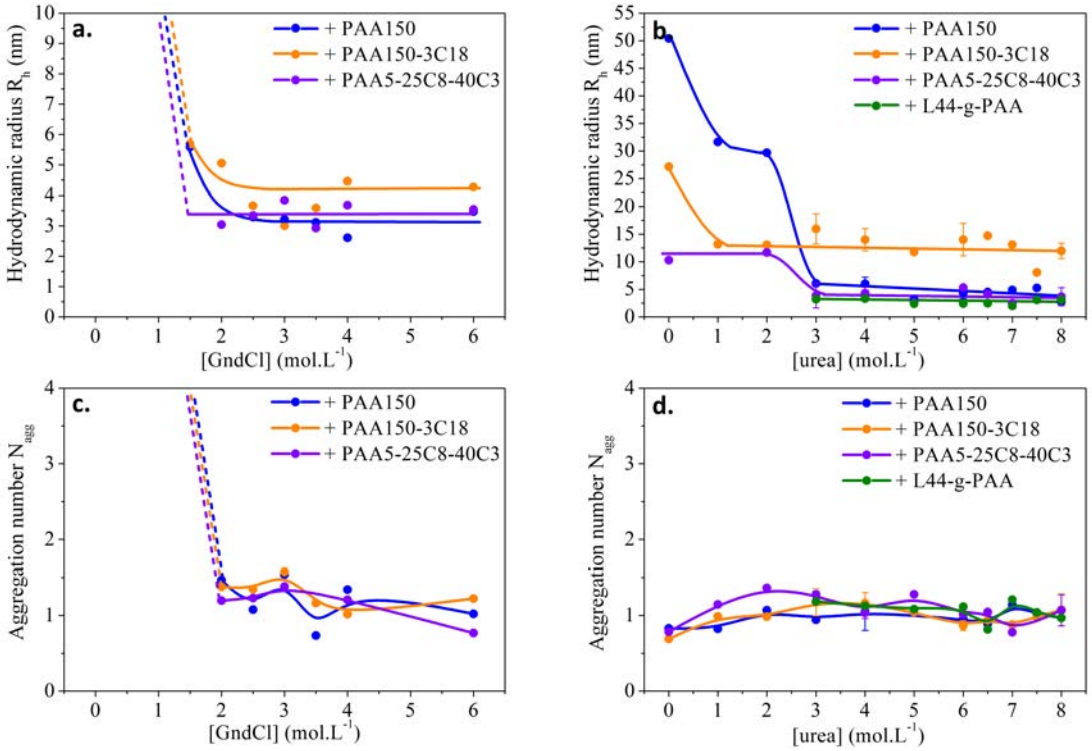


Figure 4.9: Variation upon dialysis at decreasing GndCl (a., c.) or urea (b., d.) concentration (refolding) of the hydrodynamic radius (R_h) and aggregation number (N_{agg}) of FITC-scFv:polymer mixtures measured by FCS. [scFv] = [polymer] = 0.1 mg.mL^{-1}.

several species may co-exist in the refolding mixture. MEMFCS traces point in particular to coexistence of free (unbound) proteins and complexes (see Appendix D).

The N_{agg} values seem somewhat underestimated, in particular when polymers clearly formed complexes with the protein (0-2M urea). The measured R_h values of 10-50 nm, *i.e.* higher than the sizes of the polymer chains alone, would suggest that multi-protein objects are formed (oligomers). The same care as previously mentioned as to be taken in the interpretation of N_{agg} values, which essentially reflects the order of magnitude of the degree of binding of scFv into one complex with polymer chain(s).

The results indicate that the presence of polymers has a remarkable effect on the colloidal stability of FITC-scFv during refolding in urea, but fails to protect against aggregation in GndCl. By analogy with results obtained on CAB (Chapter 3), we propose that the ionic strength of the solution is an important parameter. Electrostatic interactions between the polyanions and the fragment are shielded in GndCl used at molar concentrations, which is presumably at the origin of the poor efficiency of polymers in GndCl compared to urea. The absence of clear benefits of hydrophobic interactions (PAA150 compared to PAA150-3C18 and PAA5-25C8-40C3) suggests that Coulomb association is sufficient *per se* to avoid inter-protein association. It could however affect the structure of folded scFv, which is the question addressed in Section 4.3.

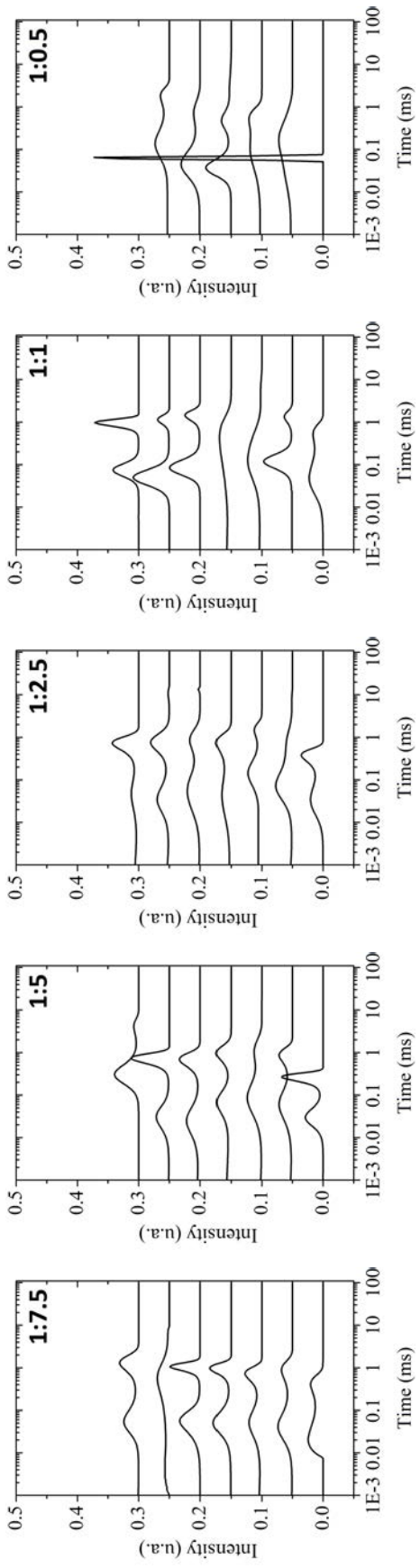


Figure 4.10: Influence of the protein:polymer weight ratio on the variation upon dialysis at decreasing urea concentration (refolding) of the distribution of diffusion times of FITC-scFv:PAA150-3C18 mixtures measured by MEMFCS. [scFv] = 0.1 mg.mL^{-1}.

4.2.2.2 Effect of scFv:polymer weight ratio

Results discussed above were obtained in the presence of excess polymer. To estimate the minimal amount of polymer required to achieve protection of scFv against aggregation, we considered here the hydrophobically-modified PAA150-3C18 as a model polymer able to develop both electrostatic and hydrophobic interactions with the proteins. Figure 4.10 shows the evolution of the distribution of diffusion times obtained using the Maximum Entropy Method to analyse FCS autocorrelation functions (see Appendix B for details) as a function of decreasing urea concentration and at different scFv:polymer weight ratios. We observe bimodal distributions all along the refolding protocol for polymer/scFv weight ratio above 1, including in 8M urea. Two modes are presumably indicative of equilibrium between free proteins (folded or not) and PAA150-3C18-associated protein.

At a scFv:polymer wt/wt ratio of 1:0.5, complexes between PAA150-3C18 and unfolded scFv in 8M urea were not detected, suggesting that these complexes became marginally stable below 0.05 $g.L^{-1}$ of polymer. The complexes were present at lower urea concentration, but were no longer able to prevent aggregation below 0.5M urea. The poor efficiency of polymer at 1:0.5 weight ratio and a complete prevention of aggregation at higher ratios (>1:1) point out that a minimal polymer/scFv weight ratio of about 1 is required.

4.3 Do polymers affect the secondary structure of scFv?

In this section, we show that formation of complexes between scFv and polymers can affect the equilibrium secondary structure in solution conditions close to destabilization of the folded conformation (with urea). The question of whether interaction with additives could stabilize non-native conformations of the scFv fragment in aqueous buffer, in the final conditions of use (no urea), is also addressed. This study was conducted in solutions containing essentially no aggregates of scFv (presence of L-arginine or polymers in the urea-based renaturation procedure, see the section above). In the following, characterizations are performed on unlabelled scFv Rendomab B1, unless specified.

The introduction of additives that have a high absorsbance in UV (urea, L-arginine and glutathione) decreases the signal and makes data recorded on bench-top CD spectrometer very noisy at low wavelength (< 220 nm), in the range containing most of the CD signatures from β-strands. This difficulty was overcome by using SRCD measurements in SOLEIL synchrotron facilities in Saclay, performed in collaboration with Frank Wien. The high intensity of the incident beam in SRCD offers several advantages over commercial circular dichroism apparatus: it allows to reach low wavelengths, even in the presence of absorbing or scattering samples thanks to the use of short path-lengths (a few tens of microns), and provides a significantly higher signal/noise ratio. Additional information on the perturbation of folding by polymers were obtained by intrinsic fluorescence measurements.

4.3.1 Secondary structure in water (no urea) at the end of renaturation

We first consider the scFv fragment after refolding from the urea-denatured state, either without polymers (but in the presence of L-arginine) or with polymers (added at 1:1 weight ratio).

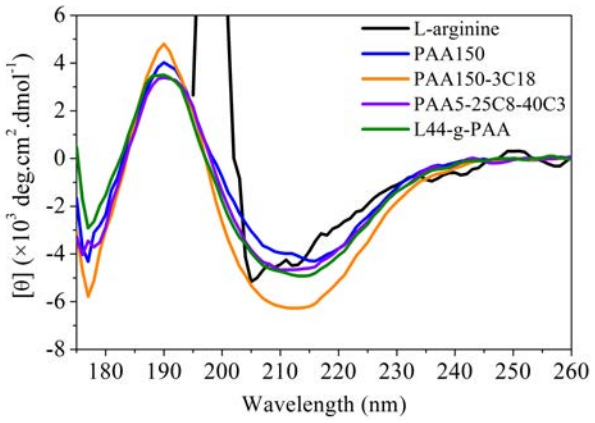


Figure 4.11: SRCD spectra of scFv Rendomab B1 at 25°C in 10 mM Tris-HCl pH 8 after refolding with or without polymers. When refolding was performed in the absence of polymers, 400 mM of L-arginine were added during the renaturation protocol as described in the main text. scFv concentration was *ca.* 5 mg.mL^{-1} with 1:1 wt/wt scFv:polymer ratio when polymers were added.

The overall shape of the spectra on Figure 4.11 was the same regardless of the polymer type (even though slight differences in the amplitude could be noticed, especially with

PAA150-3C18), suggesting that the final secondary structure reached was presumably similar with all polymers. The spectra exhibited a marked minimum at ∼215 nm and a maximum at about 190 nm, both characteristic of a predominant β-sheet structure, in consistency with the expected structure of the fragment. In the case of L-arginine, the concentration of amino acid residues of scFv (about 0.045M at 5 mg.mL^{-1}) was one order of magnitude lower than that of L-arginine (0.4M), which introduced high uncertainties in the subtraction of baselines at wavelength <200nm. The pH of the milieu was also higher (pH 10) when L-arginine was present, which could perturb the structure of the fragment.

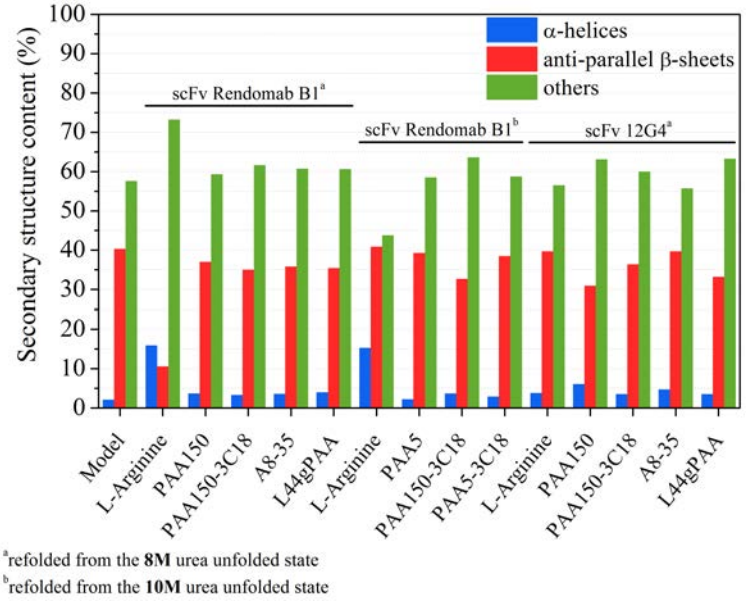


Figure 4.12: BestSel secondary structure content estimation of two scFv fragments, scFv Rendomab B1 and scFv 12G4, at 25°C in 10 mM Tris-HCl pH 8 after refolding with or without polymers. scFv Rendomab B1 was denatured in 8M or 10M urea (as specified) prior to refolding, "Model" refers to the estimation of the secondary structure content from the 3D structure of the fragment, "L-arginine" refers to refolding without polymers. scFv concentration was *ca.* 5 mg.mL^{-1} with 1:1 wt/wt scFv:polymer ratio when polymers were added.

The secondary structure content can be estimated by deconvolution of the experimental CD spectra into linear combination of contributions from elemental structures (helices, sheets, turns), which can be achieved by several softwares associated with databases of representative proteins. The widely-used DichroWeb analysis [371–373] gave large uncertainties on the amount of structural elements (not shown), probably do to a lack of predominantly β-structures in available databases. We used the yet unpublished BestSel analysis software, developed by Micsonai *et al.* [338] (BestSel was optimized for fits at low wavelengths and to include complex contributions of β-structures such as twisted β-sheets in its database, see Appendix B for details). Structural parameters fitted by BestSel are the fraction of residues belonging to a specific secondary structure. Experimental values can thus be compared with fractions estimated from the 3D model of the fragment (see Figure 4.1).

We estimated from the PDB crystal structure the proportion (in % of residues) of each secondary structure. Figure 4.12 summarizes the secondary structure content obtained from the BestSel analysis at the end of the refolding procedure (at 0M urea). Within experimental errors, the expected secondary structure content ("Model" in Figure legend) matched well with the content fitted from experimental data. Two different fragments, scFv Rendomab B1 and scFv 12G4, were refolded in the presence of polymers (either starting from stock solution of proteins in 8M or 10M urea for scFv Rendomab B1, see Appendix D). In addition, the chain length of the polymer had little impact on the native-like secondary structure recovery (see for instance comparison of PAA150 and PAA5, or PAA150-3C18 and PAA5-3C18).

At variance with polymer-protected scFv, the secondary structure obtained for the scFv Rendomab B1 refolded without polymers (referred to as "L-arginine" on Figure 4.12) – from either the 8M or the 10M urea unfolded state – did not match the expected proportions in native scFv fragments. In particular, we estimated a higher α-helix amount ($\sim$15% instead of $\sim$2%). This difference may be due to the poorly defined signal observed in the presence of L-arginine and the absence of data for wavelengths lower than $\sim$200 nm (strong absorption of the additive). For scFv 12G4, the structure of the fragment refolded without polymers appeared native-like.

The BestSel analysis can also screen the entire protein data bank (PDB) to find the class of folding that have CD spectra with high degree of similarity with the experimental one (see Appendix B for details). Structures are reported according to the CATH classification. Schematically, CATH classifies proteins depending on intrinsic features of their secondary and tertiary structures, and contains, in addition to the amount of helices, strands and/or turns, information on architecture and topology. This "fold recognition" feature enables to predict the relative frequencies of folding class, architecture and topology that best match the experimental CD spectra. Strikingly, we systematically obtained for the scFv fragments refolded in the presence of polymers more than 35% (and up to 100%) of "mainly β" class, more than 44% (and up to 83%) of "sandwich" architecture and more than 20% (and up to 52%) of "immunoglobulin-like" topology.

In summary, refolding of scFv fragments in the presence of polymers systematically resulted in formation of well-structured globules that display CD spectral features nicely compatible with refolding into a native immunoglobulin-like structure.

4.3.2 Folding transition: a semi-quantitative analysis

In this section, we address the question of the impact of association with polymers on the folding/unfolding transition of scFv. To answer the question, we focus here on scFv Rendomab B1 characterized at each step of the renaturation protocol in the presence or not of polymers. It was observed that the fragment was not completely unfolded in 8M urea buffer (see Appendix D). In the following, we hence focus on the refolding of scFv Rendomab B1 initially denatured in 10M urea to ensure its complete unfolding.

4.3.2.1 Folding transition of the scFv fragment alone

From 10M down to 4M urea, there is no need to add L-arginine, since aggregation does not occur at high denaturant concentrations (as checked by FCS). The fragment was incubated in the various urea buffers for 24 hours after simple dilution of the 10M urea unfolded sample in the appropriate buffers.

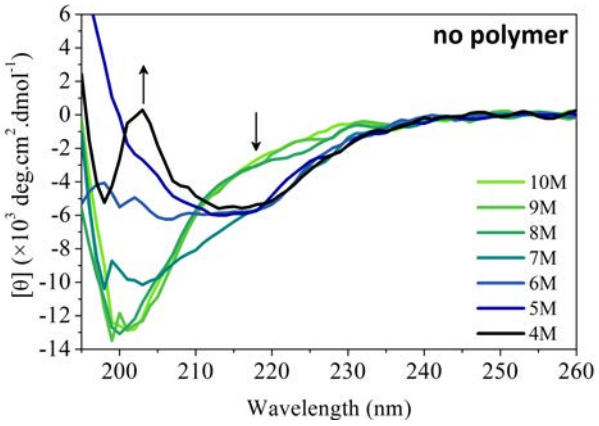


Figure 4.13: SRCD spectra of scFv Rendomab B1 in the 4-10M urea range, 10 mM Tris-HCl pH 8 at 25°C, in the absence of polymer. Samples were prepared by dilution of a stock solution of the 10M urea unfolded fragment and let equilibrated for 24 hours before SRCD measurements. [scFv] = 5 mg.mL^{-1}.

In the case of scFv alone (no polymer), the spectrum of the denatured state (at 10M urea) showed a pronounced minimum at 203 nm, characteristic of an unfolded structure, and did not vary down to 8M urea (Figure 4.13). When the concentration of urea was further diminished, we observed a progressive decrease of the absolute value of the minimum at 203 nm altogether with a sharp transition at 218 nm characterized by the appearance of a secondary minimum, attributed to (partial) folding of the fragment. The shape of the CD spectrum at 4M urea was consistent with a predominance of β-sheet structure, as already discussed above, suggesting that the fragment had reached a secondary structure that resembled the final mostly-β one.

The absence of isodichroic point indicated that the folding of the fragment could not be simply described by a two-state transition, which is not surprising for scFv as reported by Plückthun *et al.* (see the preamble)[341]. Data can be analysed semi-quantitatively by plotting the evolution of the mean molar ellipticity, $[\theta]$, at 203 nm (characteristic of the unfolded state) and at 218 nm (characteristic of the almost-folded state) as a function of the urea concentration, as plotted on Figure 4.14. A sharp transition in $[\theta]_{218\text{nm}}$ between 7M and 8M urea was observed without polymer, and was associated to the apparition of the 218 nm minimum on the CD spectra. The onset of folding thus occurred just below 8M urea. In parallel, $[\theta]_{203\text{nm}}$ increased progressively from 8M to 5M urea (Figure 4.14), which was the signature of the decreasing contribution of the unstructured elements of the protein, namely the unfolded regions.

To decrease the urea concentration below 4M, multi-step dialysis (for 24 hours each) were performed as in the genuine renaturation procedure. The evolution of the signals from 4M to 0M urea was very weak and is presented and discussed in Appendix D. It is concluded that the major folding transition is observed in the 4-8M urea range, with a strong decrease of the contribution of the unfolded regions and switch to a CD spectrum almost native-like in shape (marked minimum at 218 nm) at 4M urea.

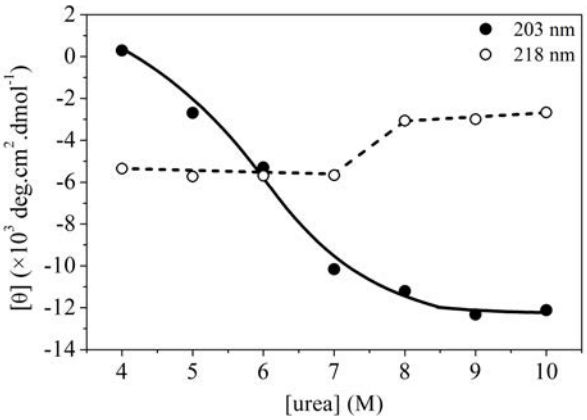


Figure 4.14: SRCD-monitored folding transition of scFv Rendomab B1 in the absence of polymer: evolution of the mean molar ellipticity $[\theta]$ at 203 and 218 nm for scFv Rendomab B1 alone in the 4-10M urea range, extracted from Figure 4.13.

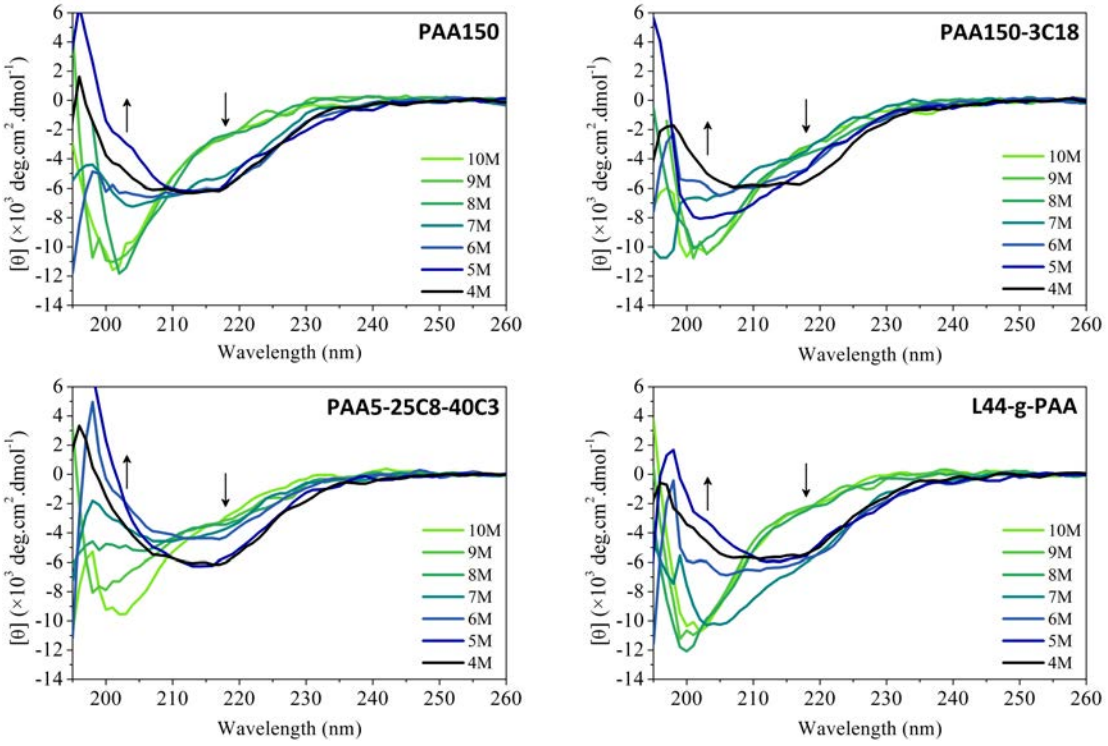


Figure 4.15: SRCD spectra of scFv Rendomab B1 in the 4-10M urea range in the presence of polymers. Samples were prepared by mixing appropriate amounts of a 10 mg.mL^{-1} stock solution of the 10M urea-unfolded fragment and 10 mg.mL^{-1} stock solutions of polymers either in 10M urea or in 10 mM Tris-HCl pH 8 and let equilibrated for 24 hours before SRCD measurements. [scFv] = 5 mg.mL^{-1}, 1:1 scFv:polymer wt/wt ratio.

4.3.2.2 Effect of the polymers on the folding transition

Polymers:scFv mixtures at 1:1 wt/wt ratio were incubated in different urea buffers for 24 hours prior to SRCD measurements. Compared to scFv alone, PAA150 had little influence on the overall shape of the CD spectra all along the refolding pathway (Figure 4.15). With PAA150-3C18 and PAA5-25C8-40C3, the minimum at 203 nm on the spectra recorded at 10M urea showed a markedly lower amplitude than for scFv alone and the evolution of spectra between 10 and 8M urea were more pronounced. The shift in the conditions of folding transition can be made more obvious in a plot of ellipticity at 203 and 218 nm (Figure 4.16).

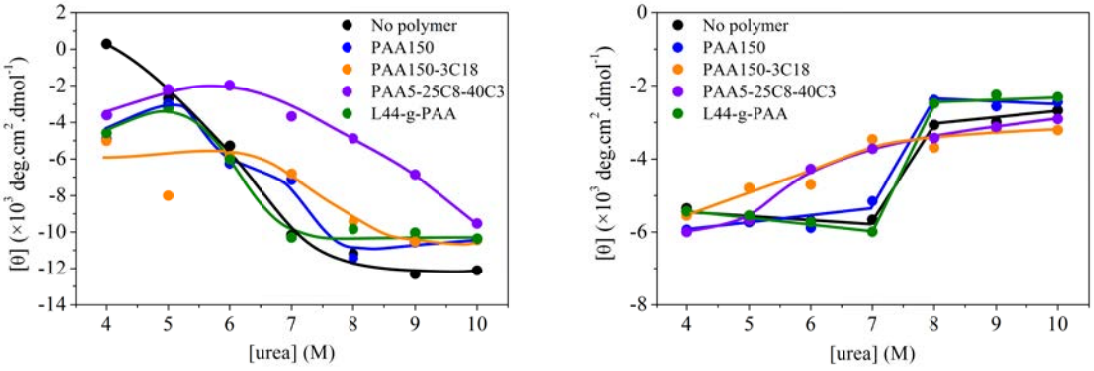


Figure 4.16: SRCD-monitored folding transition of scFv Rendomab B1 in the presence of polymers: evolution of the mean molar ellipticity $[\theta]$ at 203 nm (left) and 218 nm (right) in the 4-10M urea range, extracted from Figure 4.15.

Differences in Figure 4.16 between scFv alone, scFv:PAA150 or scFv:L44-*g*-PAA mixtures were within experimental uncertainty. The effect of polymers on the region 4-10M urea seems to arise mainly from the hydrophobically-modified chains. In the presence of PAA150-3C18 or PAA5-25C8-40C3, the transitions evidenced at either wavelength were smoother (more gradual), suggesting that amphiphilic polymers decreased the cooperativity of folding. PAA5-25C8-40C3 shifted the transition observed at 203 nm towards higher values of urea concentration, meaning that it favoured the formation of secondary structures earlier in the refolding procedure. However, the transition monitored at 218 nm showed that this structuration corresponded to spectral features significantly different from that recorded in the absence of polymer (see for instance the difference in $[\theta]_{218nm}$ at 7M urea). Altogether, these observations suggest that the polymer favours earlier folding into intermediate states that are not predominant in solutions of the fragment alone.

This result may appear counter-intuitive at first sight: usually, complexation with additives that render protein more soluble tend to favour the hydratation of peptide chains, thus facilitating disruption of intra-molecular interactions (destabilization). In the present case, structured scFv folding states are favoured by addition of PAA5-25C8-40C3.

The evolutions of α-helices, anti-parallel β-sheets, turns and unstructured elements proportions derived from the BestSel analysis are plotted on Figure 4.17 as a function or decreasing urea concentration. Surprisingly, the content of structural elements is already $\sim$25% for the unfolded protein (in 10M urea). This may arise from the fact that the reference database contains proteins well structured and characterized in water (no or

few naturally unfolded proteins for instance). The exact values may accordingly not represent the actual % of secondary structure, but variations of the estimated contents of structured elements are reliable.

The α-helix content abruptly increased (from $\sim$ 0% to $\sim$ 8-10%) between 8M and 7M urea for the fragment alone, as well as in the presence of PAA150 and L44-*g*-PAA. With the hydrophobically-modified polyanions, *ca.* 6% of α-helices already appeared at 9M urea (namely, there was a shift of the α-helix transition to higher values of urea concentration). The β-sheet content of the scFv alone increased abruptly from a plateau value of $\sim$25% to approximately 35% when the urea concentration was decreased below 7M. In the presence of polymers, the increase was more gradual, in particular with PAA150 and L44-*g*-PAA, starting as early as the 8-9M urea step, suggesting a premature but less cooperative formation of β-sheets. At lower urea concentration (0-4M urea), the secondary structure content remained almost constant, regardless of the polymer added, confirming that the folding transition (collapse) occurred above 4M urea (see Appendix D).

To sum up, the formation of secondary structures for the scFv fragment supplemented or not with polymers mainly occurs between 10M and 4M urea. Amphiphilic polymers decrease the cooperativity of folding, most-likely because they interact with partly folded intermediates and interfere with the proper association of the V_L and V_H domains. The major modification in the folding pathways seems to arise from the presence of hydrophobic grafts on the polymers, which favours the early formation of secondary structures. This result is somewhat surprising: to the best of our knowledge, the addition of polymers generally shifts the unfolding transition of soluble proteins to lower denaturant concentrations (destabilization) because association with polymer compete with intra-molecular interactions. The present observations suggest that polymers bind folded structures with higher affinity than unfolded ones (and displace the folding transition accordingly). This difference in binding strength may arise from the presence of accessible hydrophobic patches on native or partially folded scFv, unlike most of water-soluble proteins that bury the hydrophobic residues when they form a globule. The multi-domain nature of scFv shall not be overlooked neither: early association with polymers might, for instance, favour structuration of each domain by stabilizing the hydrophobic inter-domain contact area V_L-V_H.

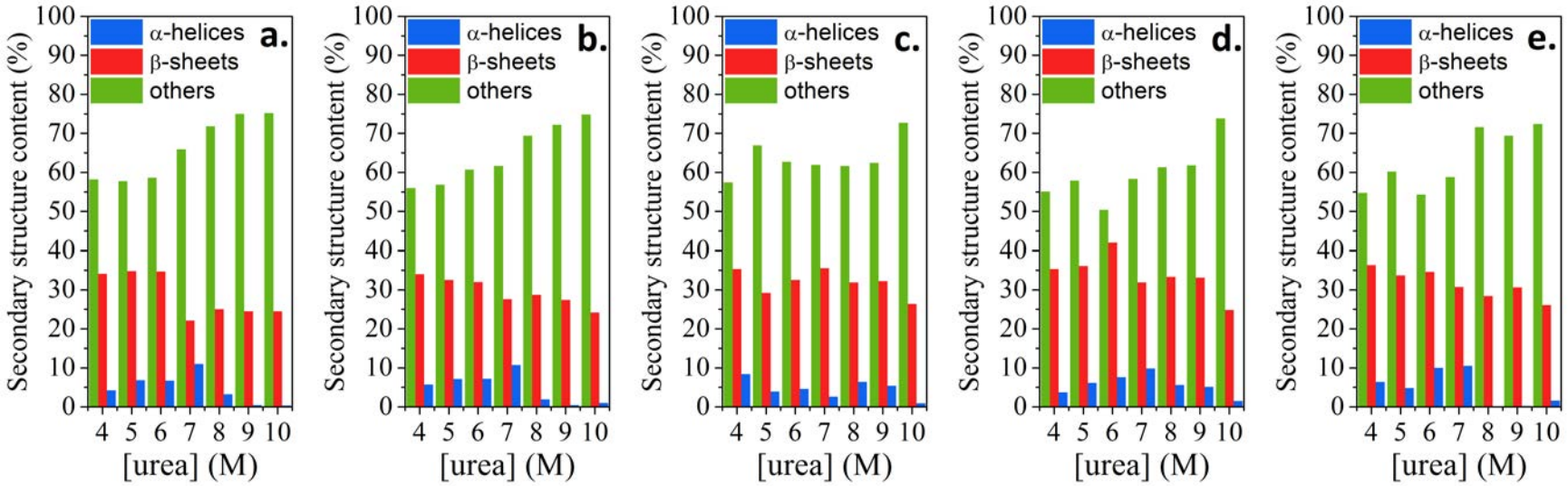


Figure 4.17: Evolution of secondary structure content via BestSel analysis in the 4-10M range. a. No polymer, b. PAA150, c. PAA150-3C18, d. PAA5-25C8-40C3, e. L44-g-PAA. "β-sheets" refers to anti-parallel β-sheets; "others" refers to turns and unstructured elements.

4.3.3 Tryptophan intrinsic fluorescence as a complement to CD study

When excited at 280 nm, tryptophan residues in proteins emit fluorescence which intensity depends on the environment of their local environment. During refolding, tryptophan residues, which are solvent-accessible in the unfolded polypeptide, are gradually buried in the hydrophobic core of the protein where they are usually less subjected to dissipative vibrations (potential enhancement of fluorescence) but where their fluorescence can be quenched (for instance by disulfide bonds). Overall, the variation of fluorescence intensity of tryptophan residues can be used to monitor the folding process, with as an outcome a fluorescence intensity integrating a complex network of intra-protein tertiary contacts (formation of a tightly packed structure).

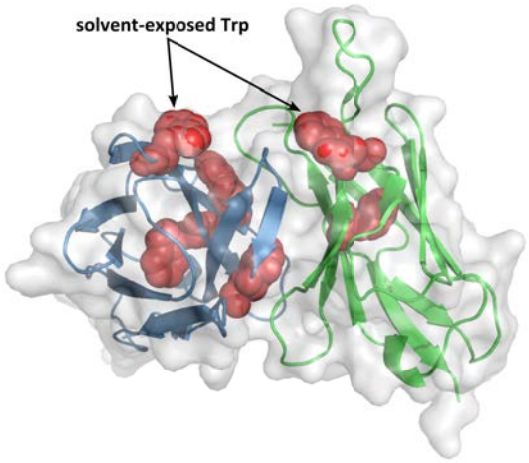


Figure 4.18: Identification of the 6 tryptophan residues in scFv Rendomab B1 (red), two of which are exposed to the solvent.

In our case, scFv Rendomab B1 comprises 6 tryptophan residues, 4 of which are buried in the hydrophobic core of the folded fragment while 2 remain relatively solvent-accessible (see Figure 4.18). The changes of fluorescence intensity during refolding may thereby not be simple to interpret. Plückthun and colleagues suggested to use the wavelength at the maximum fluorescence emission. This value indeed changes depending on the tryptophan environment and is not dependent on quenching phenomena or on the sample concentration.

Figure 4.19 shows the evolution of the wavelength at maximum fluorescence emission in the presence or not of polymers. For scFv alone, the signal strongly increased at 4M urea upon addition of L-arginine (needed to prevent aggregation). This may arise from the change in pH and ionic strength of the solution that affects the fluorescence of the tryptophan residues. Thus, we cannot obtain a reference folding transition for the fragment alone on the whole range of urea concentrations. Nonetheless, data can be compared above 4M urea (where the pH in all samples was the same). Figure 4.19 suggests that PAA150 and L44-*g*-PAA had little influence on the folding transition: the signals obtained with this two polymers matched with the one obtained for scFv alone in the range 4-10M urea. As we know from the previous section, the native-like

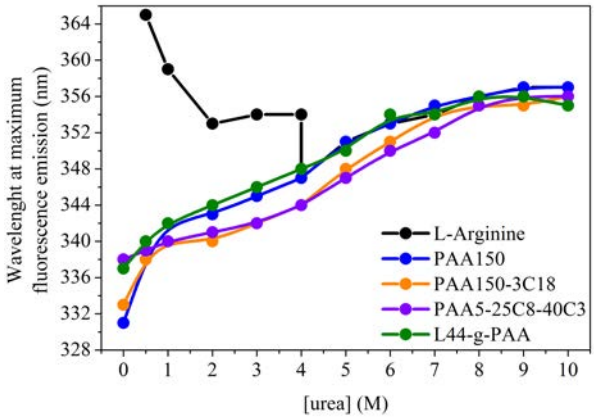


Figure 4.19: Fluorescence-monitored folding transition of scFv Rendomab B1 with or without polymers (added at 1:1 wt/wt ratio): evolution of the wavelength at maximum fluorescence emission as a function of the urea concentration. [scFv] = 0.2 mg.mL^{-1}.

secondary structure was already almost completely reached at 4M urea. Fluorescence measurements suggest yet that the tertiary structure was not completely formed at 4M urea. In consistency with shifts observed by CD measurements, hydrophobically-modified PAA shifted the fluorescence transition towards higher urea concentrations. No difference was however observed between PAA150-3C18 and PAA5-25C8-40C3, suggesting that the compaction of the protein did not depend on the content of hydrophobic moieties on polymers.

The folding transition monitored via tryptophan's intrinsic fluorescence deserves further investigation that we could not manage during this Ph.D. One could use for instance fluorescence quenchers in the refolding buffers so that tryptophan fluorescence would be quenched only if the residues are solvent-accessible. Such experiments should allow to clarify without assumption the compaction effects that occur near the 2 solvent-exposed tryptophan residues.

4.3.4 NMR to unravel the local scFv:polymer contacts: preliminary results

NMR is a powerful technique to characterize both folding of proteins and their interactions with ligands. For instance, hydrogen-deuterium exchange experiments have been widely used by Plüchthun and colleagues to unravel the folding mechanism of scFv fragments [359].

Since they provide insights into the structure and dynamics of proteins at the residue scale, ^{1}H-^{15}N Heteronuclear Single Quantum Coherence (HSQC) experiments can provide information about the local contacts between polymers and scFv fragments. ^{1}H-^{15}N HSQC measurements are easy to implement and allow the 2D mapping of the individual residues of a protein. The same residues in a slightly different environment will appear as distinct spots, but in the same region, on the ^{1}H-^{15}N plot. Accordingly, we should be able to determine what type of residue is affected by the presence of polymer.

This section illustrates preliminary results obtained with the folded fragment. We shall see that further optimization is required to get relevant information.

4.3.4.1 ^{1}H-^{15}N HSQC experiment: assessing well-defined, compact tertiary structure

ScFv Rendomab B1 was enriched in ^{15}N isotope for ^{1}H-^{15}N HSQC experiments. The labelling was performed via expression of the fragment in minimal media supplied with $^{15}NH_4Cl$ as a source of ^{15}N isotope. The urea-unfolded ^{15}N-labelled scFv Rendomab B1 (*ca.* 5 mg.mL^{-1}) was refolded in the presence of PAA5[1] (added at 1:1 wt/wt ratio) by stepwise dialysis to reach a 10 mM Tris-HCl pH 8 buffer (no urea). The sample was concentrated to *ca.* 15 mg.mL^{-1} (*i.e.* ∼0.5 mM) by centrifugation to be compatible with concentrations required for NMR measurements.

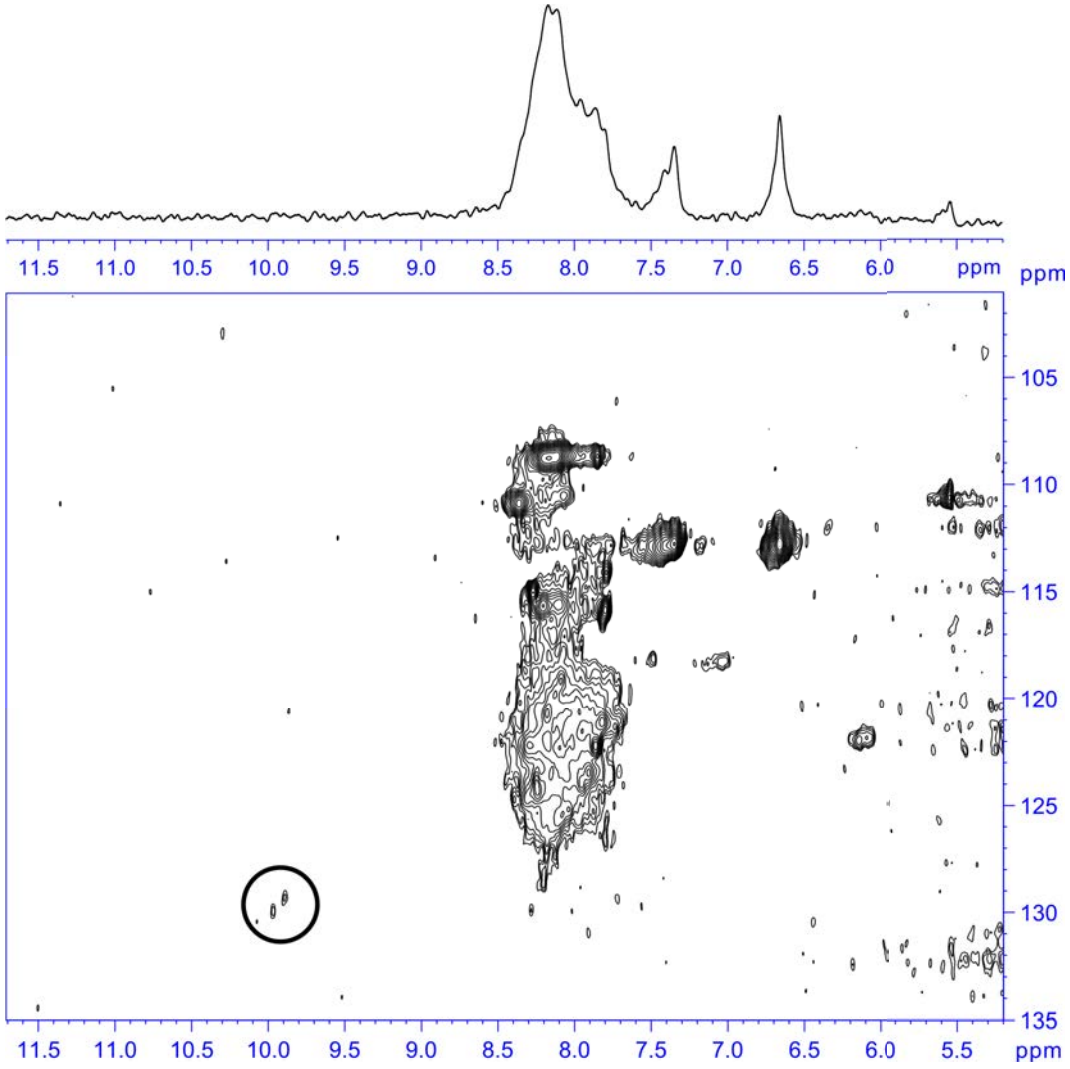


Figure 4.20: ^{1}H-^{15}N HSQC plot of scFv Rendomab B1 refolded with PAA5 (added at 1:1 wt/wt ratio) in 10 mM Tris-HCl pH 8 buffer at 10°C, and corresponding ^{1}H NMR spectrum. [scFv]∼15 mg.mL^{-1}.

Figure 4.20 shows the ^{1}H-^{15}N HSQC plot obtained for the refolded scFv Rendomab

[1] A short polymer was used here to limit the size of the complexes in order to increase the resolution of the NMR signals (higher rotational diffusion coefficient).

B1:PAA5 sample in 10 mM Tris-HCl pH 8 buffer at 10°C, as well as the corresponding ^{1}H NMR spectrum in the 5.2-11.5 ppm range. The latter shows poorly-resolved, broad peaks that do not correspond to usual spectra of folded proteins (that exhibit highly-resolved and very thin peaks). Accordingly, the ^{1}H-^{15}N HSQC plot shows poorly-defined "spots" and single residues cannot be distinguished from one another. At least two reasons can be invoked to explain the poor resolution observed: i/ the fragment (or a sub-population of it) has not acquired its compact tertiary structure (or its structure fluctuates on time-scales comparable to that of NMR signal averaging); ii/ large species (larger than the protein monomer) are formed. As far as point i/ is concerned, decreasing the temperature should reduce the dynamic structure fluctuations and favour a more compact ("frozen") conformation. However, plots obtained at the lowest temperature studied (10°C, presented in Figure 4.20) did not vary significantly from measurements performed on the same sample at higher temperature (see Appendix D). At the most, by lowering the temperature down to 10°C we can observe the appearance of spots that may correspond to signals from buried tryptophan residues (circled spots on Figure 4.20) and may suggest a better compaction at low T. Point ii/ could also explain the poor resolution as signal from large species (protein oligomers, protein:polymer complexes) that diffuse slowly are not fully averaged on the characteristic time of NMR acquisition. This hypothesis can be analysed by measuring the diffusion coefficient of species present in the NMR sample (by applying a specific magnetic field sequence involving gradients).

4.3.4.2 Determination of the diffusion coefficient: presence of large species

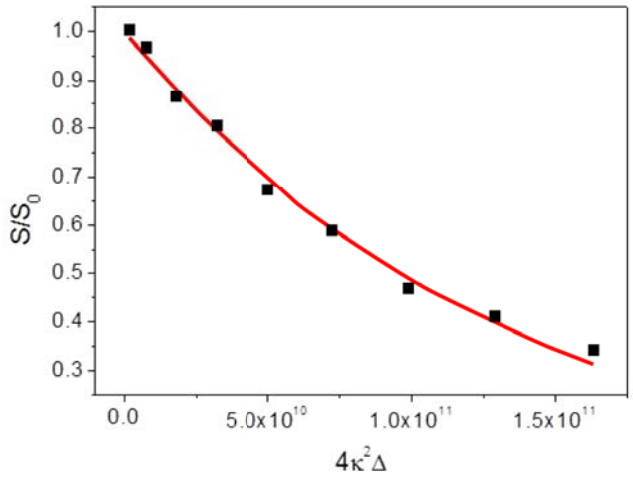


Figure 4.21: NMR determination of the diffusion coefficient of scFv Rendomab B1 refolded with PAA5 (added at 1:1 wt/wt ratio) in 10 mM Tris-HCl pH 8 buffer at 25°C. [scFv]∼15 mg.mL^{-1}.

An NMR method developed by Ferrage and co-workers [374, 375] was used to measure the translational diffusion coefficients of species present in the refolded scFv Rendomab B1:PAA5 sample. Figure 4.21 shows a typical trace obtained with this technique, which was fitted with Equation 4.1 to extract the average diffusion coefficient. The hydrodynamic radius was deduced via the Stokes-Einstein relationship. We obtained an average R_h value of 32.8 ± 2 nm. This high value compared to scFv alone is consistent

with the radius measured by FCS at 0M urea in the presence of PAA150 for scFv Sha 31 and may be the cause of the poor resolution on HSCQ spectra.

$$\frac{S}{S_0} = exp(-4\kappa^2 \Delta D) \tag{4.1}$$

where S/S_0 is the normalized signal measured, $\kappa = \gamma s g G_{max} \delta$ ($\gamma = 2.67513.10^8$ rad.s^{-1}.T^{-1} is the gyromagnetic ratio of the proton, s $= 2/\pi$ is the shape factor of the encoding and decoding gradient pulses, g is the magnetic field gradient applied for each point (gradient amplitude), $G_{max} = 0.695$ T.m^{-1} is the maximum magnetic field gradient and $\delta = 2 \times 10^{-3}$ s is the duration of the gradients), Δ is the total diffusion delay and D is the diffusion coefficient.

The analysis of local polymer:scFv contacts deserve further investigations. Other techniques that rely on the labelling of specific methylene moieties on some residues (isoleucine, leucine, valine, alanine, methionine) can extend the use of NMR to high molecular weight particles (up to ∼500 MDa) when working in a deuterated environment [376], and could hence be of help to unravel the structure and dynamics of the scFv:polymer complexes formed after (or even during) refolding.

4.4 Conclusive remarks and perspectives

The results of this study provide evidence that PAA derivatives are efficient aggregation suppressors during refolding of a two-domain model scFv fragment. FCS pointed to the formation of species of typical hydrodynamic radius that did not exceed *ca.* 50 nm in the refolded sample (no urea), suggesting that scFv:polymer complexes (or small oligomers) were stabilized. Absence of stabilization when a charged denaturant (GndCl) was used, even in the presence of hydrophobically-modified PAA, indicate that Coulomb association is the predominant factor of stabilization. L-arginine, conventionally used at high (molar) concentrations, appeared also very efficient in inhibiting scFv aggregation during refolding (stabilization of monomers). But it could lead to a non-native-like secondary structure as evidenced by SRCD studies, possibly because of an increased pH in L-arginine-containing samples. On the opposite, PAA derivatives systematically ensured recovery of a native-like structure for the refolded fragment.

The folding transition monitored by SRCD suggested that polyanions bearing no hydrophobic side groups did not (or slightly) affect the structure of the intermediates formed all along the folding pathway. On the other hand, PAA150-3C18 and PAA5-25C8-40C3 decreased the cooperativity of folding, supposedly because they interfered with proper assembly of the two scFv domains, and could shift the folding transition towards higher urea concentration. The later observation was attributed to the stabilization of structured intermediates – that differed from the ones formed in the absence of polymer – earlier in the folding pathway, which was tentatively attributed to a preferential interaction with folded of partly-folded structures that exhibit more hydrophobic surfaces than completely unfolded ones.

Overall, this work extend the use of polymers, previously reported to enhance CAB renaturation, to stabilization and refolding of a two-domain protein of therapeutic/diagnosis interest. scFv used in this study were model proteins developed for *in vivo* bio-imaging. Of practical importance, replacement of high concentrations of L-arginine with minute amount of polymers (typically 1:1 wt/wt ratio compared to the protein) should allow *in vivo* activity assays without the cytotoxicity issues inherent to L-arginine

at such concentrations (one of the polymer used in the study, L44-*g*-PAA, has been approved by the FDA to be used in therapeutic formulations). The main advantage of using scFv fragments for *in vivo* imaging reside in their small size that ensure efficient bio-distribution in target tissues. It is here envisioned that large Coulomb-based complexes formed with polymers (radius of *ca.* 50 nm or lower) be dissociated upon *in vivo* administration due to the shielding of electrostatic interactions in high ionic strength physiological milieu. Dynamic, non-covalent attachment of polymers should hence be compatible with therapeutic/diagnosis applications.

Activity measurements of the scFv fragments refolded in the presence of polymers were initiated during this Ph.D. Preliminary result suggest an enhancement of activity recovery in the presence of PAA derivatives [D. Boquet, A. Herbet, unpublished data], most-likely because of a decrease aggregation during refolding. Investigations should be pursued to confirm and quantify the positive effect of polyanions on the renaturation of scFv fragments. Identification of the local contacts between scFv fragments and polymers should also provide support to understand the mode of action of polymers at a (sub)-molecular level and predict the requirements that have to be met for polymers to be efficient aggregation inhibitors.

Part III

Amphiphilic polyelectrolytes for the stabilization of IgG

Chapter 5

Stabilization of IgG during thermal stress in the presence of poly(acrylate) derivatives

In this chapter, we show that a minute amount of poly(sodium acrylate) derivatives protects IgG against thermally-induced aggregation. We find that electrostatic and hydrophobic interactions contribute to the colloidal stability of antibodies during temperature sweep from below to above the protein unfolding/denaturation temperature. The IgG:polyanions association, as well as aggregation upon heating, are characterized by static and dynamic light scattering (SLS and DLS), capillary zone electrophoresis (CZE) and fluorescence correlation spectroscopy (FCS). Conformational stability is studied by differential scanning calorimetry (DSC) and circular dichroism (CD).

We demonstrate that electrostatic binding is strengthened upon unfolding of IgG and suffices to slow down the aggregation rate under thermal stress when working at low ionic strength. Non-specific interactions with poly(acrylates) is a generic and low-cost tool to stabilize therapeutic proteins, whilst the labile nature of association turns out to minimize detrimental effects of polymers on bioactivity of IgG in physiological milieu.

Contents

5.1 Motivation to study IgG stability 119

5.1.1 Therapeutic antibodies: promises and drawbacks 119

5.1.2 Effect of high temperature on IgG aggregation 120

5.1.3 Preparation of IgG:polymer mixtures 120

5.2 IgG:polymer complexes at room temperature 120

5.2.1 Study of complexation by capillary zone electrophoresis 121

5.2.2 Characterization of the complexes by fluorescence correlation spectroscopy 125

5.2.3 Effect of polymers on the structure and activity of native IgG . 127

5.3 Evidence of association between polymers and heat-stressed IgG 129

5.3.1 Calorimetry study of thermal denaturation of IgG 129

5.3.2 Heat-induced variation of the secondary structure of IgG . . . 132

5.4 Impact of poly(acrylate) derivatives on IgG aggregation upon thermal stress 135

5.4.1 Aggregation of heat-stressed IgG: study by light scattering . . 135

5.4.2 Aggregation kinetics by static light scattering 136

5.4.3 Aggregation of heat-stressed IgG: study by fluorescence correlation spectroscopy 139

5.5 Conclusion 142

5.1 Motivation to study IgG stability

5.1.1 Therapeutic antibodies: promises and drawbacks

Therapeutic monoclonal antibodies play an increasingly important role in the treatment of several human diseases. Their medical use and commercialization are predicted to increase rapidly over the next few years (see Chapter 1). Yet, together with the excitement generated by the efficacy of therapeutic antibodies come concerns related to their biological half-life, insufficient stability, and aggregation that is suspected to elicit occasional immunogenicity [27, 29]. In addition to therapeutic monoclonal antibodies, human polyclonal IgG (naturally occurring mixtures of many IgGs that recognize different epitopes) are important drugs on the market. Polyclonal IgG solutions are commonly used as intravenous therapeutics for substitution in antibody deficiency and immunomodulation in some autoimmune diseases [377]. But their implementation is limited to specialized health practitioners well aware of the good practices and stability issues. As for monoclonal antibodies, polyclonal antibodies are highly sensitive to aggregation under environmental perturbations: studies reported on IgG aggregation under pH changes [38, 39, 45], temperature excursions [47–51], chemical modifications [52], adsorption to air-liquid [53] and solid-liquid interfaces, high protein concentration, shaking [54], shear or lyophilization [55]. Due to the expression of a huge Ig-gene repertoire, polyclonal IgG mixtures are extremely heterogeneous, which has been shown to result in a significant propensity for aggregation (some IgG molecules are able, for instance, to recognize other IgG molecules as their antigen counterparts and form reversible complexes via secondary interactions [378], with potential evolution towards higher order oligomers and aggregates [51]).

To enhance the stability and pharmacokinetic properties of therapeutic antibodies, several approaches are actively pursued: tailoring their biological sequence [15, 29], chemical modifications [225, 379] or resorting to the addition of molecular excipients/stabilizers [380, 381] (see Chapter 2). Most stabilizers are used at concentrations too important to be of practical use in injectable drug formulations. The low protein:polymer ratio conditions reported as being efficient protection by macromolecules (*e.g.* to stabilize enzymes or antibody fragments, see previous chapters) is an exception that may be helpful for therapeutic proteins. Before the present study, there were no reports on non-covalent polymer-induced stabilization of antibodies, which is the objective of this chapter. Here, solutions of polyclonal or commercially-available monoclonal IgG are used as model for antibodies in view of the wealth of data available on their heat-induced denaturation and aggregation.

As far as pharmaceutical application is the goal, instability issues of IgG usually refer to the preservation of IgG monomers for long-term storage, which depends on a combination of chemical degradation and (partial) unfolding [32] (see Chapter 1). As a preliminary investigation, we tested the stability at ambient temperature of marketed monoclonal therapeutic antibodies (mAbs) upon storage in buffer devoid of any protectant additive. We performed time-dependent size exclusion chromatography (SEC) and light scattering measurements on Cetuximab and Infliximab alone or in the presence of polymers (see Appendix E). These control experiments showed no sign of protein aggregation for up to 20 days-long incubation (mAbs remained under their monomeric form on this time-scale in the absence of any additive). This study confirms that, nowadays, stability in aqueous formulations of marketed therapeutic proteins has been optimized (which is not the case of non-marketed biotherapeutics under development). Studying their aggregation at

ambient condition and at rest (no shear) necessitate time-consuming long-term stability trials. Since we look for evidence of general, non-specific, effects of macromolecules on IgG solubility, mimicking the route of degradation of therapeutic IgG is not the concern of the present work. Accelerated destabilisation can be obtained at higher temperature. Heat-stressed IgG solutions are certainly not representative of samples used in medical context, but this stress can be performed in aqueous buffer solution and with well-controlled conditions to produce models of unstable IgG oligomers, unfolded monomers and aggregates whose interaction with polymers can be studied in details.

5.1.2 Effect of high temperature on IgG aggregation

Thermal stress has been widely used to accelerate IgG aggregation [47–51]. The heat-induced denaturation and aggregation of IgG has been characterized in several reports, which showed that this protein unfolds stepwise and undergoes parallel (irreversible) aggregation when heated above ∼60°C (see for instance [47–51]. It is worth noting that even though high temperature is a common parameter to be selected for accelerating protein aggregation, this can involve non-Arrhenius behaviour, which makes quantitative predictions difficult [58]. High temperatures have several effects on proteins, including decreasing the thermodynamic stability (unfolding), facilitating/triggering hydrophobic association, increasing diffusion (higher frequencies of molecular collisions) and the rate of chemical reactions. All these effects accelerate the formation of aggregates [28]. Protein thermodynamic stability is particularly affected by high temperature [52]. At room temperature (and to a lesser extent at the usual storage temperatures of 2-8°C), IgG molecules under their native state are in equilibrium with partly unfolded molecules. Increasing the temperature displaces this equilibrium towards the non-native unfolded intermediates that evolve rapidly toward aggregation. We want to understand whether polymer additives can limit such aggregation. The chemical structure of the polymers used in this work, PAA, PAA-3C18 and PAA5-25C8-40C3, can be found in Chapter 2.

5.1.3 Preparation of IgG:polymer mixtures

Stock solutions of the polymers (2–20 $mg.mL^{-1}$) were prepared by dissolving freeze-dried polymer powders in deionized water under gentle stirring for at least 2 hours at room temperature. Aliquots of concentrated buffer (0.5 M NaH_2PO_4/Na_2HPO_4, pH 6.8) and, in some cases, NaCl (0.5 M) were added to the polymer and/or IgG stock solutions to reach a final concentration of 20 mM phosphate and possibly 100 mM NaCl. Solutions prepared with no added NaCl are referred to as "no NaCl" whereas solutions containing 100 mM NaCl are designated as "with NaCl".

Prior to measurements, the IgG:polymer mixed solutions were dialysed for at least 3 hours against the appropriate buffer (slide-A-lyzer, MWCO 3500, from Pierce). The IgG concentration in the dialysed solutions was determined from the absorbance at 280 nm, using the extinction coefficient of 1.4 $mL.mg^{-1}.cm^{-1}$ [Tech Tip # 6, "Extinction Coefficients", ThermoScientific], and adjusted to the desired concentration by dilution in the dialysing buffer.

5.2 IgG:polymer complexes at room temperature

Amphiphilic polyelectrolytes can associate with native proteins through a complicated combination of several intermolecular interactions. Depending on the protein and the

nature of the polymer, it is thus possible that complexes are formed with native IgG (prior to heating). Before studying the behaviour of heated IgG:polymer solution, we shall assess whether formation of complexes takes place in native IgG:polymer mixtures. We will first study the presence of complexes and the contribution of Coulomb attraction (capillary zone electrophoresis), then analyse the size of complexes and aggregation numbers (fluorescence correlation spectroscopy) and finally check the preservation or not of the native conformation of IgG (circular dichroism).

5.2.1 Study of complexation by capillary zone electrophoresis

We carried out an analysis of mixed IgG:polymer solutions by capillary zone electrophoresis (CZE), a technique that allows one to assess the effect of Coulomb binding by studying the migration of the proteins, polymers chains and complexes in aqueous buffers of various ionic strengths and pHs. IgG solutions (without polymers) were injected in the inlet of the separation capillary that had been flushed with a solution of polymer in the running buffer. The protein thus migrate through an excess of polymer. When the dynamic of protein:polymer association is fast compared to migration time, an equilibrium is established (between complexes and the (free) polymer present in the running buffer), and the apparent mobility hence reflects the average between mobilities of unbound IgG and IgG:polymer complexes (see details on the technique and on experimental conditions in Appendix B and Appendix A).

5.2.1.1 Influence of the nature of the polymer

Representative electropherograms obtained using solutions of polymers in 20 mM phosphate buffer pH 6.8 are plotted in Figure 5.1. Electropherograms of IgG alone and of polymers alone are also reported. The peak of the polyclonal IgG was broad (compared to the signal of the neutral standard mesityl oxide (MeO)), which probably reflects the polydispersity of isolectric points (pI) in the population of IgGs. The low (average) peak mobility suggests however that a predominant fraction of the proteins was close to its pI at pH 6.8.

Mobilities of the polymers were significantly higher, in consistency with the polyanionic nature of the chains (about $-32 \cdot 10^{-6}$ cm^2.V^{-1}.s^{-1} for IgG and $-350 \cdot 10^{-6}$ cm^2.V^{-1}. s^{-1} for poly(acrylate) derivatives, a value characteristic of highly charged polymers, such as PAA under its sodium salt form [224, 334]). The large difference in mobilities was favourable to separation of complexes, unbound polymers and IgG with good resolution.

Electropherograms obtained with mixed IgG:hydrophilic polymers (polymers devoid of hydrophobic side groups, PAA150 and L44-*g*-PAA), showed little evidence of IgG:polymer association at room temperature: the signal due to free IgG was slightly weaker than that of IgG alone and presented some tailing that may be ascribed to the formation of transient and weak interactions with IgG. In the presence of amphiphilic chains (PAA5-25C8-40C3, PAA150-3C18) the decrease of free IgG signal, altogether with a slower recovery of the baseline (between $-100 \cdot 10^{-6}$ cm^2.V^{-1}.s^{-1} and $-320 \cdot 10^{-6}$ cm^2.V^{-1}.s^{-1}), was the signature of IgG:polymer complexes. The strongest association was observed in IgG:PAA150-3C18 mixture. The electropherogram of IgG:PAA150-3C18 presented no detectable trace of the peak corresponding to unbound IgG. A signal appeared at higher mobility centred at $\mu \approx -320 \cdot 10^{-6}$ cm^2.V^{-1}.s^{-1}), and was attributed to tight complexes between PAA150-3C18 and native IgG (Figure 5.1 top right).

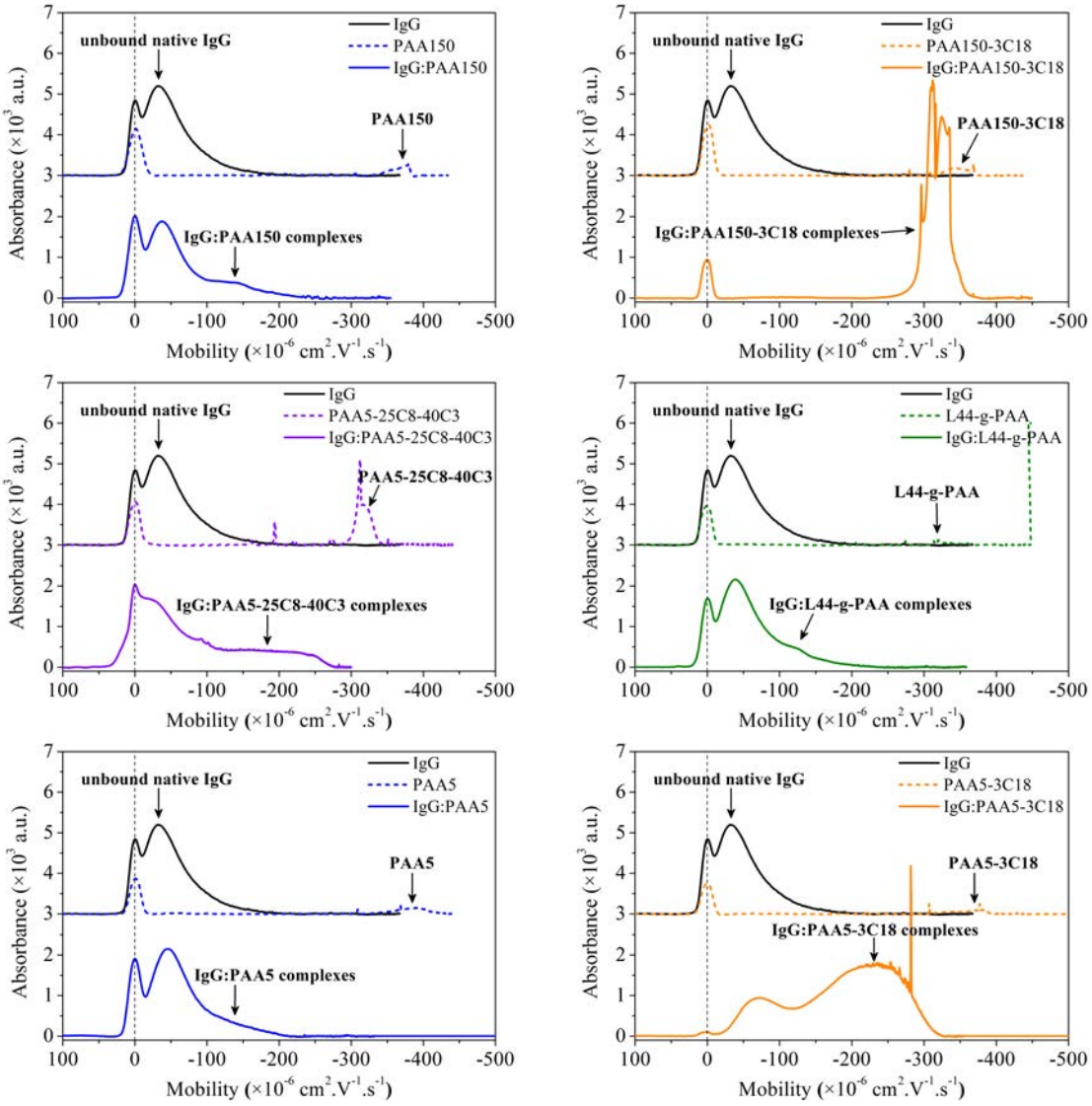


Figure 5.1: Electropherograms of IgG:polymer mixtures in 20 mM phosphate buffer pH 6.8. IgG was injected at 3 mg.mL^{-1} in a capillary filled with polymer solutions at 0.5 g.L^{-1}. The reference peak at $\mu = 0$ cm^2.V^{-1}.s^{-1} corresponds to the internal neutral standard, mesityl oxide (MeO).

Chain length probably affects the affinity. In electropherograms of IgG mixed with the shorter PAA5-3C18 polymer, the magnitude of the peak associated to unbound IgG was less diminish than with the longer PAA150-based derivative (at the same concentration of 0.5 g.L^{-1} in Figure 5.1), and the peak of complexes had a lower mobility. These differences indicate that i/ PAA5-3C18 has a lower affinity than PAA150-3C18 for IgG (less complexes were formed or they dissociated in the capillary during the separation) and ii/ the apparent charge of complexes with the short PAA5-3C18 is comprised between the charge of IgG and that of the polymer chains, *i.e.* the short polymer does not bring the large excess negative charge upon binding to IgG as does the longer polymer.

Irrespective of the chain length, comparison of the various polymers as a function of

their propensity to form complexes with unstressed IgG suggests that C18 hydrophobic side groups significantly enhance the binding, though the hydrophilic PAA chains can (weakly) associate with native IgG, presumably due to Coulomb attraction.

5.2.1.2 Influence of the ionic strength

To assess the contribution of Coulomb interaction to the stability of IgG:polymer complexes, similar experiments were carried out in the presence of 100 mM NaCl in the running phosphate buffer. Figure 5.2 compares the electrophoregrams obtained in the absence and presence of 100 mM NaCl zooming on the peak of unbound IgG. With each polymer studied, increasing the ionic strength decreased the fraction of bound IgG (higher peak of free IgG in Figure 5.2). Even with PAA150-3C18 that bound quantitatively IgG in the absence of NaCl, there was little evidence of IgG:polymer association in the presence of NaCl (slight decrease in the peak height ($< 15\%$) of unbound IgG). In the presence of the other polymers (PAA150, PAA5-25C8-40C3 and L44-*g*-PAA), the tailing of the peak betraying weak complexes without NaCl vanished upon addition of NaCl in the buffer .

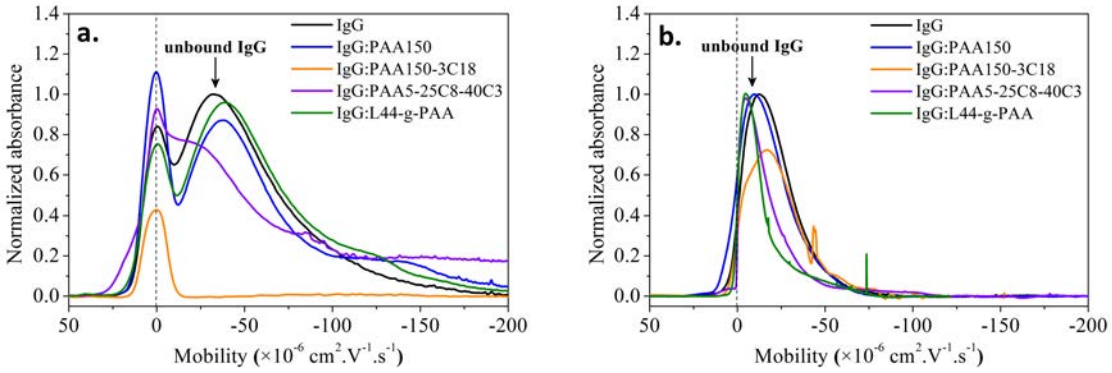


Figure 5.2: Electropherograms of unstressed IgG in the presence of polymers in the running buffer (20 mM phosphate buffer pH 6.8) in the absence (a.) or presence (b.) of 100 mM NaCl. IgG was injected at 3 mg.mL^{-1} in a capillary filled with polymer solutions at 0.5 g.L^{-1}.

We conclude that the association between IgG and PAA derivatives, including PAA150-3C18, is predominantly driven by Coulomb attraction that are shielded at high ionic strength. Hydrophobic association contributes to make the binding stronger with 3C18 derivatives. IgG concentrations around 1 g.L^{-1} are representative of stock solutions of commercial biotherapeutics. The minor fraction of bound IgG in the presence of 100 mM NaCl (except with PAA150-3C18) suggests that the complexes with PAA or L44-*g*-PAA will dissociate upon dilution of the stock solutions. Other studies presented in this chapter (CD, DSC, etc.) were carried out with IgG and polymer concentrations usually 10 times lower, and it is expected that complexes are formed essentially in the absence of NaCl, due to stronger Coulomb attraction.

5.2.1.3 Binding isotherms (PAA150-3C18)

With PAA150-3C18, the fraction of bound IgG could be measured at the working experimental concentrations enabling us to determine binding isotherms. These isotherms

provide an indication on the amount of polymer required to fully complex IgG. We performed capillary zone electrophoresis measurements by injecting a constant amount of native IgG into a capillary containing increasing concentrations of polymer in the running buffer (from 0 to 1 g.L^{-1}). The electropherograms obtained at increasing PAA150-3C18 concentration in 20 mM phosphate buffer, pH 6.8, supplemented or not with 100 mM NaCl are shown in Figure 5.3. The increasing degree of association with increasing polymer concentration is reflected in this figure by the gradual decrease of the peak of free IgG.

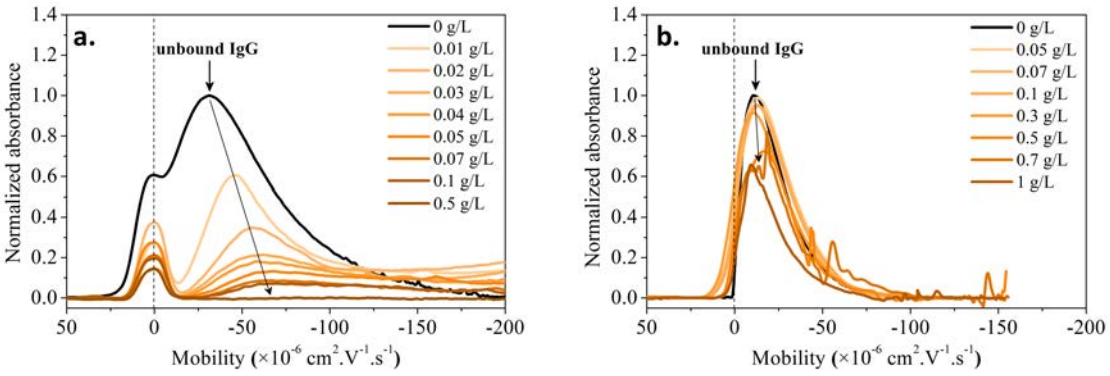


Figure 5.3: Electropherograms of unstressed IgG with increasing PAA150-3C18 concentration in the absence (a.) or presence (b.) of 100 mM NaCl. IgG was injected at 3 mg.mL^{-1} in a capillary filled with polymer solutions at varying concentrations.

The normalized area, A, of the peak of unbound IgG (a constant amount of IgG was injected irrespective of polymer concentration) can be converted into the mass of free IgG, giving the mass of complexed IgG by Equation 5.1:

$$m_{\text{complexed IgG}} = \frac{A/t_{\text{IgG}}}{A_0/t_0} \cdot [\text{IgG}] \cdot V_{\text{inj}} \tag{5.1}$$

where A (resp. A_0) is the area of the peak (in absorbance vs. migration time representation) of unbound IgG in the presence (resp. absence) of polymer, t_{IgG} (resp. t_0) is the elution time at the maximum of the peak of unbound IgG in the presence (resp. absence) of polymer, [IgG] is the IgG concentration (3 mg.mL^{-1}) and V_{inj} is the volume of stock solution injected in the capillary, calculated using the Poiseuille equation:

$$V_{\text{inj}} = \frac{\Delta P \cdot \pi \cdot d^4 \cdot t_{\text{inj}}}{128 \cdot \eta \cdot L_t} \tag{5.2}$$

where ΔP is the pressure difference between the inlet and outlet of the capillary during injection (ΔP = 0.3 psi), d is the inner diameter of the capillary, t_{inj} is the injection duration (t = 3s), η is the viscosity of the sample and L_t is the total length of the capillary.

Binding isotherms are plotted in Figure 5.4 as the mass of bound IgG as a function of the total mass of PAA150-3C18 present in the capillary (between the injection point to the detection window, *i.e.* in the segment of capillary crossed by IgG during migration.[1]

[1]This calculated amount of polymer in the capillary is not exactly the amount of polymer that IgG crosses before reaching the detection window. The negatively-charged polymer actually migrates against

Ionic strength and pH affected the isotherms (see Figure 5.4). In the absence of NaCl, the binding isotherm showed a sharp jump until the concentration of PAA150-3C18 reached 0.07 g.L^{-1}. At these concentrations, all IgG were bound and the amount of IgG-exposed polymer was *ca.* 65 ng (compared to 60 ng of injected IgG), which corresponds to a binding ratio of ∼1:1 wt/wt.

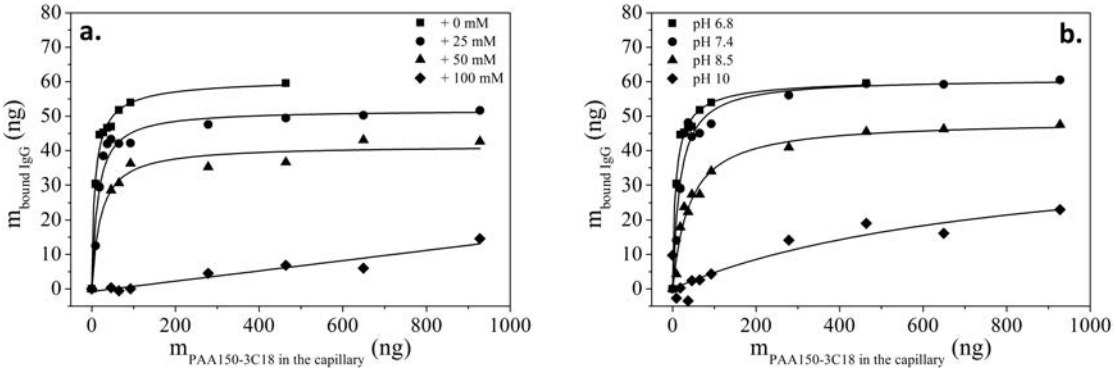


Figure 5.4: Variation of the mass of complexed IgG, based on measurements of the area under the peak of residual unbound protein monomers as a function of the amount of PAA150-3C18 present in the capillary at different ionic strengths but constant pH of 6.8 (a.) and different pH but constant 20 mM ionic strength (b.).

When increasing [NaCl] up to 50 mM, similar sharp initial increase (and absence of free IgG) was observed at low concentration of polymer which was indicative of high affinity (binding constant < μM). The bound IgG:polymer ratio decreased down to 0.6:1 wt/wt. At 100 mM NaCl, the affinity of the polymer for native IgG considerably decreased, as suggested by the presence of unbound IgG in the capillary and the linear variation of the fraction of bound IgG in the experimental concentration window. This result confirms that electrostatic attractions are almost shielded at ionic strength >100 mM. Consistently, when the pH of the buffer was increased up to pH 10[2] (at a constant ionic strength of 20 mM), the net charge of the protein became more negative and Coulomb repulsion were expected to emerge. Binding isotherms reflected this charge-driven effect by a decrease of the bound IgG:polymer ratio with increasing pH.

Finally, we conclude that PAA150-3C18 forms tight complexes with unstressed IgG at a polymer/protein weight ratio as low as 1 with a binding affinity markedly dependant on Coulomb association (strengthened by hydrophobic interactions).

5.2.2 Characterization of the complexes by fluorescence correlation spectroscopy

Size and stoichiometry of complexes can be studied *in situ* (no separation between unbound species at equilibrium with complexes) by fluorescence correlation spectroscopy (FCS, see details of the technique in Appendix B). Interestingly, FCS allows to specifically detect fluorescein-labelled IgG (FITC-IgG) within a "sea" of invisible (unlabelled) polymer chains. FITC-IgG associated to polymers were detected as larger objects (lower diffusion

the electro-osmotic flow which makes IgG go through a larger amount of polymer. The difference of crossed polymer amount was neglected in our calculations.

[2]pH 7.4 is fixed by phosphate buffer, pH 8.5 by Tris-HCl buffer and pH 10 by boric acid buffer

coefficient) than free FITC-IgG. The autocorrelation curve was analysed by the MEMFCS algorithm to extract the hydrodynamic radii of FITC-IgG-containing species and their mean aggregation number, defined as the average number of FITC-IgG per entity in the solution (complex or oligomer, see Appendix B for details).

FCS measurements were carried out with mixed solutions of a FITC-IgG and unlabelled polymers used in equal weight at a concentration of 0.02 mg.mL^{-1} in 20 mM phosphate buffer, pH 6.8, with or without 100 mM NaCl.

Table 5.1: Average hydrodynamic radius and aggregation number in FITC-IgG:polymer mixtures (20 mM phosphate buffer pH 6.8 with or without 100 mM NaCl; [FITC-IgG] = [polymer] = 0.02 mg.mL^{-1}). Hydrodynamic radii are here average values extracted from the Maximum Entropy Method (see Appendix B for details). The aggregation numbers also reflect an average value under the assumption of the presence of a single population.

Polymer	No NaCl		100 mM NaCl	
	R_h (nm)	N_{agg}	R_h (nm)	N_{agg}
No polymer	5.2	1.1	4.8	1.0
PAA5	5.8	1.1	nd	nd
PAA150	4.8	1.1	6.9	1.0
PAA5-3C18	8.7	1.0	nd	nd
PAA150-3C18	41	1.7	4.5	1.0
PAA5-25C8-40C3	5.8	1.1	4.9	1.0
L44-*g*-PAA	5.2	1.2	nd	nd

nd: not determined.

R_h of native (unstressed) FITC-IgG without polymers was $\sim$ 5 nm, in agreement with reported radius of a native IgG monomer [49]. The same R_h value was recorded for solutions of FITC-IgG mixed with either PAA5, PAA150, PAA5-25C8-40C3 or L44-*g*-PAA, independently of salt concentration, and the apparent N_{agg} remained close to 1 (Table 5.1). For mixed FITC-IgG:PAA150-3C18 solutions containing 100 mM NaCl, the R_h value was also $\sim$ 5 nm. FCS results confirm the absence of complexes in the (dilute) conditions listed above, which is consistent with results by CZE (Section 5.2.1).

In contrast, larger objects were observed in mixed solutions of FITC-IgG:PAA150-3C18 in the absence of NaCl. The R_h of the fluorescent objects in this case was $\sim$ 40 nm, a size higher than the R_h of PAA150-3C18 alone in the same buffer ($R_h \sim 16.1 \pm 2.7$ nm from FCS measurement on rhodamine-labelled PAA150-3C18), which confirms the tight association, in consistency with CZE results. FCS indicates in addition that complexes contained between 1 and 2 IgG on average. Note that for the shorter PAA5-3C18 polymer, complexes with FITC-IgG could be detected, but their size was close to the size of IgG monomers, making it difficult to separate the contribution of each species (we measured a slight increase of R_h from 5 nm to 8.7 nm). An estimation of the FITC-IgG:PAA150-3C18 stoichiometry by FCS is discussed in Appendix E and confirms the CZE result of a 1:1 wt/wt association. FCS measurement undertaken with unlabelled IgG but rhodamine-labelled polymer showed in addition that there was on average 1 polymer chain per complex (see Appendix E).

5.2.3 Effect of polymers on the structure and activity of native IgG

The question addressed in this paragraph is whether the native-like structure and activity of the protein is altered by association with polymers. We show by CD and binding assays that the presence of polymers either does not or can slightly affect the native structure of unstressed (room temperature) IgG, but does not perturb binding activity in physiological milieu.

5.2.3.1 Secondary structure monitored by circular dichroism

The effect of polymers on the secondary structure of IgG at room temperature was investigated using far-UV circular dichroism (CD). The spectrum of native IgG, plotted in Figure 5.5, was that of a typical immunoglobulin G, with a negative band at *ca.* 218 nm as well as a zero intensity at about 210 nm, which is consistent with a predominant β-sheet structure as already reported for IgG [47, 48]. The secondary structure content can be estimated using a program of deconvolution of CD data, such as the on-line program DichroWeb [372, 373]. Table 5.2 reports the values obtained with the CONTINLL analysis (reference dataset SP175), which are in agreement with values reported for monoclonal IgGs (see for instance the Protein Circular Dichroism Data Bank [382, 383].

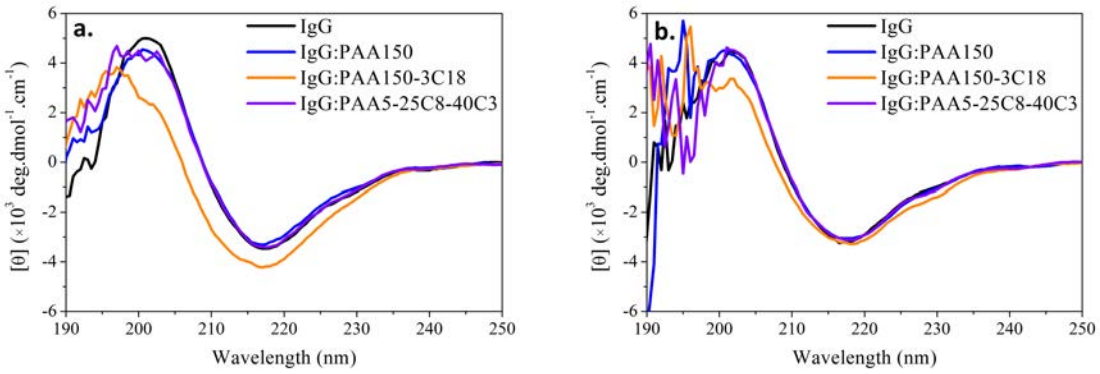


Figure 5.5: CD traces of IgG at 25°C and at 0.2 mg.mL^{-1} supplemented or not with polymers (1:1 wt/wt ratio) in 20 mM phosphate buffer pH 6.8 in the absence (a.) or presence (b.) of 100 mM NaCl.

CD spectra measured for IgG:polymer mixtures did not differ from the spectrum of native IgG alone, except in the presence of PAA150-3C18. This latter polymer seems to favour a less structured state of the protein. However, the secondary structure content as estimated with DichroWeb was not affected by this difference in the raw CD spectrum (within the accuracy of the deconvolution process: precision of ±5%). An alternative to Dichroweb is the BestSel program analysis, recently developed by Micsonai *et al.* [338] to account better for β-folds (see Appendix B for details). Results are reported in Table 5.2 for comparison. We observe that IgG still presented a predominant β-sheet structure, whereas addition of PAA150-3C18 led to a 5% decrease in anti-parallel β-sheet content altogether with an increase in parallel β-sheet content (not shown). The other polymers did not perturb the secondary structure of IgG.

PAA150-3C18 therefore slightly alters the secondary structure of native IgG (which can be referred to as a "denaturing" effect, in the sense that the polymer modifies the native structure of the protein). Figure 5.6 shows the evolution of the CD spectra of IgG,

Table 5.2: Secondary structure content of native IgG in the presence or not of polymers, in 20 mM phosphate buffer pH 6.8 ([IgG] = [polymer] = 0.2 mg.mL^{-1}).

Polymer	Secondary structure content (%)							
	DichroWeb analysis				BestSel analysis			
	α-helix	β-sheet	Turn	Coil	α-helix	β-sheet[a]	Turn	Coil
No polymer	6	46	10	38	0	50	13	37
PAA150	6	45	11	38	0	47	13	39
PAA150-3C18	7	44	11	39	1	45	10	38
PAA5-25C8-40C3	6	46	10	38	0	50	12	38

[a] For the BestSel analysis, "β-sheet" refers to anti-parallel β-sheet structures, parallel β-sheets are not shown (it is the complement to 100% of the sum of secondary structure shown in the table).

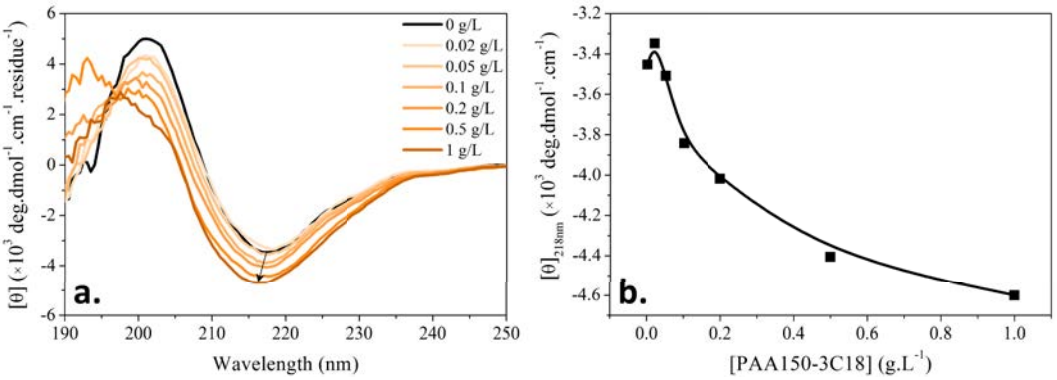


Figure 5.6: CD traces of IgG (0.2 mg.mL^{-1} at 25°C supplemented with increasing PAA150-3C18 concentration (a.) and evolution of [θ] at 218 nm as a function of [PAA150-3C18] (b.) in 20 mM phosphate buffer pH 6.8 (no NaCl).

as well as that of [θ] at 218 nm upon increasing polymer concentration. As observed, the denaturing effect of PAA150-3C18 increased as its concentration increased. Figure 5.6b suggests that this effect tend to reach a plateau for a polymer concentration above 1 g.L^{-1} of polymer.

Influence of the ionic strength

In the presence of 100 mM NaCl (in the 20 mM phosphate buffer pH 6.8), all CD spectra superimposed (Figure 5.5). In particular, the presence of PAA150-3C18 no longer affected the secondary structure of IgG in these conditions. This is consistent with the marked weakening of association between this polymer and IgG at high ionic strength, as shown by CZE and FCS in Section 5.2.1 and Section 5.2.2. The absence of structure perturbation in the presence of salt near physiological ionic strength should limit deleterious effect of polymers on the biological activity of IgG in physiological milieu, a point that is discussed in Appendix E.

5.3 Evidence of association between polymers and heat-stressed IgG

5.3.1 Calorimetry study of thermal denaturation of IgG

We describe here a study by differential scanning calorimetry (DSC) to assess the effect of poly(acrylate) derivatives on the heat-triggered denaturation of IgG.

5.3.1.1 Influence of the nature of polymers

In the absence of polymer (black line in Figure 5.7), the thermogram of the IgG solution consisted of a broad asymmetric peak spanning from $\sim$ 50 to 80°C with a maximum at *ca.* 69°C (T_m) in agreement with values found in literature [47–51]. The shape of the endotherm was characteristic of the unfolding of a multi-domain protein, which occurs in several overlapping steps that could not be resolved. The diversity of the polyclonal IgG population likely contributes to broaden the endothermic peak [51]. Above 75°C, the thermogram became quite noisy, an effect that has been attributed to protein aggregation [48]. The cooled sample recovered after heating had a milky appearance (see turbidity measurements in Appendix E), confirming the formation of large protein aggregates. This unfolding process was irreversible, as checked by reheating the samples after they had been cooled to room temperature in the microcalorimeter (not shown).

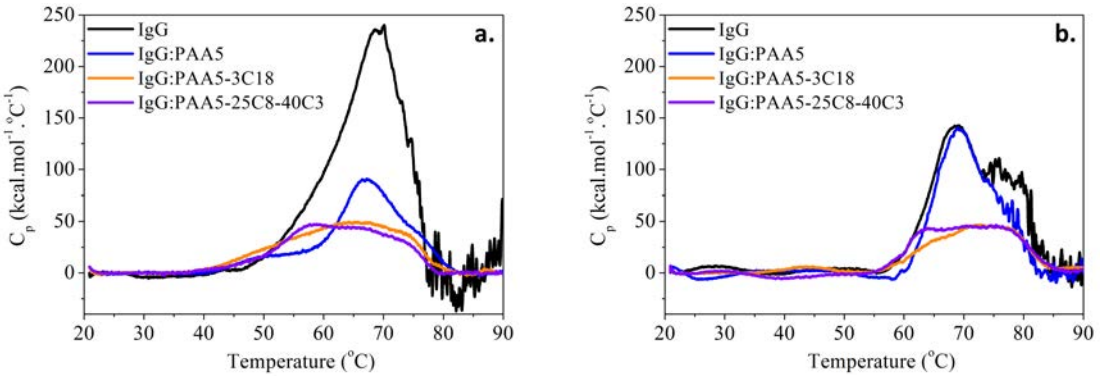


Figure 5.7: DSC thermograms (scan rate = 0.2°C.min^{-1}) of phosphate-buffered (20 mM, pH 6.8) 1:1 wt/wt IgG:polymer mixtures in the absence (a.) or in the presence (b.) of 100 mM NaCl.

Thermograms recorded for IgG:polymer mixtures in the absence of NaCl (Figure 5.7) showed significant differences compared to the thermogram of IgG alone: PAA5-3C18 and PAA5-25C8-40C3 led to broad and featureless endotherms, spanning from $\sim$ 40 to 75°C, with no well-defined maximum. Interestingly, the high temperature section of the thermograms obtained in the presence of polymers was smooth, suggesting that aggregation did not occur or, at least, took place to a much lesser extent than for IgG alone (see turbidity measurements in Appendix E). The enthalpy of the transition can be calculated from the area under the endotherm using Equation 5.3:

$$\Delta H = \int_{T_i}^{T_f} C_p \, dT \tag{5.3}$$

where C_p is the base-line corrected excess heat capacity normalized by the concentration of protein, $T_i = 20°C$ and $T_f = 90°C$.

As summed up in Table 5.3, the enthalpy of the transition for IgG in solution in the presence of polymers was significantly lower than the enthalpy associated with the thermal denaturation of IgG alone in solution. The 2.3 to 3-fold decrease of ΔH is an indication that polymers interacted with the protein during unfolding. A decreasing enthalpy of unfolding is often a signature of a decreasing contribution of intra-protein interaction, and/or increasing hydration of the residues in the native state [42]. The present results hence suggest that, upon thermal unfolding, polymer:protein associations significantly compete with intra-protein associations.

Table 5.3: Temperature and enthalpy of thermal denaturation of 0.2 mg.mL^{-1} IgG in the absence or presence of poly(acrylate) derivatives (added at 1:1 wt/wt ratio). Scan rate: 0.2°C.min^{-1}; 20 mM phosphate buffer pH 6.8 supplemented or not with 100 mM NaCl as quoted.

Polymer	T_m[a] (°C)		ΔH (kcal.mol^{-1})	
	No NaCl	100 mM NaCl	No NaCl	100 mM NaCl
No polymer	69.5	68.9	3,300	2,200
PAA5	67	68.9	1,100	2,000
PAA150	67	nd	1,050	nd
PAA5-3C18	66	broad	900	700
PAA150-3C18	64	nd	600	nd
PAA5-25C8-40C3	broad	broad	1,100	900

[a] When a shoulder or several peaks were observed, T_m of the main peak is indicated. broad: broad peak making it difficult to determine T_m; nd: not determined.

5.3.1.2 Influence of the ionic strength

The involvement of Coulomb interactions on the stability of heat-stressed IgG:polymer solutions was assessed by measurements in the presence of 100 mM NaCl in the buffer. As seen in Figure 5.7, when NaCl was added, the thermogram recorded for mixed IgG:PAA5 solutions presented all the signs of IgG aggregation and was similar to the thermogram of IgG alone in the same buffer. In contrast, thermograms recorded for solutions containing amphiphilic chains (IgG:PAA5-3C18 and IgG:PAA5-25C8-40C3) and 100 mM NaCl retained the characteristic features observed with no NaCl: the shape of the thermograms was broad, with a peak slightly shifted to lower T, and the enthalpies of the transition were similar to those obtained for the mixtures in salt-free conditions (Table 5.3). Hence, hydrophobic interactions significantly stabilize complexes of PAA5-3C18 or PAA5-25C8-40C3 with heat-stressed IgG that appeared to be still interacting with amphiphilic chains in conditions of lack of association with PAA chains.

These measurements were made in addition in mixed solutions with longer PAA150 and PAA150-3C18 polymers. No significant effect of increasing chain length could be observed (see Figure E.9 in Appendix E and Table 5.3): we determined in particular that the same 2.3 to 3 fold decrease of unfolding enthalpy of IgG occured at low ionic strength with either long or short polymers. Interestingly, this effect was significant at the 1:1

wt/wt protein:polymer ratio used, which corresponds for long chains to a 1:1 mol/mol ratio (both IgG and long polymers have the same average molecular weight of 150,000 $g.mol^{-1}$).

In conclusion, the marked salt effect on the IgG denaturation in the presence of PAA suggests that electrostatic interactions are responsible for the effect of PAA on the energy of thermal denaturation of IgG in salt-free solutions. In contrast, the lack of signature of any effect of NaCl in the endotherms of IgG mixed with amphiphilic polymers suggests that hydrophobic association is in these cases essential to interaction with heat-stressed IgG.

5.3.1.3 Importance of polymer concentration

As regards the effect of polymer concentration, studies were carried out here with the short polymers. We observed that in the presence of amphiphilic chains (PAA5-3C18 or PAA5-25C8-40C3), both T_m and ΔH decreased gradually with increasing polymer/IgG ratio (Figure 5.8). The reference experiments performed with PAA5 (in the presence of 100 mM NaCl) showed that thermal denaturation was not affected in the same range of experimental concentrations (< 1.8 $g.L^{-1}$), which confirmed the efficient screening of electrostatic interactions in these conditions. Of practical importance, the minimum quantity of amphiphilic polymers needed to protect IgG could be estimated by the onset of plateau values reached in Figure 5.8 in the window of polymer/IgG weight ratio of 1-1.5. Compared to protective osmolytes that are usually added at molar concentrations, this result suggests that millimolar concentration of the polymer repeat units is sufficient to efficiently bind and protect the heat-stressed protein (1:1 wt/wt ratio corresponds here to *ca.* 30 chains of the short polymers per IgG).

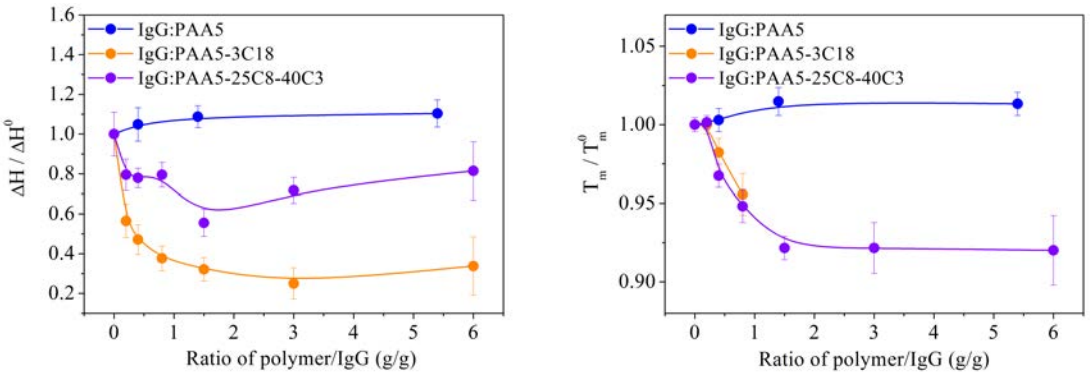


Figure 5.8: Variation of the enthalpy of thermal denaturation, ΔH, and unfolding temperature, T_m, of IgG measured by DSC as a function of the polymer/protein weight ratio (normalized by the values obtained for IgG alone). The concentration of IgG was 0.3 $mg.mL^{-1}$. Lines are shown to guide the eye. All solutions were buffered in 20 mM sodium phosphate at pH 6.8 with 100 mM NaCl. With PAA5-3C18, T_m could not be measured above a ratio of 1:1 wt/wt, because the shape of endotherms turned into several overlapping curves (see Appendix E).

We conclude that all PAA and hydrophobically-modified PAA used above 1:1 wt/wt ratio markedly affect the denaturation (decrease of the enthalpy of thermal unfolding, prevention of massive aggregation) of IgG in the buffer at low ionic strength. But only

the amphiphilic polymers (with either long or short chain length) interact with unfolding IgG intermediates in the presence of 100 mM NaCl. The polymer-induced decrease of the unfolding enthalpy is taken as an indication that polymers are bound to partially unfolded IgG, involving binding enthalpy that is of comparable magnitude as the enthalpy of folding.

5.3.2 Heat-induced variation of the secondary structure of IgG

5.3.2.1 Comparison of CD spectra before and after heating

The variation of enthalpy observed by DSC is expected to correlate with (partial) unfolding of IgG during thermal denaturation. Circular dichroism (CD) is therefore a complementary approach that provides information about structural feature of IgG folding states under the form of evolution of the secondary structure of the antibody during the thermal treatment in the presence or absence of polymers. Only the low ionic strength conditions (20 mM phosphate buffer pH 6.8 with no added NaCl) are studied in this section, since we aim at a comparison of the the polymers when they are capable to affect the denaturation process.

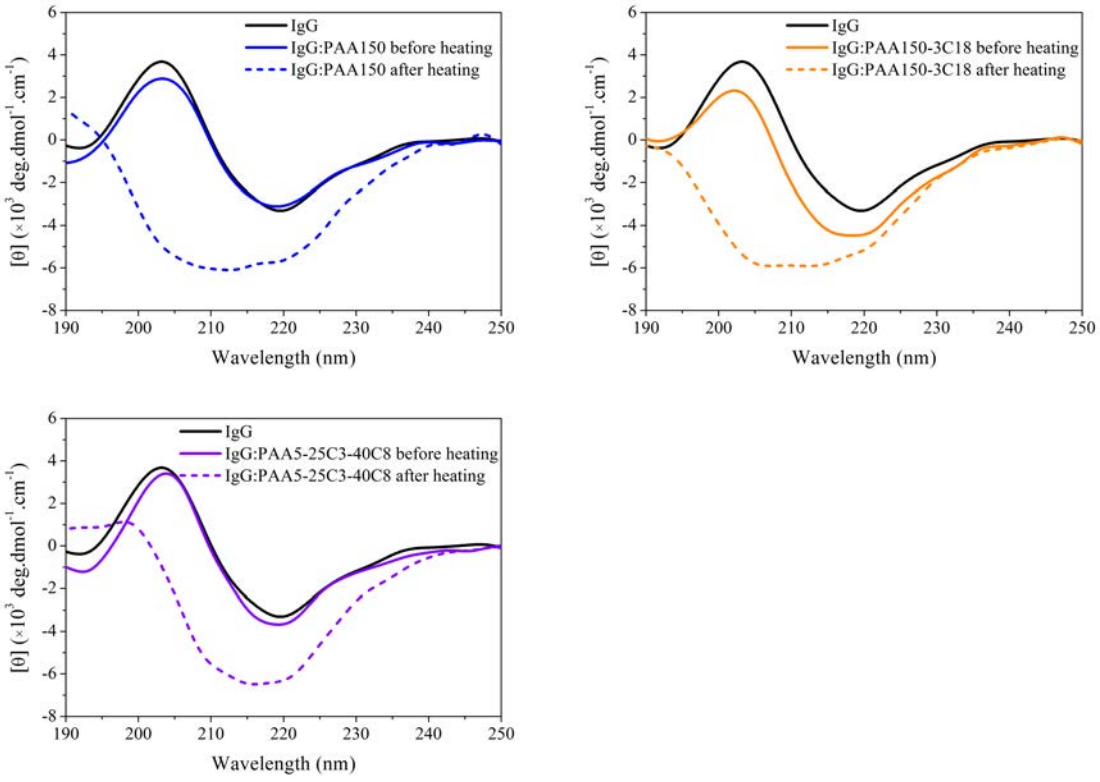


Figure 5.9: Far-UV circular dichroism traces of 1:1 wt/wt IgG:polymer mixtures before and after heating above T_m. The concentration of IgG was 0.2 mg.mL^{-1}. All solutions were buffered in 20 mM sodium phosphate at pH 6.8 (no NaCl).

Figure 5.9 shows the CD spectra measured before and after heating (up to 80°C), and cooling down to room temperature, of a 0.2 mg.mL^{-1} IgG solution supplemented or not with poly(acrylate) derivatives (added at 1:1 wt/wt ratio) in 20 mM phosphate buffer, pH 6.8 (no NaCl). After heating, we observed that the secondary structure of IgG

was irreversibly altered, even in the presence of polymers: the CD data thus confirms the irreversibility of the denaturation already reported by the DSC measurements. More precisely, the minimum at 218 nm was broadened and shifted to lower wavelengths, and a shoulder appeared at about 208 nm. The wavelength corresponding to zero intensity also shifted to a lower value.

Table 5.4: Secondary structure content of IgG in the presence or not of polymers before and after heating to 85°C, in 20 mM phosphate buffer pH 6.8 ([IgG] = [polymer] = 0.2 $g.L^{-1}$).

Polymer	Secondary structure content (%)							
	Before heating				After heating			
	α-helix	β-sheet	Turn	Coil	α-helix	β-sheet[a]	Turn	Coil
No polymer	0	46	12	42	nd	nd	nd	nd
PAA150	0	44	12	44	12	31	13	44
PAA150-3C18	1	44	12	43	9	33	13	45
PAA5-25C8-40C3	0	45	12	43	10	32	11	42

[a] "β-sheet" refers to anti-parallel β-sheet structures, parallel β-sheets are not shown (it is the complement to 100% of the sum of secondary structure shown in the table).
nd: not determined, due to IgG aggregation.

The content of secondary structures was estimated using the BestSel deconvolution software developed by Micsonai *et al.* [338] (see Appendix B for details). Table 5.4 compares the secondary structure contents before and after heating. In the absence of polymers, aggregation of IgG led to a poorly defined signal at high temperatures (the secondary structure content could not be estimated). In the presence of polymers we observed that the fraction of α-helices increased (+9-12%) after thermal treatment, while the fraction of β-sheets decreased (−11-13%). The α-helix induction observed after heating has already been reported for IgG alone (upon heating to temperatures close to T_m). The authors ascribed it to residues arriving in a non-aqueous environment upon aggregation of IgG [48]: they suggested that, after exposure of hydrophobic residues due to partial unfolding of heat-stressed IgG, aggregation takes place and makes hydrophilic peptide units come closer in space, favouring the formation of inter-protein hydrogen-bonds (instead of hydrogen bonds with water) which, in turns, induces the formation of α-helices. This was supported by the experimental observation that α-helices were induced in IgG that adsorbed on hydrophobic surfaces [384].

The fact that we also observed an increase of α-helices in the presence of polymers may be ascribed i/ to the formation of soluble IgG oligomers (no macroscopic aggregation was observed in the CD cuvette) or ii/ to the formation of IgG:polymer complexes (that could also induce the formation of α-helices). More importantly, the CD spectra show that polymers did not prevent partial unfolding/denaturation of the protein after the heating/cooling process. A substantial portion of ordered secondary structural elements remained after heating, indicating that partially unfolded intermediates were trapped by polymers (as oligomers or small aggregates) and did not completely refold after cooling.

5.3.2.2 Structural changes during the temperature sweep

As observed on the reference spectrum of native IgG and as previously reported [47, 48, 384], at about 210 nm the contribution of β-sheets to the ellipticity is essentially zero, whereas those of other structures are significant (at this wavelength, the contribution of β-turns is positive whilst formation of α-helices and random coil gives a negative contribution). We could thus monitor the changes in secondary structure content by measuring the ellipticity at 210 nm as a function of incubation at increasing temperatures.

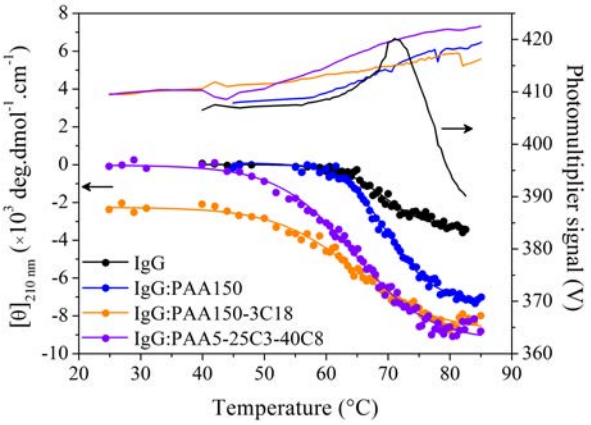


Figure 5.10: Evolution of the molar residue ellipticity at 210 nm for IgG with or without polymers (at 1:1 wt/wt ratio) upon heating (scan rate = 1°C.min^{-1}). The concentration of IgG was 0.2 mg.mL^{-1}. All solutions were buffered in 20 mM sodium phosphate at pH 6.8 (no NaCl).

Figure 5.10 shows the evolution of ellipticity at 210 nm as a function of the temperature for IgG:polymer mixtures (scan rate of 1°C.min^{-1}, faster scan rate than for DSC). In the absence of polymer, it was observed that the ellipticity measured for IgG remained constant (near zero) up to a temperature of about 60°C. Beyond this threshold temperature, the ellipticity decreased, which corresponds to the loss of β-sheets and formation of α-helices (see Table 5.4. This threshold temperature was 10°C higher than the starting unfolding temperature measured by DSC (see Figure 5.7), presumably because of the higher scan rate used here. Variations in the HT voltage (Figure 5.10) reflect variations of light scattering due to modifications of particle size and have been used to detect aggregation of proteins [47, 196, 385]. We observed that above 65°C the photomultiplier (PM) signal recorded for IgG alone (no polymer) increased abruptly, most likely because of light scattering by growing IgG aggregates. The further decrease of the PM signal at T > 72°C is attributed to the fact that large aggregates formed upon heating settled and disappeared from the solution, as reported by Vermeer *et al.* [47] (and it was consistent with the presence of visible macroscopic aggregates in the CD cuvette). We observed that at 65°C IgG did not adopt a coil-like structure and had secondary structure contents modified by only a few % compared to the native structure, indicating that aggregation starts well before IgG is unfolded [48]. Partial unfolding of IgG near the unfolding temperature suffices to transiently expose non-soluble (likely hydrophobic) segments and hence to induce aggregation.

The loss of native secondary structure started at lower temperatures in the presence of polymers, pointing to the destabilization of the native conformation of IgG by polymers.

This is an additional evidence of association between partly unfolded IgG and polymers (binding to unfolding proteins competes with intra-protein stabilizing interactions and displaces the folding equilibrium toward unfolded states). It is worth noting that the native protein structure (at room temperature, prior the heating) was already destabilized in the presence of PAA150-3C18 (see Section 5.2.3.1), thus the ellipticity value measured at 210 nm was not zero at low temperatures in this case. The PM signals measured in the presence of polymers continuously increased up to 85°C, suggesting the formation of complexes and/or oligomers that remained soluble (large aggregates that would settle were not formed, otherwise the PM signals would decrease, as for IgG alone).

Finally, this study by CD indicates that at low ionic strength all the polymers destabilize the native structure of IgG (partial unfolding occurs at lower temperatures), cannot protect IgG against irreversible loss of the native folding at $T > T_m$, but protect the protein against massive aggregation (no large, sedimentating, aggregates). In the next sections, we will analyse more precisely the aggregation propensity of IgG upon heat-induced denaturation in the presence of polymers.

5.4 Impact of poly(acrylate) derivatives on IgG aggregation upon thermal stress

5.4.1 Aggregation of heat-stressed IgG: study by light scattering

DSC and CD measurements (previous section) suggest that large aggregates are not formed in heat-stressed IgG solutions in the presence of polymers at low ionic strength or of amphiphilic polymers at high ionic strength.

5.4.1.1 Evolution of hydrodynamic radii by dynamic light scattering

We measured the hydrodynamic radius of objects formed upon heating (R_h) by dynamic light scattering after incubation of the mixtures at different temperatures for 10 minutes (see Appendix A for details on the experimental conditions). Figure 5.11 shows the temperature dependence of R_h of IgG solutions supplemented with polymers at 1:1 wt/wt ratio in 20 mM phosphate buffer, pH 6.8, with or without 100 mM NaCl as indicated. R_h of IgG alone remained constant at *ca.* 5 nm up to 60°C, then abruptly increased and reached values as high as 2µm (resp. ∼300 nm) in the absence (resp. presence) of 100 mM NaCl. When amphiphilic poly(acrylates), namely PAA5-3C18 and PAA5-25C8-40C3, were added, the measured R_h were limited to values very close to the R_h of monomeric IgG alone and did not increase above 15 nm. In the presence of PAA5, objects of R_h lower than 20 nm were also stabilized at low ionic strength, while aggregation did occur upon addition of 100 mM NaCl.

DLS results demonstrate that polymers prevent IgG thermal aggregation in several conditions: at low ionic strength (no NaCl) all polymers added at 1:1 wt/wt ratio with IgG, including the PAA parent chain, ensure the stabilization of species < 15 nm in radius; hydrophobic side groups on the polyanion enable this stabilization to be effective in the presence of 100 mM NaCl. All the experiments described above refer however to a specific procedure of temperature sweep (and particular incubation times). It is thus not distinguished here between transient stabilization (slowing down of aggregation) or colloidal stability of the heat-stressed IgG:polymer complexes. In order to establish the origin of the stabilisation, we considered measurements by SLS of the kinetics of growth

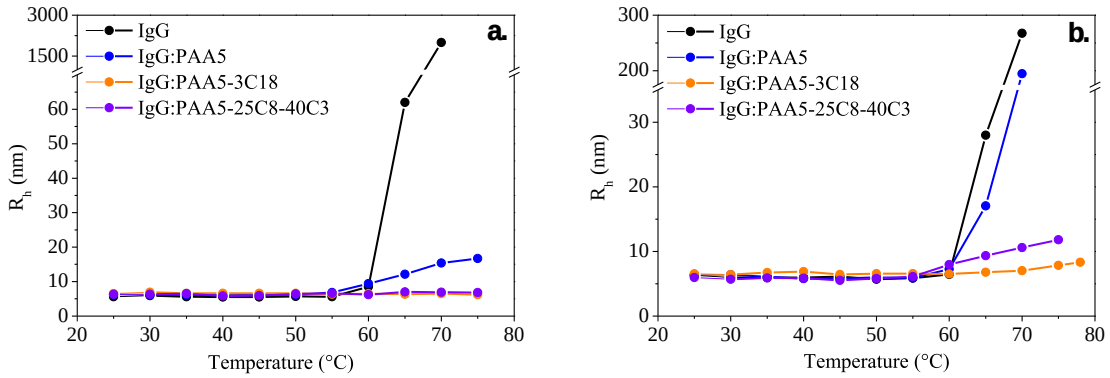


Figure 5.11: Evolution of the hydrodynamic radius of IgG alone and in the presence of polymers (at polymer:IgG ratio of 1:1 wt/wt) measured by DLS during temperature sweep in 20 mM phosphate buffer pH 6.8 without NaCl (a.) or with 100 mM NaCl (b.). The concentration of IgG was about 0.5 mg.mL^{-1}.

of oligomers and/or aggregates.

5.4.2 Aggregation kinetics by static light scattering

The increase with incubation time of the light scattered intensity measured from IgG solutions kept at constant temperature (close to T_m) in the absence or presence of polymers provides information on the colloidal stability of species formed by heat-stressed IgG (see Figure 5.12, only conditions of high ionic strength, *i.e.* in buffer containing 100 mM NaCl, were undertaken). The scattered intensity was normalized to I_0, the scattered light intensity of the solution of IgG alone prior to heating.

The rate of increase of the scattered light intensity in IgG solutions (no polymer) became abruptly more rapid as the temperature reached 65°C, and was near experimental error at T < 55°C. Thus measurements in this temperature range were indicative of heat-triggered aggregation. The initial slopes of the variation of scattered intensity from mixed IgG:PAA5 solutions were essentially the same as the ones obtained for solutions of IgG alone, confirming that this polymer did not improve the IgG stability in buffer containing 100 mM NaCl.

In mixed IgG:PAA5-3C18 and IgG:PAA5-25C8-40C3 (presented in Figure 5.12), the magnitude of increase of the scattered intensity was much smaller than in the case of IgG alone (note the difference in the ordinate scales). The change of intensity by a factor < 10 observed in these solutions betrayed a negligible contribution of large aggregates. Because of the (slow) drift of scattered intensity in mixed IgG:PAA5-25C8-40C3 solutions, it is concluded that this polymer does not confer a colloidal stability, but slows down the aggregation rate. In mixed IgG:PAA5-3C18 solutions, the variation of scattered intensity was not only close to experimental error, but could also reach a plateau (see measurement at 60°C), which suggests a true colloidal stability. Similar conclusions can be drawn from the variation of apparent hydrodynamic radii (Figure E.11 in Appendix E) measured by dynamic light scattering in the same samples.

A colloid-like aggregation mechanism was used to quantify the kinetics of inert-protein binding at the onset of aggregation. This model was shown previously to be valid to study the thermal denaturation of IgG [50]. It assumes that during the early stage of

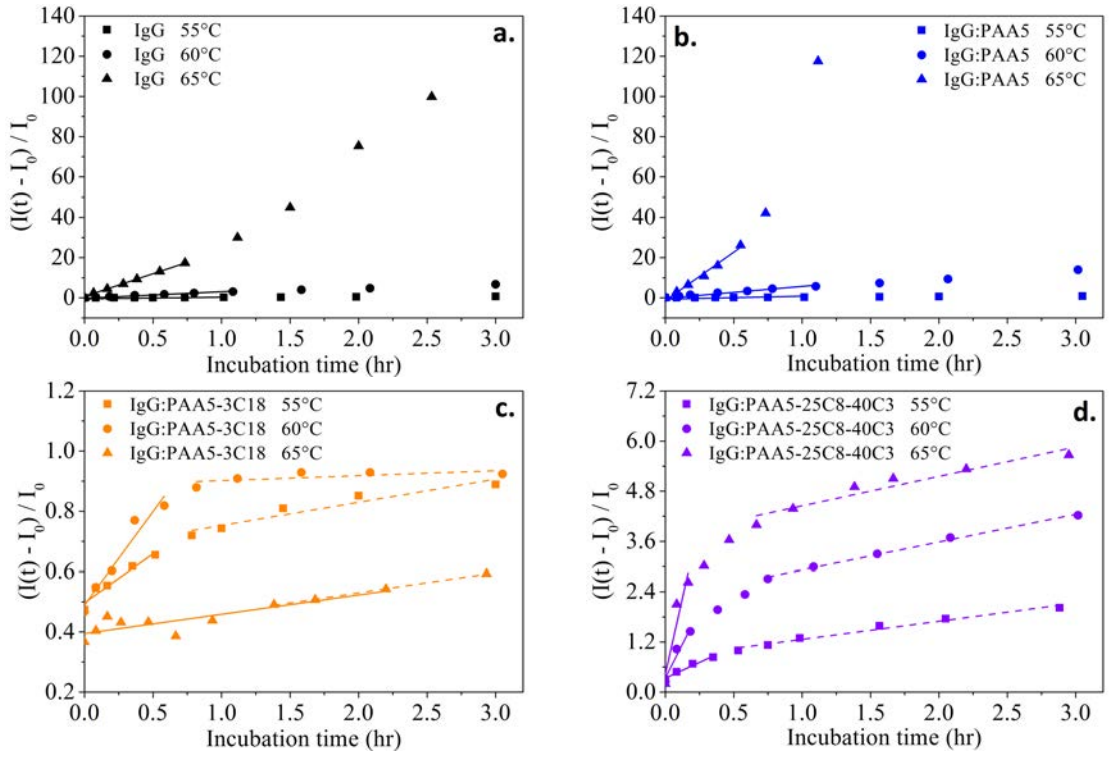


Figure 5.12: Variation of the normalized scattering intensity (I(t) - I_0)/I_0 for IgG and IgG:polymer mixtures (1:1 wt/wt ratio) in 20 mM phosphate buffer pH 6.8 supplemented with 100 mM NaCl as a function of incubation time at different temperatures. Solid lines correspond to the fits of data points at time < 20-40 minutes to Equation 5.4; dotted lines correspond to linear fits of data points beyond 1 hour incubation time. [IgG] = 0.5 mg.mL^{-1}.

aggregation, random collisions between proteins shall be the main origin of growth of oligomers, which yields a linear variation with time of the scattered intensity according to Equation 5.4 (Smoluchowski theory on kinetics of coagulation [386]):

$$I(t) = I_0\ (1 + n_0.k_s.t) \tag{5.4}$$

where I_0 is the initial (at t = 0) scattered light intensity of a monomeric IgG solution at 25°C, n_0 is the IgG concentration (in number.m^{-3}), k_s is the barrier-controlled rate constant (in m^3.s^{-1}). The slope of $(I(t) - I_0)/I_0$ gives k_s which can be expressed as:

$$k_s = \frac{{k_s}^0}{W} = \frac{4.k_B.T}{3.\eta.W} \tag{5.5}$$

In this theoretical framework, k_s varies in proportion to the reciprocal of the colloidal stability ratio, $1/W$ (Equation 5.5), and W measures the average number of collisions between IgG molecules that are required to form one protein-protein permanent association to be formed. According to this interpretation, the chance for a "sticky" collision to occur between two IgG molecules in solutions of IgG alone or in the presence of PAA5 increases by *ca.* 10 times with each 5°C increase of the temperature in the vicinity of T_m (Table 5.5).

Table 5.5: Colloidal stability ratios, W ($\times 10^{-6}$), calculated from Equations 5.4 and 5.5 and intensity variations in Figure 5.12, for IgG and IgG:polymer mixtures incubated near the temperature of thermal denaturation in 100 mM NaCl, 20 mM sodium phosphate buffer pH 6.8. [IgG] = 0.5 mg.mL^{-1}.

T (°C)	IgG	IgG:PAA5	IgG:PAA5-3C18		IgG:PAA5-25C8-40C3	
55	240	200	660[a]	na[b]	110[a]	33[b]
60	16	9.8	2900[a]	na[b]	72[a]	8.0[b]
65	2.0	1.3	720[a]	na[b]	72[a]	3.6[b]

[a] apparent W corresponding to slopes estimated by linear extrapolation beyond 1 hour incubation; [b] values corresponding to slopes at short times (<30 minutes); na: fit to Equation 5.4 not applicable (does not extrapolate to zero at time zero).

The situation in the case of mixed IgG:PAA5-3C18 and IgG:PAA5-25C8-40C3 is quite different. The scattered light intensity increased markedly in the initial phase, up to an incubation time of 1 hour and much slower at longer incubation times (Figure 5.12). Also, the overall increase in scattered light intensity was weak. Reliable W values could not be obtained from Equation 5.4 and data at short time for the IgG:PAA5-3C18 mixed solutions, since the initial increase in scattered light intensity was too abrupt and did not extrapolate to zero at time zero in Figure 5.12. It is tentatively proposed that in the first (fast) kinetic regime, complexes are formed between one or several polymer chain(s) and a few proteins (or oligomers), as evidenced by the fast increase of hydrodynamic radius (reported in Appendix E). The second regime showing slower kinetics reflects the onset of thermal aggregation.

From the rate constant at long time, we can estimate the values of W listed in Table 5.5 for mixed IgG:PAA5-25C8-40C3 solutions. High W values are good indicators of the efficiency of a polymer to shield the attractive interaction between thermally-destabilized proteins. The apparent W estimated by this method includes unavoidably the effects of i/ possible change of the fraction of aggregation-prone IgG molecules as they are sequestered by polymer chains and ii/ combinations of signals due to IgG-IgG association and/or growth of IgG:polymer complexes. In other words, the changes in scattered light intensity cannot be unequivocally ascribed to protein-protein collisions (inter-complex collisions may also generate aggregates for instance). Here, we used Equation 5.5 to estimate an apparent W as an index of the effectiveness of a kinetic protection, choosing somewhat arbitrarily to use a concentration equal to the total IgG concentration.

The increase in apparent W corresponds to both the decrease of free, or aggregation prone, proteins and to the higher colloidal stability of protein:polymer complexes, compared to free IgG. PAA5-3C18 differed from PAA5-25C8-40C3 in that it led to much higher apparent W values, due to the nearly zero drift in scattered intensity within a few hours (*e.g.* at 60°C variation are close to the experimental error) and persisting over the entire temperature range (55-65°C) (Table 5.5, values quoted with [a] exponent). The presence of PAA5-25C8-40C3 certainly slowed down the aggregation rate, but it did not prevent it entirely. Nonetheless, at 65°C the presence of PAA5-25C8-40C3 decreased the aggregation rate by a factor of about 30 compared to free IgG.

5.4.3 Aggregation of heat-stressed IgG: study by fluorescence correlation spectroscopy

We evaluated by FCS the temperature-dependent aggregation status of FITC-IgG in mixed 1:1 wt/wt ratio FITC-IgG:polymers solutions at 0.2 $mg.mL^{-1}$ in 20 mM phosphate buffer pH 6.8 (with or without 100 mM NaCl) heated from 25 to 85°C at a rate of $0.2°C.min^{-1}$. Incubations of the different mixtures were performed under the same conditions as those used for DSC experiments. However, due to the high sensitivity of FCS, aliquots taken at different temperatures had to be diluted by a factor of 10 prior to measurements. Trials to perform FCS measurements directly in a heated sample-stage were not successful (see Appendix B for details). The dilution was performed by mixing an aliquot of the concentrated sample into buffer kept at room temperature. Thus, the experiments described below report the sizes of objects that remained after 10-fold dilution and cooling down to room temperature (similar trends were observed on more concentrated mixed IgG/FITC-IgG samples, see Appendix E).

Figure 5.13 displays the temperature dependence of the hydrodynamic radii (R_h) and the number-averaged degree of aggregation (N_{agg}, see Appendix B for details on the calculations) of the fluorescent objects detected in solutions. Prior to thermal treatment, the hydrodynamic radius of FITC-IgG alone (no added polymer) was *ca.* 5 nm and the protein remained under its monomeric form in solution up to $\sim$ 70°C (close to the unfolding temperature of IgG previously reported by DSC), above which massive aggregation occurred, independently of the salt concentration (vertical lines in the plots of R_h and N_{agg} in Figure 5.13). These aggregates appeared too large to enable an estimate of their size by FCS (they created strong bursts of intensity and saturation of detectors upon crossing the confocal volume). In particular, the progressive formation of oligomers was not observed: when crossing the temperature threshold, FITC-IgG abruptly aggregated (on the time scale of the experiment, *i.e.* within a few minutes). This observation is consistent with the abrupt formation of micrometer-sized aggregates previously detected upon heating by DLS (even though DLS is more sensitive to large objects).

In salt-free solution, the presence of polymers had a remarkable effect on the aggregation of FITC-IgG: both R_h and N_{agg} remained nearly constant up to a temperature slightly below T_m of IgG ($\sim$ 60-65°C) and did not vary significantly beyond this temperature (for amphiphilic poly(acrylate) derivatives) or increased gradually (for parent PAA chain). This contrasts with the abrupt variation in the absence of polymer and confirms that IgG:polymer mixtures resist aggregation.

More precisely, PAA150-3C18 (already associated with native FITC-IgG prior to heating) formed complexes which size ($R_h \sim 40$ nm) was slightly higher than (but still comparable to) the radius of the free polymer chain ($R_h \sim 16.1 \pm 2.7$ nm from FCS measurement on rhodamine-labeled PAA150-3C18). This radius remained nearly constant in the whole experimental range of temperature, reflecting the fact that FITC-IgG:PAA150-3C18 complexes (formed at room temperature, and containing on average 2 proteins) did not aggregate up to 80°C. Similarly, a slight increase of R_h from *ca.* 5 nm to *ca.* 10 nm occurring above 60°C in the presence of PAA5-25C8-40C3 was compatible with the complexation between FITC-IgG and PAA5-25C8-40C3, though in this case the absence of complexes at low T indicates that only heat-stressed FITC-IgG associated with the polymer. This polymer limited the clustering between FITC-IgG to dimers ($N_{agg} = 2$ at 85°C). Interestingly, with PAA150, R_h was essentially constant up to 65°C and increased gradually between 65°C and 85°C, altogether with a progressive increase of

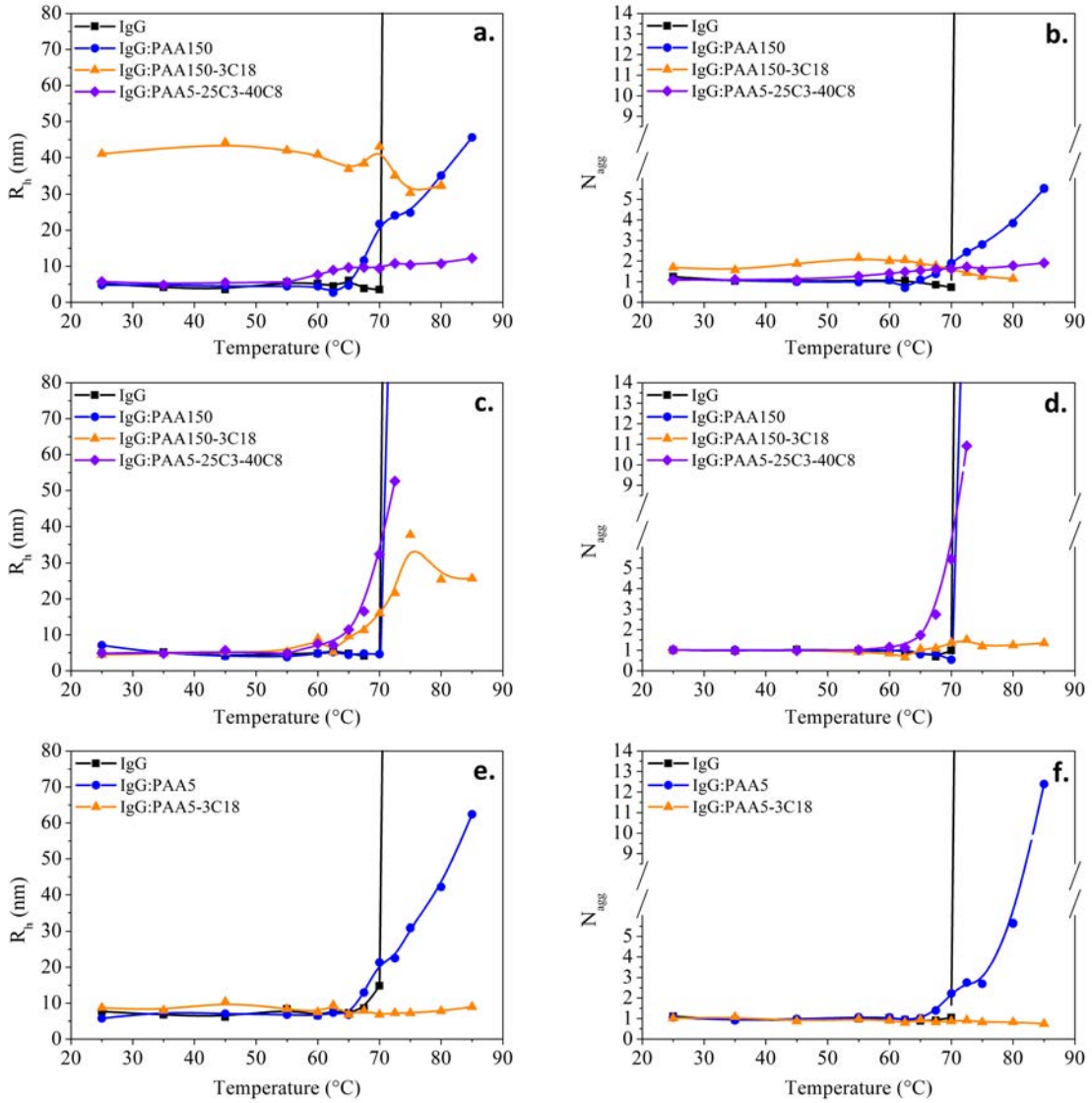


Figure 5.13: Variation upon incubation at increasing temperature of the hydrodynamic radius (R_h) and aggregation number of IgG (N_{agg}, defined as the averaged number of FITC-IgG molecules per fluorescent object in solution) measured by FCS in phosphate buffer (20 mM, pH 6.8) at 1:1 wt/wt FITC-IgG:polymer ratio, 0.02 mg.mL^{-1} FITC-IgG, in the absence (a., b.) or in the presence (c., d.) of 100 mM NaCl for the long polymers, and in the absence of 100 mM NaCl for the short polymers (e., f.).

N_{agg} from 1 (at 65°C) to 6 (at 85°C), which indicates that small oligomers predominate in the clusters of proteins formed. Coulomb interactions thus appear to be sufficient to limit massive and abrupt aggregation of FITC-IgG, though it is not as efficient as the combination of Coulomb and hydrophobic interactions.

The temperature at which complexes or oligomers started to form in the presence of polymers ($\sim$ 55-65°C) was lower than the temperature at which IgG alone aggregated ($>$ 70°C). This observation is consistent with the destabilization of IgG upon interaction with polymers, as observed the loss of native secondary structure of IgG measured by

CD at temperatures lower than T_m in the presence of polymers (Section 5.3.2.2).

FCS experiments performed on mixtures of unlabelled IgG and rhodamine-labelled polymers allowed to access the average number of polymer chains per complex formed upon heating (see Appendix E). Results indicate that complexes contained on average 1 polymer chain in the case of PAA150-3C18 in the whole temperature range, while the number of PAA150 chains gradually increase from 1 (between 25 and 70°C) to about 3 (at 85°C).

5.4.3.1 Effect of polymer chain length

At low ionic strength, in the presence of short polymers (PAA5 and PAA5-3C18), Figure 5.13 illustrates that essentially the same trends as for long polymers are observed. PAA5 prevented massive aggregation of FITC-IgG: we observed a progressive increase of N_{agg} from 5 to 50 nm and of N_{agg} from 1 to 10 when the temperature increased from 65 to 85°C.

Note that when PAA5-3C18 was used instead of the long PAA150-3C18 chain, we could not conclude on the complexation between FITC-IgG and the polymer: the hydrodynamic radius measured in the presence of the shorter polymer ($R_h \sim$ 7-8 nm) was slightly higher than the radius of FITC-IgG alone ($R_h \sim 5$ nm), but the difference was not significant. The size of the short polymer was too small to induce an apparent increase in size when the polymer binds to IgG. However, the fact that the radius, as well as the aggregation number, remained constant up to 85°C is taken as an indirect evidence that PAA5-3C18 binds IgG, and therefore protects it against aggregation.

5.4.3.2 Influence of the ionic strength

The importance of Coulomb interactions was confirmed by FCS measurements performed in the presence of 100 mM NaCl (see Figure 5.13). In the case of FITC-IgG mixed with PAA150, the partial stabilization achieved at low ionic strength, with a final $N_{agg} < 6$ (and final $R_h < 50$ nm), was no more effective in solutions with 100 mM NaCl. The size of FITC-IgG increased as without polymer added. This result validate the conclusion that the FITC-IgG:PAA150 complexes are formed in the absence of salt and owe their stability solely to electrostatic interactions.

On the other hand, amphiphilic polymers keep their protective effect in buffer with 100 mM NaCl. Remarkably low N_{agg}, typically close to 1, in the presence of PAA150-C18 indicate in Figure 5.13 that this polymer was capable to fully prevent both thermal aggregation and oligomerization, at either low or high ionic strength. Interestingly, R_h increased in solutions of FITC-IgG:PAA150-C18 with NaCl, from *ca.* 5 nm below 60°C up to $\sim$ 30 nm after the temperature sweep, which points to i/ the absence of complexes at low temperature, in consistency with CZE studies at room temperature (see Section 5.2.1) and ii/ the formation of dilution-resistant complexes between heat-stressed FITC-IgG and the polymer. PAA5-25C8-40C3 only slowed down the aggregation of FITC-IgG: oligomers were in this case progressively formed, with increasing R_h from 5 to 50 nm and N_{agg} from 1 to 10 when the temperature increased from 65°C to 72.5°C.

Finally, ranking the polymers in the order of their ability to limit thermal aggregation and oligomerization of IgG yields PAA150-3C18 $\approx$ PAA5-3C18 > PAA5-25C8-40C3 > PAA150 $\approx$ PAA5 (the latter two polymers being efficient at low ionic strength only).

5.5 Conclusion

The results of this study provide strong indication that poly(acrylate) derivatives enhance the stability of polyclonal IgG subjected to thermal stress. But as opposed to the usual assumption of shielding of hydrophobic residues exposed during protein unfolding by association with amphiphilic polymers, results from FCS, CZE, DSC, CD and DLS demonstrate that hydrophobic binding is not the sole origin of protection. Rather, Coulomb interactions drive the formation of soluble complexes, especially in solutions of low ionic strength, and, with additional stabilizing contribution of hydrophobic interaction, slow down significantly the thermal aggregation of IgG.

Complexation with amphiphilic or non-modified, hydrophilic, PAA polymers is condition-dependent (effects of ionic strength and temperature) as is the resulting degree of protection achieved against aggregation. Presented in Figure 5.14 is an overall view of which species were formed in the different conditions and whether stability, or slower aggregation, or no contribution of polymer occurred upon thermal stress. The discussion below summarizes the results that guided us to establish this schematic illustration.

First, DSC and CD results indicate that at temperature below 40-45 °C IgG is folded in the absence or presence of polymers. The fraction of (folded) IgG present under the form of complexes with polymers at low T is negligible in the concentration window studied, except in the case of PAA-3C18 at low ionic strength. From this result, it appears that binding on folded IgG is not necessarily required to achieve protection. Complexation is temperature dependent as shown by FCS results. In 100 mM NaCl solutions, IgG associates with the amphiphilic polymers as the solution reaches temperatures near the onset of unfolding. At lower ionic strength in the absence of NaCl, the formation of complexes at the onset of IgG unfolding is also effective with the hydrophilic non-modified PAA chains.

FCS points to a low IgG:polymer chain stoichiometry of the complexes (near T_m, N_{agg} with PAA150-3C18 is of the order of one, whereas complexes with PAA150 at low ionic strength have $N_{agg} < 6$). A simplified picture shown in Figure 5.14 of one (destabilized and partially unfolded) IgG surrounded by one long polymer chain is thus representative of the state of association reached at the initial stage of the thermal stress. The colloidal stability of these complexes depends on the hydrophobicity of the polymer and of the ionic strength. An increase of the aggregation number with increasing temperature, as measured by FCS (PAA), or the slow but continuous aggregation as characterized by light scattering (PAA-25C8-40C3) point to the improvement of metastability of IgG (*i.e.* a decrease of the probability of IgG-IgG sticky collision). But both PAA and PAA-25C8-40C3 fail to fully prevent aggregation, notably at high ionic strength. The lower capacity of PAA-25C8-40C3 to develop hydrophobic association with IgG (the polymer hydrophobic side groups are buried in polymer micelles) presumably accounts for the differences with the results obtained with PAA-3C18.

Finally, PAA-3C18 polymers were the best protective agents that preserved both low N_{agg} and, within experimental uncertainties, arrested the kinetics of aggregation, which is indicated in Figure 5.14 by the term "protection". Prevention of aggregation was not accompanied by enhanced conformational stability, as shown by the persistence of DSC peak(s) in a similar range of T irrespective of the presence or not of polymers. The marked effect of polymer complexation on the enthalpy of IgG denaturation suggests in addition that association with PAA and its derivatives significantly perturbs the unfolding of IgG. In general, complexation of proteins with polyelectrolytes favours unfolding. Future

optimization of protection may therefore focus on combining the colloidal stabilization with better thermodynamic stability, for instance by introducing kosmotropic side groups in the polymer chains.

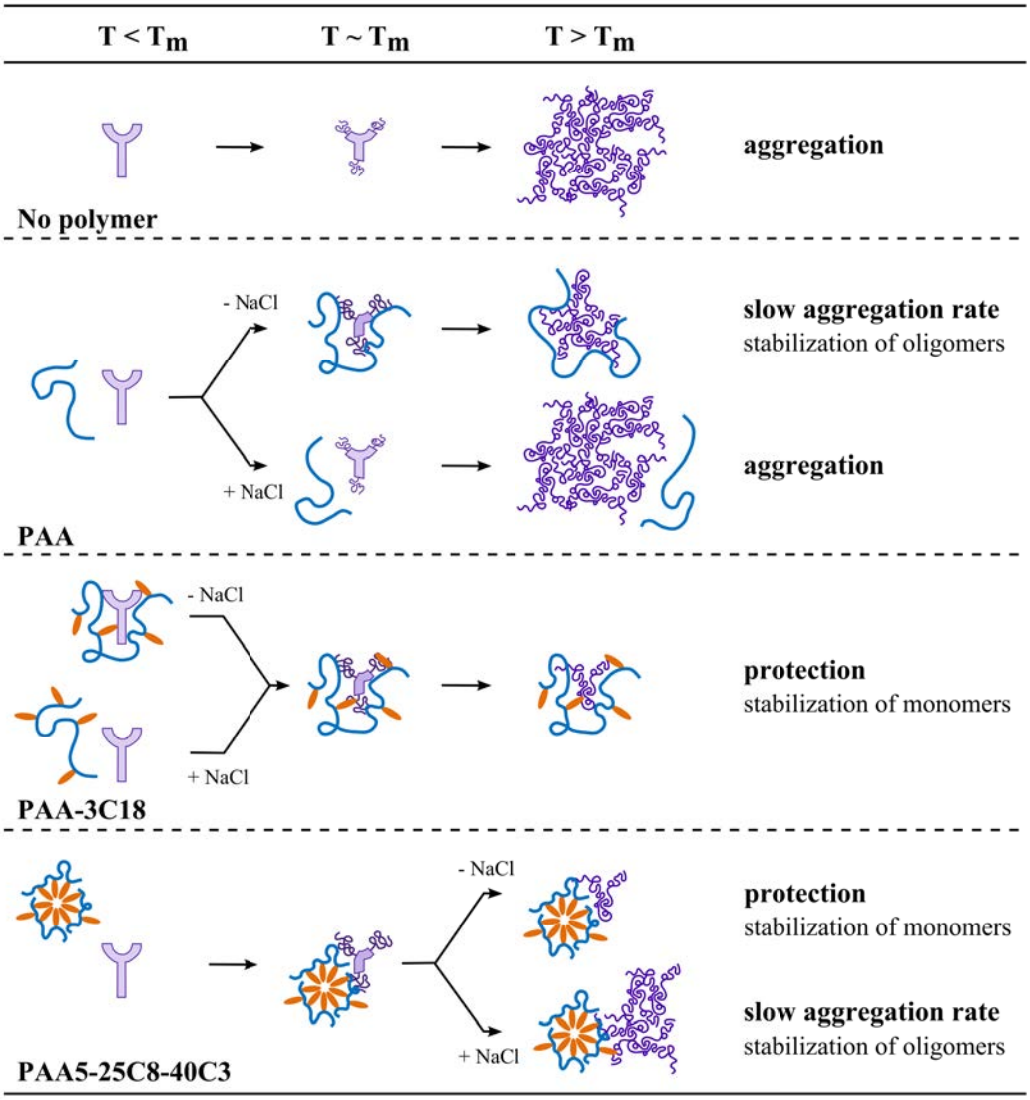


Figure 5.14: Schematic summary describing the temperature-dependent interactions between IgG and amphiphlic polyanions.

Our observations also extend the studies on stabilization of proteins in the presence of polyelectrolytes to multi-domain proteins of pharmaceutical interest. It is important to note that most of the previous studies exploited electrostatic interactions between oppositely-charged proteins and polymers. In the studies described here, both partners are negatively charged, albeit with IgG close to its isoelectric point, as observed by capillary electrophoresis. Coulomb interactions with PAA5 or PAA150, in solutions of low ionic strength, also protect proteins close to their isoelectric point, irrespective of the presence or not of hydrophobes on the polymer chain. Such electrostatically-driven binding between polyelectrolytes and antibodies may be a general phenomenon, as suggested by

a recent study of systems containing monoclonal antibodies and alginate [387].

From the viewpoint of applications, Coulomb complexation of IgG with polyelectrolytes has the additional advantage that it can be weakened with increasing ionic strength up to *ca.* 100 mM, which may facilitate the release of active proteins under physiological conditions.

Conclusion and perspectives

Hydrophobically-modified PAA and non modified PAA significantly affect the stability of the model proteins used in this work, enabling us to identify key requisites for chaperone-like properties of polyelectrolytes and possible applications on protection of biotherapeutics against stress-induced aggregation. Poly(sodium acrylate) of varying hydrophobicity appeared highly efficient in minimizing protein aggregation, both during refolding from a chemically-denatured state (for model CAB and scFv) or under an external heat stress (for IgG). Prevalence of hydrophobic association often reported in the literature is however questioned in this work. We demonstrate that electrostatic binding of polymers onto partly folded/unfolded protein conformers is sufficient to slow down aggregation (at low ionic strength). The need for providing an hydrophobic interface to non-polar residues exposed to contact with water thus appears vastly overrated. Rather, sequestration of partly-folded conformers in host macromolecules and controlled, gradual release turn out to be the true objectives if one aims at reducing aggregation, regardless of details about the nature of interactions. Modulation of Coulomb binding between polyelectrolyte and proteins appears in practice easier to achieve than modulation of hydrophobicity as long as the ionic strength can be varied. Interestingly, aggregation minimization was general to all proteins tested, pointing to the little influence of the peculiar structure of the polypeptide, and suggesting that amphiphilic polyelectrolytes could constitute generic artificial chaperone systems. In addition, low stoichiometry, close to 1:1 mol/mol, and protection in dilute conditions (<mM concentrations) are important features, specific to polymer:protein protective complexes and to chaperones. These latter two points indicates that the affinities of PAAs for the conformers of the proteins (native and non native) were in the μM-mM range. It is likely that affinities can be tuned by adjustment of experimental parameters, including the chemical nature of the polymer. As regards Coulomb attraction, however, PAA is among the polyelectrolyte chains having the highest charge density, suggesting that sub-micromolar (Coulomb) affinities should be difficult to reach. This possibility deserve further studies.

The slowing down of the aggregation rate, general to all tested polymers, was extended to a true colloidal stabilisation (for IgG) when the PAA backbone was functionnalized with weakly hydrophobic moieties, presumably because of transient isolation of aggregation-prone, amphiphilic conformers into non-aggregating protein:polymer complexes. It is essential to recognize that Coulomb association may nevertheless not stop denaturation (*e.g* thermal denaturation of IgG), despite an obvious prevention of aggregation. Misfolding, or oligomerization may occur in polymer:protein complexes. Higher renaturation yields (for CAB) were achieved when the association was compatible with spontaneous

release of the proteins from dynamic equilibrium of free and bound forms (under experimental conditions that were compatible with spontaneous refolding). At the present time, we have no evidence of any contribution of the polymer hydrophobicity to refolding. Tight hydrophobic binding may even trap the system into non-native complex states. Tailoring the degree of hydrophobicity is accordingly a delicate point. Conformational destabilization of proteins upon association with PAA derivatives (hydrophobic or not) is a general rule when natural proteins are used, but our work suggest that artificial ones (*e.g.* antibody scFv fragments) could be stabilized presumably by an association of the polymers with water-exposed unstable regions/patches. Polymer-activated (stimulated) switch between protein conformers could be imagined, though it was not observed in the present study.

Within the scope of the use of amphiphilic polyelectrolytes as artificial chaperones for refolding of proteins, questions remain unsolved. Future investigations on the molecular structure and dynamics of protein:polymer complexes all along the refolding pathway are needed to clearly identify the locus of contacts between the two partners and hence rationalize the impact of the chemical structure of polymers on the conformation of proteins. The affinity between polyanions and proteins and life-time of complexes with unstable protein conformers are identified to be key issues, with possible modulation of association/release with appropriate external stimuli (ionic strength, pH, light). Interestingly, the physico-chemical properties (*e.g.* charge density, hydrophobicity) of polyelectrolytes as well as their architecture (branched, brushes, multi-layers...) and formulation can be easily tailored to achieve optimal attractive/repulsive balance with a protein and control inter-complexes repulsions while allowing dissociation of the thermodynamically stable native structure. The design of a generic, controllable artificial chaperone has now to integrate the diversity of polyelectrolytes structures achievable by conventional chemical synthesis, as well as by biological synthesis, that provides vast opportunities to investigate the detailed effects of these macromolecular additives on the folding and stability of proteins.

Appendix A

Materials and methods

Contents

A.1 Chemical and biological materials 148
A.2 Fluorescent labelling of proteins 148
A.3 Hydrophobic moieties grafting onto PAA parent chain . . . 149
A.4 Expression and purification of scFv fragments 149
A.5 Refolding protocols 150
A.5.1 Denaturation and refolding protocol of CAB 150
A.5.2 scFv renaturation protocol 151
A.6 Fluorescence correlation spectroscopy (FCS) 151
A.6.1 Experimental set-up and acquisitions 151
A.6.2 Heating of IgG 152
A.6.3 Refolding of scFv 152
A.6.4 Refolding of CAB 152
A.7 Capillary zone electrophoresis (CZE) 152
A.8 Differential scanning calorimetry (DSC) 153
A.9 Dynamic and static light scattering (DLS, SLS) 153
A.9.1 Aggregation kinetics of IgG by SLS 153
A.9.2 Size measurement of heated IgG by DLS 153
A.9.3 Aggregation of CAB 153
A.10 Circular dichroism (CD) 154
A.10.1 Conventional circular dichroism 154
A.10.2 Synchrotron-radiation circular dichroism (SRCD) 154
A.11 Steady-state fluorescence emission spectroscopy 154
A.12 Electrostatic modelling 155
A.13 Activity assays 155
A.13.1 Enzymatic activity of CAB by UV-visible spectroscopy 155
A.13.2 Antibody binding assays by flow cytometry 155
A.14 Nuclear Magnetic Resonance (NMR) 156

A.1 Chemical and biological materials

Water was deionized with a MilliQ Millipore purification system. ChromPure Human IgG (Code Num. 009-000-003) was purchased from Jackson ImmunoResearch Labs Inc. (as a 11.1 mg.mL^{-1} stock solution). Poly(acrylic acid) (PAA) samples (nominal average molecular weight (M_w) 5,000 g.mol^{-1} (PAA5) or 150,000 g.mol^{-1} (PAA150)), carbonic anhydrase from bovine erythrocytes II (CAB), urea, guanidine hydrochloride (GndCl), L-arginine, *para*-nitrophenylacetate, anhydrous dimethylsulfoxide (DMSO) and buffering chemicals were purchased from Sigma-Aldrich. PAA5-25C8-40C3 (M_w 9,000–10,000 g.mol^{-1}) was purchased from ANATRACE (Amphipol A8-35, Affymetrix). L44-*g*-PAA was supplied by SupraTek Pharma Inc. (Montreal, Canada). Fluorescein isothiocyanate (FITC) was purchased from Fluka. FITC-labelled scFv Sha 31, unlabelled scFv Rendomab B1 and scFv 12G4, as well as ^{15}N-enriched scFv Rendomab B1 were supplied by Didier Boquet (LIAS, CEA Saclay, see expression protocol below).

A.2 Fluorescent labelling of proteins

A solution of protein (IgG or CAB, 2 mg.mL^{-1}) in a 0.5 M $NaHCO_3 - Na_2CO_3$ buffer pH 9.5 was dialysed against the same buffer for one hour. An aliquot of a freshly-prepared FITC solution in anhydrous DMSO (5 mg.mL^{-1}) was added to the protein solution (50 µg FITC / 1 mg of IgG,) to reach a final ratio of FITC/protein of about 20:1 mol/mol). The reaction mixture was kept at room temperature for two hours, then dialysed against the working buffer (20 mM sodium phosphate, pH 6.8, with or without 100 mM NaCl for IgG, or 50 mM Tris-HCl, pH 7.75, for CAB) for one hour to remove unreacted FITC. The dialysate was purified by gel permeation chromatography (GPC) using a Sephacryl® 300 HR resin (Sigma-Aldrich) eluted with the working buffer.

The concentration of FITC-protein in the collected fractions was assessed by UV-Vis spectrometry according to the relationship:

$$[\text{protein}](\text{mg.mL}^{-1}) = \frac{A_{280} - 0.31A_{495}}{\varepsilon}$$

where A_{280} and A_{495} are the absorbances at 280 nm and 495 nm respectively, 0.31 is a correction factor accounting for the absorption of the dye at 280 nm and 1.4 mg.mL^{-1} is the extinction coefficient of the protein in mL.mg^{-1}.cm^{-1} (ε = 1.4 mL.mg^{-1}.cm^{-1} for IgG and ε = 1.83 mL.mg^{-1}.cm^{-1} for CAB).

The molar ratio FITC:protein (*ca.* 3:1) was determined from the relationship:

$$\frac{\text{FITC}}{\text{protein}} = \frac{A_{495}/69,000}{[\text{protein}](\text{mg.mL}^{-1})/M_w}$$

where 69,000 mol^{-1}.L.cm^{-1} is the molar extinction coefficient of FITC at 495 nm (Application note from Pierce FITC Antibody Labelling Kit, ThermoScientific) and M_w (g.mol^{-1}) is the molar mass of the protein (M_w = 150,000 g.mol^{-1} for IgG and M_w = 29,000 g.mol^{-1} for CAB).

After purification, solution could be concentrated (if too diluted) by centrifugation using a Microcon® centrifugal filter device (MWCO 100,000 for IgG and 10,000 for CAB).

A.3 Hydrophobic moieties grafting onto PAA parent chain

Functionalization of a few mol percent of carboxylic acids with hydrophobic moieties on a poly(acrylic acid) backbone has been developed for several years in the group. The grafting is performed through a peptidic coupling reaction. A great variety of primary amines has already been grafted onto PAA backbone, such as isoproylamine, amino-(alkyl)-azobenzenes and several *n*-akylamines [258, 288].

The grafting of primary amines is performed in *N*-methyl-pyrrolidone (NMP) on the acidic form of PAA in the presence of a coupling agent, *N*, *N*′-dicyclohexyl-carbodiimide (DCC). DCC is an electrophilic reactant which, in the presence of acrylic acid motifs, forms an activated ester intermediate capable of reacting with an amine. This reaction has been used to graft *N*-*n*-octadecylamine but also NH_2-rhodamine (to get fluorescently-labelled polymers) onto a PAA backbone. The case of NH_2-rhodamine is briefly described here as a typical coupling protocol.

Coupling of ∼2 mol% of NH_2-rhodamine onto a PAA chain
To a limpid solution of the acidic form of PAA5 (200 mg, 2.78 mmol of acrylic acid units) in *N*-methylpyrrolidone (∼7 mL), obtained after stirring at 45°C for 1 hour, were added NH_2-rhodamine (114 µL of a 0.26 g.mL^{-1} solution in DMSO, 0.056 mmol, 0.02 equiv.) and DCC (12 mg, 0.058 mmol, 0.021 equiv.). After being stirred at 40°C for 24 hours, the mixture was cooled to 4°C, transferred into a Falcon tube, then MeONa 5M in MeOH (1.1 mL, 5.56 mmol, 2 equiv.) was added dropwise. The reaction mixture was stirred for one hour, then the formed gel was centrifuged and the supernatant eliminated. The collected gel is rinsed twice with MeOH, then dissolved in water and purified by precipitation in MeOH (repeated twice). The precipitate is filtered and dried over vacuum to recover the rhodamine-functionnalized PAA.

In each case, the grafting ratio was determined by ^{1}H NMR. The molar mass (M_w) and polydispersity index (PI) of the polymers in the sodium acrylate form measured by GPC using a Waters system equipped with Waters 2414 Refractive Index and Waters 2487 UV-Visible absorbance detectors, and Waters Styragel HR 5E (4 columns) eluted with 0.5 M LiNO3 were M_w = 6,500 g.mol^{-1}, PI ∼ 2 (PAA5) and M_w ∼ 130,000 g.mol^{-1}, PI ∼ 4 (PAA150) based on a calibration curve using poly(ethylene oxide) standards [258].

As far as L44-*g*-PAA is concerned (formula: EO_{10}-PO_{23}-EO_{10}-*g*-$AA_{7.6}$), the polymer is composed of 7.6 acrylic acid units on average per chain, as determined via ^{1}H NMR and titration experiments. It has a LCST of about 60°C and a cmc of *ca.* 1.5 g.L^{-1} in phosphate buffer saline (as determined by fluorescence measurements with the pyrene probe).

A.4 Expression and purification of scFv fragments

Conventional micro-organisms culture and expression techniques were used to produced the scFv fragments used in this thesis. Briefly, the expression was carried out in chemically competent BL21 (DE3) *E. Coli* bacteria transformed with an expression vector containing the lactose operon and the gene of the scFv fragment of interest. Bacteria were isolated on solid medium, after which a colony was transferred into a liquid culture medium for expansion. Absorbance measurements of the medium were used to monitor the bacterial growth and determine the appropriate moment for the

induction of the lactose operon (typically OD∼0.6), triggered though the addition of isopropyl β-D-1-thiogalactopyranoside (IPTG) in the milieu for a few hours. scFv was hence produced.

During this over-expression of scFv fragments, the nascent polypeptide chains aggregate into insoluble inclusion bodies (IBs) where native disulfide bridges cannot form due to the reducing environment of the bacterial cytoplasm. It is worth noting at this stage that expression of scFv in the periplasm of bacteria (via a signalling peptide) would allow formation of disulfide bonds (non-reducing environment), thereby expression of fragments in their soluble form, but usually leads to lower production yields [341, 388, 389].

After over-expression in inclusion bodies, a first centrifugation step was used to isolate and recover the bacteria cells. Ultrasound-induced bacterial lysis then allowed, after a second centrifugation step, to recover the soluble fraction containing small cellular debris as well as proteins and the inclusion bodies of interest. The latter had to be solubilized in high denaturant concentrations (6M guanidine hydrochloride or 8M urea) and in the presence of reducing thiol compounds to break non-native disulfide bonds that might have formed during cell lysis.

Purification was performed using an affinity column that retains specifically proteins labelled with a histidine-tag (a molecular label made of 6 histidine that binds to the solid matrix through nickel cations-mediated complexation). Major part of proteins was not retained by the affinity column during the washing procedure then the scFv fragments were eluted with a buffer containing imidazole a competitor of the his-tag/nickel association. The elution buffer contained high denaturant concentrations (typically here 8M urea) to maintain the protein in its unfolded state and therefore avoid aggregation. Further purification on a size exclusion chromatography column allowed recovery of a highly pure monomeric form of unfolded scFv. Concentration and purity of the fragment in the collected fractions were respectively assessed with BCA assay and SDS-PAGE polyacrylamide gel.

A.5 Refolding protocols

A.5.1 Denaturation and refolding protocol of CAB

The denaturation and refolding protocol of CAB was adapted from Hanson and Gellman [161]. Urea-denatured CAB stock solution (25 $mg.mL^{-1}$) was prepared by dissolving freeze-dried CAB in 10M urea aqueous solution. Mixed CAB/polymers stock solutions (at 1:1 wt/wt ratio) were prepared by dissolving an aliquot of the freeze-dried polymer in the urea-denatured CAB stock solution to reach the final polymer concentration of 25 $mg.mL^{-1}$.

CAB and mixed CAB/polymer solutions were incubated for 24 hours at room temperature, and heated (70°C for 6 minutes) just before being abruptly diluted ($\times$40 to $\times$250 fold) in a refolding buffer down to a final CAB concentration of 0.1 $mg.mL^{-1}$ (CD experiments) or 0.6 $mg.mL^{-1}$ (for light scattering measurements), and 0.03 or 0.6 $g.L^{-1}$ (for activity and solubility assays). Except when specified, refolding buffer were 10 mM TRIS-HCl pH 7.75, or 10 mM MES pH 5.9.

As a reference blank experiment, we implemented the detergent-assisted refolding previously reported by Hanson and Gellman [161]: the urea-denatured CAB solution, heated at 70°C for 6 minutes, was diluted to reach the CAB concentration of 0.043 $g.L^{-1}$ in 50 mM TRIS buffer pH 7.75 containing STS at 0.57 $mmol.L^{-1}$. Mixed CAB/STS

solution was incubated for 2 hours, and then supplemented with Me-β-CD added in excess (as the STS stripping agent, final concentrations 0.03 g.L^{-1} CAB, 0.4 mmol.L^{-1} STS, 4 mmol.L^{-1} Me-β-CD). The mixed solution was incubated for 2 additional hours prior to solubility and enzymatic activity assays.

CAB concentration was determined by UV-Vis measurement on a Thermo Scientific Evolution Array spectrophotometer using an extinction coefficient of 1.83 mg^{-1}.mL.cm^{-1} at 280 nm [320] after subtraction of the absorbance value at 314 nm (to limit the contribution of light scattering).

A.5.2 scFv renaturation protocol

The refolding protocol of scFv in the presence of polymers was adapted from the procedure optimized at CEA Saclay in the absence of polymers. The refolding is performed at 0.4 mg.mL^{-1} of scFv ($\sim$15 µM, as determined by UV-visible spectroscopy at 280 nm by using the predicted molar extinction coefficients given in Table **??**) unless stated otherwise. The fragments are purified and recovered as their denatured state. The 8M urea-unfolded (resp. 6M GndCl-unfolded) form of scFv is dialysed against 100 mM (or 10 mM) Tris-HCl pH 8 buffers of decreasing concentration of denaturant (4M for 48 h, 2M for 12-24 h, 1M for 12-24 h, 0.5M for 12-24 h and 0M for 12-24 h) containing 0.4M of L-arginine aimed at preventing aggregation of refolding intermediates. At the 1M and 0.5M denaturant steps, reduced glutathione (500× molar excess compared to scFv, *i.e.* 7.5mM for [scFv]$\sim$15 µM) and oxidized glutathione (50× molar excess, *i.e.* 0.75 mM) are added so that the electrochemical potential is set to a value allowing rapid exchange and formation of disulfide bonds.

In the presence of polymers, the same refolding protocol is performed, but L-arginine is not added. Polymers are added directly in the denaturant-unfolded scFv stock solution at 1:1 wt/wt ratio compared to the protein. In practice, a concentrated solution of polymers in 8M urea or 6M GndCl is prepared and a given volume of the solution is added to a certain volume of the denaturant-unfolded scFv stock solution. The latter is then subjected to dialysis against buffers of decreasing denaturant concentration. The electrochemical potential is also adjusted at the 1M and 0.5M denaturant stages.

A.6 Fluorescence correlation spectroscopy (FCS)

A.6.1 Experimental set-up and acquisitions

FCS measurements were performed on a home-built two-photon excitation system equipped with a mode-locked Ti:Sapphire laser (Mira900, Coherent, Auburn, CA) pumped by a solid-state laser at 532 nm (Verdi, Coherent). The sample (typically a few µL of solution) was placed on a microscope stage between two cover slips (Menzel-Gläser, # 1) held together with double-sided adhesive tape.

The laser beam (780 nm, $\sim$ 100-fs pulse width) was focused into the sample using a 60× water immersion microscope objective (1.2 NA, UPlanApo, Olympus). The power was kept below 10 mW by means of neutral filters. The fluorescence signal was collected through the same objective lens, reflected by a dichroic mirror to select fluorescein fluorescence (wavelength 580 $\pm$ 30 nm), and filtered through short pass filters to absorb any possible diffused excitation infrared light. The collected light was then separated by a beam splitter and focused on the 200 µm^2 working surfaces of two avalanche photodiode modules, APDs (SPCM-AQR-14, PerkinElmer, Vaudreuil, Canada). The signal outputs

of the APDs (TTL pulses) were acquired by a digital autocorrelator module (ALV-6000, ALV-GmbH, Langen, Germany) which computed online the cross-correlation function of the fluorescence fluctuations, $g(t)$.

The background contribution to the collected fluorescence intensity was about 100-300 Hz. The concentration of FITC-labelled proteins in the sample was chosen so that the fluorescence intensity collected was not less than 3 kHz (typically 3-50 kHz) to get a sufficiently high signal/noise ratio. Typically, 10 to 30 acquisitions of 60 seconds acquisitions of intensity fluctuations were averaged to compute the autocorrelation curve.

A.6.2 Heating of IgG

IgG/polymer solutions were prepared in 20 mM phosphate buffer pH 6.8 with or without 100 mM NaCl as described in Chapter 3, with both IgG and polymer concentrations of 0.2 $mg.mL^{-1}$. Each sample was heated at a rate of 0.2°C.min^{-1} from 25°C to 85°C. Aliquots (1 µL) of the sample were collected at various temperatures during the scan. They were diluted into 9 µL of buffer and kept at room temperature 10 minutes prior to fluorescence fluctuation recording (ten sets of 60-seconds acquisition).

A.6.3 Refolding of scFv

Refolding of scFv was performed as detailed in Section A.5.2, in the absence or presence of polymers (added at 1:1 wt/wt ratio). At each dialysis step, aliquots of *ca.* 2 µL were collected and deposited on a microscope glass plate in the FCS apparatus to perform a measurement at 25°C, which consisted of 10 acquisitions of 60 seconds each.

A.6.4 Refolding of CAB

A 2 µL aliquot of a pre-heated (70°C, 6 minutes) mixed CAB:polymer solution at 1.35 $mg.mL^{-1}$ in 10M urea was diluted in 198 µL of the renaturation buffer (either Tris-HCl 10 mM pH 7.75 or MES 10 mM pH 5.9) and then incubated at room temperature. Regularly, a 2 µL sampling was deposited on a microscope glass plate in the FCS apparatus to perform a measurement at 25°C, which consisted of 10 acquisitions of 60 seconds each.

A.7 Capillary zone electrophoresis (CZE)

CZE was performed using a Beckman P/ACE system MDQ instrument equipped with a diode array UV/visible detector (Beckman Instruments Fullerton, CA), a working wavelength of 220 nm, operating at 25°C and fitted with bare silica capillaries of 75 µm × 31 cm, effective length of 21 cm (Chromoptic, France). The capillary was flushed daily with 1M NaOH, followed by a water rinse, and finally was allowed to equilibrate with the running buffer (20 mM phosphate buffer pH 6.8 with or without 100 mM NaCl, and with or without polymers).

Solutions of IgG (3 $mg.mL^{-1}$) in the running buffer containing mesityl oxide as marker of the electro osmotic flow (EOF) were injected using the pressure injection mode (3 s at 0.5 psi – for IgG – or 0.3 psi – for MeO). A voltage of 10 kV (resp. 5 kV) was applied in the absence (resp. presence) of 100 mM NaCl in running buffer. The mobility (μ) was calculated from Equation A.1, where t_{samp} is the sample migration time, t_{EOF} is the migration time of the EOF marker, L_t is the total length of the capillary, L_d is the length to the detector, and E is the electric field.

$$\mu = \frac{L_t L_d}{E}\left(\frac{1}{t_{samp}} - \frac{1}{t_{EOF}}\right) \quad (A.1)$$

A.8 Differential scanning calorimetry (DSC)

DSC measurements were performed on a VP DSC microcalorimeter (MicroCal Inc.) with a cell volume of 0.520 mL and under an external pressure of *ca.* 180 kPa. The heating rate was set at 0.2°C.min^{-1} in the range of 20-95°C. The experimental data were analysed using the Origin 7.0 software supplied by the manufacturer.

Solutions were kept at 20°C for 1 hour and degassed at 20°C under mild vacuum for 15 minutes prior to loading into sample and reference cells. The reference cell was filled with the same buffer as the IgG and IgG/polymer solutions. All measurements were carried out in duplicates. A scan recorded with buffer in the sample and reference cells was subtracted from the sample data to remove baseline contributions.

A.9 Dynamic and static light scattering (DLS, SLS)

A.9.1 Aggregation kinetics of IgG by SLS

The aggregation kinetics of IgG with NaCl were assessed by measuring the intensity of the light scattered at a fixed angle of 90°using an ALV/CGS-3 Compact Goniomerer System equipped with a 22 mW HeNe laser operating at a wavelength of 632.8 nm. Toluene was used as the standard to normalize the intensity. Prior to measurement, the samples were filtered through Anotop10 filters (pore size: 20 nm, Whatman). The concentration of IgG after filtration was $\sim$ 0.5 mg.mL^{-1}, as determined by the solution absorbance at 280 nm using an extinction coefficient of 1.4 mL.mg^{-1}.cm^{-1}. The polymer:IgG ratio was $\sim$ 1:1 wt/wt. The scattering intensity recorded for solutions at room temperature prior to thermal treatment is defined as intensity at time 0. Subsequently, the IgG solutions were kept at a fixed temperature (55, 60 or 65°C). Changes in the scattering intensity were measured as a function of incubation time at each of the three selected temperatures.

A.9.2 Size measurement of heated IgG by DLS

Before DLS measurements, 1 mL aliquots of the IgG(:polymer) solution at 0.5 mg.mL^{-1} in a 10×75 mm cylinder cell (VWR, Canada) for light scattering were heated for 10 min with gentle shaking in a water bath at 25, 30, 35, 40, 45, 50, 55, 60, 65, 70°C. The samples were cooled back to room temperature prior to characterization.

DLS experiments were performed on an ALV/CGS-3 Compact Goniomerer System equipped with a 22 mW HeNe laser operating at a wavelength of 633 nm. The correlation functions were measured at 25°C with an angle of 90°. The hydrodynamic radius was calculated using the Stokes-Einstein equation. The size distribution was also obtained using the CONTIN regularized fit.

A.9.3 Aggregation of CAB

An index of aggregation of CAB was assessed by measuring the intensity of the light scattered at a fixed angle of 90°using a BI-200SM Goniomerer System (Brookhaven Instruments Corporation) equipped with a 30 mW laser LED operating at a wavelength

of 637 nm. The time at which we dilute urea-denatured mixed CAB:polymer (or CAB) in the refolding buffer is defined as time 0. The diluted CAB solutions were kept at 25°C and variations in the scattering intensity were measured as a function of incubation time.

Hydrodynamic radii were measured with the same set-up in the dynamic mode, and derived from the autocorrelation curve via the non-negative least-squares fitting procedure.

A.10 Circular dichroism (CD)

A.10.1 Conventional circular dichroism

CD measurements were carried out at 20°C with a Jasco J/815 spectrophotometer using quartz cells of 1 mm path length. The molar ellipticity $[\theta]$ was calculated according to the equation:

$$[\theta] = \frac{0.1\ \theta\ M_R}{l\ c} \tag{A.2}$$

where θ is the measured ellipticity in degrees, M_R is the mean residue molar mass, l is the path length (in cm) of the cell and c is the protein concentration (in $mg.mL^{-1}$).

A typical CD trace consisted of the average of three acquisitions at a scan rate of 100 $nm.min^{-1}$ (integration constant: 0.25 second, 1 point every 0.5 nm).

A.10.2 Synchrotron-radiation circular dichroism (SRCD)

SRCD was performed on the DISCO beamline at SOLEIL. Stock solutions of scFv at 10 $mg.mL^{-1}$ and polymer at the same concentration were prepared in in 10 or 8M urea and in 10 mM Tris-HCl buffer pH 8. Specific volumes of the four solutions (scFv in urea, scFv in Tris buffer, polymer in urea, polymer in Tris buffer) were mixed to prepare mixtures of final urea concentration in the range 5-10M. Lower urea concentration were accessed through dialysis of the scFv/polymer mixtures in 5M urea against buffers of decreasing urea concentration after equilibration for 24 hours (as in the refolding protocol detailed above). In the absence of polymers, the refolding was performed with 0.4M L-arginine.

Measurements were carried out at 25°C on $\sim$ 5 µL of solution placed in between two calcium fluoride windows separated by an optical path-length of 0.012 cm (for urea- or L-arginine-containing samples) or 0.055 cm (for sample devoid of urea or L-arginine). For each sample, three acquisitions were performed and averaged (integration time: 1200 ms, wavelength step: 1 nm). (1R)-(−)-10-camphorsulfonic acid (CSA) was used as a calibration standard.

A.11 Steady-state fluorescence emission spectroscopy

Corrected fluorescence spectra upon one-photon excitation were recorded on a Photon Technology International QuantaMaster QM-1 spectrofluorimeter (PTI, Monmouth Junction, NJ) that was equipped with a Peltier cell-holder (TLC50, Quantum Northwest, Shoreline, WA). Solutions for the fluorescence measurements were adjusted to concentrations such that the absorption maximum was about 0.15 at the excitation wavelength.

A.12 Electrostatic modelling

PyMol was used to visualize the 3D structure of proteins (PDB files). Electrostatic calculations were performed with the adaptative Poisson-Boltzmann solver (APBS). Briefly, the .pdb file was converted into a .pqr file via the on-line PDB2PQR software [390], which is required to prepare the .pdb file to electrostatic potential calculations via the APBS tool. This .pdb to .pqr conversion results in:

- the addition of a limited set of heavy atoms missing in the structure,
- the determination of the residues' pKas,
- the positioning of missing hydrogen atoms,
- the optimisation of the protein *vis-á-vis* of the favourable hydrogen bonds,
- the assignment of charge and radius parameters according to a specified forcefield (we chose here the PARSE forcefield).

The PROPKA software [391–394] was used to assign the pKa values of each residue and therefore fix their protonation state at a chosen pH. After the .pqr file has been generated, the electrostatic surface potential can be calculated with the APBS plug-in in the PyMol visualization software. For these calculations, the ionic strength can be adjusted at will.

In addition, Patch Finder Plus [365] is an on-line software that extracts the largest positive patch on the surface of a protein from the entry .pdb file, by using a cut-off of ± 2 kT/e. Here, pH (resp. ionic strength) is set to 7 (resp. 150 mM). Hydrogen atoms are automatically added with the PDB2PQR software.

A.13 Activity assays

A.13.1 Enzymatic activity of CAB by UV-visible spectroscopy

To determine the activity of CAB after incubation in refolding buffers (0.6 mg.mL^{-1} CAB in either 10 mM Tris-HCl pH 7.75 or 10 mM MES pH 5.9), measurements of the initial rate of hydrolysis of *p*-nitrophenyl acetate (*p*-NPA) were performed in Tris-HCl 50 mM pH 7.75 using an excess of *p*-NPA substrate. Since the enzymatic activity of CAB depends on pH and the protein is completely inactive at pH 5.9, activity assays were performed at pH 7.75 (by 20× dilution into a 50 mM Tris-HCl pH 7.75 buffer of aliquots of the CAB solutions incubated in refolding buffer).

Typically, a 25 µL sampling of the CAB preparation at 0.6 mg.mL^{-1} (ca. 21 µM) was diluted in 500 µL of 50 mM Tris-HCl buffer pH 7.75, and supplemented at time zero with 5 µL of 100 mM *p*-NPA in acetonitrile (1 mmol). The absorbance at 400 nm was monitored for 200 seconds in an Evolution Array spectrophotometer (ThermoScientific), and we determined the slope, S, of initial variation of the absorbance with time. Similar measurements without CAB or with freshly solubilized native CAB gave the background self-hydrolysis rate, S_0 (buffer only), and the maximal rate, S_{ref} (solution of 0.03 mg.mL^{-1} CAB freshly prepared in Tris-HCl buffer pH 7.75 from the stock protein powder). The % activity recovery is given by $(S - S_0)/(S_{\text{ref}} - S_0)$.

A.13.2 Antibody binding assays by flow cytometry

The IgG:polymer solutions were prepared at *ca.* 0.2 mg.mL^{-1} (and 1:1 wt/wt protein:polymer ratio) and incubated for 1 hour in 20 mM phosphate buffer pH 6.8 at room temperature. The mixtures were then added to ∼ 300,000 CHO cells (WT and

ETBR ones) suspended in phosphate buffer saline containing 5% of goat serum and 1% of bovine serum albumin (to limit non specific binding of IgG onto cell membrane) to reach a final concentration of about 100 nM. After incubation at 4°C for 3 hours, cells were centrifugated (4,000 RPM, 10 minutes) and the cell-containing pellets were washed twice with buffer to eliminate unbound IgG. After re-suspension, an AlexaRed-labelled secondary antibody, directed against a specific sequence of the Fc region of the Rendomab-B1, was added at *ca.* 100 nM and let react with Rendomab-B1 for 1 hour at 4°C. Additional washing steps were last performed to remove unbound secondary antibody before the flow cytometry measurements, that were carried out on a GUAVA flow cytometer (Guava Easycyte Plus, Millipore) and mean fluorescence intensity (MFI) of samples was measured.

A.14 Nuclear Magnetic Resonance (NMR)

Nuclear magnetic resonance (NMR) experiments were performed on a Bruker Avance III 600 MHz spectrometer equipped with a 4 mm Shigemi tube at temperatures varying between 283 and 308K. ^{15}N-enriched scFv Rendomab B1 was refolded at *ca.* 5 mg.mL^{-1} in the presence of PAA5 (added at 1:1 wt/wt ratio) according to the procedure described above. The refolded sample (no urea) was concentrated up to *sim* 15 mg.mL^{-1} via centrifugation on an Amicon Ultra-15 centrifugal filter unit (MWCO 3,000 g.mol^{-1}). About 100-150 µL of concentrated sample were used for an experiment. D_2O was added (*ca.* 5-10 wt%) to lock the NMR signal.

Appendix B

Experimental techniques

Contents

B.1 Fluorescence Correlation Spectroscopy (FCS) 158
B.1.1 FCS: a powerful technique 158
B.1.2 Principle 158
B.1.3 Analysis of the experimental data 160
B.1.4 Common artefacts and calibrations 163
B.1.5 Practical considerations 168
B.2 Capillary zone electrophoresis (CZE) 168
B.3 Circular dichroism (CD) 170
B.3.1 Principle 170
B.3.2 Deconvolution programs 170

B.1 Fluorescence Correlation Spectroscopy (FCS)

B.1.1 FCS: a powerful technique

The size of objects in the nano- to micro-metric range in solution is commonly estimated by measurements of hydrodynamic radii with dynamic light scattering. Yet, this conventional technique cannot readily discriminate the different entities of an inherently heterogeneous mixture (proteins, polymers, protein/polymer complexes, oligomers or aggregates in our case), especially if sizes are close to each other. The high sensitivity to large objects (*e.g.* protein aggregates), which contribute significantly to the scattered intensity, as well as the relatively elevated concentrations required to get reliable hydrodynamic radius values ($\sim$ 1 to a few mg.mL^{-1}) are all drawbacks of this familiar technique. Accordingly, we have chosen to implement another experimental technique in order to measure sizes of protein-based objects in a more specific way, namely by easily distinguishing the different "states" of the protein of interest (monomer, oligomer or complexed by polymers): fluorescence correlation spectroscopy (FCS).

Introduced by the pioneering work of Madge, Elson and Webb in 1972 [395], FCS is an experimental technique used to access dynamic properties (translational diffusion coefficients, kinetic constants, molecular interaction, conformational changes, aggregation...) through statistical analysis of spontaneous fluorescence intensity fluctuations of a fluorescently-labelled entity at thermal equilibrium.

As we shall see, FCS allows to study dynamic molecular event on a wide time range (from microseconds to seconds) with samples of typical concentration in the nanomolar to micromolar range. Unlike the conventional light scattering technique used to measure sizes, fluorescent entities are selectively observed by FCS, without perturbation of dust or unlabelled objects.

B.1.2 Principle

The objects studied by FCS (proteins such as IgG, scFv, CAB; or polymers) have to be labelled with a fluorophore to be detected (see Appendix A for the labelling procedure). The sample is irradiated with an incident LASER beam which energy is adjusted so that fluorophore excitation (and hence emission of fluorescence) is only possible after simultaneous absorption of two photons: the expression "two-photon FCS" is used to refer to the technique (as opposed to the conventional one-photon FCS where the excitation wavelength exactly matches that of the fluorophore). In order to get a reasonable probability of such a three-body event, the incident photon density must be high enough. To this purpose, a pulsed excitation is used (pulses of $\sim$ 100 fs) so that the photon density per pulse is higher than the mean photon density of the LASER. The two-photon absorption is in these conditions possible only in close vicinity of the focal point of the incident beam, which generates an excitation volume (or confocal volume) of about 1 femtolitre (while one-photon FCS generates in the same conditions an illumination cone, see Figure B.1). This volume is assumed to be Gaussian, with radial and axial dimensions respectively designed by ω_{xy} and ω_z. The small size of the excited volume makes FCS a single-molecule detection technique.

In a FCS experiment, temporal fluorescence intensity fluctuations emitted from the excited entities in the confocal volume are recorded: they arise either from the movement of objects in and out of the excitation volume (brownian motion, active transport...) or to physical of chemical dynamics that facilitate the interconversion between a fluorescent

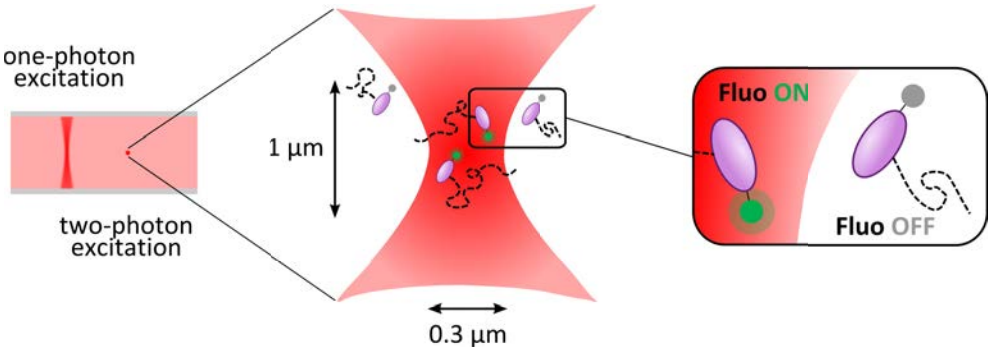


Figure B.1: Schematic illustration of the confocal volume (in red) generated by a two-photon excitation where fluorescently-labelled entities are subjected to brownian motion.

and a non-fluorescent state of the considered fluorophore (see Figure B.2).

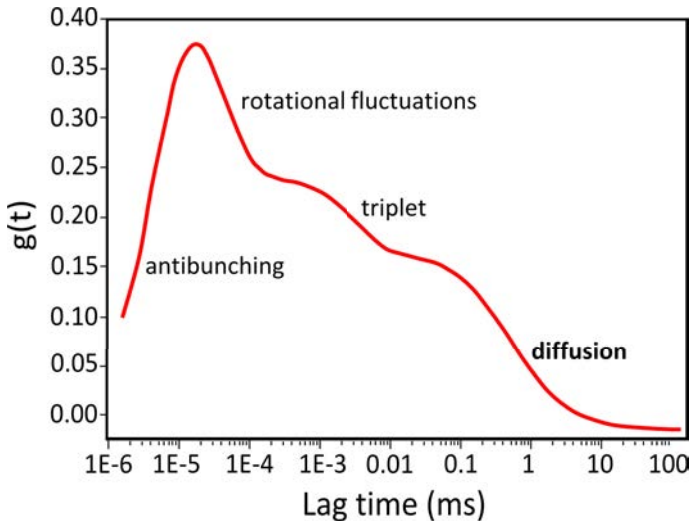


Figure B.2: Time-scales of various processes monitored by FCS autocorrelation analysis.

We are here interested in the Brownian motion of fluorescently-labelled biological entities (antibodies and fragments, or other proteins) in the presence or not of polymers in order to extract the size distribution (in terms of hydrodynamic radii) of the objects formed in solution. Polymers that are potentially added are not fluorescent and are thereby not directly detected: one can already sense how FCS will allow to discriminate the different entities in a mixture. In particular, the technique enables specific detection of objects involving labelled proteins, unlike light scattering. The diffusion coefficient accessible by FCS will be affected by the aggregation of proteins, but also by their interaction with polymers as illustrated on Figure B.3 (in both cases, larger objects are formed).

We shall see in the following how the knowledge of the mean fluorescence intensity emitted by labelled entities, coupled to the measurement of fluorescence intensity fluctuations, can be used to extract the average number N_{agg}, of fluorescently-labelled proteins

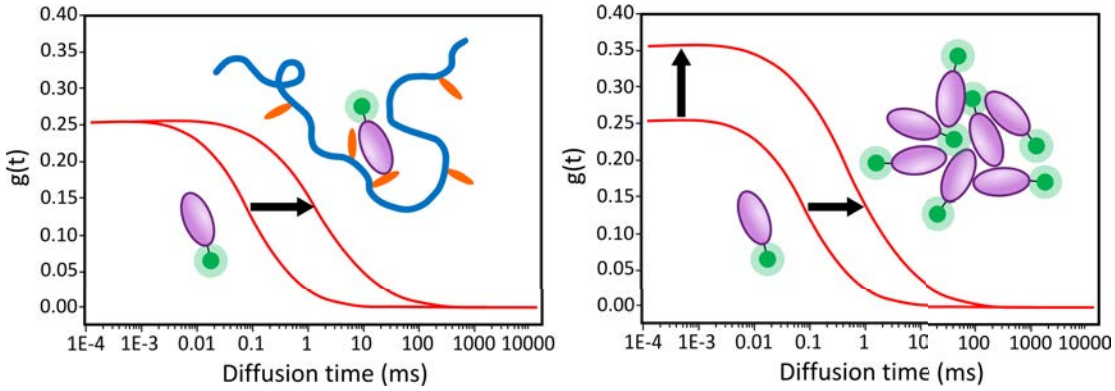


Figure B.3: Schematic illustration of the evolution of the FCS autocorrelation curve upon complexation with polymers or oligomerization. Upon protein complexation with polymers, the diffusion time increases, and the value at the plateau remains constant if complexes contain only one protein (or increases if multi-protein complexes are formed, see below). Upon protein aggregation, both the diffusion time and the value at the plateau are expected to increase, because fewer but larger entities are formed (see below the relationship between the value at the plateau and the average number of objects in solution).

per oligomer or complex (and thereby distinguish *in fine* oligomers from protein:polymer complexes of similar size).

B.1.3 Analysis of the experimental data

In order to extract molecular dynamics properties of the considered sample, fluorescence intensity fluctuations are analysed via the calculation of the auto-correlation function, $g(t)$, which contains information on the mean number of fluorescent entities in the confocal volume, their mean residence time in this excited volume as well as photophysical or photochemical features. In our case, the incident power light is kept below 10 mW so that contribution of the triplet state can be neglected. The shape and characteristic decay time of the autocorrelation functions gives access to the underlying dynamics and especially to the translational diffusion coefficient, and thus the hydrodynamic radius, of species. More theoretical details can be found in [396]. Different models have been developed to extract the diffusion coefficient. Some of them are discussed in the following.

B.1.3.1 Single-component diffusion

In the case of a single-component sample that can diffuse freely and independently in three dimension due to Brownian motion, and under the assumption of a Gaussian confocal volume, the autocorrelation function writes:

$$g(t) = \frac{1}{\bar{N}} \left(\frac{1}{1 + \frac{t}{\tau_D}} \right) \left(\frac{1}{1 + \left(\frac{\omega_{xy}}{\omega_z} \right)^2 \frac{t}{\tau_D}} \right)^{1/2} \tag{B.1}$$

where $\bar{N}$ is the mean number of fluorescent entities in the excited volume and τ_D is the their characteristic diffusion time across the volume.

In practice, the 3D system can be fairly approximated by a two-dimensional diffusion in the x y plane because $\omega_z \gg \omega_{xy}$. The smaller dimensions determine the relaxation of fluctuations of the number of proteins in the confocal volume. In that 2D-diffusion case, the autocorrelation function can be simplified to:

$$g(t) = \frac{1}{\bar{N}} \left(\frac{1}{1 + \frac{t}{\tau_D}} \right) \tag{B.2}$$

Determination of the average hydrodynamic radius
From Equation B.2, it is possible to extract the characteristic diffusion time τ_D of the single species in the sample. This diffusion time is related to the radial size of the excited volume and to the diffusion coefficient via the relationship:

$$\tau_D = \frac{\omega_{xy}^2}{8D} \tag{B.3}$$

To extract the diffusion coefficient of the considered species, one needs to know the radial size of the confocal volume. Calibration is performed by using a fluorescein as standard of known diffusion coefficient, $D^{\text{fluorescein}} = 4.25 \times 10^{-6} \pm 0.01$ cm^2.s^{-1} [397]. Therefore, one can simply write:

$$D^{\text{protein}} = \frac{\tau_D^{\text{fluorescein}}}{\tau_D^{\text{protein}}} D^{\text{fluorescein}} \tag{B.4}$$

where $\tau_D^{\text{fluorescein}}$ (resp. τ_D^{protein}) is the diffusion time measured for fluorescein (resp. the protein).

Under the simplified assumption of a spherical globular protein (which is not the case for IgG), the Stokes-Einstein relationship can be used to finally obtain the average value of the hydrodynamic radius:

$$\mathrm{R_h^{protein}} = \frac{k_B T}{6\pi\eta D^{\text{protein}}} \tag{B.5}$$

where η is the viscosity of the sample at the temperature T.

Estimation of the average aggregation number
As can be seen in Equations B.1 and B.2, the amplitude of the correlation function, g_0, varies as the inverse of the average number of fluorescent objects in the confocal volume. Is is then possible to access the aggregation number $\mathrm{N_{agg}}$ defined as the average number of proteins per fluorescent entity in the solution. Indeed, the mean fluorescence intensity is given by $I = \bar{n} \times i$, where $\bar{n}$ is the total average number of fluorescent proteins in the excited volume and i is the fluorescence intensity of a single FITC-protein. This, of course, strictly holds only if there is no quenching of fluorescence (or change in quantum yield) upon formation of multi-protein objects.

The average fluorescence intensity per object is $I \times g_0 = I/\bar{N} = (i \times \bar{n})/\bar{N} = i \times \mathrm{N_{agg}}$, where $\mathrm{N_{agg}}$ accounts for emission from free (unbound) FITC-protein monomers, FITC-protein complexes with polymers and FITC-protein oligomers or aggregates. The $\mathrm{N_{agg}}$

value can be determined using $i = I/\bar{n} = (I \times g_0)_0$, where $(I \times g_0)_0$ is the value of $I \times g_0$ for FITC-protein monomers in the absence of polymer, in conditions where the protein does not aggregate.

The autocorrelation curve calculated from the fluorescence fluctuations serves to estimate the size distribution of objects in the considered sample. As we will see, the low-time plateau value of the autocorrelation function can be used to extract the aggregation number defined as the number of single fluorescently-labelled entity in objects observed in the excited volume.

B.1.3.2 Multi-component diffusion

When more than one species coexist in the sample, the autocorrelation has to be adapted to take into account contributions of the different populations. In the case of two species, one can write for a 3D diffusion [396]:

$$\begin{aligned} g(t) = & \frac{Q_1^2 \bar{N}_1}{(Q_1\bar{N}_1 + Q_2\bar{N}_2)^2} \left(\frac{1}{1 + \frac{t}{\tau_{D_1}}} \right) \left(\frac{1}{1 + \left(\frac{\omega_{xy}}{\omega_z}\right)^2 \frac{t}{\tau_{D_1}}} \right)^{1/2} \\ + & \frac{Q_2^2 \bar{N}_2}{(Q_1\bar{N}_1 + Q_2\bar{N}_2)^2} \left(\frac{1}{1 + \frac{t}{\tau_{D_2}}} \right) \left(\frac{1}{1 + \left(\frac{\omega_{xy}}{\omega_z}\right)^2 \frac{t}{\tau_{D_2}}} \right)^{1/2} \end{aligned} \tag{B.6}$$

where Q_i is the brightness of species i, $\bar{N}_i$ is the mean number of entities of species i in the confocal volume and τ_{D_i} their mean diffusion time.

In Equation B.6, each species can be described as a single diffusing component. The hydrodynamic radius of each species can be readily accessed through the determination of the diffusion time, as described in the previous section. However, at variance with Equation B.1, the amplitude of each contribution not only depends on the mean number of entities of each species in the confocal volume but also on their brightness. Accordingly, a more subtle analysis is required if one wants to extract the aggregation number.

Let's first redefine the amplitude of each component as g_{01} and g_{02} and consider that species *1* is the free FITC-protein and species *2* is a polymer-bound or oligomer of FITC-protein containing $\mathrm{N_{agg}}$ proteins. The total number of single FITC-protein ($\bar{n}$) that contributes to the average fluorescence intensity I collected in the confocal volume can be written as: $\bar{n} = \bar{N_1} + \bar{N_2}\mathrm{N_{agg}}$. Besides, under the assumption of a conserved brightnes of FITC-protein upon complexation or oligomerization (no quenching nor change of quantum yield), we can write: $Q_2 = \mathrm{N_{agg}} \times Q_1$. Accordingly:

$$g_{01} = \frac{Q_1^2 \bar{N}_1}{(Q_1\bar{N}_1 + Q_2\bar{N}_2)^2} = \frac{\bar{N}_1}{\bar{n}^2} \qquad \text{and} \qquad g_{02} = \frac{Q_2^2 \bar{N}_2}{(Q_1\bar{N}_1 + Q_2\bar{N}_2)^2} = \frac{\mathrm{N_{agg}^2}\bar{N}_2}{\bar{n}^2}$$

In addition, the average fluorescence intensity collected during the experiment is related to the total number of single FITC-proteins, $\bar{n}$ (under the hypothesis of conserved brightnesses when forming oligomers or complexes) via: $I = \bar{n} \times i$, where i is the fluorescence per single FITC-protein, which is a constant that can be measured in an experiment without polymer and where proteins do not aggregate. Therefore, we can determine

systematically $\bar{n}$ in conditions where there is an equilibrium between free proteins and protein/polymer complexes or protein oligomers. Fitting of the autocorrelation function gives g_{01} and g_{02}, so that we can calculate $\bar{N_1} = g_{01} \times \bar{n}^2$ and $\mathrm{N}_{\mathrm{agg}}^2 \bar{N_2} = g_{02} \times \bar{n}^2$.

We can also access: $\mathrm{N}_{\mathrm{agg}} \bar{N_2} = \bar{n} - \bar{N_1}$ and finally determine $\mathrm{N}_{\mathrm{agg}}$. By combining all the expressions, we can write:

$$\mathrm{N}_{\mathrm{agg}} = \frac{g_{02} \times \bar{n}^2}{\bar{n} - g_{01} \times \bar{n}^2} = \frac{g_{02} \times (I/i)}{1 - g_{01} \times (I/i)}$$

In the case of multiple components (more than 2), the expression of the autocorrelation function can be generalized as:

$$g(t) = \frac{1}{\left(\sum_{i=1}^{k} Q_k \bar{N_k}\right)^2} \sum_{j=1}^{k} Q_j^2 \bar{N_j} \left(\frac{1}{1 + \frac{t}{\tau_{D_j}}}\right) \left(\frac{1}{1 + \left(\frac{\omega_{xy}}{\omega_z}\right)^2 \frac{t}{\tau_{D_j}}}\right)^{1/2} \tag{B.7}$$

B.1.3.3 Maximum Entropy Method for highly heterogeneous systems

In the case of highly heterogeneous samples (more than 2 species, or very polydisperse species), it can be convenient to have access to the effective distribution of diffusion times. To this purpose, data can be analysed with the Maximum Entropy Method (called MEMFCS) that has been developed by Sengupta *et al.* precisely for heterogeneous mixtures [398].

Briefly, the MEMFCS algorithm describes the autocorrelation function as a discrete sum of k components, as in the multi-component diffusion case:

$$g(t) = \sum_{i=1}^{k} \alpha_i \left(\frac{1}{1 + \frac{t}{\tau_{D_i}}}\right) \left(\frac{1}{1 + \left(\frac{\omega_{xy}}{\omega_z}\right)^2 \frac{t}{\tau_{D_i}}}\right)^{1/2} \tag{B.8}$$

where k is the number of components that can each be described by a single diffusion coefficient, α_i is a global parameter that reflects both their concentration and their brightness (*vide supra* the multi-component case), τ_{D_i} their characteristic diffusion time and ω_{xy} and ω_z the radial and axial dimensions, respectively, of the observation volume.

The algorithm attempts to minimize the normalized value of χ^2 while maximizing the entropic term, defined as $S = -\sum_i p_i \ln p_i$ where $p_i = \alpha_i / \sum_i \alpha_i$ [398]. The result is given as a seemingly continuous distribution of diffusion times, as illustrated on Figure **??**. It can hence be useful to describe highly heterogeneous systems, in particular when we do not know how many species have to be taken into account to correctly fit the autocorrelation function.

B.1.4 Common artefacts and calibrations

B.1.4.1 Refractive index mismatch at high concentrations of additive. Calibration of the confocal volume

During the intermediate steps of the refolding procedure of scFv fragments, samples may contain high concentrations of urea or guanidinium chloride (above 1M). Such

high concentrations affect the refractive index of the sample (refractive index mismatch with the water-immersion objective) so that the confocal volume size changes, resulting in wrong determinations of the sample concentration, or aggregation numbers. Error has been shown to remain below 12% up to a refractive index of 1.38 [399]. To limit the refractive index mismatch, the collar setting of the objective is adjusted for each denaturant concentration so as to maximize the mean fluorescence intensity collected. Moreover, the intensity collected for a sample of fluorescein of known concentration is used as calibration for each buffer.

B.1.4.2 High-temperature measurements

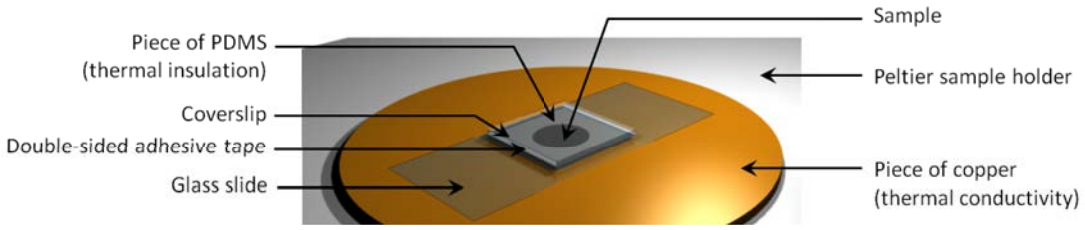


Figure B.4: Schematic illustration of the FCS set-up used for *in situ* heating.

Chapter 5 presents results about the variation of hydrodynamic radii and aggregation number of FITC-IgG/polymer mixtures upon heating. Measurements were performed after the sample had been cooled down to room temperature though (*ex-situ* heating). The possibility of measuring the size of FITC-IgG oligomers or complexes with polymers upon heating directly on the FCS objective was investigated. The experimental set-up was adapted to ensure proper thermal equilibration on the Peltier sample stage. Briefly, a piece of copper (good thermal conductor) was placed between the sample and the sample holder in order to maximize their contact surface (see Figure B.4), while a piece of poly(dimethylsiloxane) (PDMS) on top of the sample ensured thermal isolation (to avoid convection phenomena).

Calibration with Rhodamine B

FCS measurements were carried out with an water-immersion objective. The temperature of the later was not controlled, therefore thermal losses could occur through it. As a result, the nominal temperature given by the Peltier system did not match the effective temperature of the sample. In order to get the sample temperature, a fluorescent dye was used, rhodamine B. It is well-established that the fluorescence intensity of this dye decreases as the temperature increases.

We first measured the fluorescence intensity emitted by rhodamine B (10 µM in 100 mM Tris-HCl buffer pH 8) at different temperatures with an air objective ($\lambda_e x = 780$ nm, emission filter at 625 nm). The nominal temperature is then supposed to be equal to the real temperature of the sample (since there is no contact here between the sample and the objective).

The intensity measured at 25°C was taken as the reference: we could plot the ratio $I_T/I_{25°C}$ (Figure B.5) as a function of increasing temperature. The measurement was repeated twice with increasing temperature and once with decreasing temperature. Samples were let to reach thermal equilibrium for 10 minutes between each acquisition

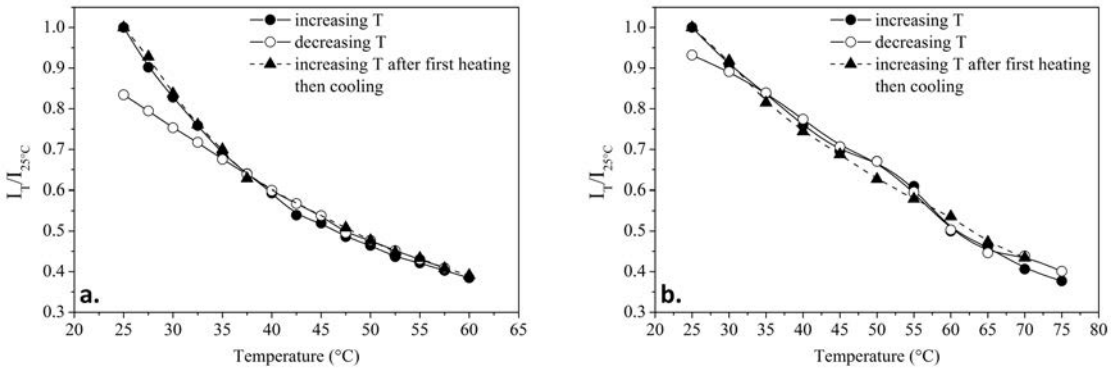


Figure B.5: Evolution of $I_T/I_{25°C}$ as a function of temperature for rhodamine B excited with two-photons using an air (left) or a water (right) objective.

(*i.e.* every 2.5°C). The same protocol was carried out with a water-immersion objective. Measurements were repeated three times with increasing temperature, and all three measurements are identical (Figure B.5).

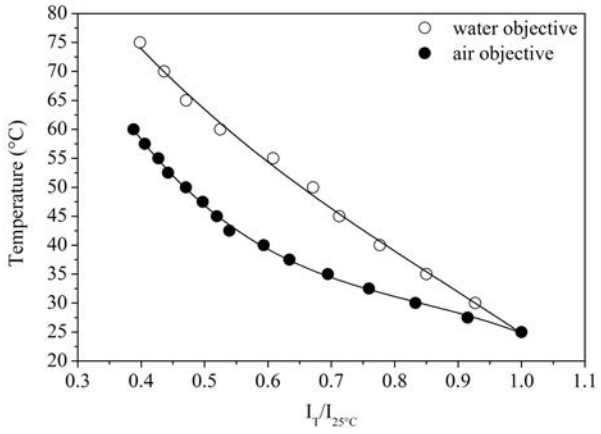


Figure B.6: Evolution of temperature as a function of $I_T/I_{25°C}$ for the air objective and the immersion objective, as quoted.

The two experiments are compared on Figure B.6: the plot for the water objective is shifted to higher temperatures compared to the air objective, which results from the thermal loss through the immersion objective. These plots can further be fitted by a third-order polynomial function:

$$T = a + b\frac{I_T}{I_{25°C}} + c\left(\frac{I_T}{I_{25°C}}\right)^2 + c\left(\frac{I_T}{I_{25°C}}\right)^3$$

.

The a, b, c, d coefficients obtained are listed in Table B.1 and compared to values reported in the literature for rhodamine B. It is then possible to plot the evolution of the sample effective temperature as a function of the nominal temperature read on the Peltier controller (Figure B.7).

Table B.1: Values of the coefficient of the polynomial fit of T=f($I_T/I_{25°C}$). The values from literature are extracted from [400].

	a (°C)	b (°C)	c (°C)	d (°C)
Air objective	164	-424	471	-187
Water objective	137	-212	161	-61
Ross *et al.*	132	-250	220	-79
Fu *et al.*	149.15	-317.84	323.41	-131.84
Samy *et al.*	141.53	-250.25	228.02	-96.904

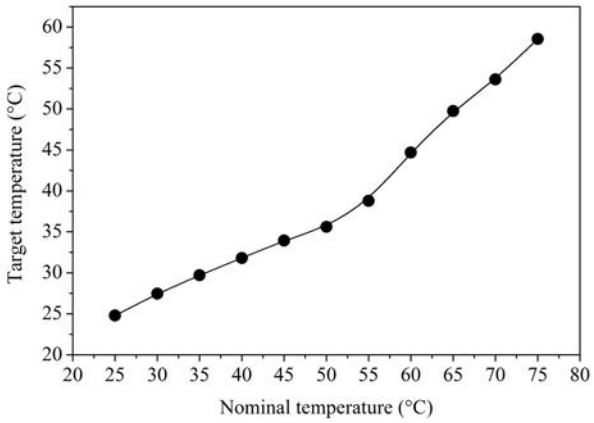


Figure B.7: Evolution of the target temperature as a function of the nominal temperature (in the case of the water objective)

Diffusion coefficient of fluorescein

To assess the goodness of the calibration, we proceeded to the measurement of the diffusion time of fluorescein as a function of temperature (using the relation between nominal temperature and sample temperature as determined previously). The autocorrelation functions were fitted using the MEMFCS algorithm (see above). The diffusion coefficient of fluorescein at 25°C is known from literature studies (4.25×10^{-10} $m^2.s^{-1}$), therefore we can calculate the diffusion coefficients expected at higher temperatures with the relationship:

$$D_T = \frac{\tau_{25°C}}{\tau_T} \cdot D_{25°C} \tag{B.9}$$

where $\tau_{25°C}$ (resp. τ_T) is the diffusion time measured for fluorescein at 25°C (resp. at T).

With the evolution of water viscosity as a function of temperature (Figure B.8), we can normalize these diffusion coefficient with the temperature and viscosity (Figure **??**), according to Equation B.10:

$$D_{\text{normalized}} = \frac{\frac{\eta}{\eta_0}}{\frac{T}{T_0}} \cdot D_T \tag{B.10}$$

where η (resp. η_0) is the viscosity of the buffer at the temperature T (resp. at T_0).

The normalization should give a constant value (dotted line on Figure B.9), which is

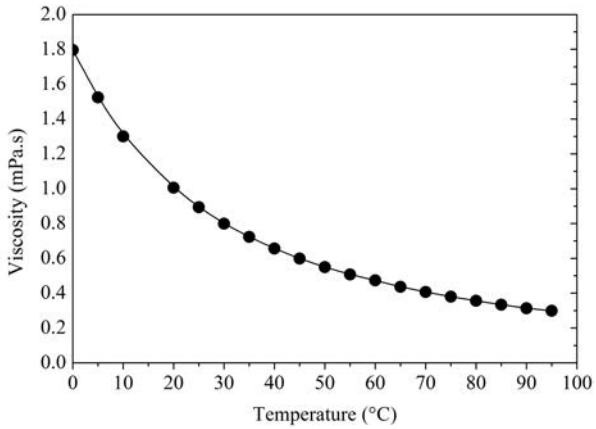


Figure B.8: Evolution of water viscosity as a function of T. From [401].

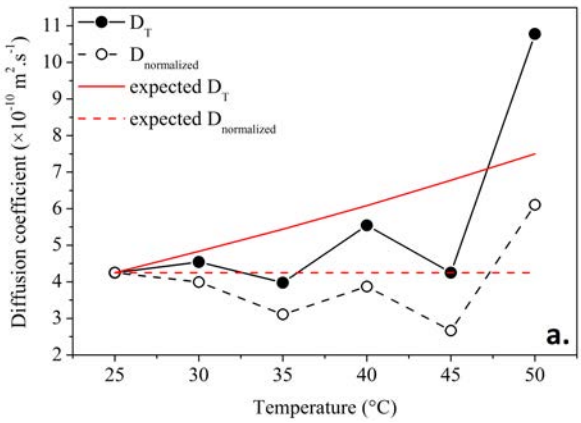


Figure B.9: Evolution of diffusion coefficient of fluorescein as a function of temperature (water objective).

not exactly the case here. Fluctuations around the expected mean value may be due to thermal convection phenomena in the sample.

Diffusion coefficient of quantum dots

Since the correlation signal of fluorescein was weak, we tried the same calibration with quantum dots (better signal/noise ratio). The diffusion coefficients obtained are plotted on Figure B.10, before and after normalization. The normalization does not give a constant value of diffusion coefficient. This presumably results from the thermal convection in the sample, even with the precautions taken (PDMS on top of the sample).

Similar measurements with FITC-IgG also showed that convection biased the measured diffusion coefficients. In the main text, we thus turned to heating the sample before measuring the sizes of objects by FCS at room temperature.

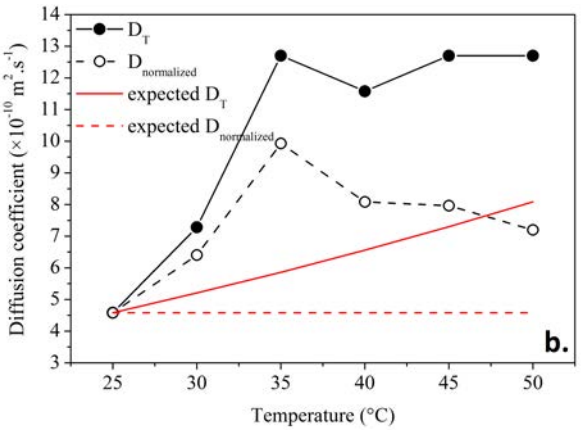


Figure B.10: Evolution of diffusion coefficient of quantum dots as a function of temperature (water objective).

B.1.5 Practical considerations

Cover slides (Menzel-Gräser, # 1) were rinsed with ethanol before use, then passivated by immersion in a 0.5 wt % BSA solution for at least 15 minutes. After water rinsing, a few µL of sample was added at the center of a "cavity" formed by a double-sided adhesive tape and sealed with a second cover slide.

In practice, 10-30 acquisitions of 60 seconds fluorescence intensity fluctuations were recorded and averaged before fitting. However, the amplitude of the autocorrelation function, which roughly depends on the average number of particles in the excited volume, may fluctuate from one acquisition to another, because of unspecific adsorption of proteins to sample container, variation of stoichiometry of binding to polymers, or other phenomena. This change in amplitude reflects a systematic error inherent of the sample and leads to overestimated standard deviations, which results in inaccurate fits [402]. Accordingly, each autocorrelation curve was first normalized by its own amplitude, after which all normalized curves were averaged, as suggested by Wohland *et al.* [402]. The appropriately chosen model was then applied to extract the hydrodynamic radius and, potentially, the aggregation number in the considered sample.

B.2 Capillary zone electrophoresis (CZE)

CZE is a complementary technique to conventional chromatography methods that enables the separation of molecules based on their differential migration under an electric field. The migration is the result of two transport mechanisms: electro-migration and electro-osmosis.

Electro-migration
Electro-migration defines the movement of a charged specie under an electric field. The linear velocity it acquires (or electrophoretic velocity, v_{ep}) depends on the value of the electric field and on the electrophoretic mobility of the specie via the relationship:

$$v_{ep} = \mu_{ep} E \tag{B.11}$$

where v_{ep} is the electrophoretic velocity ($cm.s^{-1}$), E is the electric field ($V.cm^{-1}$) and μ_{ep} is the electrophoretic mobility ($cm^2.V^{-1}.s^{-1}$).

The electrophoretic mobility can be determined experimentally from the migration time and the value of the electric field via:

$$\mu_{ep} = \frac{L_t L_d}{E}\left(\frac{1}{t_{samp}}\right) \tag{B.12}$$

where L_t is the total length of the capillary, L_d is the distance from the inlet to the detection point and t_{samp} is the migration time of the sample.

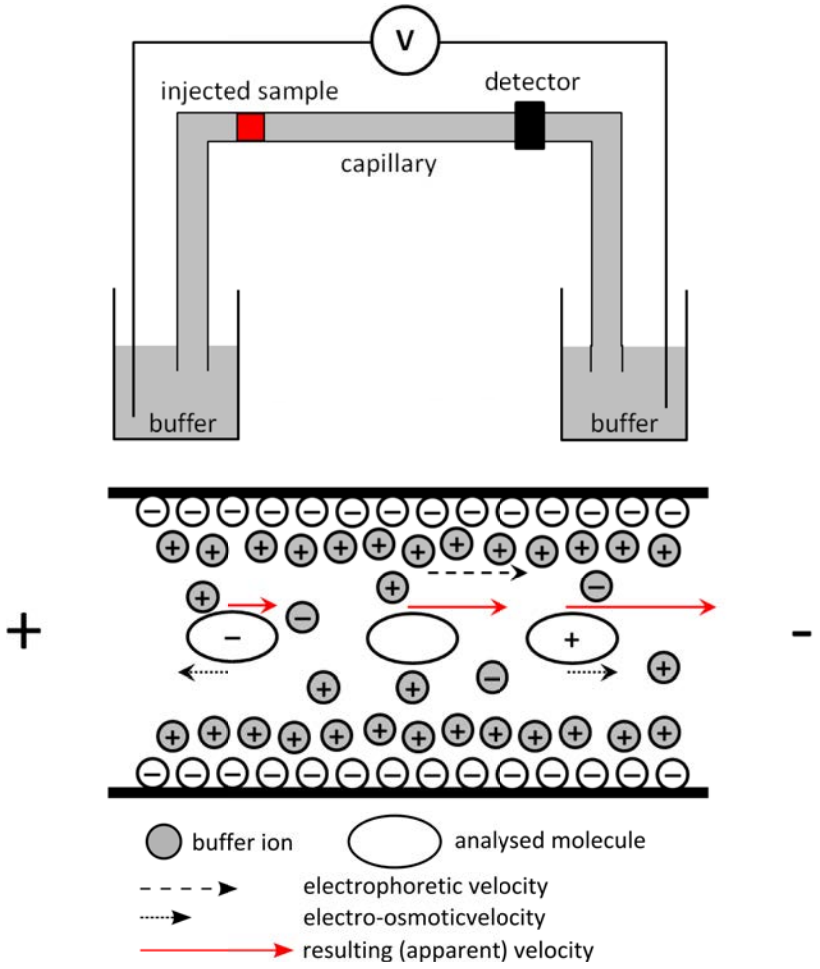


Figure B.11: Schematic illustration of the mobility of different species in capillary electrophoresis.

Electro-osmosis

Electro-osmosis corresponds to the motion of a liquid induced by an applied electric field across a capillary tube which internal wall carries a surface charge. In the case of a fused silica capillary, surface charges are negative at the usual working pHs. When the capillary is filled with a buffer, cations are attracted to the negative charges on the surface of the capillary, and form a electrical double layer. When an electric field is applied to the fluid,

cations in the electrical double layer migrate towards the cathode, inducing a flow the fluid contained in the capillary. The linear velocity of this motion, v_{eo}, is proportional to the intensity of the electric field, E, and the electro-osmotic mobility, μ_{eo}:

$$v_{eo} = \mu_{eo} E \tag{B.13}$$

where the electro-osmotic mobility μ_{eo} is defined as: $\mu_{eo} = (\varepsilon\zeta)/\eta$, where ζ is the zeta potential of the capillary wall, ε is the relative permittivity of the buffer solution and η its viscosity.

Experimentally, the electro-osmotic mobility is determined by measuring the retention time of a neutral analyte, in our case mesityl oxide.

Summary
Finally, the migration velocity of a given species depends on both the electrophoretic and electro-osmotic velocities via:

$$v_{app} = \mu_{app} E \tag{B.14}$$

where μ_{app} is the apparent mobility: $\mu_{app} = \mu_{ep} + \mu_{eo}$.

This apparent mobility is the one that is measured. It reflects the competition between the two transport modes. In a fused-silica capillary, the electro-osmotic velocity is generally higher than the electrophoretic one, so that all species migrate towards the cathode (positively-charged molecules will arrive first, see Figure B.11).

B.3 Circular dichroism (CD)

B.3.1 Principle

Circular dichroism characterizes materials or molecules that absorb differently light depending on its circular polarization. Proteins are optically active macromolecules. Their circular dichroism signature depends on their secondary and tertiary structures. Two spectral regions of interest can be identified: i/ the far-UV region (170–250 nm) is dominated by the absorption of peptide bonds and ii/ the near-UV region (250–300 nm) is dominated by the absorption of aromatic amino acids. The far-UV signal is particularly interesting because it gives information on the secondary structure of the protein. Absorption in this wavelength range is indeed highly sensitive to ordered structures.

B.3.2 Deconvolution programs

The different structures give rise to very different shapes of the measured signals. One can thus extract the relative amount of secondary structures through deconvolution programs. Two different program are used in this work: the well-known DichroWeb on-line software [372, 373] and the yet unpublished BestSel program [338]. The DirchroWeb analysis was performed by using the CONTINLL program with the Set 4 database. The choice depends mainly on the available wavelength range (details are available on-line).

The BestSel analysis offers many advantages over the DichroWeb program. BestSel was optimized for fits at low wavelengths and to include complex contributions of β-structures such as twisted β-sheets in its database. The program fits the experimental CD curve by the linear combination of fixed basis components to get the proportion

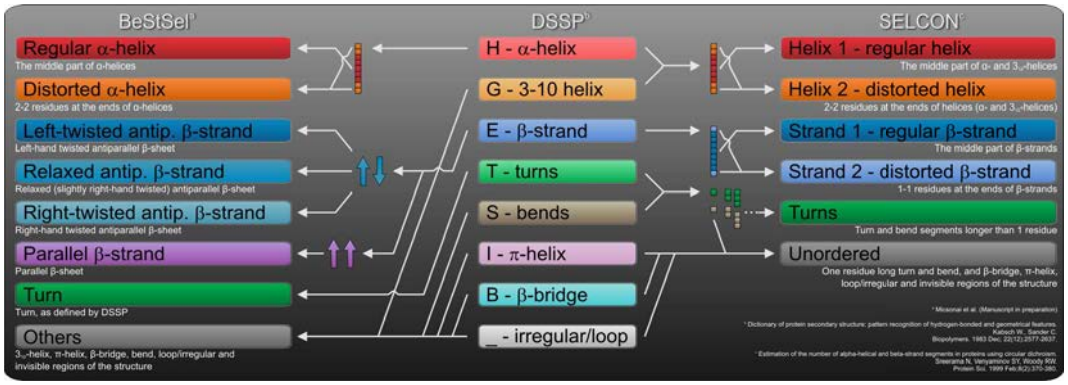


Figure B.12: Eight basis components of BestSel in relation to the dictionary of protein secondary structure (DSSP). For comparison, basis components of SELCON3 algorithm, which are also used for CONTIN and CDSSTR in CDPro, are presented.

of the eight structural elements detailed in Figure B.12. BestSel also gives the closest structure on the entire PDB of 71430 structures. The latter are presented by their PDB ID, secondary structure content, sequence length, number of chains and CATH domains contained (class, architecture, topology, homodomain superfamily). This function is especially useful in case of multi-domain proteins.

Appendix C

Supplementary data on CAB refolding assisted with PAA derivatives

Contents

C.1 Conformational stability of CAB in the presence of PAA derivatives 174

C.1.1 Monitoring the folding transition 174

C.1.2 Extracting the unfolding energies and m values 175

C.1.3 Comparison of CD- and fluorescence-monitored transitions . . 177

C.1.4 Reversibility of the electrostatic-based association with partly-folded CAB intermediates 179

C.1 Conformational stability of CAB in the presence of PAA derivatives

C.1.1 Monitoring the folding transition

An overview on CAB conformational stability study is presented here, with PAA150 and PAA150-3C18 as additives. Fluorescence and CD measurements are used to monitor the folding transition of CAB in the presence or not of polymers and at both pHs. CAB:polymer solutions are prepared at *ca.* 0.2 mg.mL^{-1} in various urea concentrations starting either from a urea-denatured CAB solution (folding) or from a native CAB solution (unfolding) and incubated for 24 hours before measurements.

C.1.1.1 CD traces

Evolution of molar ellipticity at 222 nm as a function of urea concentration for the folding and unfolding conditions with or without polymers are presented on Figure C.1 at both pHs. The first thing that can be noticed is the reversibility of the folding/unfolding transition: the signals obtained either with the urea-unfolded CAB or the native protein indeed completely superimpose, at least on the 2-10M range. There seems yet to be aggregation when the 10M urea-denatured CAB is diluted in buffers containing less than 2M urea, thus CD spectra are not acquired in those cases.The reversibility suggests that there is no irreversible aggregation in the 2M-10M urea range, even in the absence of additive.

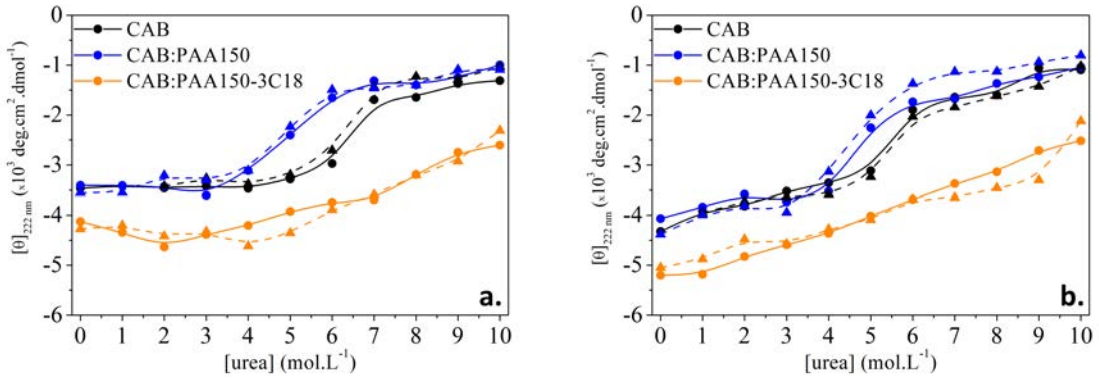


Figure C.1: Evolution of $[\theta]_{222nm}$ of CAB(:polymer) mixtures as a function of urea concentration at pH 7.75 (a.) or pH 5.9 (b.). Urea-unfolded CAB (circles,solid lines) or native CAB (triangles, dotted lines) were incubated in the absence or presence of polymers in different urea buffers for 24 hours prior to the measurements (at *ca.* 0.2 mg.mL^{-1}).

The folding/unfolding transitions are shifted to lower values of urea concentrations in the presence of PAA150, meaning that the polyanion destabilises the protein. This results is an evidence of association between PAA150 and partly folded intermediates: destabilisation is attributed to intermolecular interactions between both partners that compete with intramolecular protein interactions. The reversibility of the transition is yet still preserved.

In the presence of PAA150-3C18, the secondary structure if CAB is highly affected all along the folding transition. Values of molar ellipticity at 222 nm are systematically

lower than for CAB alone or CAB:PAA150 mixtures. The polymer already disrupted the structure of native or 10M urea-unfolded CAB (see Chapter 3). The present results suggest that the polymer affects all the folding intermediates and associate with native and unfolded CAB in a way that traps off-pathway or misfolded protein intermediates.

C.1.1.2 Fluorescence monitoring

The transition can also be monitored by fluorescence spectroscopy. The intrinsic fluorescence of tryptophan residues indeed varies according to their local environment. To avoid inherent variations of protein concentration from one sample to another, it can be useful to follow the shift of the maximum fluorescence emission (with $\lambda_{exc} = 280$ nm) instead of the fluorescence intensity. Figure C.2 plots such evolution as a function of urea concentration (only for the unfolding case, *i.e.* starting with a native CAB stock solution).

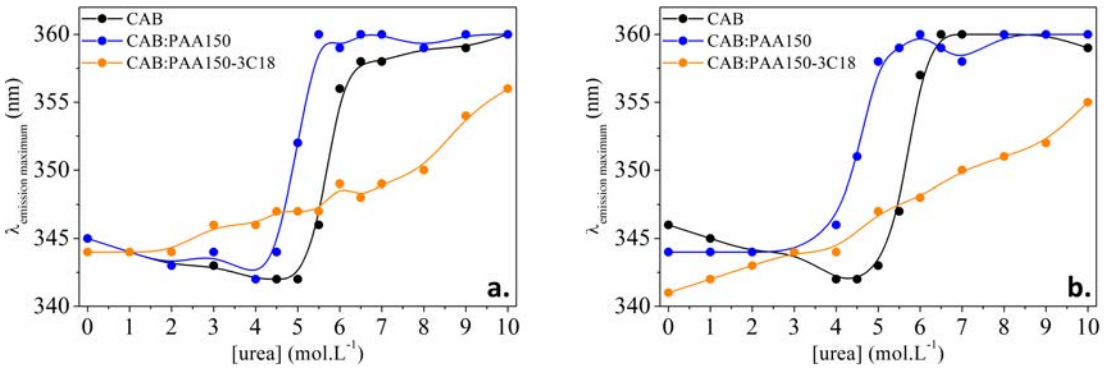


Figure C.2: Evolution of the wavelength at maximum tryptophan fluorescence emission ($\lambda_{exc} = 280$ nm) of CAB(:polymer) mixtures as a function of urea concentration at pH 7.75 (a.) or pH 5.9 (b.). Urea-unfolded CAB was incubated in the absence or presence of polymers in different urea buffers for 24 hours prior to the measurements (at *ca.* 0.2 mg.mL^{-1}).

Similar conclusions as those established by CD results can be proposed, namely a destabilisation of CAB with PAA150 and the predominance of off-pathway intermediate states with PAA150-3C18.

C.1.2 Extracting the unfolding energies and m values

Owing to the reversibility of the transition, the signals obtained for the folding and the unfolding of CAB can be averaged and normalized to the values measured for native or denatured CAB alone. The normalized value Σ is obtained via the relationship:

$$\Sigma = \frac{S - S_F^0}{S_U^0 - S_F^0} \tag{C.1}$$

where S_U^0 (resp. S_F^0) is the value of molar ellipticity at 222 nm measured for the 10M urea-unfolded CAB alone (resp. the native CAB alone).

Normalized folding transitions are plotted on Figure C.3. Under the assumption of a two-state reversible transition (no kinetics accumulation of intermediates), it has been

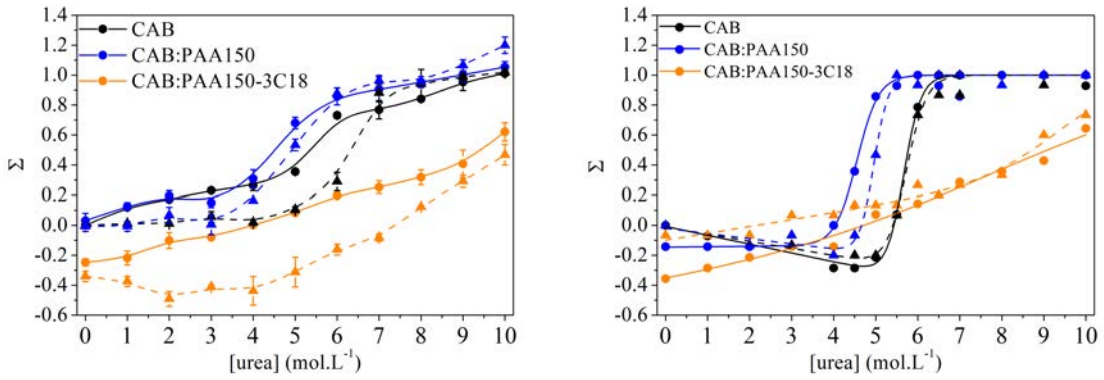


Figure C.3: Normalized folding transition from CD (a.) or fluorescence (b.) measurements. N.B.: in the case of CD, results obtained with the folding and unfolding procedures were averaged (possible because of the observed reversibility of the transition). The lines correspond to fits with Equation C.6.

proposed empirically that the unfolding energy ΔG (defined as the difference in Gibbs free energy between the unfolded and the folded states) varies linearly with the molar concentration of denaturant, x in the region of the unfolding transition [403, 404]. This has led to the widely used linear extrapolation method to estimate the conformational stability of proteins at 0M denaturant concentration:

$$\Delta \mathrm{G} = -RT\ lnK = \Delta \mathrm{G}^{\mathrm{H_2O}} - m\ x \tag{C.2}$$

where $\Delta \mathrm{G}^{\mathrm{H_2O}}$ corresponds to the value of ΔG linearly extrapolated to zero molar denaturant, m reflects the dependence of the free energy on the denaturant concentration and K is the thermodynamic folding/unfolding equilibrium constant.

The m value actually reflects the steepness, or cooperativity, of the transition curve and has been shown to be strongly correlated with the change in accessible surface area upon unfolding [405]. Here, the linear extrapolation method can be used to extract the thermodynamic parameters of the folding/unfolding of CAB in the absence or presence of polymers. Briefly, the thermodynamic equilibrium constant K for a simple $F \rightleftharpoons U$ equilibrium can be expressed in terms of the normalized signal Σ:

$$K = \frac{[\mathrm{F}]}{[\mathrm{U}]} = \frac{\Sigma_{\mathrm{F}} - \Sigma}{\Sigma - \Sigma_{\mathrm{U}}} \tag{C.3}$$

In the pre- and post-folding zones, the signals may vary with urea concentration due to variations of physico-chemical properties with varying buffer composition. These signal drifts are usually described by linear functions:

$$\begin{aligned} \Sigma_{\mathrm{F}} &= \Sigma_{\mathrm{F}}^{0} + m_{\mathrm{F}}\ x \\ \Sigma_{\mathrm{U}} &= \Sigma_{\mathrm{U}}^{0} + m_{\mathrm{U}}\ x \end{aligned} \tag{C.4}$$

where Σ_{F}^{0} and Σ_{U}^{0} (resp. m_{F} and m_{U}) are the y-intercepts (resp. the slopes) of the linear signal variations in the pre- and post- folding zones.

By combining Equation C.2, C.3 and C.4, we get:

$$\Delta G = -RT\ ln\frac{(\Sigma_F^0 + m_F\ x) - \Sigma}{\Sigma - (\Sigma_U^0 + m_U\ x)} \tag{C.5}$$

and finally:

$$\Sigma = \frac{\Sigma_F^0 + m_F\ x + (\Sigma_U^0 + m_U\ x)e^{\left(-\frac{1}{RT}(\Delta G^{H_2O} + m\ x)\right)}}{1 + e^{\left(-\frac{1}{RT}(\Delta G^{H_2O} + m\ x)\right)}} \tag{C.6}$$

In our experiments, the plateau at high urea concentration may not be reached experimentally due to the limited solubility of urea (no measurements above 10M urea). Accordingly, values of Σ_U^0 and m_U are respectively set to 1 and 0. The fits of the normalized CD and fluorescence signal are shown on Figure C.3. Table C.1 summarizes the values of the different parameters, including the unfolding energy ΔG and the m value. One can also derive the urea concentration at mid-transition as $C_m = \Delta G/|m|$.

Both experiment give different results in terms of unfolding energy and m values when comparing CAB alone and CAB:PAA150 situations, suggesting a different impact of the polymer on the tertiary (fluorescence) and secondary (CD) structures of the enzyme. Overall, PAA150 systematically decreases C_m (favoured unfolding), while PAA150-3C18 increases it, suggesting the stabilization of partly-structured intermediates that do not completely unfold, even in 10M urea.

C.1.3 Comparison of CD- and fluorescence-monitored transitions

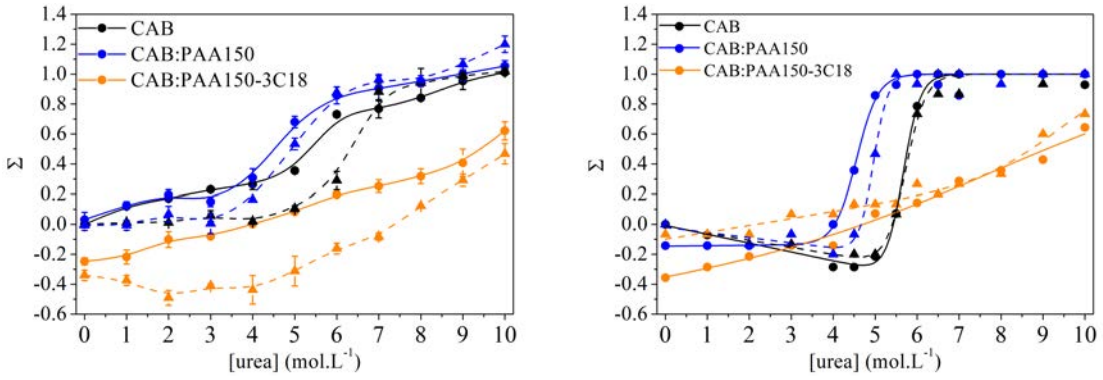


Figure C.4: Comparison of the normalized folding transition from CD and fluorescence measurements at pH 7.75 (a.) or pH 5.9 (b.) measurements.

Figure C.4 compares the normalized evolution of CD and fluorescence data. It is observed that:

- at pH 5.9, the secondary structures form gradually, with a slightly more marked variation between 5-6M urea for CAB alone and 4-5M urea for CAB:PAA150 mixture, while tryptophan fluorescence varies abruptly (in the same concentration range). This suggest differences in the cooperativity of the secondary or tertiary structure loss/acquisition.
- at pH 7.75, the secondary structures and tryptophan fluorescence vary in a similar way (more abrupt jump).

Table C.1: Fitting parameters of CD data according to Equation C.6.

		pH 5.9			pH 7.75		
		no polymer	PAA150	PAA150-3C18	no polymer	PAA150	PAA150-3C18
CD	ΔG^{H_2O} (kcal.mol^{-1})	14.0	21.8	7.8	47.3	22.9	7.9
	m (kcal.mol^{-2}.L^{-1})	-2.3	-4.5	-0.96	-7.4	-4.6	-1.1
	Σ_F^0	0.039	0.091	-0.30	-0.0044	0.00097	-0.40
	m_F (L.mol^{-1})	0.041	0.023	0.024	0.014	0.0051	-0.077
	Σ_U^0	1	1	1	1	1	1
	m_U (L.mol^{-1})	0	0	0	0	0	0
	C_m (mol.L^{-1})	6.2	4.8	8.2	6.4	5.0	7.4
Fluorescence	ΔG^{H_2O} (kcal.mol^{-1})	68.8	43.7	8.0	59.3	71.6	25.7
	m (kcal.mol^{-2}.L^{-1})	-12.2	-9.6	-0.91	-10.4	-14.5	-2.7
	Σ_F^0	-0.0073	-0.15	-0.41	-0.012	-0.019	-0.099
	m_F (L.mol^{-1})	-0.059	0.0029	0.039	-0.047	-0.035	0.046
	Σ_U^0	1	1	1	1	1	1
	m_U (L.mol^{-1})	0	0	0	0	0	0
	C_m (mol.L^{-1})	5.7	4.6	8.8	5.7	5.0	9.6

C.1.4 Reversibility of the electrostatic-based association with partly-folded CAB intermediates

Fluorescence and CD measurements showed that PAA150 destabilises CAB, presumably because of an interaction with partly-folded intermediates. Fluorescence measurements were used to assess the reversibility of this association. By working at 5M urea, the biggest difference is observed between CAB alone and CAB:PAA150 mixture. Figure C.5 shows the evolution of the wavelength at maximum tryptophan fluorescence emission in 5M urea buffer at pH 7.75 as a function of PAA150 concentration (and fixed 10 mM ionic strength and CAB concentration of .2 mg.mL^{-1}, black line) or NaCl concentration (and fixed PAA150 concentration of 0.2 mg.mL^{-1}, blue line).

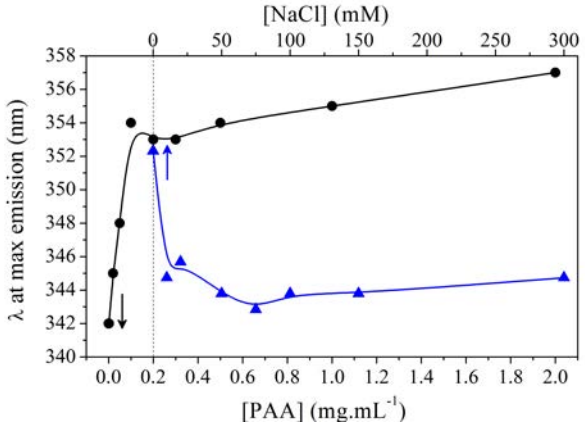


Figure C.5: Evolution of λ at maximum tryptophan fluorescence emission in 5M urea, pH 7.75, as a function of [PAA150] (fixed ionic strength of 10 mM, fixed [CAB] = 0.2 mg.mL^{-1}) or [NaCl] (fixed [PAA150] = [CAB] = 0.2 mg.mL^{-1}).

It is observed that addition of PAA150 to CAB in 5M urea (apparently folded CAB by fluorescence) leads to an increase of λ at maximum emission (unfolding) up to a pseudo-plateau for a polymer concentration higher than 0.2 mg.mL^{-1}, which corresponds to a 1:1 wt/wt ratio compared to the protein. Addition of NaCl on the 5M urea-incubated CAB:PAA150 mixture (at 1:1 wt/wt ratio) restores the value λ at maximum emission observed in the absence of polymers, suggesting that the shielding of electrostatic interactions dissociate the partly-folded CAB:PAA150 complexes and allows CAB to fold.

Appendix D

Supplementary data on scFv refolding assisted with PAA derivatives

Contents

D.1 Physico-chemical characteristics of scFv fragments 182

D.2 Electrostatic modelling at varying pHs and ionic strengths 182

D.3 Additional FCS data on the refolding of FITC-scFv 183

D.3.1 Fluorescence intensity traces measured by FCS 183

D.3.2 Distributions given by the MEMFCS algorithm during refolding of FITC-scFv(:polymer) solutions 184

D.4 Additional SRCD data on the refolding of scFv 186

D.4.1 Influence of the denaturing conditions on the secondary structure of scFv 186

D.4.2 Evolution of SRCD spectra in the 0-4M urea range 186

D.5 Additional NMR data on scFv Rendomab B1:PAA150 mixture (no urea) 189

D.1 Physico-chemical characteristics of scFv fragments

Table D.1: Physico-chemical characteristics of scFv fragments computed by the on-line ProtParam tool (on the ExPAsY bioinformatics resource portal).

	scFv Rendomab B1	scFv Sha 31	scFv 12G4
M_w	30,394.8	29,050.0	28,341.4
pI	9.02	8.25	8.26
ε ($M^{-1}.cm^{-1}$)[a]	58,580	47,580	62,590
number of residues	283	272	267

[a] assuming that all cysteines are involved in disulfide bridges.

D.2 Electrostatic modelling at varying pHs and ionic strengths

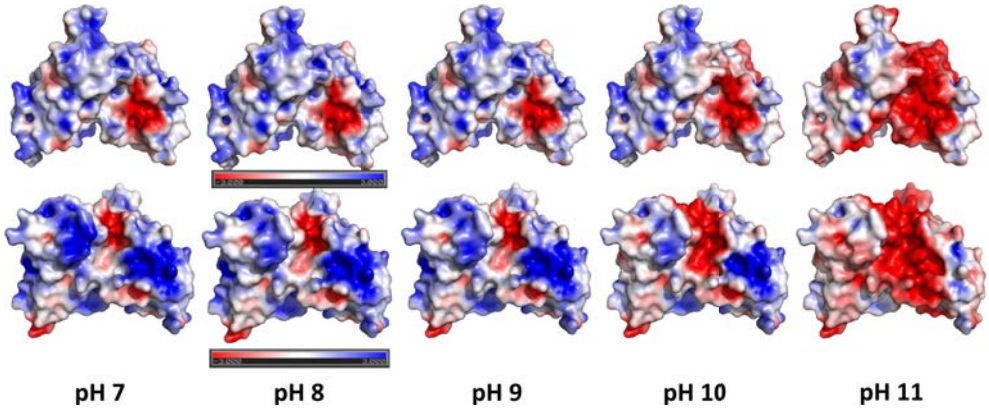


Figure D.1: Electrostatic surface potential (at ±3kT/e) of scFv Rendomab B1 at varying pHs and fixed 10 mM ionic strength (blue: positive regions, red: negative regions).

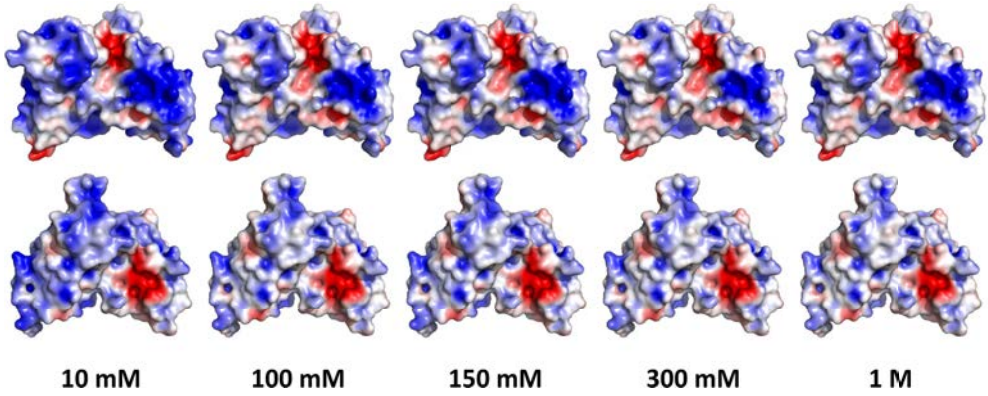


Figure D.2: Electrostatic surface potential (at ±3kT/e) of scFv Rendomab B1 at varying ionic strengths and fixed pH 8 (blue: positive regions, red: negative regions).

D.3 Additional FCS data on the refolding of FITC-scFv

D.3.1 Fluorescence intensity traces measured by FCS

Figure D.3 shows typical normalized fluorescence intensity traces observed by FCS after or during the refolding of FITC-scFv. Bursts of intensity observed at 3M urea in the absence of any additive contrasted with the absence of large fluorescent species when L-arginine or polymers were added.

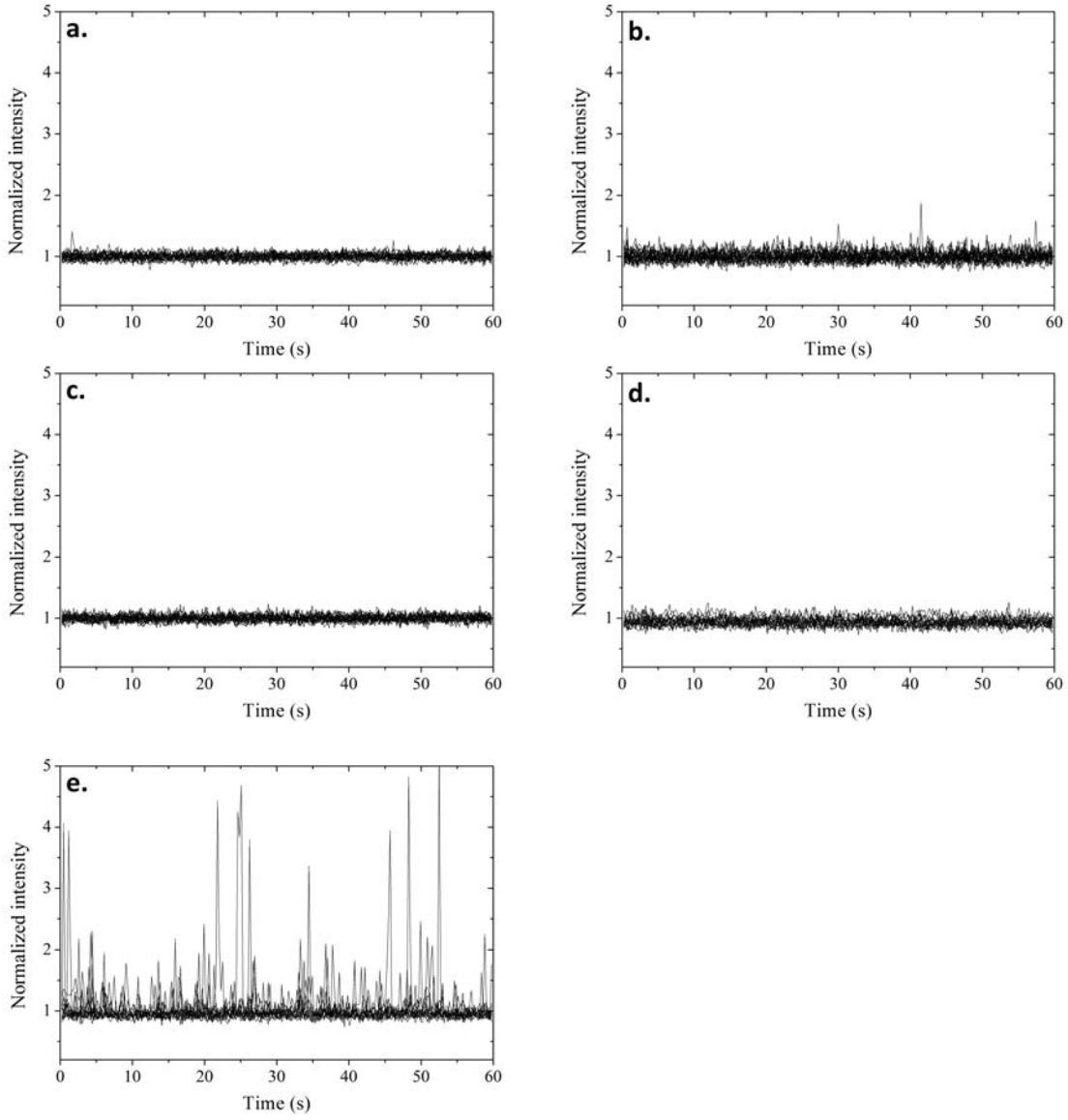


Figure D.3: Typical normalized fluorescence intensity traces observed by FCS for FITC-scFv at 0M urea (a., b., c., d.) or 3M urea (e.), in the presence of a. L-arginine, b. PAA150, c. PAA150-3C18, d. PAA5-25C8-40C3 or e. in the absence of any additive.

D.3.2 Distributions given by the MEMFCS algorithm during refolding of FITC-scFv(:polymer) solutions

Distributions given by the MEMFCS algorithm (see Appendix B) obtained all along the refolding procedure of FITC-scFv (until aggregation occurs) either in GndCl or urea, in the presence of additives or not, are plotted in Figure D.4. Mono-modal distributions when refolding was performed in GndCl (no interaction with polymers) contrasted with bi-modal distributions typically obtained in the presence of polymers when refolding was performed in urea. MEMFCS traces hence point to a potential equilibrium between free (unbound) proteins and complexes in urea.

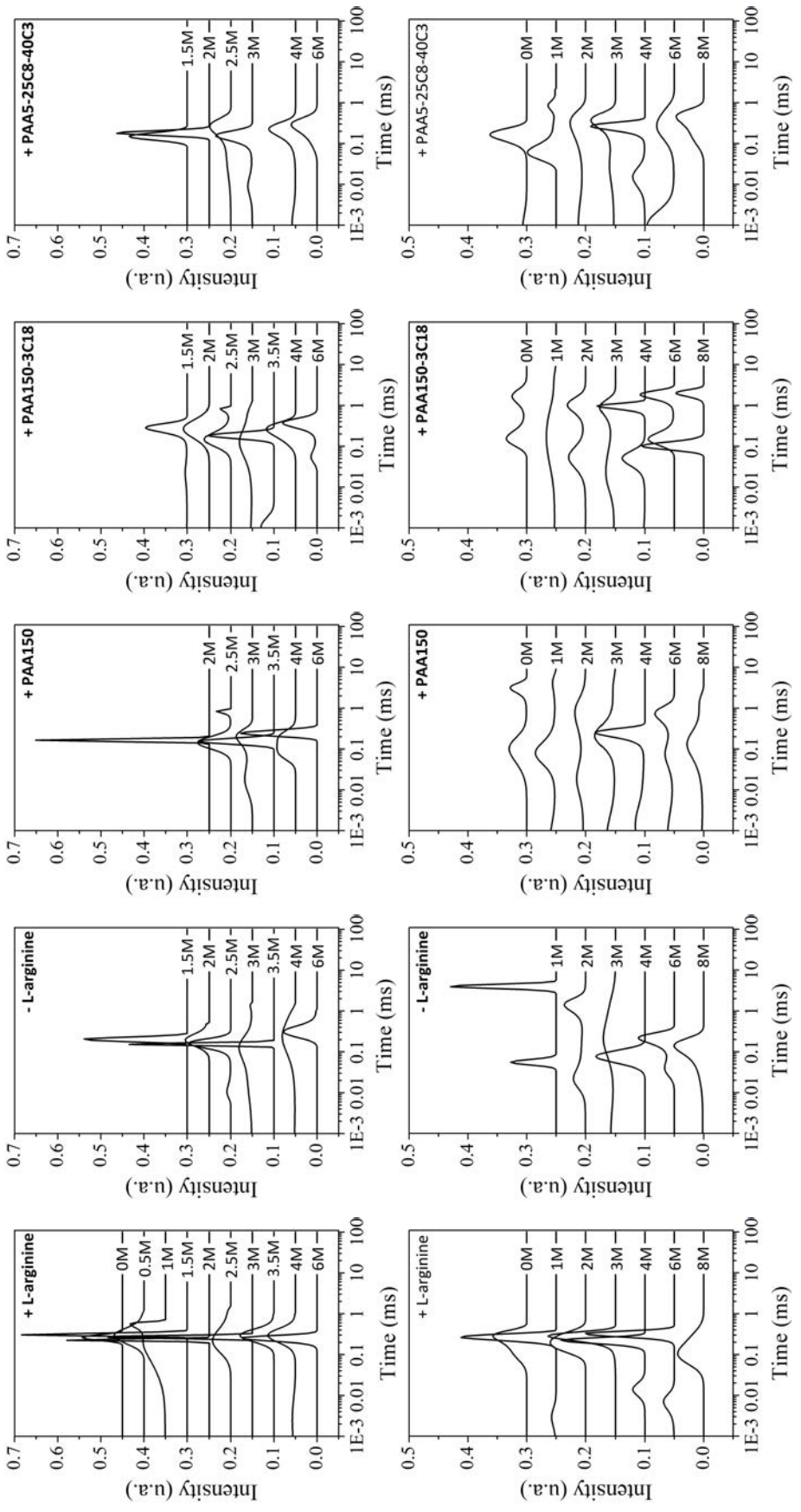


Figure D.4: Distributions given by the MEMFCS algorithm during refolding of FITC-scFv(:polymer) solutions. Top: refolding in GndCl, bottom: refolding in urea.

D.4 Additional SRCD data on the refolding of scFv

D.4.1 Influence of the denaturing conditions on the secondary structure of scFv

Prior to its refolding, scFv Rendomab B1 was denatured either in 8M or 10M urea. Figure D.5 compares the normalized CD spectra obtained for the unfolded fragment in both cases. The CD spectrum of the 10M urea unfolded fragment exhibited a marked minimum at 200-203 nm, which is a signature of an unstructured polypeptide as expected. On the other hand, the fragment was not completely unfolded in 8M urea as can be seen on the CD spectrum from the less pronounced minimum at about 203 nm altogether with a shoulder at *ca.* 215 nm, which are signs of residual secondary structure. In addition, when incubating the 10M-urea-unfolded scFv fragment in 8M urea for 24 hours, the fragment remained completely unstructured (see Figure D.5).

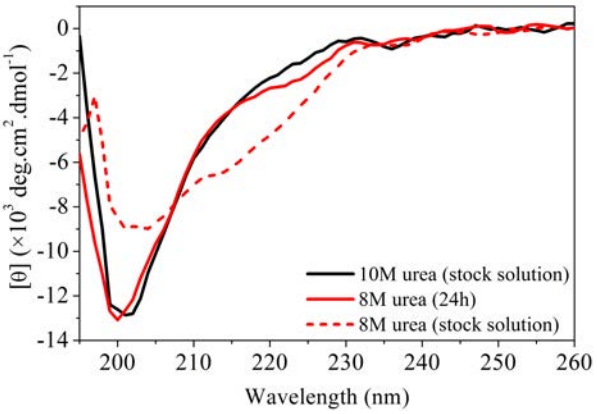


Figure D.5: SRCD spectra of scFv Rendomab B1 unfolded in 10M or 8M urea, 10 mM Tris-HCl pH 8 at 25°C. Stock solutions of the fragment were prepared at both 8M and 10M urea and stored at room temperature for a few days prior to use. The spectrum after incubation of the 10M-urea-unfolded fragment in 8M urea for 24 hours is also plotted for comparison. [scFv] = 5 mg.mL^{-1}.

Altogether, these observations suggest that i/ long-term storage of the 8M urea unfolded fragment on the bench may favour the premature formation of structural elements, in consistency with residual structures observed for other proteins unfolded in urea [406], and ii/ the initial denaturing conditions presumably solely affect the early stages of refolding, but are not decisive for obtaining a native-like secondary structure for the refolded fragment (see Section 4.3.1 in Chapter 4).

D.4.2 Evolution of SRCD spectra in the 0-4M urea range

Figure D.6 and Figure D.7 respectively show the SRCD spectra of scFv Rendomab B1 in the 0-4M urea range and the evolution of secondary structure content via BestSel analysis in the same urea range. Little variation is observed (except in the presence of

L-arginine, that also changes the buffering pH), indicating that the fragment has acquired most of its secondary structure elements in 4M urea.

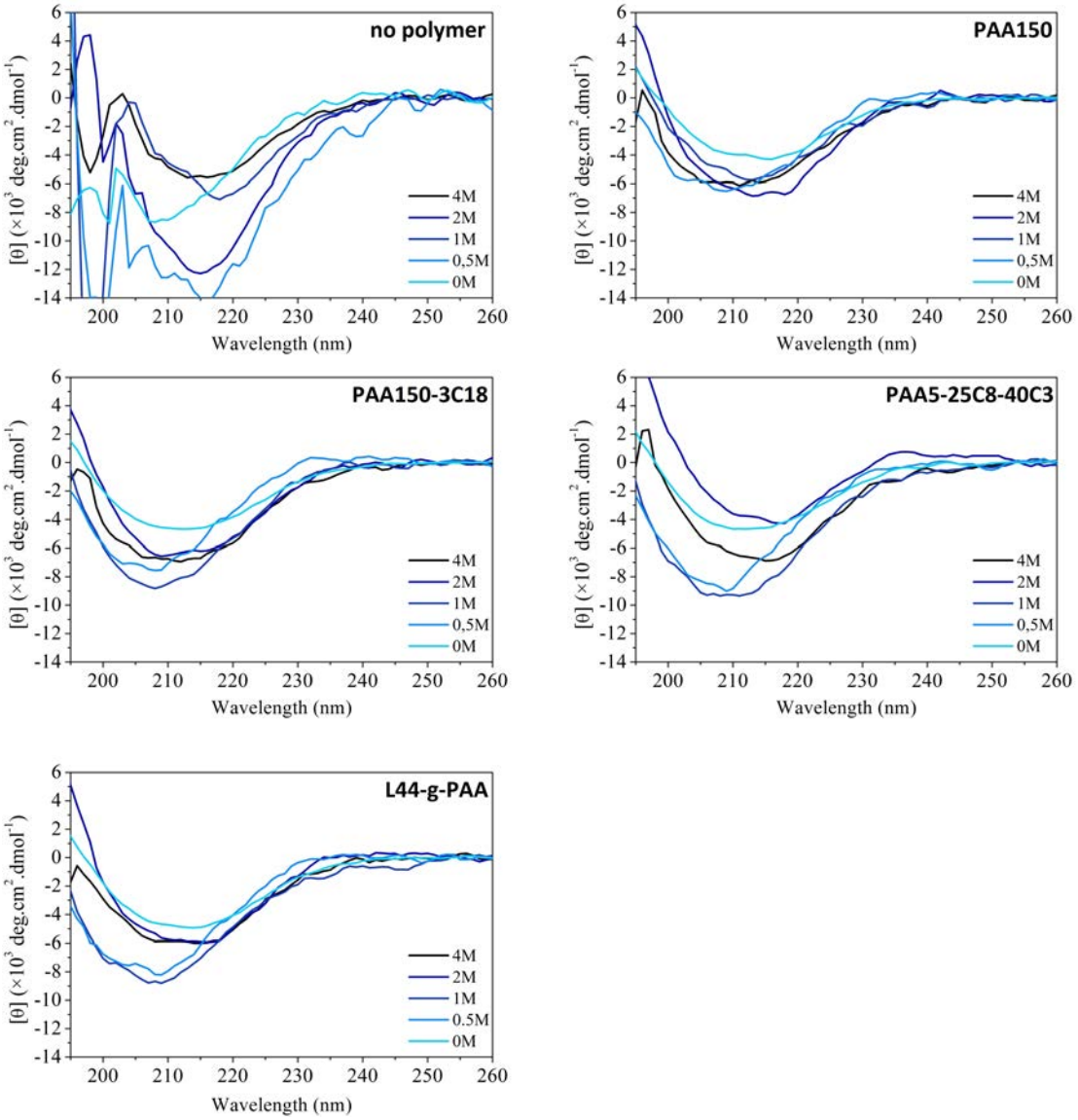


Figure D.6: SRCD spectra of scFv Rendomab B1 in the 0-4M urea range in the absence or presence (1:1 scFv:polymer wt/wt ratio) of polymers. [scFv] = 5 mg.mL^{-1}.

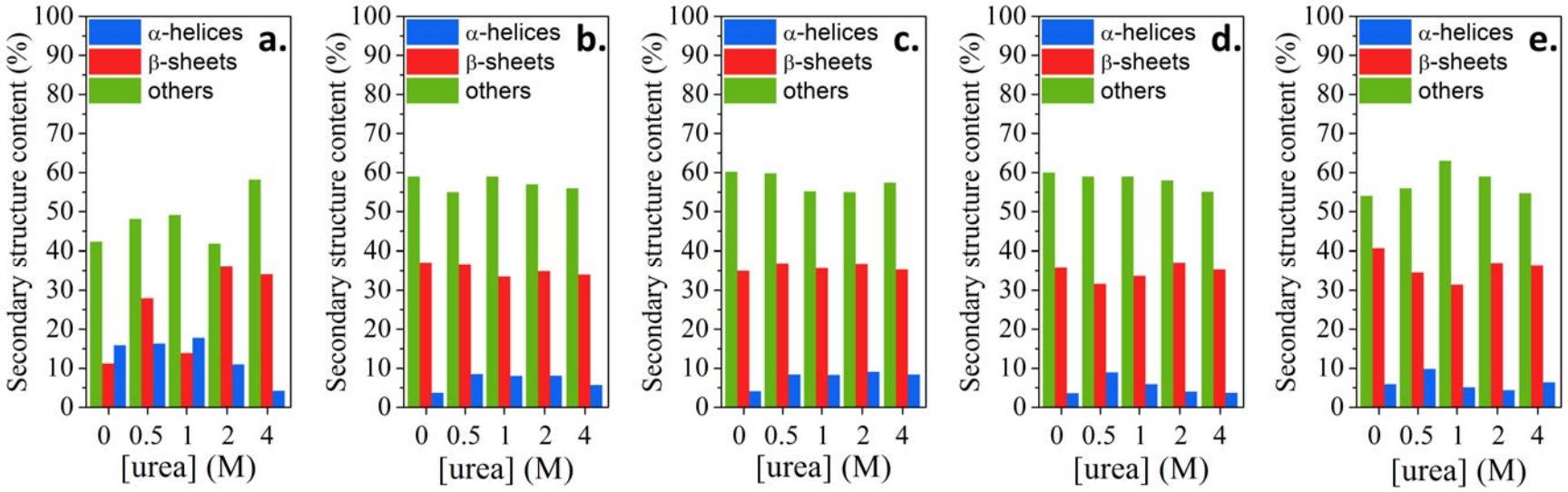


Figure D.7: Evolution of secondary structure content via BestSel analysis in the 0-4M range. a. No polymer, b. PAA150, c. PAA150-3C18, d. PAA5-25C8-40C3, e. L44-g-PAA. "β-sheets" refers to anti-parallel β-sheets; "others" refers to turns and unstructured elements.

D.5 Additional NMR data on scFv Rendomab B1:PAA150 mixture (no urea)

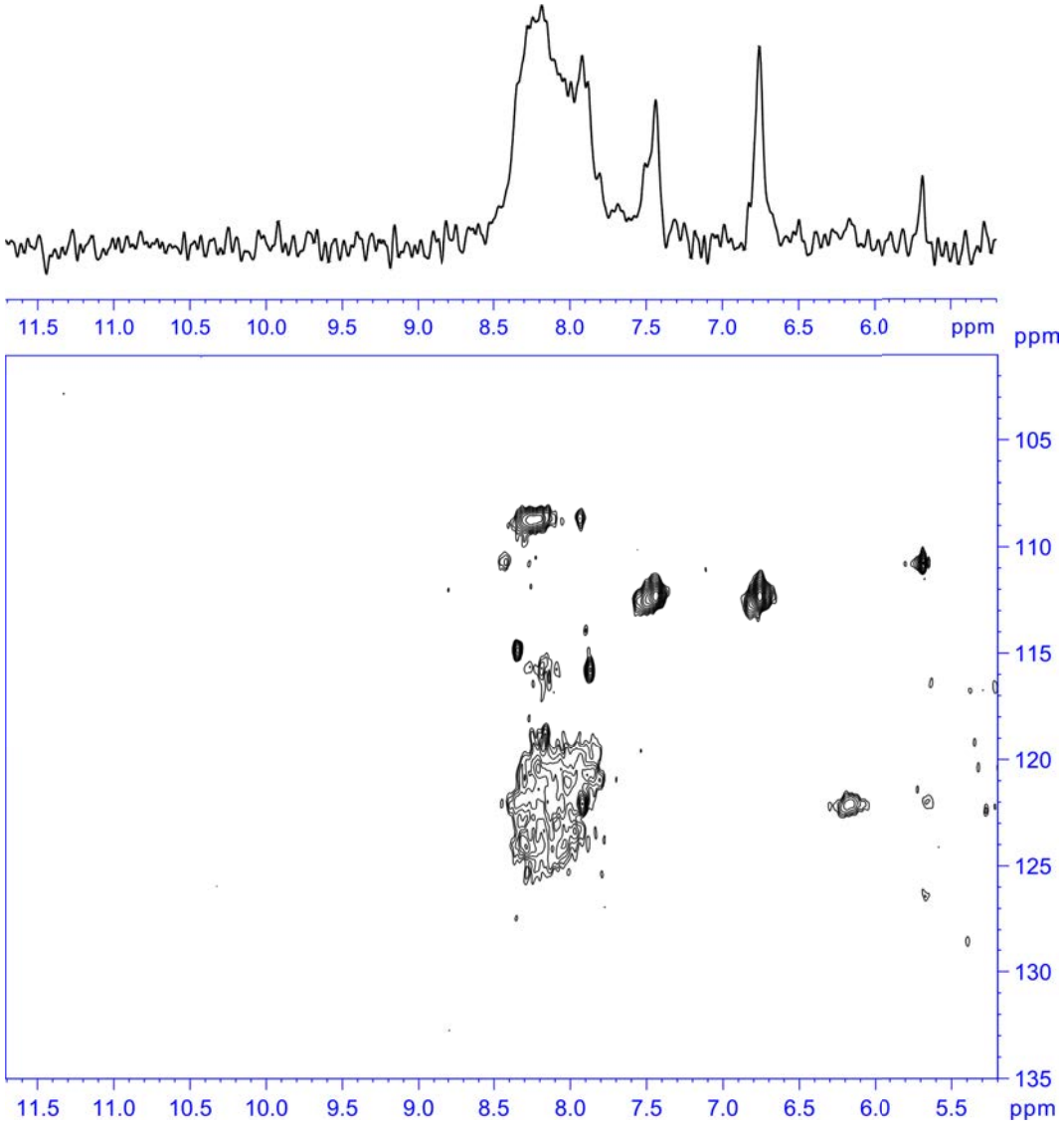


Figure D.8: ^{1}H-^{15}N HSQC plot of scFv Rendomab B1 refolded with PAA5 (added at 1:1 wt/wt ratio) in 10 mM Tris-HCl pH 8 buffer at 25°C, and corresponding ^{1}H NMR spectrum. [scFv]∼15 mg.mL^{-1}.

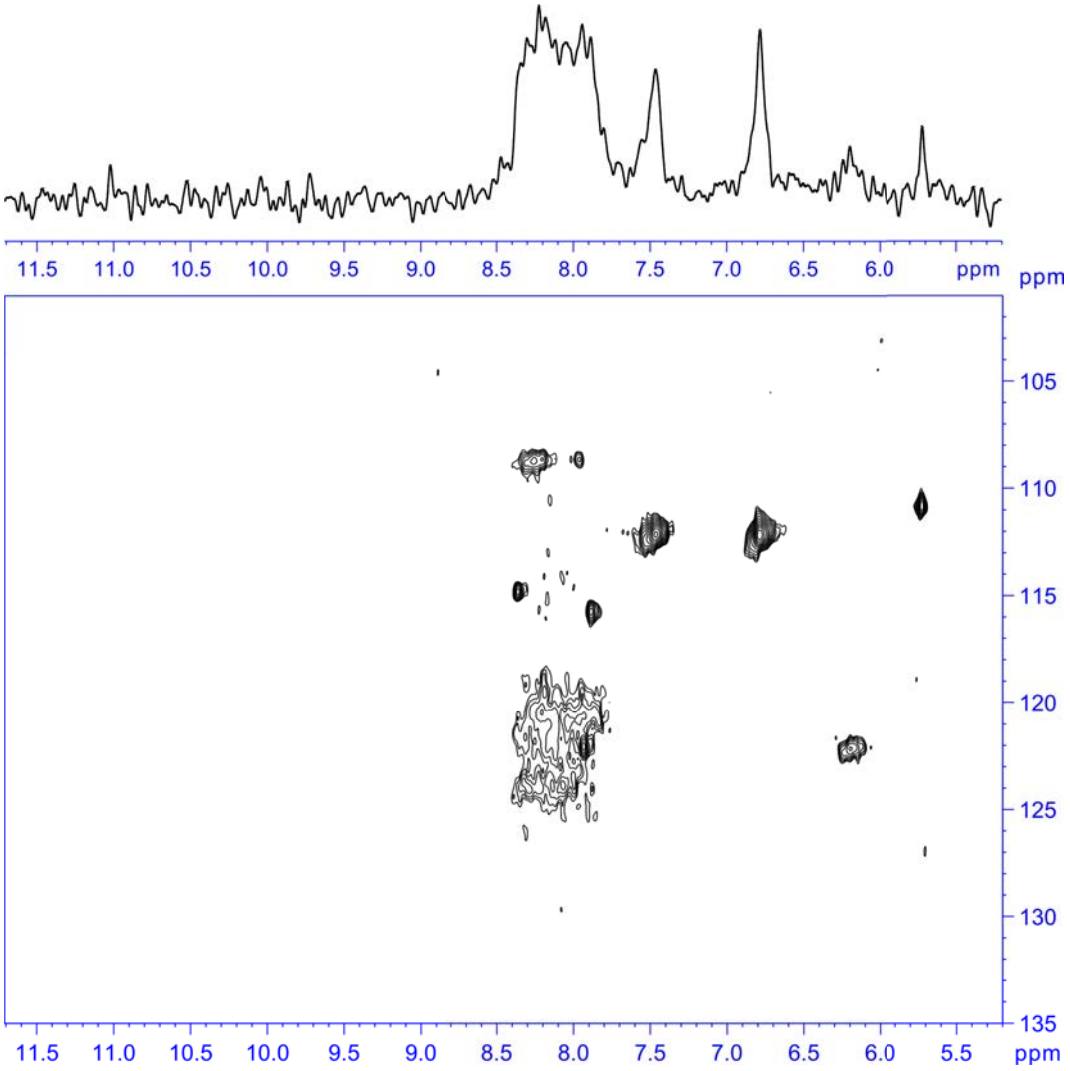


Figure D.9: ^{1}H-^{15}N HSQC plot of scFv Rendomab B1 refolded with PAA5 (added at 1:1 wt/wt ratio) in 10 mM Tris-HCl pH 8 buffer at 30°C, and corresponding ^{1}H NMR spectrum. [scFv]∼15 mg.mL^{-1}.

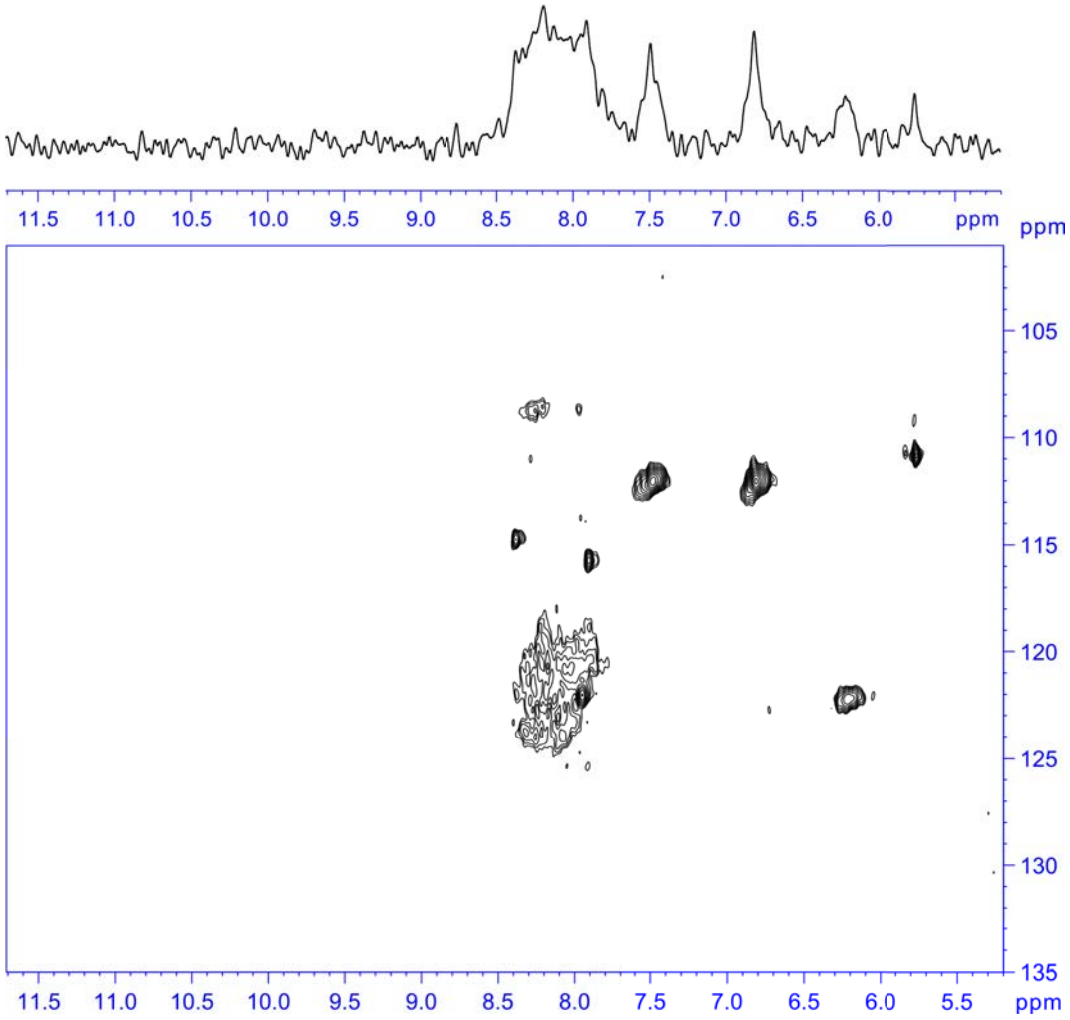


Figure D.10: ^{1}H-^{15}N HSQC plot of scFv Rendomab B1 refolded with PAA5 (added at 1:1 wt/wt ratio) in 10 mM Tris-HCl pH 8 buffer at 35°C, and corresponding ^{1}H NMR spectrum. [scFv]∼15 mg.mL^{-1}.

Appendix E

Supplementary data on thermally-induced IgG aggregation in the presence of PAA derivatives

Contents

E.1 A few results on monoclonal IgG 194
E.1.1 Stability studies on marketed therapeutic monoclonal antibodies 194
E.1.2 Preservation of IgG activity: a study by flow cytometry 197
E.2 Additional FCS data on thermally-induced aggregation of IgG 198
E.2.1 Estimation of native IgG:PAA150-3C18 stoichiometry by FCS . 198
E.2.2 FCS measurements on unlabelled IgG:rhodamine-labelled polymers mixtures 199
E.2.3 Influence of IgG concentration (and labelling) on the thermally-induced aggregation observed by FCS 200
E.3 UV-visible absorption spectroscopy 201
E.4 Thermograms of IgG in the presence of polymers with varying molecular weights and concentrations 202
E.5 Kinetics of aggregation: evolution of R_h by dynamic light scattering 205

E.1 A few results on monoclonal IgG

E.1.1 Stability studies on marketed therapeutic monoclonal antibodies

The stability of two marketed monoclonal antibodies, Cetuximab and Infliximab, was assessed after removal of most of the additives in the original formulation (through elution on a PD10 desalting column) by size exclusion chromatography (SEC) and light scattering in the absence or presence of polymers (and in 20 mM phosphate buffer pH 6.8 with no added NaCl, typical IgG concentration of 1 $g.L^{-1}$).

SEC elution profiles (Figure E.1) at t=0 (in practice, *ca.* 10 minutes after elution on the PD10 column) and t=15 days showed for Cetuximab (similar results not shown obtained for Infliximab) one single peak that was attributed to the monomer species (calibration of the column using protein standards gave a molar mass of about 160,000 $g.mol^{-1}$). It is concluded that the antibody did not aggregate on a 15 days-long time-scale. A similar single peak at the same elution volume was measured in the presence of polymers at t=15 days.

Light scattering measurements were also performed all along the sample incubation. Figure E.2 shows that the light scattered by Infliximab samples supplemented or not with polymers remained constant up to 22 days, after which part of the sample was buffered to pH 9 by addition of concentrated Tris-HCl buffer (60 mM, pH 9) to favour antibody self-association and aggregation (the isoelectric point reported for Infliximab is close to 9, so the protein becomes neutral which decreases electrostatic repulsions). Even then, no aggregation was observed. At the most, the scattered intensity of Infliximab alone (or with PAA150) slightly increased, which may betray formation of dimers, but no time-dependent variation was monitored.

It is concluded that the monoclonal antibodies tested are stable on days-long incubation (note that part of the original formulations may not have been totally removed after elution on the PD10 desalting column).

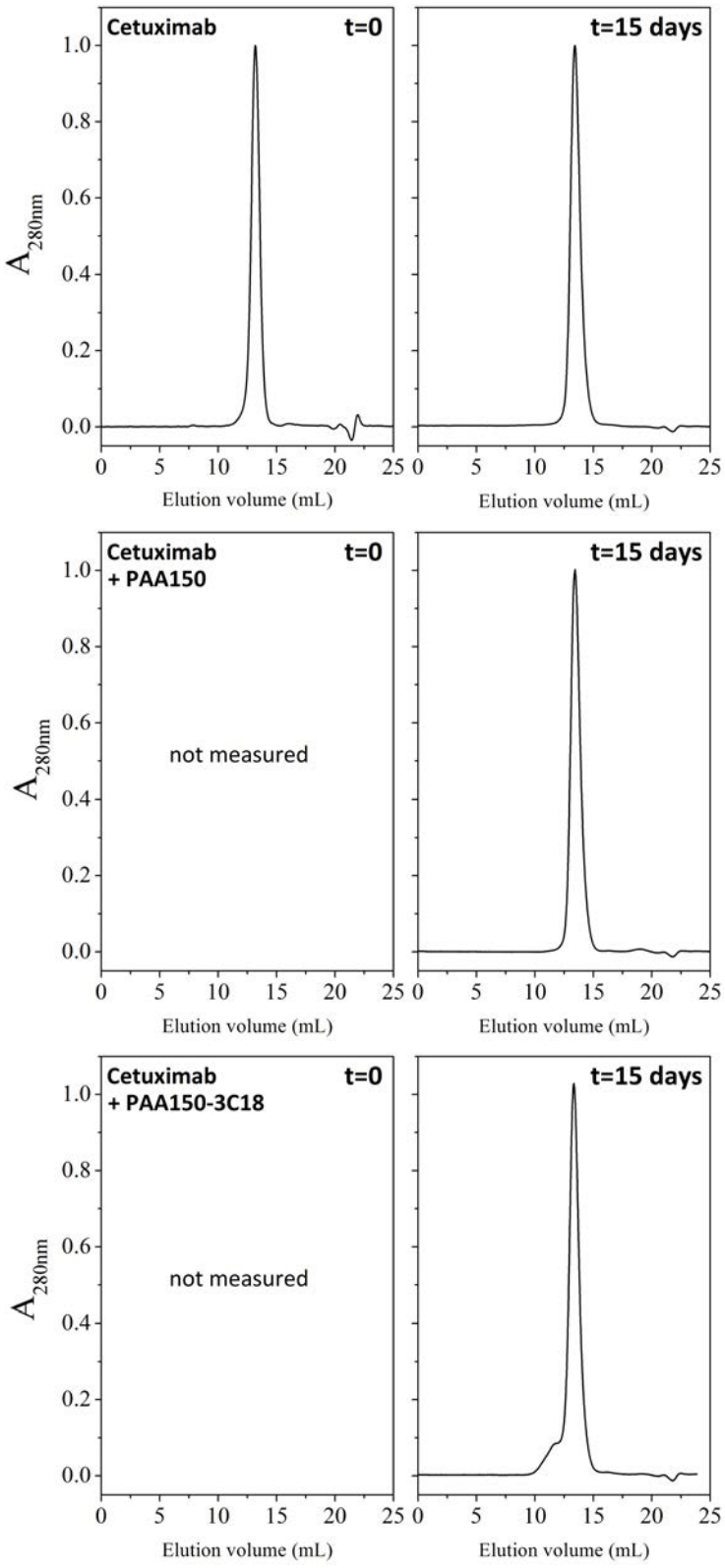


Figure E.1: SEC elution profiles of Cetuximab in the absence of presence of polymers at t=0 and after 15 days of incubation in 20 mM phosphate buffer pH 6.8 at *ca.* 1 $g.L^{-1}$.

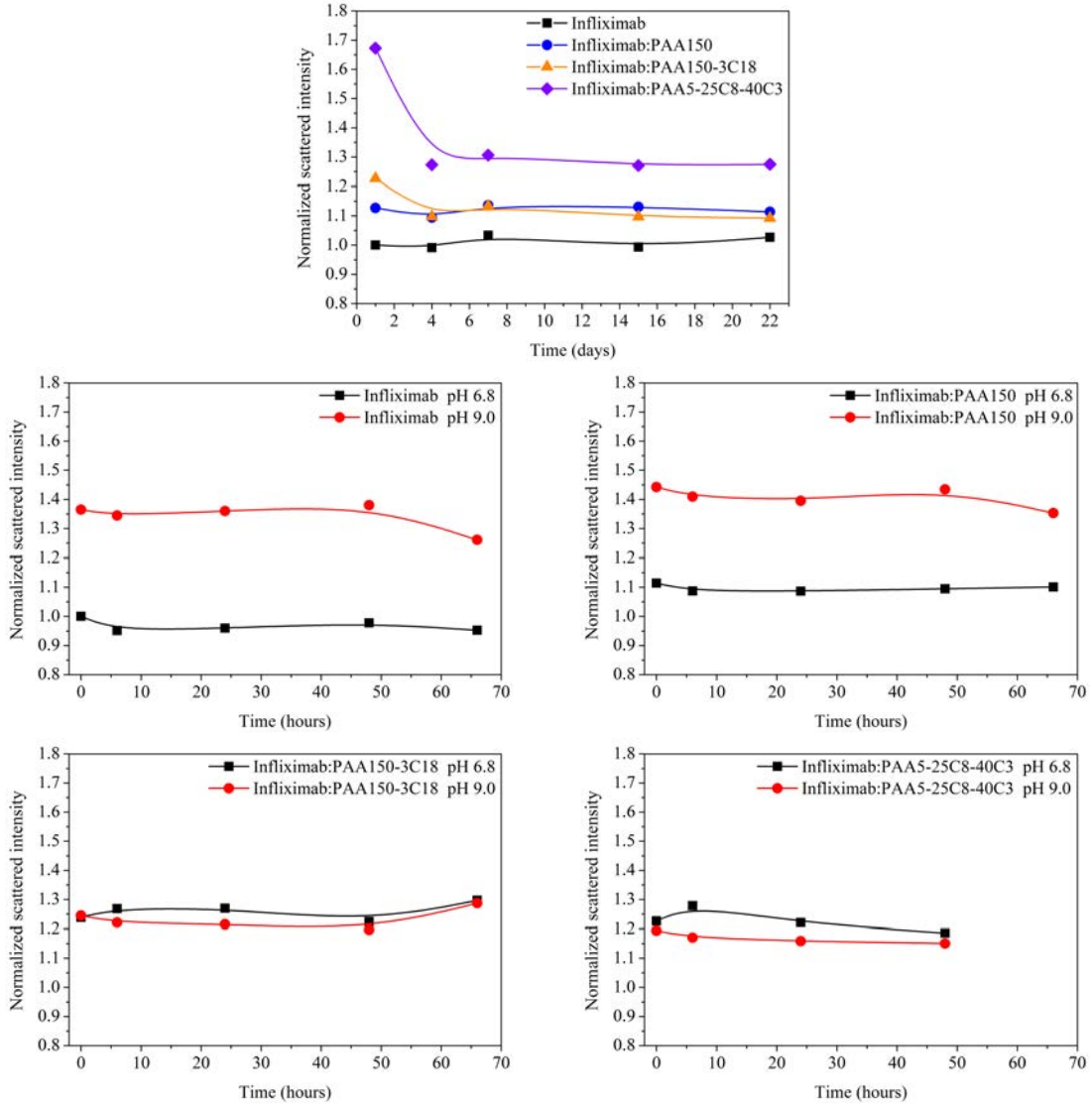


Figure E.2: SEC elution profiles of Cetuximab in the absence of presence of polymers at t=0 and after 15 days of incubation in 20 mM phosphate buffer pH 6.8 at *ca.* 1 g.L^{-1}.

E.1.2 Preservation of IgG activity: a study by flow cytometry

Activity assays: the chosen model antibody and practical considerations

The activity of immunoglobulins G is based on their ability to recognize and bind a specific antigen, which can be for instance a particular peptidic sequence or a specific local three-dimensional region of a protein. As opposed to previous physico-chemical characterizations, which were carried out on polyclonal IgG[1] (commercially available at low cost in large quantities), activity assays require the use of a specific monoclonal antibody. The team of Didier Boquet at CEA Saclay develops a monoclonal IgG, Rendomab-B1, directed against the extracellular regions of a membrane protein over-expressed in cancer cells, the endothelin receptor B (ETBR) [352] (see Chapter 4). Because the polymer studied were considered as promising stabilizing agent for application in imaging techniques based of such targets, we used here Rendomab B1 as a model for activity assays.

Saclay's team developed cell lines capable of over-expression of the membrane receptor of interest (in our case Chinese hamster ovary (CHO) cells) to produce suspensions of cells prone to bind Rendomab-B1. The presence of membrane-bound antibody was revealed via a secondary fluorescently-labelled monoclonal antibody directed against the Fc fragment of Rendomab-B1 (see Appendix A for details). The level of fluorescence was detected by flow cytometry, which allowed to count cells depending on the fluorescence they emit. The higher the fluorescence, the higher the activity of Rendomab-B1 for ETBR. Control experiments were performed in parallel with wild-type (WT) CHO cells (which did not over-express ETBR).

Effect of polymers on the activity of Rendomab-B1

Comparison of the mean fluorescence intensity (MFI) measured for Rendomab-B1 incubated with or without polymers (added at 1:1 wt/wt ratio) either on wild-type or ETBR-functionnalized CHO cells is shown in Figure E.3.

Cell over-expressing ETBR in their membrane bound Rendomab-B1 and hence were detected at a high level of fluorescence compared to the control experiments on WT cells (the low fluorescence signal corresponds to cells autofluorescence and possibly to non-specific binding of Rendomab-B1). Interestingly, the same fluorescence signal was monitored when the antibody was incubated in the presence of polymers ($\sim$ 270 MFI). In addition, the non-specific fluorescence signal (on wild-type cells) did not vary in the presence of polymers, indicating that the high level of fluorescence measured on ETBR cells can effectively be ascribed to the specific binding of Rendomab-B1 (and is not due for instance to non-specific interactions between the polymers and cell membranes). These results indicate that complexes between unstressed IgG and polymers (see in particular the case of 3C18-grafted PAA) do not perturb the activity of our model antibody. As a control (blank) experiment, we also checked that mixtures of polymers and another monoclonal antibody, which does not bind to ETBR, did not give rise to an increased fluorescence signal after incubation of the fluorescently-labelled secondary antibody (Figure E.3, antibody ARH6).

[1] A similar decrease of unfolding enthalpy as that measured for polyclonal IgG in the presence of PAA derivatives was observed for monoclonal Rendomab B1 by DSC (not shown).

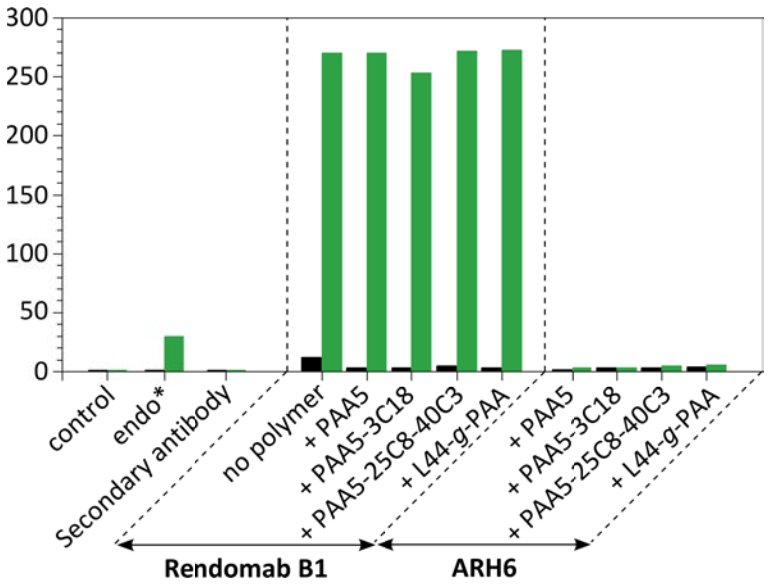


Figure E.3: Activity of Rendomab B1 in the presence of polymers

E.2 Additional FCS data on thermally-induced aggregation of IgG

E.2.1 Estimation of native IgG:PAA150-3C18 stoichiometry by FCS

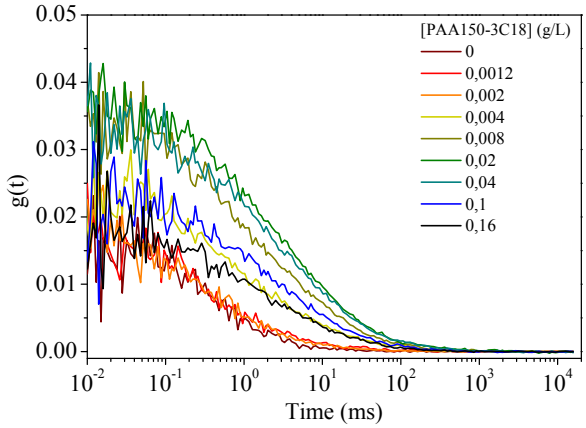


Figure E.4: FCS-determined autocorrelation curves of FITC-IgG in the presence of increasing concentrations of PAA150-3C18 in 20 mM phosphate buffer pH 6.8. [FITC-IgG] = 0.04 g.L^{-1}.

PAA150-3C18 readily associates to native FITC-IgG in conditions of low ionic strength. In order to estimate the stoichiometry between the two partners, FCS measurements were carried out at constant [FITC-IgG] of 0.04 mg.mL^{-1} and increasing amounts of polymer from 0 to 0.16 g.L^{-1} in 20 mM phosphate buffer, pH 6.8. Mixtures were incubated for 24 hours before measurements.

The autocorrelation curves obtained at polymer concentration above 0.002 mg.mL^{-1}

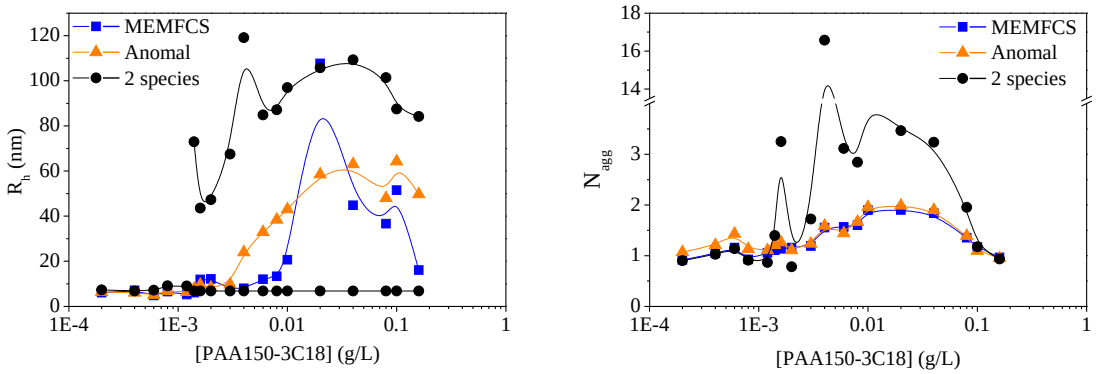


Figure E.5: Hydrodynamic radii and aggregation numbers of FITC-IgG in the presence of increasing concentrations of PAA150-3C18 in 20 mM phosphate buffer pH 6.8. [FITC-IgG] = 0.04 g.L^{-1}.

presented the signs of a polydisperse distribution of sizes (Figure E.4), and could thus be analysed under two different hypothesis: i/ an equilibrium between free IgG and IgG:polymer complexes (two-component diffusion model); ii/ the intrinsic polydispersity of the polymer chains, that can lead to polydisperse complexes (single-component stretched diffusion model or MEMFCS calculation, see Appendix B). Figure E.5 compares the evolution of R_h and N_{agg} vs. polymer concentration extracted with the three different analysis. The N_{agg} value remained below 3. In addition, the same overall trend is observed (even if the absolute values of radii differ according to the fit used), namely a constant R_h for low polymer concentrations (typically below 0.002 mg.mL^{-1}), then an increase of R_h at higher polymer concentrations up to a pseudo-plateau for polymer concentration above 0.04^{-1}, which correspond to a 1:1 wt/wt ratio compared to FITC-IgG, in consistency with CZE studies.

E.2.2 FCS measurements on unlabelled IgG:rhodamine-labelled polymers mixtures

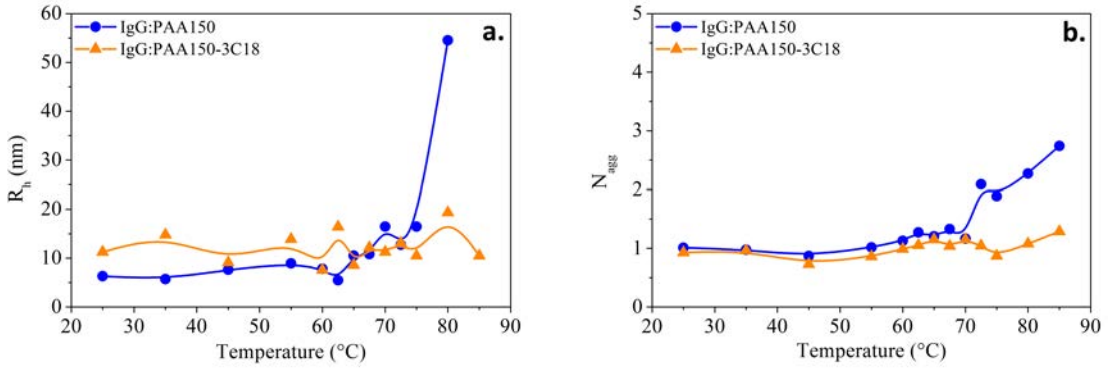


Figure E.6: Hydrodynamic radius (a.) and aggregation number (b.) of unlabelled IgG:rhodamine-labelled polymer mixtures upon heating in 20 mM phosphate buffer pH 6.8. [IgG] = [polymers] = 0.04 g.L^{-1}.

E.2.3 Influence of IgG concentration (and labelling) on the thermally-induced aggregation observed by FCS

In order to determine if the 10-fold dilution step of the heated IgG sample had an effect on the aggregation of the protein or on its complexation with polymers, we repeated the FCS experiments by incubating a 10:1 mol/mol ratio of IgG:FITC-IgG solution, at a total IgG concentration of 0.2 mg.mL^{-1}, in the presence or not of polymers, added at 1:1 wt/wt ratio compared to the total amount of IgG. In these mixtures, the FITC-IgG concentration is therefore compatible with FCS measurements, with no need of dilution. The mixtures are heated from 25 to 85°C (scan rate of 0.2°C.min^{-1}) and aliquots are taken at the desired temperatures and cooled down to 25°C (but not diluted) prior to FCS measurements.

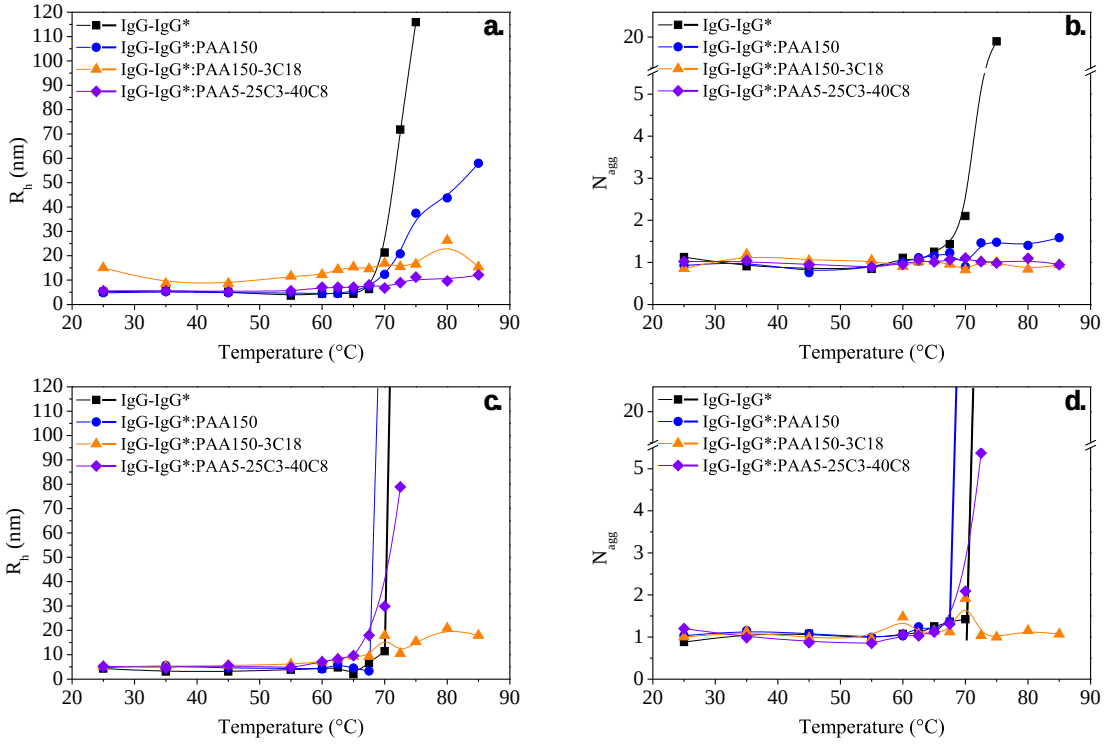


Figure E.7: Variation upon incubation at increasing temperature of the hydrodynamic radius (R_h) and aggregation number of IgG (N_{agg}, defined as the averaged number of IgG molecules per fluorescent object in solution) measured by FCS in phosphate buffer (20 mM, pH 6.8) at 1:1 wt/wt IgG:polymer ratio, 0.2 mg.mL^{-1} IgG:FITC-IgG (at 10:1 mol/mol ratio), in the absence (a., b.) or in the presence (c., d.) of 100 mM NaCl.

Figure E.7 shows the evolution of R_h and N_{agg} obtained for these mixtures. Interestingly, we observe similar trends as described on diluted FITC-IgG:polymer samples. In particular, IgG:FITC-IgG mixtures with no polymer still aggregated above 70°C, as evidenced by the simultaneous increase of R_h and N_{agg}. In the salt-free solutions, all polymers prevented IgG:FITC-IgG aggregation, with similar features as in the dilution case, namely PAA150-3C18 associated with native FITC-IgG and subsequent heating did not change the observed R_h, PAA5-25C8-40C3 bound FITC-IgG upon unfolding and preserved a monomeric form of the protein while in the presence of PAA150 we observed

a progressive increase of R_h as the temperature increased from 65 to 85°C. This suggests here again that oligomers growing in size were gradually formed in the presence of the PAA chain. However, this increase in radius was not accompanied by an increase in N_{agg} which remained close to 1 over the entire temperature range. This may be ascribed to the fact that complexes/oligomers of proteins formed upon heating contain on average only 1 FITC-IgG (their brightness is then the same as the monomeric form of FITC-IgG) but may contain other unlabelled IgG proteins, as expected from the higher N_{agg} values measured when only FITC-IgG was used. In the presence of 100 mM NaCl, only hydrophobically-modified poly(acrylates) still succeeded in preventing IgG:FITC-IgG aggregation, whilst the screening of electrostatic interactions prevented PAA150 from stabilizing the protein, confirming the important role played by electrostatics.

E.3 UV-visible absorption spectroscopy

UV-visible spectra of IgG solutions before and after DSC measurements in the presence or not of polymers and at low (no NaCl) or high (100 mM NaCl) are presented in Figure E.8. It is observed that IgG alone presented marked signs of turbidity after heating, at both ionic strengths. On the opposite, in the presence of all polymers, there was no sign of turbidity after heating at low ionic strength, indicating that polymers, including PAA parent chain, prevented the formation of micrometer- (or sub-micromiter-) sized aggregates.

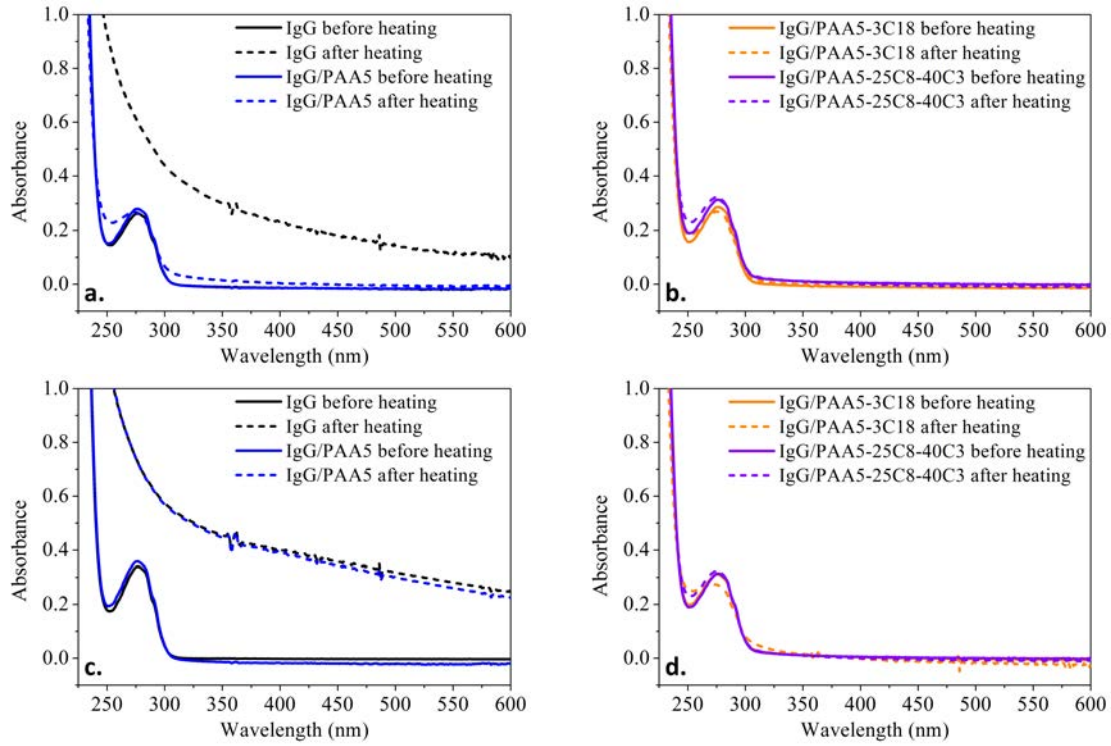


Figure E.8: Absorption spectra of IgG alone and with polymers (at 1:1 wt/wt ratio) prior and after heating at 90°C, in 20 mM phosphate buffer pH 6.8 in the absence (a., b.) or in the presence (c., d.) of 100 mM NaCl. The concentration of IgG was 0.3 $mg.mL^{-1}$.

Upon addition of 100 mM NaCl, only hydrophobically-modified PAAs still prevented the increase of turbidity, while the UV-visible spectrum obtained in solutions containing PAA5 showed the same trends as solution of IgG alone.

E.4 Thermograms of IgG in the presence of polymers with varying molecular weights and concentrations

DSC measurements shown in this appendix were obtained with human IgG from the same provider as data shown in the main text (Jackson ImmunoResearch Labs Inc.), but using a different batch. The unavoidable batch to batch variation of polyclonal IgG slightly affected the thermogram of IgG alone (shift in the average T_m by less than 1°C, and Δ H by 10%). The same batch was accordingly used to study the effect of polymers concentrations and to compare thermograms in the presence of different polymers. Thermograms of IgG in the presence of PAA (or PAA-3C18) with molecular weight of 5,000 g.mol^{-1} and 150,000 g.mol^{-1} at a IgG:polymer ratio of 1:1.3 wt/wt showed no significant difference (Figure E.9); the corresponding T_m and Δ H are shown in Table E.1.

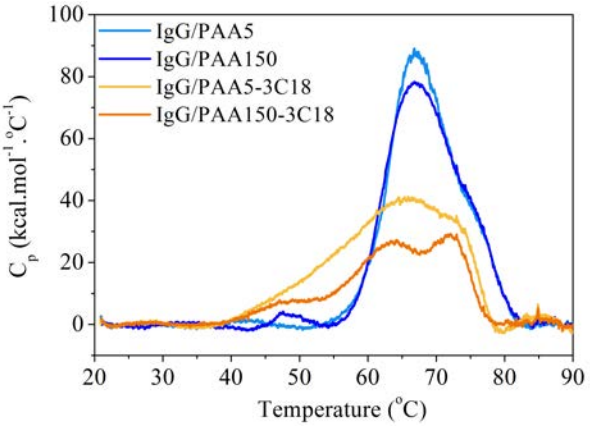


Figure E.9: Thermograms of IgG in the presence of PAA and PAA-3C18 of 5,000 or 150,000 g.mol^{-1}. The solutions were buffered in 20 mM phosphate buffer at pH 6.8. Scan rate: 0.2°C.min^{-1}; [IgG] = [polymer] = 0.2 mg.mL^{-1}.

Table E.1: Influence of the polymer chain length on the temperature and enthalpy of thermal denaturation of IgG.

	IgG:PAA5	IgG:PAA150	IgG:PAA5-3C18	IgG:PAA150-3C18
T_m (°C)	67	67	66	64/72
Δ H (kcal.mol^{-1})	1,100	1,050	900	600

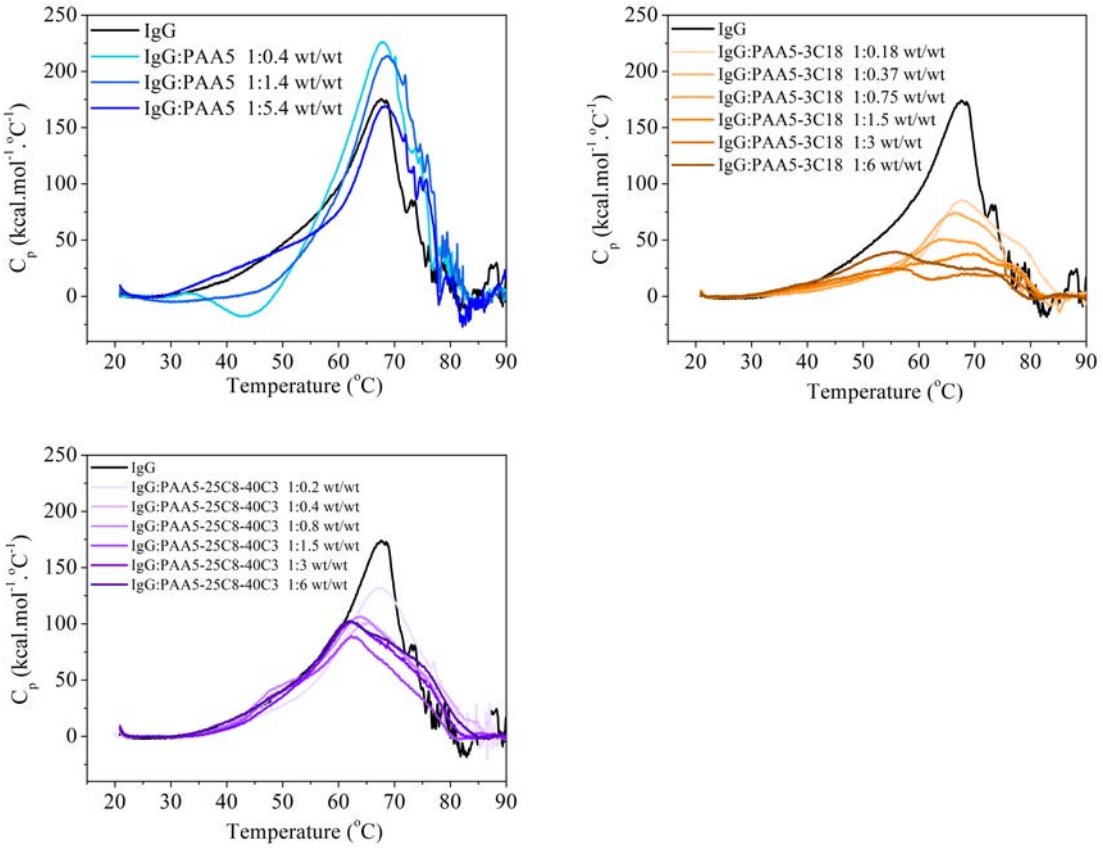


Figure E.10: Thermograms of IgG and mixtures of IgG:polymers at different weight ratios. All solutions were in 100 mM NaCl and 20 mM phosphate buffer, pH 6.8. Only one typical trace for each sample is shown here to make it clear. Scan rate: 0.2°C.min^{-1}; [IgG] = [polymer] = 0.2 mg.mL^{-1}.

Table E.2: Influence of the IgG:PAA5 weight ratio on the temperature and enthalpy of thermal denaturation of IgG.

	no polymer	1:0.4	1:1.4	1:5.4
T_m (°C)	67.6 ± 0.3	67.8 ± 0.5	68.6 ± 0.6	68.5 ± 0.5
Δ H (kcal.mol^{-1})	3,080 ± 340	3,230 ± 260	3,350 ± 170	3,400 ± 210

Table E.3: Influence of the IgG:PAA5-3C18 weight ratio on the temperature and enthalpy of thermal denaturation of IgG.

	no polymer	1:0.2	1:0.4	1:0.8	1:1.5	1:3.0	1:6.0
T_m (°C)	67.6 ± 0.3	67.6 ± 0.4	66.4 ± 0.6	64.6 ± 0.9	n.a.	n.a.	n.a.
Δ H (kcal.mol^{-1})	3,080 ± 340	1,740 ± 260	1,450 ± 230	1,160 ± 190	990 ± 180	720 ± 240	1,040 ± 450

Table E.4: Influence of the IgG:PAA5-25C8-40C3 weight ratio on the temperature and enthalpy of thermal denaturation of IgG.

	no polymer	1:0.2	1:0.4	1:0.8	1:1.5	1:3.0	1:6.0
T_m (°C)	67.6 ± 0.3	67.7 ± 0.3	65.4 ± 0.5	64.1 ± 0.7	62.3 ± 0.5	62.3 ± 1.1	62.2 ± 1.5
Δ H (kcal.mol^{-1})	3,080 ± 340	2,450 ± 240	2,400 ± 150	2,450 ± 190	1,710 ± 210	2,210 ± 200	2,510 ± 450

E.5 Kinetics of aggregation: evolution of R_h by dynamic light scattering

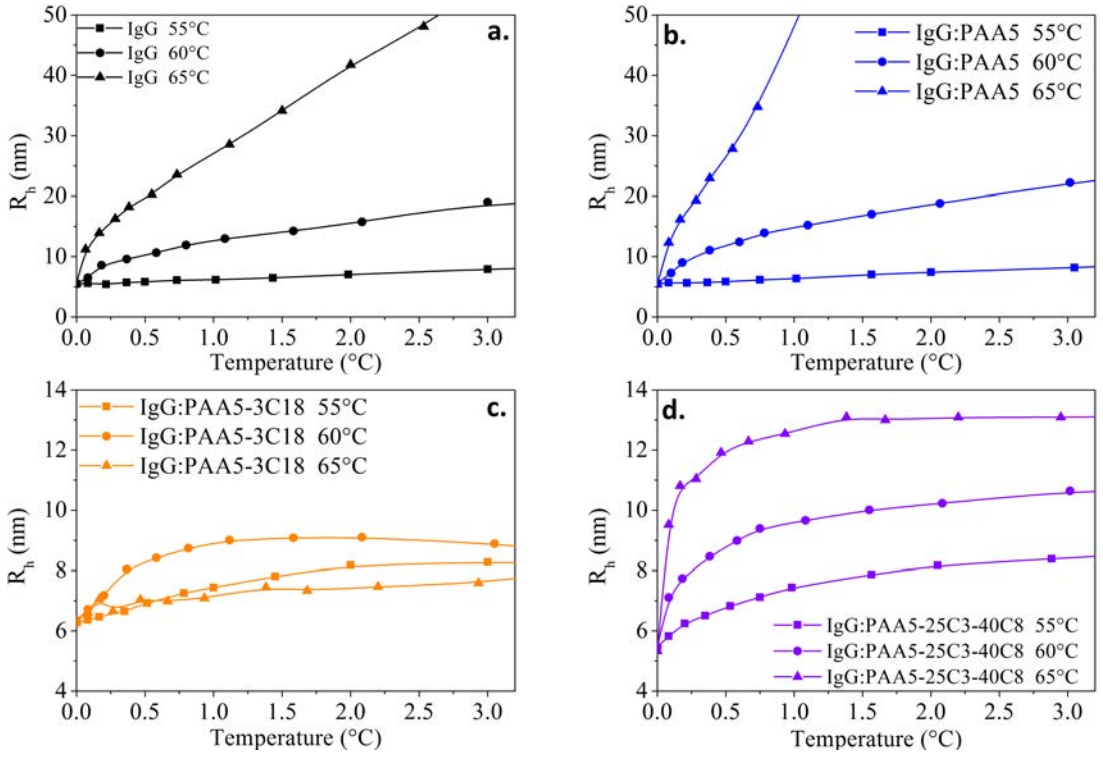


Figure E.11: Plot of R_h of IgG in the absence/presence of polymers as a function of time. The solutions were buffered in 20 mM phosphate buffer at pH 6.8 + 100 mM NaCl. [IgG] = [polymer] = 0.5 mg.mL^{-1}.

Bibliography

[1] Scannell, J.W.; Blanckley, A.; Boldon, H.; Warrington, B. Diagnosing the decline in pharmaceutical R&D efficiency. *Nat. Rev. Drug Discov.* **2012**, *11*, 191–200

[2] Hay, M.; Thomas, D.W.; Craighead, J.L.; Economides, C.; Rosenthal, J. Clinical development success rates for investigational drugs. *Nat. Biotechnol.* **2014**, *32*, 40–51

[3] Klein, F.; Mouquet, H.; Dosenovic, P.; Scheid, J.F.; Scharf, L.; Nussenzweig, M.C. Antibodies in HIV-1 vaccine development and therapy. *Science* **2013**, *341*, 1199–1204

[4] Chan, A.C.; Carter, P.J. Therapeutic antibodies for autoimmunity and inflammation. *Nat. Rev. Immunol.* **2010**, *10*, 301–316

[5] Sliwkowski, M.X.; Mellman, I. Antibody therapeutics in cancer. *Science* **2013**, *341*, 1192–1198

[6] Adams, G.P.; Weiner, L.M. Monoclonal antibody therapy of cancer. *Nat. Biotechnol.* **2005**, *23*, 1147–1157

[7] Weiner, L.M.; Surana, R.; Wang, S. Monoclonal antibodies: versatile platforms for cancer immunotherapy. *Nat. Rev. Immunol.* **2010**, *10*, 317–327

[8] Brekke, O.H.; Sandlie, I. Therapeutic antibodies for human diseases at the dawn of the twenty-first century. *Nat. Rev. Drug Discov.* **2003**, *2*, 52–62

[9] Davies, D.R.; Chacko, S. Antibody structure. *Acc. Chem. Res.* **1993**, *26*, 421–427

[10] Cruse, J.; Lewis, R. *Atlas of Immunology, Third Edition.* Taylor & Francis **2010**

[11] Schroeder, J.H.W.; Cavacini, L. Structure and function of immunoglobulins. *J. Allergy Clin. Immunol.* **2010**, *125*, S41–S52

[12] Rousseaux, J.; Rousseaux-Prevost, R.; Bazin, H. Optimal conditions for the preparation of Fab and $F(ab')_2$ fragments from monoclonal IgG of different rat IgG subclasses. *J. Immunol. Methods* **1983**, *64*, 141–146

[13] Köhler, G.; Milstein, C. Continuous cultures of fused cells secreting antibody of predefined specificity. *Nature* **1975**, *256*, 495–497

[14] Nelson, A.L.; Dhimolea, E.; Reichert, J.M. Development trends for human monoclonal antibody therapeutics. *Nat. Rev. Drug Discov.* **2010**, *9*, 767–774

[15] Beck, A.; Wurch, T.; Bailly, C.; Corvaia, N. Strategies and challenges for the next generation of therapeutic antibodies. *Nat. Rev. Immunol.* **2010**, *10*, 345–352

[16] Morrison, S.L.; Johnson, M.J.; Herzenberg, L.A.; Oi, V.T. Chimeric human antibody molecules: mouse antigen-binding domains with human constant region domains. *Proc. Natl. Acad. Sci.* **1984**, *81*, 6851–6855

[17] Jones, P.T.; Dear, P.H.; Foote, J.; Neuberger, M.S.; Winter, G. Replacing the complementarity-determining regions in a human antibody with those from a mouse. *Nature* **1986**, *321*, 522–525

[18] Riechmann, L.; Clark, M.; Waldmann, H.; Winter, G. Reshaping human antibodies for therapy. *Nature* **1988**, *332*, 323–327

[19] McCafferty, J.; Griffiths, A.D.; Winter, G.; Chiswell, D.J. Phage antibodies: filamentous phage displaying antibody variable domains. *Nature* **1990**, *348*, 552–554

[20] Elvin, J.; Couston, R.; van der Walle, C. Therapeutic antibodies: market considerations, disease targets and bioprocessing. *Int. J. Pharma.* **2013**, *440*, 83–98

[21] Chari, R.V.; Miller, M.L.; Widdison, W.C. Antibody–drug conjugates: An emerging concept in cancer therapy. *Angew. Chem. Int. Ed.* **2014**, *53*, 3796–3827

[22] Holliger, P.; Hudson, P.J. Engineered antibody fragments and the rise of single domains. *Nat. Biotechnol.* **2005**, *23*, 1126–1136

[23] Nelson, A.L. Antibody fragments: hope and hype. *mAbs* **2010**, *2*, 77–83

[24] Cuesta, Á.M.; Sainz-Pastor, N.; Bonet, J.; Oliva, B.; Álvarez-Vallina, L. Multivalent antibodies: when design surpasses evolution. *Trends Biotechnol.* **2010**, *28*, 355–362

[25] Fink, A.L. Protein aggregation: folding aggregates, inclusion bodies and amyloid. *Fold. Des.* **1998**, *3*, R9–R23

[26] De Bernardez Clark, E. Refolding of recombinant proteins. *Curr. Opin. Biotechnol.* **1998**, *9*, 157–163

[27] Wang, W.; Singh, S.; Zeng, D.L.; King, K.; Nema, S. Antibody structure, instability, and formulation. *J. Pharm. Sci.* **2007**, *96*, 1–26

[28] Wang, W.; Roberts, C. *Aggregation of Therapeutic Proteins.* Wiley **2010**

[29] Manning, M.; Chou, D.; Murphy, B.; Payne, R.; Katayama, D. Stability of protein pharmaceuticals: An update. *Pharm. Res.* **2010**, *27*, 544–575

[30] Demeule, B.; Lawrence, M.J.; Drake, A.F.; Gurny, R.; Arvinte, T. Characterization of protein aggregation: The case of a therapeutic immunoglobulin. *Biochim. Biophys. Acta – Proteins and Proteomics* **2007**, *1774*, 146–153

[31] Ratanji, K.D.; Derrick, J.P.; Dearman, R.J.; Kimber, I. Immunogenicity of therapeutic proteins: Influence of aggregation. *J. Immunotoxicol.* **2013**, *11*, 99–109

[32] Wang, W.; Nema, S.; Teagarden, D. Protein aggregation–Pathways and influencing factors. *Int. J. Pharm.* **2010**, *390*, 89–99

[33] Narhi, L.O.; Schmit, J.; Bechtold-Peters, K.; Sharma, D. Classification of protein aggregates. *J. Pharm. Sci.* **2012**, *101*, 493–498

[34] Joubert, M.K.; Luo, Q.; Nashed-Samuel, Y.; Wypych, J.; Narhi, L.O. Classification and characterization of therapeutic antibody aggregates. *J. Biol. Chem.* **2011**, *286*, 25118–25133

[35] Morris, A.; Watzky, M.; Finke, R. Protein aggregation kinetics, mechanism and curve-fitting: a review of the literature. *Biochim. Biophys. Acta* **2009**, *1794*, 375–397

[36] Etzel, M.R. Bulk protein crystallization – Principles and methods. *BIOTECHNOLOGY AND Bioprocessing Series* **2007**, *31*, 159

[37] Prausnitz, J.M. Molecular thermodynamics for some applications in biotechnology. *J. Chem. Thermodyn.* **2003**, *35*, 21–39

[38] Arosio, P.; Rima, S.; Lattuada, M.; Morbidelli, M. Population balance modelling of antibodies aggregation kinetics. *J. Phys. Chem. B* **2012**, *116*, 7066–7075

[39] Arosio, P.; Rima, S.; Morbidelli, M. Aggregation mechanism of an IgG2 and two IgG1 monoclonal antibodies at low ph: From oligomers to larger aggregates. *Pharm. Res.* **2013**, *30*, 641–654

[40] Chi, E.; Krishnan, S.; Randolph, T.; Carpenter, J. Physical stability of proteins in aqueuous solution: mechanism and driving forces in nonnative protein aggregation. *Pharm. Res.* **2003**, *20*, 1325–1336

[41] Santoro, M.M.; Bolen, D.W. A test of the linear extrapolation of unfolding free energy changes over an extended denaturant concentration range. *Biochem.* **1992**, *31*, 4901–4907

[42] Creighton, T.E. *Proteins: Structures and Molecular Properties, 2nd ed.* W. H. Freeman: New York **1992**

[43] Taverna, D.M.; Goldstein, R.A. Why are proteins marginally stable? *Proteins: Structure, Function, and Bioinformatics* **2002**, *46*, 105–109

[44] Tokuriki, N.; Tawfik, D.S. Protein dynamism and evolvability. *Science* **2009**, *324*, 203–207

[45] Wu, H.; Kroe-Barrett, R.; Singh, S.; Robinson, A.; Roberts, C. Competing aggregation pathways for monoclonal antibodies. *FEBS Lett.* **2014**, *588*, 936–941

[46] Sahin, E.; Grillo, A.O.; Perkins, M.D.; Roberts, C.J. Comparative effects of pH and ionic strength on protein-protein interactions, unfolding, and aggregation for IgG1 antibodies. *J. Pharm. Sci.* **2010**, *99*, 4830–4848

[47] Vermeer, A.; Bremer, M.G.; Norde, W. Structural changes of IgG induced by heat treatment and by adsorption onto a hydrophobic Teflon surface studied by circular dichroism spectroscopy. *Biochim. Biophys. Acta* **1998**, *1425*, 1–12

[48] Vermeer, A.W.P.; Norde, W. The thermal stability of immunoglobulin: unfolding and aggregation of a multi-domain protein. *Biophys. J.* **2000**, *78*, 394–404

[49] Ahrer, K.; Buchacher, A.; Iberer, G.; Jungbauer, A. Thermodynamic stability and formation of aggregates of human immunoglobulin G characterised by differential scanning calorimetry and dynamic light scattering. *J. Biochem. Bioph. Methods* **2006**, *66*, 73–86

[50] Andersen, C.B.; Manno, M.; Rischel, C.; Thorolfsson, M.; Martorana, V. Aggregation of a multidomain protein: a coagulation mechanism governs aggregation of a model IgG1 antibody under weak thermal stress. *Protein Sci.* **2010**, *19*, 279–290

[51] Szenczi, A.; Kardos, J.; Medgyesi, G.A.; Závodszky, P. The effect of solvent environment on the conformation and stability of human polyclonal IgG in solution. *Biologicals* **2006**, *34*, 5–14

[52] Luo, Q.; Joubert, M.K.; Stevenson, R.; Ketchem, R.R.; Narhi, L.O.; Wypych, J. Chemical modifications in therapeutic protein aggregates generated under different stress conditions. *J. Biol. Chem.* **2011**, *286*, 25134–25144

[53] Rudiuk, S.; Cohen-Tannoudji, L.; Huille, S.; Tribet, C. Importance of the dynamics of adsorption and of a transient interfacial stress on the formation of aggregates of IgG antibodies. *Soft Matter* **2012**, *8*, 2651–2661

[54] Jayaraman, M.; Buck, P.M.; Ignatius, A.A.; King, K.R.; Wang, W. Agitation-induced aggregation and subvisible particulate formation in model proteins. *Eur. J. Pharm. Biopharm.* **2014**, *87*, 299–309

[55] Sane, S.U.; Wong, R.; Hsu, C.C. Raman spectroscopic characterization of drying-induced structural changes in a therapeutic antibody: Correlating structural changes with long-term stability. *J. Pharm. Sci.* **2004**, *93*, 1005–1018

[56] Zhang, L.; Lu, D.; Liu, Z. How native proteins aggregate in solution: A dynamic Monte Carlo simulation. *Biophys. Chem.* **2008**, *133*, 71–80

[57] Roberts, C.J. Kinetics of irreversible protein aggregation: analysis of extended Lumry-Eyring models and implications for predicting protein shelf life. *J. Phys. Chem. B* **2003**, *107*, 1194–1207

[58] Weiss, W.F.; Young, T.M.; Roberts, C.J. Principles, approaches, and challenges for predicting protein aggregation rates and shelf life. *J. Pharm. Sci.* **2009**, *98*, 1246–1277

[59] Roberts, C. Non-native protein aggregation kinetics. *Biotechnol. Bioeng.* **2007**, *98*, 927–938

[60] Sanchez-Ruiz, J.M.; Makhatadze, G.I. To charge or not to charge? *Trends in biotechnology* **2001**, *19*, 132–135

[61] Sali, D.; Bycroft, M.; Fersht, A.R. Surface electrostatic interactions contribute little to stability of barnase. *J. Mol. Biol.* **1991**, *220*, 779 – 788

[62] Frankenberg, N.; Welker, C.; Jaenicke, R. Does the elimination of ion pairs affect the thermal stability of cold shock protein from the hyperthermophilic bacterium *Thermotoga maritima*? *FEBS Lett.* **1999**, *454*, 299–302

[63] Broersen, K.; Weijers, M.; de Groot, J.; Hamer, R.J.; de Jongh, H.H. Effect of protein charge on the generation of aggregation-prone conformers. *Biomacromolecules* **2007**, *8*, 1648–1656

[64] Dong, A.; Prestrelski, S.; Allison, S.; Carpenter, J. Infrared spectroscopic studies of lyophilization-induced and temperature-induced protein aggregation. *J. Pharm. Sci.* **1995**, *64*, 415–424

[65] Calamai, M.; Canale, C.; Relini, A.; Stefani, M.; Chiti, F.; Dobson, C.M. Reversal of protein aggregation provides evidence for multiple aggregated states. *J. Mol. Biol.* **2005**, *346*, 603–616

[66] Dobson, C. Protein folding and misfolding. *Nature* **2003**, *426*, 884–890

[67] Dill, K.; MacCallum, J. The protein-folding probelm, 50 years on. *Science* **2012**, , 1042–1046

[68] Kim, P.; Baldwin, R. Specific intermediates in the folding reaction of small proteins and the mechanisms of protein folding. *Annu. Rev. Biochem.* **1982**, *51*, 459–489

[69] Kim, P.; Baldwin, R. Intermediates in the folding reactions of small proteins. *Annu. Rev. Biochem.* **1990**, *59*, 631–660

[70] Ptitsyn, O. Protein folding: hypotheses and experiments. *J. Protein Chem.* **1987**, , 273–293

[71] Daggett, V.; Fersht, A. Is there a unifying mechanims for protein folding? *Trends Biochem. Sci.* **2003**, *28*, 18–25

[72] Kauzmann, W. Some factors in the interpretation of protein denaturation. *Adv. Protein Chem.* **1959**, *14*, 1–63

[73] Chandler, D. Interfaces and the driving force of hydrophobic assembly. *Nature* **2005**, *437*, 640–647

[74] Ben-Naim, A. Solvent-induced forces in protein folding reflections on the protein folding problem. *Curr. Opin. Colloid Interface Sci.* **2013**, *18*, 502–509

[75] Rose, G.; Fleming, P.; Banavar, J.; Maritan, A. A backbone-based theory ofprotein folding. *Proc. Natl. Acad. Sci.* **2006**, *103*, 16623–16633

[76] Sun, T.; Lin, F.H.; Campbell, R.L.; Allingham, J.S.; Davies, P.L. An antifreeze protein folds with an interior network of more than 400 semi-clathrate waters. *Science* **2014**, *343*, 795–798

[77] Dill, K.A.; Ozkan, S.B.; Shell, M.S.; Weikl, T.R. The protein folding problem. *Annu. Rev. Biophys.* **2008**, *37*, 289–316

[78] Uversky, V.; Fink, A. The chicken-egg scenario of protein folding revisited. *FEBS Lett.* **2002**, *515*, 79–83

[79] Lin, M.; Zewail, A. Hydrophobic forces and the length limit of foldable protein domains. *Proc. Natl. Acad. Sci.* **2012**, *109*, 9851–9856

[80] Kamtekar, S.; Schiffer, J.M.; Xiong, H.; Babik, J.M.; Hecht, M.H. Protein design by binary patterning of polar and nonpolar amino acids. *Science* **1993**, *262*, 1680–1685

[81] Ghosh, K.; Dill, K. Theory for protein folding cooperativity: helix bundles. *J. Am. Chem. Soc.* **2009**, *131*, 2306–2312

[82] Garbuzynskiy, S.; Ivankov, D.; Bogatyreva, N.; Finkelstein, A. Golden triangle for folding rates of globular proteins. *Proc. Natl. Acad. Sci.* **2013**, *110*, 147–150

[83] Baldwin, R.L. The search for folding intermediates and the mechanism of protein folding. *Annu. Rev. Biophys.* **2008**, *37*, 1–21

[84] Ekman, D.; Bjorklund, A.; Frey-Scott, J.; Elofsson, A. Multi-domain proteins in the three kingdom of life: orphan domains and other unassigned regions. *J. Mol. Biol.* **2005**, *348*, 231–243

[85] Apic, G.; Gough, J.; Teichmann, S. Domain combinations in archael, eubacterial and eukariotic proteomes. *J. Mol. Biol.* **2001**, *310*, 311–325

[86] Levitt, M. Nature of the protein universe. *Proc. Natl. Acad. Sci.* **2009**, *106*, 11079–11084

[87] Murzin, A.; Brenner, S.; Hubbard, T.; Clothia, C. SCOP: a structural classification of proteins database for the investigation of sequences and structures. *J. Mol. Biol.* **1995**, *247*, 536–540

[88] Savageau, M. Proteins of *Escherichia Coli* come in sizes that are multiples of 14 kDa: domain concepts and evolutionary implications. *Proc. Natl. Acad. Sci.* **1986**, *83*, 1198–1202

[89] Rothlisberger, D.; Honegger, A.; Pluckthun, A. Domain interactions in the Fab fragment: a comparative evaluation of the single-chainFv and Fab format engineered with variable domains of different stability. *J. Mol. Biol.* **2005**, *347*, 773–789

[90] Han, J.H.; Batey, S.; Nickson, A.; Teichmann, S.; Clarke, J. The folding and evolution of multidomain proteins. *Nat. Rev.* **2007**, *8*, 319–330

[91] Itoh, K.; Sasai, M. Cooperativity, connectivity, and folding patwhays of multidomain proteins. *Proc. Natl. Acad. Sci.* **2008**, *105*, 13865–13870

[92] Batey, S.; Nickson, A.; Clarke, J. Studying the folding of multidomain proteins. *HFSP Journal* **2008**, *2*, 365–377

[93] Arviv, O.; Levy, Y. Folding of multidomain proteins: biophysical consequences of tethering even in apparently independent folding. *Proteins Struct. Funct. Bioinf.* **2012**, *80*, 2780–2798

[94] Chennamsetty, N.; Voynov, V.; Kayser, V.; Helk, B.; Trout, B.L. Design of therapeutic proteins with enhanced stability. *Proc. Natl. Acad. Sci.* **2009**, *106*, 11937–11942

[95] Chennamsetty, N.; Voynov, V.; Kayser, V.; Helk, B.; Trout, B. Prediction of aggregation prone regions of therapeutic proteins. *J. Phys. Chem. B* **2010**, *114*, 6614–6624

[96] Pawar, A.; DuBAY, K.; Zurdo, J.; Chiti, F.; Vendruscolo, M.; Dobson, C. Prediction of "aggregation-prone" and "aggregation-susceptible" regions in proteins associated with neurodegenerative diseases. *J. Mol. Biol.* **2005**, *350*, 379–392

[97] Nieba, L.; Honegger, A.; Krebber, K.; Pl¨ uckthun, A. Disrupting the hydrophobic patches at the antibody variable/constant domain interface: improved *in vivo* folding and physical chracterization of an engineered scFv fragment. *Protein Eng.* **1997**, *10*, 435–444

[98] Santner, A.A.; Croy, C.H.; Vasanwala, F.H.; Uversky, V.N.; Van, Y.Y.J.; Dunker, A.K. Sweeping away protein aggregation with entropic bristles: Intrinsically disordered protein fusions enhance soluble expression. *Biochemistry* **2012**, *51*, 7250–7262

[99] Kubetzko, S.; Sarkar, C.A.; Plückthun, A. Protein PEGylation decreases observed target association rates via a dual blocking mechanism. *Mol. Pharmacol.* **2005**, *68*, 1439–1454

[100] Yang, K.; Basu, A.; Wang, M.; Chintala, R.; Hsieh, M.C.; Liu, S.; Hua, J.; Zhang, Z.; Zhou, J.; Li, M.; *et al.* Tailoring structure–function and pharmacokinetic properties of single-chain Fv proteins by site-specific PEGylation. *Protein Eng.* **2003**, *16*, 761–770

[101] Chapman, A.P.; Antoniw, P.; Spitali, M.; West, S.; Stephens, S.; King, D.J. Therapeutic antibody fragments with prolonged *in vivo* half-lives. *Nat. Biotechnol.* **1999**, *17*, 780–783

[102] Chapman, A.P. PEGylated antibodies and antibody fragments for improved therapy: a review. *Adv. Drug. Del. Rev.* **2002**, *54*, 531–545

[103] Chen, C.; Constantinou, A.; Deonarain, M. Modulating antibody pharmacokinetics using hydrophilic polymers. *Expert Opin. Drug Deliv.* **2011**, *8*, 1221–1236

[104] Rudolph, R.; Lilie, H. *In vitro* folding of inclusion body proteins. *FASEB J.* **1996**, *10*, 49–56

[105] Wang, W. Protein aggregation and its inhibition in biopharmaceutics. *Int. J. Pharm.* **2005**, *289*, 1–30

[106] Tsumoto, K.; Ejima, D.; Kumagai, I.; Arakawa, T. Practical considerations in refolding proteins from inclusion bodies. *Protein Expres. Purif.* **2003**, *28*, 1–8

[107] Hamada, H.; Arakawa, T.; Shiraki, K. Effect of additives on protein aggregation. *Curr. Pharm. Biotechnol.* **2009**, *10*, 400–407

[108] Yancey, P.; Clark, M.; Hand, S.; Bowlus, R.; Somero, G. Living with water stress: evolution of osmolyte systems. *Science* **1982**, *217*, 1214–1222

[109] Arakawa, T.; S.N., T. The stabilization of proteins by osmolytes. *Biophys. J.* **1985**, *47*, 411–414

[110] Creighton, T.E. *Protein Structure, a Practical Approach.* Oxford University Press **1997**

[111] Auton, M.; R¨ osgen, J.; Sinev, M.; Holthauzen, L.; Bolen, D. Osmolyte effects on protein stability and solubility: A balancing act between backbone and side-chains. *Biophys. Chem.* **2011**, *159*, 90–99

[112] Street, T.; Bolen, D.; Rose, G. A molecular mechanism for osmolyte-induced protein stability. *Proc. Natl. Acad. Sci.* **2006**, *103*, 13997–14002

[113] Auton, M.; Bolen, D. Predicting the energetics of osmolyte-induced protein folding/unfolding. *Proc. Natl. Acad. Sci.* **2005**, *102*, 15065–15068

[114] Lilie, H.; Schwarz, E.; Rudolph, R. Advances in refolding of proteins produced in *e. coli. Curr. Opin. Biotechnol.* **1998**, *9*, 497–501

[115] Lange, C.; Rudolph, R. Suppression of protein aggregation by l-arginine. *Curr. Pharm. Bitoechnol.* **2009**, *10*, 408–414

[116] Tsumoto, K.; Umetsu, M.; Kumagai, I.; Ejima, D.; Philo, J.S.; Arakawa, T. Role of arginine in protein refolding, solubilization, and purification. *Biotechno. Prog.* **2004**, *20*, 1301–1308

[117] Arakawa, T.; Tsumoto, K. The effects of arginine on refolding of aggregated proteins: not facilitate refolding, but suppress aggregation. *Bioche. Biophys. Res. Comm.* **2003**, *304*, 148–152

[118] Tischer, A.; Lilie, H.; Rudolph, R.; Lange, C. L-arginine hydrochloride increases the solubility of folded and unfolded recombinant plasminogen activator rPA. *Prot. Sci.* **2010**, *19*, 1783–1795

[119] Schneider, C.P.; Trout, B.L. Investigation of cosolute-protein preferential interaction coefficients: New insight into the mechanism by which arginine inhibits aggregation. *J. Phys. Chem. B* **2009**, *113*, 2050–2058

[120] Li, J.; Garg, M.; Shah, D.; Rajagopalan, R. Solubilization of aromatic and hydrophobic moieties by arginine in aqueous solutions. *J. Chem. Phys.* **2010**, *133*, 054902

[121] Arakawa, T.; Ejima, D.; Tsumoto, K.; Obeyama, N.; Tanaka, Y.; Kita, Y.; Timasheff, S.N. Suppression of protein interactions by arginine: a proposed mechanism of the arginine effects. *Biophys. Chem.* **2007**, *127*, 1–8

[122] Schneider, C.; Shukla, D.; Trout, B. Aginine and the hofmeister series: role of ion-ion interactions in protein aggregation suppression. *J. Phys. Chem. B* **2011**, *115*, 7447–7458

[123] Baynes, B.M.; Wang, D.I.; Trout, B.L. Role of arginine in the stabilization of proteins against aggregation. *Biochemistry* **2005**, *44*, 4919–4925

[124] Das, U.; Hariprasad, G.; Ethayathulla, A.S.; Manral, P.; Das, T.K.; Pasha, S.; Mann, A.; Ganguli, M.; Verma, A.K.; Bhat, R.; *et al.* Inhibition of protein aggregation: supramolecular assemblies of arginine hold the key. *PLoS One* **2007**, *2*, e1176

[125] Vagenende, V.; Han, A.; Mueller, M.; Trout, B. Protein-associated cation clusters in aqueous arginine solutions and theireffect on protein stability and size. *ACS Chem. Biol.* **2013**, *8*, 416–422

[126] Blobel, J.; Brath, U.; Bernadó, P.; Diehl, C.; Ballester, L.; Sornosa, A.; Akke, M.; Pons, M. Protein loop compaction and the origin of the effect of arginine and glutamic acid mixtures on solubility, stability and transient oligomerization of proteins. *Eur. Biophy. J.* **2011**, *40*, 1327–1338

[127] Brockwell, D.; Radford, S. Intermediates: ubiquitous species on folding energy landscapes? *Curr. Opin. Struct. Biol.* **2007**, *17*, 30–37

[128] Lu, J.; Deutsch, C. Folding zones inside the ribosomal exit tunnel. *Nat. Struct. Mol. Biol.* **2005**, *12*, 1123–1129

[129] Kramer, G.; Boehringer, D.; Ban, N.; Bukau, B. The ribosome as a platform for cotranslational processing, folding and targeting of newly synthesized proteins. *Nat. Struct. Mol. Biol.* **2009**, *16*, 589–597

[130] Hartl, F.U.; Hayer-Hartl, M. Converging concepts of protein folding in vitro and in vivo. *Nature Struct. Mol. Biol.* **2009**, *16*, 574–581

[131] Hartl, F.; Hayer-Hartl, M. Molecular chaperones in the cytosol: from nascent chain to folded protein. *Science* **2002**, *295*, 1852–1858

[132] Ellis, R.; Minton, A. Protein aggregation in crowded environments. *Biol. Chem.* **2006**, *387*, 485–497

[133] Hartl, F.; Bracher, A.; Hayer-Hartl, M. Molecular chaperones in protein folding and proteostasis. *Nature* **2011**, *475*, 324–332

[134] Bucciantini, M.; Giannoni, E.; Chiti, F.; Baroni, F.; Formigli, L.; Zurdo, J.; Taddei, N.; Ramponi, G.; Dobson, C.; Stefani, M. Inherent toxicity of aggregates implies a common mechanism for protein misfolding diseases. *Nature* **2002**, *416*, 507–511

[135] Ravid, T.; Hochstrasser, M. Diversity of degradation signals in the ubiquitin-proteasome system. *Nat. Rev. Mol. Cell Biol.* **2008**, *9*, 679–689

[136] Tyedmers, J.; Mogk, A.; Bukau, B. Cellular strategies for controlling protein aggregation. *Nat. Rev. Mol. Cell Biol.* **2010**, *11*, 777–788

[137] Ellis, R. Proteins as molecular chaperones. *Nature* **1987**, *328*, 378

[138] Hartl, F. Molecular chaperones in cellular protein folding. *Nature* **1996**, *381*, 571–580

[139] Saibil, H. Chaperone machines for protein folding, unfolding and disaggregation. *Nat. Rev. Mol. Cell Biol.* **2013**, *14*, 630–642

[140] Doyle, S.; Genest, O.; Wickner, S. Protein rescue from aggregates by powerful molecular chaperone machines. *Nat. Rev. Mol. Cell Biol.* **2013**, *14*, 617–629

[141] Tompa, P.; Csermely, P. The role of structural disorder in the function ofRNA and protein chaperones. *FASEB J.* **2004**, *18*, 1169–1175

[142] Reichamnn, D.; Xu, Y.; Cremers, C.; Ilbert, M.; Mittelman, R.; Fitzgerald, M.; Jakob, U. Order out of disorder: working cycle of an intrinsically unfolded chaperone. *Cell* **2012**, *148*, 947–957

[143] Bukau, B.; Horwich, A. The Hsp70 and Hsp60 chaperone machines. *Cell* **1998**, *92*, 351–366

[144] Farr, G.; Furtakl, K.; Rowland, M.B.; Ranson, N.; Saibil, H.; Kirchhausen, T.; Horwich, A. Mutlivalent binding of nonnative substrate proteins by the chaperonin GroEL. *Cell* **2000**, *100*, 561–573

[145] Ewalt, K.; Hendrick, J.; Houry, W.; Hartl, F. *In vivo* observation of polypeptide flux through the bacterial chaperonin system. *Cell* **1997**, *90*, 491–500

[146] Shtilerman, M.; Lorimer, G.; Englander, S. Chaperonin function: folding by forced unfolding. *Science* **1999**, *284*, 822–825

[147] Ellis, R. Protein folding : Inside the cage. *Nature* **2006**, *442*, 360–362

[148] Priya, S.; Sharma, S.; Sood, V.; Mattoo, R.; Finka, A.; Azem, A.; De Los Rios, P.; Goloubinoff, P. GroEL and CCT are catalytic unfoldases mediating out-of-cage polypeptide refolding without ATP. *Proc. Natl. Acad. Sci.* **2013**, *110*, 7199–7204

[149] Brinker, A.; Pfeifer, G.; Kerner, M.; Naylor, D.; Hartl, F.; Hayer-Hartl, M. Dual function of protein confinement in chaperonin-assisted protein folding. *Cell* **2001**, *107*, 223–233

[150] Tandon, S.; Horowitz, P. Detergent-assisted refolding of guanidinium chloride-denatured rhodanese - The effect of lauryl maltoside. *J. Biol. Chem.* **1986**, *261*, 15615–15681

[151] Tandon, S.; Horowitz, P. Detergent-assisted refolding of guanidinium chloride-denatured rhodanese - The effect of concentration and type of detergent. *J. Biol. Chem.* **1987**, *262*, 4486–4491

[152] Zardeneta, G.; Horowitz, P. Detergent, liposome and micelle-assisted protein refolding. *Anal. Biochem.* **1994**, *223*, 1–6

[153] Yoshimoto, M.; Kuboi, R. Oxidative refolding of denatured/reduced lysozyme utilizing the chaperone-like function of liposomes and immobilized liposome chromatography. *Biotechnol. Prog.* **1999**, *15*, 480–487

[154] Kuboi, R.; Yoshimoto, M.; Walde, P.; Luisi, P. Refolding of carbonic anhydrase assisted by 1-palmitoyl-2-oleoyl-*sn*-glycero-3-phosphocholine liposomes. *Biotechnol. Prog.* **1997**, *13*, 828–836

[155] Kuboi, R.; Mawatari, T.; Yoshimoto, M. Oxidative refolding of lysozyme assisted by negatively charged liposomes: Relationship with lysozyme-mediated fusion of liposomes. *J. Biosci. Bioeng.* **2000**, *90*, 14–19

[156] Yoshimoto, M.; Shimanouchi, T.; Umakoshi, H.; Kuboi, R. Immobilized liposome chromatography for refolding and purification of protein. *J. Chromatogr. B* **2000**, *743*, 93–99

[157] Taylor, K.M.P.; Roseman, M.A. Effect of cholesterol, fatty acyl chain composition, and bilayer curvature on the interaction of cytochrome b5 with liposomes of phosphatidylcholines. *Biochemistry* **1995**, *34*, 3841–3850

[158] Yoshimoto, M.; Kuboi, R.; Yang, Q.; Miyake, J. Immobilized liposome chromatography for studies of protein-membrane interactions and refolding of denatured bovine carbonic anhydrase. *J. Chromatogr. B* **1998**, *712*, 59–71

[159] Dubey, P.; Gautam, S.; Kumar, P.P.P.; Sadanandan, S.; Haridas, V.; Gupta, M.N. Dendrons and dendrimers as pseudochaperonins for refolding of proteins. *RSC Adv.* **2013**, *3*, 8016–8020

[160] Rozema, D.; Gellman, S. Artificial chaperones: protein refolding via sequential use of detergent and cyclodextrin. *J. Am. Chem. Soc.* **1995**, *117*, 2373–2374

[161] Hanson, P.E.; Gellman, S.H. Mechanistic comparison of artificial-chaperone-assisted and unassisted refolding of ureadenatured carbonic anhydrase B. *Fold. Des.* **1998**, *3*, 457–468

[162] Rozema, D.; Gellman, S. Artificial chaperone-assisted refolding of carbonic anhydrase B. *J. Biol. Chem.* **1996**, *271*, 3478–3487

[163] Rozema, D.; Gellman, S. Artificial chaperone-assisted refolding of denatured-reduced lysozyme: modulation of the competition between renaturation and aggregation. *Biochem.* **1996**, *35*, 15760–15771

[164] Yazdanparast, R.; Khodarahmi, R. Evaluation of artificial chaperoning behavior of an insoluble cyclodextrin-rich copolymer: Solid-phase assisted refolding of carbonic anhydrase. *Int. J. Biol. Macromol.* **2007**, *40*, 319–326

[165] Badruddoza, A.; Hidajat, K.; Uddin, M. Synthesis and characterization of β-cyclodextrin-conjugated magnetic nanoparticles and their uses as solid-phase artificial chaperones in refolding of carbonic anhydrase bovine. *J. Coll. Int. Sci.* **2010**, *346*, 337–346

[166] Lu, D.; Zhang, M.; Zheng, L. Protein refolding assisted by an artificial chaperone using temperature stimuli responsive polymer as the stripper. *Biochem. Eng. J.* **2005**, *25*, 141–149

[167] Akiyoshi, K.; Sasaki, Y.; Sunamoto, J. Molecular chaperone-like activity of hydrogel nanoparticles of hydrophobized pullulan: thermal stabilization with refolding of carbonic anhydrase B. *Bioconjuagte Chem.* **1999**, *10*, 321–324

[168] Nomura, Y.; Sasaki, Y.; Takagi, M.; Narita, T.; Aoyama, Y.; Akiyoshi, K. Thermoresponsive controlled association of protein with a dynamic nanogel of hydrophobized polysahharide and cyclodextrin: heat-shock protein-like activity of artificial molecular chaperone. *Biomacromolecules* **2005**, *6*, 447–452

[169] Sawada, S.; Sasaki, Y.; Nomura, Y.; Akiyoshi, K. Cyclodextrin-responsive nanogel as an artificial chaperone for horseradish peroxidase. *Colloid Polym. Sci.* **2011**, *289*, 685–691

[170] Nomura, Y.; Ikeda, M.; Yamaguchi, N.; Aoyama, Y.; Akiyoshi, K. Protein refolding assisted by self-assembled nanogels as novel artificial molecular chaperone. *FEBS Lett.* **2003**, *553*, 271–276

[171] Asayama, W.; Sawasa, S.; Taguchi, K.; Akiyoshi, K. Comparison of refolding activities between nanogel artificial chaperone and groel systems. *Int. J. Biol. Macromol.* **2008**, *42*, 241–246

[172] Sasaki, Y.; Nomura, Y.; Sawada, S.; Akiyoshi, K. Polysaccharide nanogel–cyclodextrin system as an artificial chaperone for *in vitro* protein synthesis of green fluorescent protein. *Polymer J.* **2010**, *42*, 823–828

[173] Sasaki, Y.; Asayama, W.; Niwa, T.; Sawada, S.; Ueda, T.; Taguchi, H.; Akiyoshi, K. Amphiphilic polysaccharides nanogels as artificial chaperones in cell-free protein synthesis. *Macromol. Biosci.* **2011**, *11*, 814–820

[174] Akiyoshi, K.; Nishikawa, T.; Mitsui, Y.; Miyata, T.; Kodama, M.; Sunamoto, J. Self-assembly of polymer amphiphiles: Thermodynamics of complexation between bovine serum albumin and self-aggregate of cholesterol-bearing pullulan. *Coll. Surf. A - Physicochem. Eng. Aspects* **1996**, *112*, 91–95

[175] Nishikawa, T.; Akiyoshi, K.; Sunamoto, J. Supramolecular assembly between nanoparticles of hydrophobized polysaccharide and soluble protein complexation between the self-aggregate of cholesterol-bearing pullulan and α-chymotrypsin. *Macromolecules* **1994**, *27*, 7654–7659

[176] Nishikawa, T.; Akiyoshi, K.; Sunamoto, J. Macromolecular complexation between bovine serum albumin and the self-assembled hydrogel nanoparticle of hydrophobized polysaccharides. *J. Am. Chem. Soc.* **1996**, *118*, 6110–6115

[177] Takahashi, H.; Sawada, S.; Akiyoshi, K. Amphiphilic polysaccharide nanoballs: a new building block for nanogel biomedical engineering and artificial chaperones. *ACS Nano* **2011**, *5*, 337–345

[178] Hirakura, T.; Nomura, Y.; Aoyama, Y.; Akiyoshi, K. Photoresponsive nanogels formed by the self-assembly of spiropyrane-bearing pullulan that act as artificial molecular chaperones. *Biomacromolecules* **2004**, *5*, 1804–1809

[179] Lin, S.C.; Lin, K.L.; Chiu, H.C.; Lin, S. Enhanced protein renaturation by temperature-responsive polymers. *Biotechnol. Bioengineer.* **2000**, *67*, 505–511

[180] Chen, Y.; Huang, L.; Chiu, H.; Lin, S. Temperature-responsive polymer-assisted protein refolding. *Enzyme Microb. Technol.* **2003**, *32*, 120–130

[181] Lu, D.; Liu, Z.; Zhang, M.; Zheng, L.; Zhou, H. The mechanism of PNIPAAm-assisted refolding of lysozyme denatured by urea. *Biochem. Eng. J.* **2005**, *24*, 55–64

[182] Lu, D.; Liu, Z.; Zhang, M.; Wang, X.; Zheng, L. Temperature sensitive PNIPAAm assisted protein refolding *in vitro*. *Acta Polym. Sin.* **2004**, -, 573–579

[183] Lu, D.; Liu, Z.; Zhang, M.; Wang, X.; Zheng, L. Dextran-grafted-PNIPAAm as an artificial chaperone for protein refolding. *Biochem. Eng. J.* **2006**, *27*, 336–343

[184] Lu, D.; Wu, J.; Liu, Z. Dynamic control of protein folding pathway with a polymer of tunable hydrophobicity. *J. Phys. Chem. B* **2007**, *111*, 12303–12309

[185] Ge, X.; Guan, Y.X.; Chen, J.; Yao, Z.; Cao, K.; Yao, S.J. Refolding of lysozyme *in vitro* assisted by colloidal thermosensitive poly(N-isopropylacrylamide) brushes grafted onto the surface of uniform polystyrene cores. *J. Appl. Polym. Sci.* **2009**, *114*, 1270–1277

[186] Cui, Z.F.; Guan, Y.X.; Chen, J.L.; Yao, S.J. Thermosensitive poly(N-isopropylacrylamide) hydrogel for refolding of recombinant bovine prethrombin-2 from E. Coli inclusion bodies. *J. Appl. Polym. Sci.* **2005**, *96*, 1734–1740

[187] Tao, Q.; Li, A.; Liu, X.; Ma, R.; An, Y.; Shi, L. Protecting enzymes against heat inactivation by temperature-sensitive polymer in confined space. *Phys. Chem. Chem. Phys.* **2011**, *13*, 16265–16271

[188] Liu, X.; Liu, Y.; Zhang, Z.; Huang, F.; Tao, Q.; Ma, R.; An, Y.; Shi, L. Temperature-responsive mixed-shell polymeric micelles for the refolding of thermally denatured proteins. *Chem. Eur. J.* **2013**, *19*, 7437–7442

[189] Cleland, J.; Randolph, T. Mechanism of polyethylene glycol interaction with the molten globule folding intermediate of bovine carbonic anhydrase B. *J. Biol. Chem.* **1992**, *267*, 3147–3153

[190] Cleland, J.; Hedgepeth, C.; Wang, D. Polyethylene glycol enhanced refolding of bovine carbonic anhydrase B. *J. Biol. Chem.* **1992**, *267*, 13327–13334

[191] Cleland, J.; Wang, D. Cosolvent assisted protein refolding. *Biotechnol.* **1990**, *8*, 1274–1278

[192] Kuboi, R.; Morita, S.; Ota, H.; Umakoshi, H. Protein refolding using stimuli-responsive polymer-modified aqueous two-phase systems. *J. Chromatogr. B: Biomed. Sci. Appl.* **2000**, *743*, 215–223

[193] Yoshimoto, N.; Hashimoto, T.; Felix, M.; Umakoshi, H.; Kuboi, R. Artificial chaperone-assisted refolding of bovine carbonic anhydrase using molecular assemblies of stimuli-responsive polymers. *Biomacromolecules* **2003**, *4*, 1530–1538

[194] Tomita, S.; Nagasaki, Y.; Shiraki, K. Different mechanisms of action of poly(ethylenglycol) and arginine on thermal inactivation of lysozyme and ribonuclease A. *Biotech. Bioeng.* **2012**, *109*, 2543–2552

[195] Muraoka, T.; Adachi, K.; Ui, M.; Kawasaki, S.; Sadhukhan, N.; Obara, H.; Tochio, H.; Shirakawa, M.; Kinbara, K. A structured monodispersed PEG for the effective suppression of protein aggregation. *Angew. Chem.* **2013**, *125*, 2490–2494

[196] Muraoka, T.; Sadhukhan, N.; Ui, M.; Kawasaki, S.; Hazemi, E.; Adachi, K.; Kinbara, K. Thermal-aggregation suppression of proteins by a structured PEG analogue: importance of denaturation temperature for effective aggregation suppression. *Biochem. Eng. J.* **2014**, *86*, 41–48

[197] Cavalieri, F.; Chiessi, E.; Paradossi, G. Chaperone-like activity of nanoparticles of hydrophobized poly(vinyl alcohol). *Soft Matter* **2007**, *3*, 718–724

[198] De, M.; Rotello, V. Synthetic "chaperones": nanoparticle-mediated refolding of thermally denatured proteins. *Chem. Commun.* **2008**, *30*, 3504–3506

[199] Raghava, S.; Singh, P.; Rao, A.; Dutta, V.; Gupta, M. Nanoparticles of unmodified titanium dioxide faciliatate protein refolding. *J. Mater. Chem.* **2009**, *19*, 2830–2834

[200] Wang, X.; Lu, D.; Austin, R.; Argawal, A.; Mueller, L.; Liu, Z.; Wu, J.; Feng, P. Protein refolding assisted by periodic mesoporous organosilicas. *Langmuir* **2007**, *23*, 5735–5739

[201] Chiku, H.; Kawai, A.; Ishibashi, T.; Takehara, M.; Yanai, T.; Mizukami, F.; Sakaguchi, K. A novel protein refolding method using a zeolite. *Anal. Biochem.* **2006**, *348*, 307–314

[202] Nara, T.; Togashi, H.; Sekikawa, C.; Kawakami, M.; Yaginuma, N.; Sakaguchi, K.; Mizukami, F.; Tsunoda, T. Use of zeolite to refold a disulfide-bonded protein. *Colloid Surf. B* **2009**, *68*, 68–73

[203] Qiao, S.; Yu, C.; Xing, W.; Hu, Q.; Djojoputro, H.; Lu, G. Synthesis and bioadsorptive properties of large-pore periodic mesoporous organosilica rods. *Chem. Mater.* **2005**, *17*, 6172–6176

[204] Kameta, N.; Masuda, M.; Shimizu, T. Soft nanotube hydrogels functioning as artificial chaperones. *ACS Nano* **2012**, *6*, 5249–5258

[205] Morawetz, H.; Hugues, W. The interaction of proteins with synthetic polyelectrolytes. I. Complexation of bovine serum albumin. *J. Phys. Chem.* **1951**, *51*, 64–69

[206] Cooper, C.L.; Dubin, P.L.; Kayitmazer, A.B.; Turksen, S. Polyelectrolyte-protein complexes. *Curr. Opin. Colloid Interface Sci.* **2005**, *10*, 52–78

[207] Kayitmazer, A.; Seeman, D.; Minsky, B.; Dubin, P.; Xu, Y. Protein–polyelectrolyte interactions. *Soft Matter* **2013**, *9*, 2553–2583

[208] Mattison, K.W.; Dubin, P.L.; Brittain, I.J. Complex formation between bovine serum albumin and strong polyelectrolytes: effect of polymer charge density. *J. Phys. Chem. B* **1998**, *102*, 3830–3836

[209] Shalova, I.N.; Asryants, R.A.; Sholukh, M.V.; Saso, L.; Kurganov, B.I.; Muronetz, V.I.; Izumrudov, V.A. Interaction of polyanions with basic proteins, 2^a – Influence of complexing polyanions on the thermoaggregation of oligomeric enzymes. *Macromol. Biosci.* **2005**, *5*, 1184–1192

[210] Cooper, C.L.; Goulding, A.; Kayitmazer, A.B.; Ulrich, S.; Stoll, S.; Turksen, S.; Yusa, S.i.; Kumar, A.; Dubin, P.L. Effects of polyelectrolyte chain stiffness, charge mobility, and charge sequences on binding to proteins and micelles. *Biomacromolecules* **2006**, *7*, 1025–1035

[211] Sedlak, E.; Fedunova, D.; Vesela, V.; Sedlakova, D.; Antalik, M. Polyanion hydrophobicity and protein basicity affect protein stability in protein-polyanion complexes. *Biomacromolecules* **2009**, *10*, 2533–2538

[212] Izumrudov, V.A.; Kharlampieva, E.; Sukhishvili, S.A. Multilayers of a globular protein and a weak polyacid: Role of polyacid ionization in growth and decomposition in salt solutions. *Biomacromolecules* **2005**, *6*, 1782–1788

[213] Gao, G.; Dubin, P. Binding of proteins to copolymers of varying hydrophobicity. *Biopolymers* **1999**, *49*, 185–193

[214] Gao, G.; Yao, P. Structure and activity transition of lysozyme on interacting with and releasing from polyelectrolyte with different hydrophobicity. *J. Polym. Sci. A - Polym. Chem.* **2008**, *46*, 4681–4690

[215] Porcar, I.; Gareil, P.; Tribet, C. Formation of complexes between protein particles and long amphiphilic polymers: binding isotherms versus size and surface of the particles. *J. Phys. Chem. B* **1998**, *102*, 7906–7909

[216] Porcar, I.; Cottet, H.; Gareil, P.; Tribet, C. Association between protein particles and long amphiphilic polymers: effect of the polymer hydrophobicity on binding isotherms. *Macromolecules* **1999**, *32*, 3922–3929

[217] Stogov, S.; Izumrudov, V.; Muronetz, V. Structural changes of a protein bound to a polyelectrolyte depend on the hydrophobicity and polymerization degree of the polyelectrolyte. *Biochemsitry (Moscow)* **2010**, *75*, 437–442

[218] Capito, F.; Skudas, R.; Stanislawski, B.; Kolmar, H. Polyelectrolyte-protein interaction at low ionic strength: required chain flexibility depending on protein average charge. *Colloid Polym. Sci.* **2013**, *291*, 1759–1769

[219] de Vries, R.; Stuart, M. Theory and simulations of macroion complexation. *Curr. Opin. Colloid Interface Sci.* **2006**, *11*, 295–301

[220] Park, J.; Muhoberac, B.; Dubin, P.; Xia, J. Effects of protein charge heterogeneity in protein-polyelectrolyte complexation. *Macromolecules* **1992**, *25*, 290–295

[221] Serefoglou, E.; Oberdisse, J.; Staikos, G. Characterization of the soluble nanoparticles formed through coulombic interaction of bovine serum albumin with anionic graft copolymers at low pH. *Biomacromolecules* **2007**, *8*, 1195–1199

[222] Becker, A.; Henzler, K.; Welsch, N.; Ballauff, M.; Borisov, O. Proteins and polyelectrolytes: a charged relationship. *Curr. Opin. Colloid Interface Sci.* **2012**, *17*, 90–96

[223] de Vries, R.; Weinbreck, F.; de Kruif, C. Theory of polyelectrolyte adsorption on heterogeneously charged surfaces applied to soluble protein–polyelectrolyte complexes. *J. Chem. Phys.* **2003**, *118*, 4649–4659

[224] Seyrek, E.; Dubin, P.L.; Tribet, C.; Gamble, E.A. Ionic strength dependence of protein-polyelectrolyte interactions. *Biomacromolecules* **2003**, *4*, 273–282

[225] Chen, K.; Xu, Y.; Rana, S.; Miranda, O.R.; Dubin, P.L.; Rotello, V.M.; Sun, L.; Guo, X. Electrostatic selectivity in protein–nanoparticle interactions. *Biomacromolecules* **2011**, *12*, 2552–2561

[226] Li, Y.; Vries, R.d.; Kleijn, M.; Slaghek, T.; Timmermans, J.; Stuart, M.C.; Norde, W. Lysozyme uptake by oxidized starch polymer microgels. *Biomacromolecules* **2010**, *11*, 1754–1762

[227] Lindhoud, S.; Voorhaar, L.; de Vries, R.; Schweins, R.; Cohen Stuart, M.A.; Norde, W. Salt-induced disintegration of lysozyme-containing polyelectrolyte complex micelles. *Langmuir* **2009**, *25*, 11425–11430

[228] Lindhoud, S.; de Vries, R.; Schweins, R.; Stuart, M.A.C.; Norde, W. Salt-induced release of lipase from polyelectrolyte complex micelles. *Soft Matter* **2009**, *5*, 242–250

[229] Constancis, A.; Meyrueix, R.; Bryson, N.; Huille, S.; Grosselin, J.M.; Gulik-Krzywicki, T.; Soula, G. Macromolecular colloids of diblock poly(amino acids) that bind insulin. *J. Coll. Int. Sci.* **1999**, *217*, 357–368

[230] Wittemann, A.; Haupt, B.; Ballauff, M. Adsorption of proteins on spherical polyelectrolyte brushes in aqueous solution. *Phys. Chem. Chem. Phys.* **2003**, *5*, 1671–1677

[231] Tribet, C. *Complexation between amphiphilic polyelectrolytes and proteins: from necklaces to gels in Physical chemistry of polyelectrolytes*. CRC Press **2001**

[232] Salmaso, S.; Caliceti, P. Self-assembling nanocomposites for protein delivery: supramolecular interactions of soluble polymers with protein drugs. *Int. J. Pharma.* **2013**, *440*, 111–123

[233] Henzler, K.; Haupt, B.; Lauterbach, K.; Wittemann, A.; Borisov, O.; Ballauff, M. Adsorption of β-lactoglobulin on spherical polyelectrolyte brushes: direct proof of counterion release by isothermal titration calorimetry. *J. Am. Chem. Soc.* **2010**, *132*, 3159–3163

[234] van der Gucht, J.; Spruijt, E.; Lemmers, M.; Cohen Stuart, M. Polyelectrolyte complexes: bulk phases and colloidal systems. *J. Coll. Int. Sci.* **2011**, *361*, 407–422

[235] Ball, V.; Winterhalter, M.; Schwinte, P.; Lavalle, P.; Voegel, J.C.; Schaaf, P. Complexation mechanism of bovine serum albumin and poly(allylamine hydrochloride). *J. Phys. Chem. B* **2002**, *106*, 2357–2364

[236] Wittemann, A.; Ballauff, M. Interaction of proteins with linear polyelectrolytes and spherical polyelectrolyte brushes in aqueous solution. *Phys. Chem. Chem. Phys.* **2006**, *8*, 5269–5275

[237] da Silva, F.L.B.; Lund, M.; Jönsson, B.; Åkesson, T. On the complexation of proteins and polyelectrolytes. *J. Phys. Chem. B* **2006**, *110*, 4459–4464

[238] da Silva, F.L.B.; Jönsson, B. Polyelectrolyte–protein complexation driven by charge regulation. *Soft Matter* **2009**, *5*, 2862–2868

[239] Barroso da Silva, F.L.; Boström, M.; Persson, C. Effect of charge regulation and ion–dipole interactions on the selectivity of protein–nanoparticle binding. *Langmuir* **2014**, *30*, 4078–4083

[240] Lund, M.; Åkesson, T.; Jönsson, B. Enhanced protein adsorption due to charge regulation. *Langmuir* **2005**, *21*, 8385–8388

[241] Lund, M.; Jönsson, B. On the charge regulation of proteins. *Biochem.* **2005**, *44*, 5722–5727

[242] Xia, J.; Dubin, P.L.; Kim, Y.; Muhoberac, B.B.; Klimkowski, V.J. Electrophoretic and quasi-elastic light scattering of soluble protein-polyelectrolyte complexes. *J. Phys. Chem.* **1993**, *97*, 4528–4534

[243] Mattison, K.W.; Brittain, I.J.; Dubin, P.L. Protein–polyelectrolyte phase boundaries. *Biotechnol. Prog.* **1995**, *11*, 632–637

[244] Kizilay, E.; Kayitmazer, A.; Dubin, P. Complexation and coacervation of polyelectrolytes with oppositely charged colloids. *Adv. Colloid Interface Sci.* **2011**, *167*, 24–37

[245] Antonov, M.; Mazzawi, M.; Dubin, P.L. Entering and exiting the protein-polyelectrolyte coacervate phase via nonmonotonic salt dependence of critical conditions. *Biomacromolecules* **2010**, *11*, 51–59

[246] Kayitmazer, A.B.; Quinn, B.; Kimura, K.; Ryan, G.L.; Tate, A.J.; Pink, D.A.; Dubin, P.L. Protein specificity of charged sequences in polyanions and heparins. *Biomacromolecules* **2010**, *11*, 3325–3331

[247] de Kruif, C.G.; Weinbreck, F.; de Vries, R. Complex coacervation of proteins and anionic polysaccharides. *Curr. Opin. Coll. Int. Sci.* **2004**, *9*, 340–349

[248] Xu, Y.S.; Mazzawi, M.; Chen, K.M.; Sun, L.H.; Dubin, P.L. Protein purification by polyelectrolyte coacervation: Influence of protein charge anisotropy on selectivity. *Biomacromolecules* **2011**, *12*, 1512–1522

[249] McDonald, P.; Victa, C.; Carter-Franklin, J.; Fahrner, R. Selective antibody precipiation using polyelectrolytes: a novel approach to the purification of monoclonal antibodies. *Biotechnol. Bioeng.* **2008**, *102*, 1141–1151

[250] Peram, T.; McDonald, P.; Carter-Franklin, J.; Fahrner, R. Monoclonal antibody purification using cationic polyelectrolytes: An alternative to column chromatography. *Biotechnol. Prog.* **2010**, *26*, 1322–1331

[251] Ma, J.; Hoang, H.; Myint, T.; Peram, T.; Fahrner, R.; Chou, J.H. Using precipitation by polyamines as an alternative to chromatographic separation in antibody purification processes. *J. Chrom. B* **2010**, *878*, 798–806

[252] Lindhoud, S.; de Vries, R.; Norde, W.; Stuart, M.A.C. Structure and stability of complex coacervate core micelles with lysozyme. *Biomacromolecules* **2007**, *8*, 2219–2227

[253] Kurinomaru, T.; Maruyama, T.; Izaki, S.; Handa, K.; Kimoto, T.; Shiraki, K. Protein–poly(amino acid) complex precipitation for high-concentration protein formulation. *J. Pharm. Sci.* **2014**, *103*, 2248–2254

[254] Tribet, C.; Porcar, I.; Bonnefont, P.; Audebert, R. Association between hydrophobically modified polyanions and negatively charged bovine serum albumin. *J. Phys. Chem. B* **1998**, *102*, 1327–1333

[255] Tribet, C.; Audebert, R.; Popot, J. Amphipols: polymer that keep membrane proteins soluble in aqueous solutions. *Proc. Natl. Acad. Sci.* **1996**, *93*, 15047–15050

[256] Tribet, C.; Audebert, R.; Popot, J. Stabilization of hydrophobic colloidal dispersions in water with amphiphilic polymers: application to integral membrane proteins. *Langmuir* **1997**, *13*, 5570–5576

[257] Petit, F.; Audebert, R.; Iliopoulos, I. Interactions of hydrophobically modified poly(sodium acrylate) with globular proteins. *Colloid Polym. Sci.* **1995**, *273*, 777–781

[258] Borrega, R.; Tribet, C.; Audebert, R. Reversible gelation in hydrophobic polyelectrolyte/protein mixtures: an example of cross-links between soft and hard colloids. *Macromolecules* **1999**, *32*, 7798–7806

[259] Popot, J.L.; Berry, E.A.; Charvolin, D.; Creuzenet, C.; Ebel, C.; Engelman, D.; Flotenmeyer, M.; Giusti, F.; Gohon, Y.; Hong, Q.; Lakey, J.; Leonard, K.; Shuman, H.; Timmins, P.; Warschawski, D.; Zito, F.; Zoonens, M.; Pucci, B.; Tribet, C. Amphipols: polymeric surfactants for membrane biology research. *Cell Mol. Life. Sci.* **2003**, *60*, 1553–1574

[260] Zoonens, M.; Catoire, L.; Giusti, F.; Popot, J.L. NMR study of a membrane protein in detergent-free aqueous solution. *Proc. Natl. Acad. Sci.* **2005**, *102*, 8893–8898

[261] Zoonens, M.; Giusti, F.; Zito, F.; Popot, J.L. Dynamics of membrane protein/amphipol association studied by Förster resonance energy transfer: implications for *in vitro* studies of amphipol-stabilized membrane proteins. *Langmuir* **2007**, *23*, 4303–4309

[262] Catoire, L.; Zoonens, M.; van Heijenoort, C.; Giusti, F.; Guittet, E.; Popot, J.L. Solution NMR mapping of water-accsible resiudes in the transmembrane beta-barrel of ompx. *Eur. Biophys. J.* **2010**, *39*, 623–630

[263] Tribet, C.; Diab, C.; Dahmane, T.; Zoonens, M.; Popot, J.L.; Winnik, F. Thermodynamic characterization of the exchange of detergents and amphipols at the surfaces of integral membrane proteins. *Langmuir* **2009**, *25*, 12623–12634

[264] Karayianni, M.; Pispas, S.; Chryssikos, G.D.; Gionis, V.; Giatrellis, S.; Nounesis, G. Complexation of lysozyme with poly(sodium(sulfamate-carboxylate)isoprene). *Biomacromolecules* **2006**, *12*, 1697–1706

[265] Ivinova, O.N.; Izumrudov, V.A.; Muronetz, V.I.; Galaev, I.Y.; Mattiasson, B. Influence of complexing polyanions on the thermostability of basic proteins. *Macromol. Biosci.* **2003**, *3*, 210–215

[266] Kuramoto, N.; Sakamoto, M.; Komiyama, J.; Iijima, T. Complex formation between bovine serum albumin and poly(acrylic acid) as studied by viscosimetry, circular dichroism and fluorescence. *Makromol. Chem.* **1984**, *185*, 1419–1427

[267] Xia, J.; Dubin, P.; Kokufuta, E.; Havel, H.; Muhoberac, B. Light scattering, cd and ligand binding studies of ferrihemoglobin-polyelectrolyte complexes. *Biopolymers* **1999**, *50*, 153–161

[268] Kreft, O.; Prevot, M.; Möhwald, H.; Sukhorukov, G. Shell-in-shell microcapsules: A novel tool for integrated, spatially confined enzymatic reactions. *Angew. Chem. Int. Ed.* **2007**, *46*, 5605–5608

[269] Lee, H.; Jeong, Y.; Park, T.G. Shell cross-linked hyaluronic acid/polylysine layer-by-layer polyelectrolyte microcapsules prepared by removal of reducible hyaluronic acid microgel cores. *Biomacromolecules* **2007**, *8*, 3705–3711

[270] Crouzier, T.; Ren, K.; Nicolas, C.; Roy, C.; Picart, C. Layer-by-layer films as a biomimetic reservoir for rhBMP-2 delivery: Controlled differentiation of myoblasts to osteoblasts. *Small* **2009**, *5*, 598–608

[271] Shutava, T.G.; Kommireddy, D.S.; Lvov, Y.M. Layer-by-layer enzyme/polyelectrolyte films as a functional protective barrier in oxidizing media. *J. Am. Chem. Soc.* **2006**, *128*, 9926–9934

[272] Weidinger, I.M.; Murgida, D.H.; Dong, W.f.; Möhwald, H.; Hildebrandt, P. Redox processes of cytochrome c immobilized on solid supported polyelectrolyte multilayers. *J. Phys. Chem. B* **2006**, *110*, 522–529

[273] Tezcaner, A.; Hicks, D.; Boulmedais, F.; Sahel, J.; Schaaf, P.; Voegel, J.C.; Lavalle, P. Polyelectrolyte multilayer films as substrates for photoreceptor cells. *Biomacromolecules* **2006**, *7*, 86–94

[274] Vodouhê, C.; Schmittbuhl, M.; Boulmedais, F.; Bagnard, D.; Vautier, D.; Schaaf, P.; Egles, C.; Voegel, J.C.; Ogier, J. Effect of functionalization of multilayered polyelectrolyte films on motoneuron growth. *Biomaterials* **2005**, *26*, 545–554

[275] Yuan, W.; Dong, H.; Li, C.M.; Cui, X.; Yu, L.; Lu, Z.; Zhou, Q. pH-controlled construction of chitosan/alginate multilayer film: Characterization and application for antibody immobilization. *Langmuir* **2007**, *23*, 13046–13052

[276] Schwinte, P.; Ball, V.; Szalontai, B.; Haikel, Y.; Voegel, J.C.; Schaaf, P. Secondary structure of proteins adsorbed onto or embedded in polyelectrolyte multilayers. *Biomacromolecules* **2002**, *3*, 1135–1143

[277] Cousin, F.; Gummel, J.; Ung, D.; Boué, F. Polyelectrolyte–protein complexes: Structure and conformation of each specie revealed by SANS. *Langmuir* **2005**, *21*, 9675–9688

[278] Gao, G.; Yunfeng, Y.; Pispas, S.; Yao, P. Sustained and extended release with structural and activity recovery of lysozyme from complexes with sodium (sulfamate carboxylate) isoprene/ethylene oxide block copolymer. *Macromol. Biosci.* **2010**, *10*, 139–146

[279] Ganguli, S.; Yoshimoto, K.; Tomita, S.; Sakuma, H.; Matsuoka, T.; Shiraki, K.; Nagasaki, Y. Regulation of lysozyme activity based on thermotolerant protein/smart polymer complex formation. *J. Am. Chem. Soc.* **2009**, *131*, 6549–6553

[280] Ganguli, S.; M.B., H. Polymeric switch on lysozyme activity: Role of hydrophobic and electrostatic interactions. *J. Pure App. Chem. Res.* **2013**, *2*, 93–101

[281] Ganguli, S.; Yoshimoto, K.; Tomita, S.; Sakuma, H.; Matsuoka, T.; Shiraki, K.; Nagasaki, Y. Improving the heat resistance of ribonuclease A by the addition of poly(N,Ndiethylaminoethyl methacrylate)-graft-poly(ethylene glycol) (PEAMA-g-PEG). *Macromol. Biosci.* **2010**, *10*, 853–859

[282] Ganguli, S. Switching the enzymatic activity of ribonuclease A based on enzyme/polymer complex formation. *J. Biosci.* **2012**, *20*, 33–39

[283] Kurinomaru, T.; Tomita, S.; Kudo, S.; Ganguli, S.; Nagasaki, Y.; Shiraki, K. Improved complementary polymer pair system: switching for enzyme activity by PEGylated polymers. *Langmuir* **2012**, *28*, 4334–4338

[284] Tomita, S.; Shiraki, K. Poly(acrylic acid) is a common noncompetitive inhibitor for cationic enzymes with high affinity and reversibility. *J. Polym. Sci. A* **2011**, *49*, 3835–3841

[285] Kurinomaru, T.; Tomita, S.; Hagihara, Y.; Shiraki, K. Enzyme hyperactivation system based on a complementary charged pair of polyelectrolytes and substrates. *Langmuir* **2014**, *30*, 3826–3831

[286] Fedunova, D.; Antalik, M. Prevention of thermal induced aggregation of cytochrome c at isoelectric ph values by polyanions. *Biotechno. Bioeng.* **2006**, *93*, 485–493

[287] Wittemann, A.; Ballauff, M. Temperature-induced unfolding of ribonuclease A embedded in spherical polyelectrolyte brushes. *Macromol. Biosci.* **2005**, *5*, 13–20

[288] Sun, J.; Ruchmann, J.; Pallier, A.; Jullien, L.; Desmadril, M.; Tribet, C. Unfolding of cytochrome C upon interaction with azobenzene-modified copolymers. *Biomacromolecules* **2012**, *13*, 3736–3746

[289] Stogov, S.; Muronetz, V.; Izumrudov, V. Basic guidelines for the selection of polyelectrolytes that can effectively prevent thermal aggregation of enzymes without any substantial loss in their catalytic activity. *Polym. Sci. C* **2011**, *53*, 97–106

[290] Shalova, I.N.; Naletova, I.N.; Saso, L.; Muronetz, V.I.; Izumrudov, V.A. Interaction of polyelectrolytes with proteins, 3 – influence of complexing polycations on the thermoaggregation of oligomeric enzymes. *Macromol. Biosci.* **2007**, *7*, 929–939

[291] Giger, K.; Vanam, R.P.; Seyrek, E.; Dubin, P. Suppression of insulin aggregation by heparin. *Biomacromolecules* **2008**, *9*, 2338–2344

[292] Xu, Y.; Seeman, D.; Yan, Y.; Sun, L.; Post, J.; ; Dubin, P.L. Effect of heparin on protein aggregation: Inhibition versus promotion. *Biomacromolecules* **2012**, *13*, 1642–1651

[293] Chung, K.; Kim, J.; Cho, B.K.; Ko, B.J.; Hwang, B.Y.; Kim, B.G. How does dextran sulfate prevent heat induced aggregation of protein? The mechanism and its limitation as aggregation inhibitor. *Biochim. Biophys. Acta (BBA) - Proteins and Proteomics* **2007**, *1774*, 249–257

[294] Mounsey, J.S.; O'Kennedy, B.T.; Fenelon, M.A.; Brodkorb, A. The effect of heating on β-lactoglobulin–chitosan mixtures as influenced by pH and ionic strength. *Food Hydrocolloids* **2008**, *22*, 65–73

[295] Calamai, M.; Kumita, J.R.; Mifsud, J.; Parrini, C.; Ramazzotti, M.; Ramponi, G.; Taddei, N.; Chiti, F.; Dobson, C. Nature and significance of the interactions between amyloid fibrils and biological polyelectrolytes. *Biochemistry* **2006**, *45*, 12806–2815

[296] Cohlberg, J.A.; Li, J.; Uversky, V.N.; Fink, A.L. Heparin and other glycosaminoglycans stimulate the formation of amyloid fibrils from alpha-synuclein in vitro. *Biochemistry* **2002**, *41*, 1502–1511

[297] Goedert, M.; Jakes, R.; Spillantini, M.G.; Hasegawa, M.; Smith, M.J.; Crowther, R.A. Assembly of microtubule-associated protein tau into alzheimer-like filaments induced by sulphated glycosaminoglycans. *Nature* **1996**, *383*, 550–553

[298] Solomon, J.P.; Bourgault, S.; Powers, E.T.; Kelly, J.W. Heparin binds 8 kDa gelsolin cross-beta-sheet oligomers and accelerates amyloidogenesis by hastening fibril extension. *Biochemistry* **2011**, *50*, 2486–2498

[299] Bourgault, S.; Solomon, J.P.; Reixach, N.; Kelly, J.W. Sulfated glycosaminoglycans accelerate transthyretin amyloidogenesis by quaternary structural conversion. *Biochemistry* **2011**, *50*, 1001–1015

[300] McLaurin, J.and Franklin, T.; Zhang, X.; Deng, J.; Fraser, P.E. Interactions of alzheimer amyloid-beta peptides with glycosaminoglycans effects on fibril nucleation and growth. *Eur. J. Biochem.* **1999**, *266*, 1101–1110

[301] Mukrasch, M.D.; Biernat, J.; von Bergen, M.; Griesinger, C.; Mandelkow, E.; Zweckstetter, M. Sites of tau important for aggregation populate beta-structure and bind to microtubules and polyanions. *J. Biol. Chem.* **2005**, *280*, 24978–24986

[302] Ojha, B.; Liu, H.; Dutta, S.; Rao, P.P.N.; Wojcikiewicz, E.P.; Du, D. Poly(4-styrenesulfonate) as an inhibitor of Aβ40 amyloid fibril formation. *J. Phys. Chem. B* **2013**, *117*, 13975–13984

[303] Taluja, A.; Bae, Y. Role of a novel excipient poly(ethylene glycol)-b-poly(l-histidine) in retention of physical stability of insulin in aqueous solutions. *Pharm. Res.* **2007**, *24*, 1517–1526

[304] Ai Tran, H.N.; Sousa, F.; Moda, F.; Mandal, S.; Chanana, M.; Vimercati, C.; Morbin, M.; Krol, S.; Tagliavini, F.; Legname, G. A novel class of potential prion drugs: preliminary *in vitro* and *in vivo* data for multilayer coated gold nanoparticles. *Nanoscale* **2010**, *2*, 2724–2732

[305] Roy, I.; Gupta, M. pH-responsive polymer-assisted refolding of urea- and organic solvent-denatured alpha-chymotrypsin. *Protein Eng.* **2003**, *16*, 1153–1157

[306] Roy, I.; Mondal, K.; Sharma, A.; Gupta, M. Simultaneous refolding/purification of xylanase with a microwave treated smart polymer. *Biochim. Biophys. Acta* **2005**, *1747*, 179–187

[307] Huang, Z.; Leong, S.S. Molecular-assisted refolding: study of two different ionic forms of recombinant human fibroblast growth factors. *J. Biotechnol.* **2009**, *142*, 157–163

[308] Ye, C.; Ilghari, D.; Niu, J.; Xie, Y.; Wang, Y.; Wang, C.; Li, X.; Liu, B.; Huang, Z. A comprehensive structure–function analysis shed a new light on molecular mechanism by which a novel smart copolymer, NY-3-1, assists protein refolding. *J. Biotechnol.* **2012**, *160*, 169–175

[309] Sharma, A.; Roy, I.; Gupta, M. Affinity precipitation and macroaffinity ligand facilitated three-phase partitioning for refolding and simultaneous purification of urea-denatured pectinase. *Biotechnol. Prog.* **2004**, *20*, 1255–1258

[310] Mondal, K.; Bohidar, H.B.; Roy, R.P.; Gupta, M.N. Alginate-chaperoned facile refolding of *Chromobacterium viscosum* lipase. *Biochim. Biophys. Acta – Proteins and Proteomics* **2006**, *1764*, 877–886

[311] K., M.; Raghava, S.; Barua, B.; Varadarajan, R.; Gupta, M. Role of stimuli-sensitive polymers in protein refolding: alpha-amylase and CcdB (controller of cell division or death B) as model proteins. *Langmuir* **2007**, *23*, 70–75

[312] Gautam, S.; Dubey, P.; Singh, P.; Kesavardhana, S.; Varadarajan, R.; Gupta, M.N. Smart polymer mediated purification and recovery of active proteins from inclusion bodies. *J. Chrom. A* **2012**, *1235*, 10–25

[313] Singh, P.; Gupta, M. Simultaneous refolding and purification of a recombinant lipase with an intein tag by affinity precipitation with chitosan. *Biochim. Biophys. Acta* **2008**, *1784*, 1825–1829

[314] Khodagholi, F.; Farahmand, S.; Tusi, S. Designing a highly efficient chemical chaperone system using chitosan-coated alginate. *Prot. J.* **2010**, *29*, 343–349. ISSN 1572–3887

[315] Pocanschi, C.L.; Dahmane, T.; Gohon, Y.; Rappaport, F.; Apell, H.J.; Kleinschmidt, J.H.; Popot, J.L. Amphipathic polymers: tools to fold integral membrane proteins to their active form. *Biochemistry* **2006**, *45*, 13954–13961

[316] Dahmane, T.; Damian, M.; Mary, S.; Popot, J.L.; Banères, J.L. Amphipol-assisted *in vitro* folding of G protein-coupled receptors. *Biochemistry* **2009**, *48*, 6516–6521

[317] Bazzacco, P.; Billon-Denis, E.; Sharma, K.S.; Catoire, L.J.; Mary, S.; Bon, C.L.; Point, E.; Banères, J.L.; Durand, G.; Zito, F.; Pucci, B.; Popot, J.L. Non-ionic homopolymeric amphipols: Application to membrane protein folding, cell-free synthesis, and solution NMR. *Biochemistry* **2012**, *51*, 1416–1430

[318] Thorslund, A.; Lindskog, S. Studies of the esterase activity and the anion inhibition of bovine zinc and cobalt carbonic anhydrases. *Eur. J. Biochem.* **1967**, *3*, 117–123

[319] Verpoorte, J.A.; Mehta, S.; Edsall, J.T. Esterase activities of human carbonic anhydrases B and C. *J.Biol. Chem.* **1967**, *242*, 4221–4229

[320] Pocker, Y.; Stone, J.T. The catalytic versatility of erythrocyte carbonic anhydrase. III. kinetic studies of the enzyme-catalyzed hydrolysis of p-nitrophenyl acetate. *Biochem.* **1967**, *6*, 668–678

[321] Saito, R.; Sato, T.; Ikai, A.; Tanaka, N. Structure of bovine carbonic anhydrase II at 1.95 A resolution. *Acta Crystallogr. Sect. D. Biol. Crystallogr.* **2004**, *60*, 792–795

[322] Krishnamurthy, V.M.; Kaufman, G.K.; Urbach, A.R.; Gitlin, I.; Gudiksen, K.L.; Weibel, D.B.; Whitesides, G.M. Role of a novel excipient poly(ethylene glycol)-b-poly(l-histidine) in retention of physical stability of insulin in aqueous solutions. *Chem. Rev.* **2008**, *108*, 946–1051

[323] Mirarefi, P.; Lee Jr, C.T. Photo-induced unfolding and inactivation of bovine carbonic anhydrase in the presence of a photoresponsive surfactant. *Biochim. Biophys. Acta - Proteins and Proteomics* **2010**, *1804*, 106–114

[324] Ko, B.P.N.; Yazgan, A.; Yeagle, P.L.; Lottich, S.C.; Henkens, R.W. Kinetics and mechanism of refolding of bovine carbonic anhydrase. A probe study of the formation of the active site. *Biochemistry* **1977**, *16*, 1720–1725

[325] McCoy, L.F.; Wong, K.P. Renaturation of bovine erythrocyte carbonic anhydrase B denatured by acid, heat, and detergent. *Biochemistry* **1981**, *20*, 3062–3067

[326] Dolgikh, D.; Kolomiets, A.; Bolotina, I.; Ptitsyn, O. 'molten-globule state accumulates in carbonic anhydrase folding. {*FEBS*} *Letters* **1984**, *165*, 88–92

[327] Semisotnov, G.; Rodionova, N.; Kutyshenko, V.; Ebert, B.; Blanck, J.; Ptitsyn, O. Sequential mechanism of refolding of carbonic bovine anhydrase B. *FEBS Lett.* **1987**, *224*, 9–13

[328] Uversky, V.; Ptitsyn, O. Further evidence on the equilibrium "pre-molten globule state": four-state guanidinium chloride-induced unfolding of carbonic anhydrase B at low temperature. *J. Mol. Biol.* **1996**, *255*, 215–228

[329] Semisotnov, G.V.; Uversky, V.N.; Sokolovsky, I.V.; Gutin, A.M.; Razgulyaev, O.I.; Rodionova, N.A. Two slow stages in refolding of bovine carbonic anhydrase B are due to proline isomerization. *J. Mol. Biol.* **1990**, *213*, 561

[330] Cleland, J.L.; Wang, D.I.C. Refolding and aggregation of bovine carbonic anhydrase B: quasi-elastic light scattering analysis. *Biochem.* **1990**, *29*, 11072–11078

[331] Prokhorov, D.A.; Timchenko, A.A.; Uversky, V.N.; Khristoforov, V.S.; Kihara, H.; Kimura, K.; Kutyshenko, V.P. Dynamics of oligomer formation by denatured carbonic anhydrase II. *Biochim. Biophys. Acta – Proteins and Proteomics* **2008**, *1784*, 11072–11078

[332] Cleland, J.L.; Wang, D.I.C. *Equilibrium association of a molten globule intermediate in the refolding of bovine carbonic anhydrase in Protein Refolding.* ACS Symposium Series, vol.470 **1991**

[333] Ruchmann, J.; Fouilloux, S.; Tribet, C. Light-responsive hydrophobic association of surfactants with azobenzene-modified polymers. *Soft Matter* **2008**, *4*, 2098–2108

[334] Pouliquen, G.; Tribet, C. Light-triggered association of bovine serum albumin and azobenzene-modified poly(acrylic acid) in dilute and semidilute solutions. *Macromolecules* **2006**, *39*, 373–383

[335] Gitlin, I.; Gudiksen, K.; Whitesides, G. Effects of surface charge on denaturation of bovine carbonic anhydrase. *Chem. Bio. Chem.* **2006**, *7*, 1241–1250

[336] Piaggio, M.V.; Peirotti, M.B.; Deiber, J.A. Effect of background electrolyte on the estimation of protein hydrodynamic radius and net charge through capillary zone electrophoresis. *Electrophoresis* **2005**, *26*, 3232–3246

[337] Cleland, J.L.; Wang, D.I.C. Transient association of the first intermediate during the refolding of bovine carbonic anhydrase B. *Biotechnol. Prog.* **1992**, *8*, 97–103

[338] Micsonai, A.; Jozsef, K.; *et al. In preparation.*

[339] Baty, D.; Chames, P. Approved antibodies for imaging and therapeutic: an update. *Immuno-analyse & biologie spécialisée* **2006**, *21*, 255–263

[340] Plückthun, A. Monovalent and bivalent antibody fragments produced in *escherichia coli*: engineering, folding and antigen-binding. *Immunolog. Rev.* **1992**, *130*, 151–188

[341] Wörn, A.; Plückthun, A. Stability engineering of antibody single-chain Fv fragments. *J. Mol. Biol.* **2001**, *305*, 989–1010

[342] Whitlow, M.; Bell, B.; Feng, S.; Filpula, D.; Hardman, K.; S.L., H.; Rollence, M.; Wood, J.; Schott, M.; Milenic, D.; *et al.* An improved linker for single-chain Fv with reduced aggregation and enhanced proteolytic stability. *Protein Eng.* **1993**, *6*, 989–995

[343] Alfthan, K.; Takkinen, K.; Sizmann, D.; Söderlund, H.; Teeri, T.T. Properties of a single-chain antibody containing different linker peptides. *Protein Eng.* **1995**, *8*, 725–731

[344] Monnier, P.P.; Vigouroux, R.J.; Tassew, N.G. In vivo applications of single chain Fv (variable domain)(scFv) fragments. *Antibodies* **2013**, *2*, 193–208

[345] Ahmad, Z.A.; Yeap, S.K.; Ali, A.M.; Ho, W.Y.; Alitheen, N.B.M.; Hamid, M. scFv antibody: principles and clinical application. *J. Immunol. Res.* **2012**, *2012*, 1–15

[346] Hudson, P.; Kortt, A. High avidity scFv multimers: diabodies and triabodies. *J. Immunol. Methods* **1999**, *231*, 548–557

[347] Yokota, T.; Milenic, D.E.; Whitlow, M.; Schlom, J. Rapid tumor penetration of a single-chain Fv and comparison with other immunoglobulin forms. *Cancer Res.* **1992**, *52*, 3402–3408

[348] Scott, A.M.; Wolchok, J.D.; Old, L.J. Antibody therapy of cancer. *Nat. Rev. Cancer* **2012**, *12*, 278–287

[349] Kobayashi, N.; Odaka, K.; Uehara, T.; Imanaka-Yoshida, K.; Kato, Y.; Oyama, H.; Tadokoro, H.; Akizawa, H.; Tanada, S.; Hiroe, M.; *et al.* Toward in vivo imaging of heart disease using a radiolabeled single-chain Fv fragment targeting tenascin-C. *Anal. Chem.* **2011**, *83*, 9123–9130

[350] Prusiner, S. Novel proteinaceous infections particles cause scrapie. *Science* **1982**, *216*, 136–144

[351] Ortega, C.; Herbet, A.; Richard, S.; Kersual, N.; Costa, N.; Pelegrin, A.; Ducancel, F.; Couraud, J.Y.; Navarro-Teulon, I.; Boquet, D. High-level prokariotic expression of anti-müllerian inhibitng substance type II receptor diabody, a new recombinant

antibody for *in vivo* ovarian cancer imaging. *J. Immunol. Methods* **2013**, *387*, 11–20

[352] Allard, B.; Wijkhuisen, A.; Borrull, A.; Deshayes, F.; Priam, F.; Lamourette, P.; Ducancel, F.; Boquet, D.; Couraud, J.Y. Generation and characterization of rendomab-B1, a monoclonal antibody displaying potent and specific antagonism of the human endothelin receptor B. *mAbs* **2013**, *5*, 56–69

[353] Padlan, E.A. Anatomy of the antibody molecule. *Mol. Immunol.* **1994**, *31*, 169–271

[354] Wörn, A.; Plückthun, A. Different equilibrium stability behavior of scFv fragments: identification, classification, and improvement by protein engineering. *Biochemistry* **1999**, *38*, 8739–8750

[355] Goto, Y.; Hamaguchi, K. The role of the intrachin disulfide bond in the conformation and stability of the constant fragment of the immunoglobulin light chain. *J. Biochem.* **1979**, *86*, 1433–1441

[356] Goto, Y.; Tsunenaga, M.; Kawata, Y.; Hamaguchi, K. Conformation of the constant fragment of the immunoglobulin light chain: effect of cleavage of the the polypeptide chain and the disulfide bond. *J. Biochem.* **1987**, *101*, 319–329

[357] Frisch, C.; Kolmar, H.; Schmidt, A.; Kleemann, G.; Reinhardt, A.; Pohl, E.; Usón, I.; Schneider, T.; Fritz, H. Contribution of the intramolecular disulfide bridge to the folding stability of REI(v), the variable domain of a human immunoglobulin kappa light chain. *Folding Des.* **1996**, *1*, 431–440

[358] Pedroso, I.; un, M.P.I.; Machicado, C.; Sancho, J. Four-state equilibrium unfolding of an scFv antibody fragment. *Biochemistry* **2002**, *41*, 9873–9884

[359] Jäger, M.; Gehrig, P.; Plückthun, A. The scFv fragment of the antibody hu4D5-8: evidence for early premature domain interaction in refolding. *J. Mol. Biol.* **2001**, *305*, 1111–1129

[360] Freund, C.; Gehrig, P.; Baici, A.; Holak, T.; Pl¨ uckthun, A. Parallel pathways in the folding of a short-term denatured scfv fragment of an antibody. *Fold. Des.* **1997**, *3*, 39–49

[361] Jäger, M.; Plückthun, A. The rate-limiting steps for the folding of an antibody scFv fragment. *FEBS Lett.* **1997**, *418*, 106–110

[362] Hoyer, W.; Ramm, K.; Plückthun, A. A kinetic trap is an intrinsic feature in the folding pathway of single-chain Fv fragments. *Biophys. Chem.* **2002**, *96*, 273–284

[363] Glockshuber, R.; Malia, M.; Pfitzinger, I.; Pl¨ uckthun, A. A comparison of strategies to stabilize immunoglobulin Fv fragments. *Biochemistry* **1990**, *29*, 1362–1367

[364] Hugo, N.; Lafont, V.; Beukes, M.; Altschuh, D. Functional aspects of co-variant surface charges in an antibody fragment. *Protein Sci.* **2002**, *11*, 2697–2705

[365] Shazman, S.; Celniker, G.; Haber, O.; Glaser, F.; Mandel-Gutfreund, Y. Patch Finder Plus (PFplus): a web server for extracting and displaying positive electrostatic patches on protein surfaces. *Nuclei Acids Res.* **2007**, *35*, 526–530

[366] Dayhoff, M.O.; Schwartz, R.M. *A model of evolutionary change in proteins.* In Atlas of protein sequence and structure **1978**

[367] Tsumoto, K.; Shinoki, K.; Kondo, H.; Uchikawa, M.; Juji, T.; Kumagai, I. Highly efficient recovery of functional single-chain Fv fragments from inclusion bodies overexpressed in *Escherichia Coli* by controlled introduction of oxidizing reagent – application to a human single-chain Fv fragment. *J. Immunol. Methods* **1998**, *219*, 119–129

[368] Umetsu, M.; Tsumoto, K.; Hara, M.; Ashish, K.; Goda, S.; Adschiri, T.; Kumagai, I. How additives influence the refolding of immunoglobulin-folded proteins in a stepwise dialysis system: Spectroscopic evidence for highly efficient refolding of a single-chain Fv fragment. *J. Biol. Chem.* **2003**, *278*, 8979–8987

[369] Arakawa, T.; Kita, Y.; Ejima, D. Refolding technology for scfv using a new detergent, N-Lauroyl-L-glutamate and arginine. *Antibodies* **2012**, *1*, 215–238

[370] Kudou, M.; Ejima, D.; Sato, H.; Yumioka, R.; Arakawa, T.; Tsumoto, K. Refolding single-chain antibody (scFv) using lauroyl-L-glutamate as a solubilization detergent and arginine as a refolding additive. *Protein Expr. Purif.* **2011**, *77*, 68–74

[371] Lobely, A.; Whitmore, L.; Wallace, B. DICHROWEB: an interactive website for the analysis of protein secondary structure from circular dichroism spectra. *Bioinformatics* **2002**, *18*, 211–212

[372] Whitmore, L.; Wallace, B. DICHROWEB: an online server for protein secondary structure analyses from circular dichroism spectroscopic data. *Nucleic Acids Res.* **2004**, *32*, 668–673

[373] Whitmore, L.; Wallace, B. Protein secondary structure analyses from circular dichroism spectroscopy: methods and reference databases. *Biopolymers* **2008**, *89*, 392–400

[374] Augustyniak, R.; Ferrage, F.; Paquin, R.; Lequin, O.; Bodenhausen, G. Methods to determine slow diffusion coefficients of biomolecules. Applications to Engrailed 2, a partially disordered protein. *J. Biomol. NMR* **2011**, *50*, 209–218

[375] Augustyniak, R.; Ferrage, F.; Damblon, C.; Bodenhausen, G.; Pelupessy, P. Efficient determination of diffusion coefficients by monitoring transport during recovery delays in NMR. *Chem. Commun.* **2012**, *48*, 5307–5309

[376] Ruschak, A.M.; Kay, L.E. Methyl groups as probes of supra-molecular structure, dynamics and function. *J. Biomol. NMR* **2010**, *46*, 75–87

[377] Schroeder, H.W., J.; Dougherty, C. Review of intravenous immunoglobulin replacement therapy trials for primary humoral immunodeficiency patients. *Infection* **2012**, *40*, 601–611

[378] Tankersley, D.; Preston, M.; Finlayson, J. Immunoglobulin g dimer: an idiotype–anti-idiotype complex. *Mol. Immunol.* **1988**, *25*, 41–48

[379] Ryan, S.M.; Mantovani, G.; Wang, X.X.; Haddleton, D.M.; Brayden, D.J. Advances in PEGylation of important biotech molecules: delivery aspects. *Expert Opin. Drug Deliv.* **2008**, *5*, 371–383

[380] Frokjaer, S.; Otzen, D.E. Protein drug stability: A formulation challenge. *Nat. Rev. Drug Discov.* **2005**, *4*, 298–306

[381] Manache, L.; Dulieu, C.; Boussif, O. Anticorps thérapeutiques - Importance de la galénique pour l'efficacité et la sécurité. *Med. Sci. (Paris)* **2009**, *25*, 1063–1069

[382] Lees, J.G.; Miles, A.J.; Wien, F.; Wallace, B.A. A reference database for circular dichroism spectroscopy covering fold and secondary structure space. *Bioinformatics* **2006**, *22*, 1955–1962

[383] Whitmore, L.; Woollett, B.; Miles, A.J.; Klose, D.P.; Janes, R.W.; Wallace, B.A. PCDDB: the protein circular dichroism data bank, a repository for circular dichroism spectral and metadata. *Nucleic Acids Res.* **2011**, *39*, D480–D486

[384] Vermeer, A.W.; Giacomelli, C.E.; Norde, W. Adsorption of IgG onto hydrophobic Teflon. Differences between the F_{ab} and F_c domains. *Biochim. Biophys. Acta* **2001**, *1526*, 61–69

[385] Benjwal, S.; Verma, S.; Röhm, K.H.; Gursky, O. Monitoring protein aggregation during thermal unfolding in circular dichroism experiments. *Protein Sci.* **2006**, *15*, 635–639

[386] Hunter, R. *Foundations of Colloid Science*. Oxford University Press **2001**

[387] Schweizer, D.; Schonhammer, K.; Jahn, M.; Gopferich, A. Protein-polyanion interactions for the controlled release of monoclonal antibodies. *Biomacromolecules* **2013**, *14*, 75–83

[388] de Marco, A. Strategies for successful recombinant expression of disulfide bond-dependent proteins in *Escherichia Coli*. *Microb. Cell Fact.* **2009**, *8*, 26

[389] Berkmen, M. Production of disulfide-bonded proteins in *Escherichia Coli*. *Protein Express. Purif.* **2012**, *82*, 240–251

[390] Dolinsky, T.J.; Nielsen, J.E.; McCammon, J.A.; Baker, N.A. PDB2PQR: an automated pipeline for the setup of Poisson–Boltzmann electrostatics calculations. *Nucl. Acids Res.* **2004**, *32*, W665–W667

[391] Li, H.; Robertson, A.D.; Jensen, J.H. Very fast empirical prediction and rationalization of protein pKa values. *Proteins: Structure, Function, and Bioinformatics* **2005**, *61*, 704–721

[392] Bas, D.C.; Rogers, D.M.; Jensen, J.H. Very fast prediction and rationalization of pKa values for protein–ligand complexes. *Proteins: Structure, Function, and Bioinformatics* **2008**, *73*, 765–783

[393] Olsson, M.H.M.; Sondergaard, C.R.; Rostkowski, M.; Jensen, J.H. PROPKA3: Consistent treatment of internal and surface residues in empirical pKa predictions. *J. Chem. Th. Comp.* **2011**, *7*, 525–537

[394] Sondergaard, C.R.; Olsson, M.H.M.; Rostkowski, M.; Jensen, J.H. Improved treatment of ligands and coupling effects in empirical calculation and rationalization of pKa values. *J. Chem. Th. Comp.* **2011**, *7*, 2284–2295

[395] Magde, D.; Elson, E.; Webb, W. Thermodynamic fluctuations in a reacting system – measurement by fluorescence correlation spectroscopy. *Phys. Rev. Lett.* **1972**, *29*, 705–708

[396] Krichevsky, O.; Bonnet, G. Fluorescence correlation spectroscopy: the technique and its applications. *Rep. Prog. Phys.* **2002**, *65*, 251–297

[397] Culbertson, C.; Jacobson, S.; Ramsey, J. Diffusion coefficient measurements in microfluidic devices. *Talanta* **2002**, *56*, 365–373

[398] Sengupta, P.; Garai, K.; Balaji, J.; Periasamy, N.; Maiti, S. Measuring size distribution in highly heterogeneous systems with fluorescence correlation spectroscopy. *Biophys. J.* **2003**, *84*, 1977–1984

[399] Enderlein, J.; Gregor, I.; Patra, D.; Fitter, J. Art and artefact of fluorescence correlation spectroscopy. *Curr. Pharm. Biotechnol.* **2004**, *5*, 155–161

[400] Shah, J.J.; Gaitan, M.; Geist, J. Generalized temperature measurement equations for rhodamine B dye solution and its application to microfluidics. *Anal. Chem.* **2009**, *81*, 8260–8263

[401] Kampmeyer, P.M. The temperature dependence of viscosity for water and mercury. *J. App. Phys.* **1952**, *23*, 99–102

[402] Wohland, T.; Rigler, R.; Vogel, H. The standard deviation in fluorescence correlation spectroscopy. *Biophys. J.* **2001**, *80*, 2987–2999

[403] Greene, R.F.; Pace, C.N. Urea and guanidine hydrochloride denaturation of ribonuclease, lysozyme, α-chymotrypsin, and β-lactoglobulin. *J. Biol. Chem.* **1974**, *249*, 5388–5393

[404] Santoro, M.M.; Bolen, D. Unfolding free energy changes determined by the linear extrapolation method. 1. Unfolding of phenylmethanesulfonyl α-chymotrypsin using different denaturants. *Biochemistry* **1988**, *27*, 8063–8068

[405] Myers, J.K.; Nick Pace, C.; Martin Scholtz, J. Denaturant m values and heat capacity changes: relation to changes in accessible surface areas of protein unfolding. *Protein Sci.* **1995**, *4*, 2138–2148

[406] Shortle, D.; Ackerman, M. Persistence of native-like topology in a denatured protein in 8 m urea. *Science* **2001**, *293*, 487–489

List of Figures

1.1 The structure of immunoglobulins G 8
1.2 Schematic illustration of the main biological roles of IgG 9
1.3 Schematic illustration of the advantages of using antibody-based therapies in cancer 10
1.4 The top 10 best-selling drugs in 2013 (in terms of worldwide sales) 11
1.5 A selection of engineered antibody fragments. 11
1.6 The development of therapeutic antibodies. 13
1.7 A unified view of some of the types of structure that can be formed by polypeptide chains during folding 18
1.8 Schematic view of protein folding 19
1.9 Domain interface and folding dependency in multi-domain proteins 20
1.10 Schematic view of preferential interaction, preferential hydration and neutral crowding 22

2.1 Working cycle of the GroEL/GroES chaperonin system 29
2.2 Artificial chaperone system developed by Rozema and Gellman 32
2.3 Hydrophobically-modified pullulan nanogels developed by Akiyoshi and coll. 33
2.4 Hydrophobically-modified enzymatically synthesized glycogen developed by Akiyoshi and coll. 34
2.5 Protein refolding in a temperature sweep in the presence of a thermo-sensitive polymer 35
2.6 Schematic illustration of protecting CAB against heat inactivation by PNIPAM in microemulsion developed by Tao *et al.* 36
2.7 Comparison of CAB activity recovery in the presence of PNIPAM or PNIPAM-PEG copolymer in bulk solution or PNIPAM confined in microemulsion droplets 37
2.8 Stabilization and refolding of the heat-denatured proteins assisted by thermo-responsive mixed shell polymeric micelles 38
2.9 Suppression of protein aggregation by triangular PEG developed by Kinbara and coll. 39
2.10 Nanoparticles of hydrophobized poly(vinyl alcohol) to suppress heat-induced protein aggregation 40
2.11 Protein refolding assisted by negatively-charged nanoparticles 41
2.12 Protein refolding assisted by periodic mesoporous organosilicas 42

2.13 Release of counterions upon complexation between proteins and polyelectrolytes . . . 46
2.14 Schematic illustration of the different types of protein:amphiphilic polyelectrolytes complexes . . . 47
2.15 Interaction between lysozyme and PAEMA-*g*-PEG . . . 49
2.16 Destabilization of proteins upon association with polyelectrolytes . . . 51
2.17 Effect of azobenzene-bearing copolymers on the urea-induced unfolding of ferri-cytochrome c . . . 52
2.18 Switching for enzyme activity by PEGylated polycations . . . 53
2.19 Chemical structures of the polymers used in the thesis . . . 56
2.20 Structure of the model proteins used in the thesis . . . 57

3.1 3D structure of CAB . . . 63
3.2 Renaturation protocol of urea-denatured CAB supplemented or not with polymers . . . 64
3.3 Visual aspect of 5h-old solutions in renaturation buffers of urea-denatured CAB or mixed urea-denatured CAB:PAA150 . . . 66
3.4 Time-dependence of the light scattering intensity of solutions of CAB during refolding . . . 67
3.5 Time-dependence of the light intensity scattered during CAB refolding in the presence of polymers . . . 68
3.6 Time-dependence of the light intensity scattered during CAB refolding in the presence of light-sensitive polymers . . . 70
3.7 Time-dependence of the hydrodynamic radius measured by FCS in solutions of urea-denatured FITC-CAB during refolding with or without polymers . . . 72
3.8 Far-UV CD spectra of native CAB:polymer mixtures . . . 73
3.9 Far-UV CD spectra of unfolded CAB:polymer mixtures . . . 74
3.10 Time-dependence of far-UV CD spectra of urea-unfolded CAB during refolding in the absence of polymers . . . 74
3.11 Time-dependence of far-UV CD spectra of CAB during refolding in the presence of polymers . . . 75
3.12 Time-dependence of enzyme activity recovery in mixed urea-denatured CAB:polymer solutions . . . 77
3.13 Dependence of enzyme activity on PAA150/CAB weight ratio after a 5-hours long renaturation of urea-denatured CAB . . . 78
3.14 Activity recovery of urea-denatured CAB in the presence of PAA150-3C6azo 80
3.15 Electrostatic surface isocontour (±1kT/e) of CAB . . . 81

4.1 The structure of scFv . . . 86
4.2 Possible equilibrium unfolding schemes of scFv fragments . . . 88
4.3 Exposed hydrophobicity on the scFv Rendomab B1 surface . . . 90
4.4 Electrostatic surface potential of scFv Rendomab B1 . . . 91
4.5 Residues involved in the positively-charged patches on the scFv Rendomab B1 surface . . . 92
4.6 Sequence alignment of scFv Sha 31, 12G4 and Rendomab B1: conserved residues and conserved positive-charges . . . 93
4.7 Optimized refolding protocol of scFv fragments . . . 95

4.8 Variation upon dialysis at decreasing GndCl or urea concentration (refolding) of the hydrodynamic radius and aggregation number of FITC-scFv (FCS measurement) . . . 96
4.9 Variation upon dialysis at decreasing GndCl or urea concentration (refolding) of the hydrodynamic radius and aggregation number of FITC-scFv (FCS measurement) . . . 98
4.10 Influence of the protein:polymer weight ratio on the variation upon dialysis at decreasing urea concentration (refolding) of the distribution of diffusion times of FITC-scFv:PAA150-3C18 mixtures (MEMFCS) . . . 99
4.11 SRCD spectra of scFv Rendomab B1 after refolding with or without polymers 101
4.12 BestSel secondary structure content estimation of two scFv fragments after refolding with or without polymers . . . 102
4.13 SRCD spectra of scFv Rendomab B1 in the 4-10M urea range in the absence of polymer . . . 104
4.14 SRCD-monitored folding transition of scFv Rendomab B1 in the absence of polymer . . . 105
4.15 SRCD spectra of scFv Rendomab B1 in the 4-10M urea range in the presence of polymers . . . 105
4.16 SRCD-monitored folding transition of scFv Rendomab B1 in the presence of polymers . . . 106
4.17 Evolution of secondary structure content via BestSel analysis in the 4-10M range . . . 108
4.18 Identification of the 6 tryptophan residues in scFv Rendomab B1 . . . 109
4.19 Fluorescence-monitored folding transition of scFv Rendomab B1 with or without polymers . . . 110
4.20 ^{1}H-^{15}N HSQC of scFv Rendomab B1 refolded with PAA5 . . . 111
4.21 NMR determination of the diffusion coefficient of scFv Rendomab B1 refolded with PAA5 . . . 112

5.1 Electropherograms of IgG:polymer mixtures in 20 mM phosphate buffer, pH 6.8 . . . 122
5.2 Electropherograms of unstressed IgG in the presence of polymers in the running buffer, in the absence or presence of 100 mM NaCl . . . 123
5.3 Electropherograms of unstressed IgG with increasing PAA150-3C18 concentration in the absence or presence of 100 mM NaCl . . . 124
5.4 Variation of the mass of complexed IgG, based on measurements of the area under the peak of residual unbound protein monomers as a function of the amount of PAA150-3C18 present in the capillary at different ionic strengths and pHs . . . 125
5.5 CD traces of IgG at 25°C supplemented or not with polymers in the absence or presence of 100 mM NaCl . . . 127
5.6 CD traces of IgG at 25°C supplemented with increasing PAA150-3C18 concentration in the absence of 100 mM NaCl . . . 128
5.7 DSC thermograms of IgG:polymer mixtures . . . 129
5.8 Variation of the enthalpy of thermal denaturation, ΔH, and unfolding temperature, T_m, of IgG measured by DSC as a function of the polymer/protein weight ratio . . . 131

5.9 Far-UV circular dichroism traces of 1:1 wt/wt IgG:polymer mixtures before and after heating above T_m . . . 132
5.10 Evolution of the molar residue ellipticity at 210 nm for IgG with or without polymers (at 1:1 wt/wt ratio) upon heating . . . 134
5.11 Evolution of the hydrodynamic radius of IgG alone and in the presence of polymers during temperature sweep (DLS measurement) . . . 136
5.12 Variation of the normalized scattering intensity (I(t) - I_0)/I_0 for IgG and IgG:polymer mixtures as a function of incubation time at different temperatures . . . 137
5.13 Variation upon incubation at increasing temperature of the hydrodynamic radius and aggregation number of FITC-IgG:polymer mixtures (FCS measurement) . . . 140
5.14 Schematic summary describing the temperature-dependent interactions between IgG and amphiphlic polyanions . . . 143

B.1 Schematic illustration of the confocal volume generated by a two-photon excitation . . . 159
B.2 Time-scales of various processes monitored by FCS autocorrelation analysis 159
B.3 Schematic illustration of the evolution of the FCS autocorrelation curve upon complexation with polymers or oligomerization . . . 160
B.4 Schematic illustration of the FCS set-up used for *in situ* heating . . . 164
B.5 Evolution of $I_T/I_{25°C}$ as a function of temperature for rhodamine B excited with two-photons using an air or a water objective . . . 165
B.6 Evolution of temperature as a function of $I_T/I_{25°C}$ for the air objective and the immersion objective . . . 165
B.7 Evolution of the target temperature as a function of the nominal temperature (in the case of the water objective) . . . 166
B.8 Evolution of water viscosity as a function of T . . . 167
B.9 Evolution of diffusion coefficient of fluorescein as a function of temperature (water objective) . . . 167
B.10 Evolution of diffusion coefficient of quantum dots as a function of temperature (water objective) . . . 168
B.11 Schematic illustration of the mobility of different species in capillary electrophoresis . . . 169
B.12 Eight basis components of BestSel in relation to the dictionary of protein secondary structure . . . 171

C.1 Evolution of $[\theta]_{222nm}$ of CAB(:polymer) mixtures as a function of urea concentration . . . 174
C.2 Evolution of the wavelength at maximum tryptophan fluorescence emission of CAB(:polymer) mixtures as a function of urea concentration . . . 175
C.3 Normalized folding transition from CD or fluorescence measurements . . . 176
C.4 Comparison of the normalized folding transition from CD and fluorescence measurements . . . 177
C.5 Evolution of λ at maximum tryptophan fluorescence emission as a function of PAA150 or NaCl concentrations in 5M urea, pH 7.75 . . . 179

D.1 Electrostatic surface potential of scFv Rendomab B1 at varying pHs and fixed 100 mM ionic strength . . . 182

D.2 Electrostatic surface potential of scFv Rendomab B1 at varying ionic strengths and fixed pH 8 . . . 182
D.3 Typical normalized fluorescence intensity traces observed by FCS after or during the refolding of FITC-scFv . . . 183
D.4 Distributions given by the MEMFCS algorithm during refolding of FITC-scFv(:polymer) solutions . . . 185
D.5 SRCD spectra of scFv Rendomab B1 unfolded in 10M or 8M urea . . . 186
D.6 SRCD spectra of scFv Rendomab B1 in the 0-4M urea range in the absence or presence of polymers . . . 187
D.7 Evolution of secondary structure content via BestSel analysis in the 0-4M range . . . 188
D.8 ^{1}H-^{15}N HSQC of scFv Rendomab B1 refolded with PAA150 . . . 189
D.9 ^{1}H-^{15}N HSQC of scFv Rendomab B1 refolded with PAA150 . . . 190
D.10 ^{1}H-^{15}N HSQC of scFv Rendomab B1 refolded with PAA150 . . . 191

E.1 SEC elution profiles of Cetuximab in the absence of presence of polymers at t=0 and after 15 days of incubation . . . 195
E.2 SEC elution profiles of Cetuximab in the absence of presence of polymers at t=0 and after 15 days of incubation . . . 196
E.3 Activity of Rendomab B1 in the presence of polymers . . . 198
E.4 FCS-determined autocorrelation curves of FITC-IgG in the presence of increasing concentrations of PAA150-3C18 . . . 198
E.5 Hydrodynamic radii and aggregation numbers of FITC-IgG in the presence of increasing concentrations of PAA150-3C18 . . . 199
E.6 Hydrodynamic radius and aggregation number of unlabelled IgG:rhodamine-labelled polymer mixtures upon heating . . . 199
E.7 Variation upon incubation at increasing temperature of the hydrodynamic radius and aggregation number of IgG:FITC-IgG:polymer mixtures (FCS measurement) . . . 200
E.8 Absorption spectra of IgG alone and with polymers prior and after heating 201
E.9 Thermograms of IgG in the presence of short or long polymers . . . 202
E.10 Thermograms of IgG in the presence of short or long polymers . . . 203
E.11 Plots of R_h of IgG in the absence/presence of polymers as a function of time 205

List of Tables

1.1 Classification of protein aggregates proposed by Narhi *et al.* [33] 14

3.1 Solubility of urea-denatured CAB diluted after 5 hours of incubation in renaturation buffers with or without polymers 67
3.2 Scattered intensity by native CAB and polymer solutions and native CAB:polymer mixtures 69
3.3 Characteristic features determined by light scattering measurements of mixed urea-denatured CAB:polymer solutions diluted in renaturation buffer 69
3.4 Hydrodynamic radius R_h of native or 10M urea-denatured FITC-CAB measured by FCS in the absence or presence of polymers 71
3.5 Secondary structure content of native CAB in the presence or not of polymers 73
3.6 Enzymatic activity of urea-denatured CAB diluted after 5 hours of incubation in renaturation buffers with or without polymers 79
3.7 Enzymatic activity of native CAB in the presence of polymers 79

4.1 List and occurrence of highly conserved positively-charged residues on scFv fragments 94

5.1 Average hydrodynamic radius and aggregation number in IgG:polymer mixtures 126
5.2 Secondary structure content of IgG in the presence or not of polymers . . 128
5.3 Temperature and enthalpy of thermal denaturation of IgG in the absence or presence of poly(acrylate) derivatives 130
5.4 Secondary structure content of IgG in the presence or not of polymers before and after heating 133
5.5 Colloidal stability ratios, W ($\times 10^{-6}$), for IgG and IgG:polymer mixtures incubated near the temperature of thermal denaturation 138

B.1 Values of the coefficient of the polynomial fit of T=f($I_T/I_{25°C}$) 166

C.1 Fitting parameters of CD data according to Equation C.6 178

D.1 Physico-chemical characteristics of scFv fragments 182

E.1 Influence of the polymer chain length on the temperature and enthalpy of thermal denaturation of IgG 202

E.2 Influence of the IgG:PAA5 weight ratio on the temperature and enthalpy of thermal denaturation of IgG 203
E.3 Influence of the IgG:PAA5-3C18 weight ratio on the temperature and enthalpy of thermal denaturation of IgG 204
E.4 Influence of the IgG:PAA5-25C8-40C3 weight ratio on the temperature and enthalpy of thermal denaturation of IgG 204

Résumé

Les anticorps à visée thérapeutique sont en pleine expansion. Le développement de ces protéines issues de la bioingénierie est toutefois entravé par leur tendance naturelle à l'agrégation, particulièrement critique au cours des étapes de repliement. L'association réversible (non covalente) de protéines avec des polymères solubles pourrait permettre de résoudre ce problème. Nous avons ici étudié les interactions entre des protéines modèles et des dérivés hydrophobes du poly(acrylate de sodium) (PAA) grâce à des techniques expérimentales incluant la spectroscopie de corrélation de fluorescence, le dichroïsme circulaire sous radiation synchrotron, la diffusion de lumière, l'électrophorèse capillaire et la calorimétrie différentielle à balayage. Comme preuve de concept, nous avons démontré que les dérivés du PAA augmentent le rendement de renaturation d'une enzyme modèle, l'anhydrase carbonique bovine, grâce à la protection des conformères partiellement repliés. La stabilisation colloïdale au cours du repliement a été étendue à des fragments d'anticorps de type scFv, qui sont d'importants modèles de biothérapeutiques sensibles à l'agrégation. L'éfficacité des polymères a aussi été validée pour des immunoglobulines G soumises à un stress thermique. La prédominance de l'association hydrophobe est remise en cause dans cette étude. L'ancrage électrostatique des chaines de PAA s'avère suffisant pour minimiser l'agrégation des protéines, grâce à des associations dynamiques avec les conformères partiellement repliés. Un avantage majeur de ces polymères est la faible quantité nécessaire comparé aux osmolytes conventionnels et l'absence de modification chimique des protéines.

Mots clefs: renaturation; chaperonne artificielle; anticorps; agrégation; polyélectrolyte modifié hydrophobe; complexes polymères:protéines

Abstract

Antibodies constitute the fastest growing class of human biopharmaceuticals. The development of these engineered proteins is yet hampered by their natural propensity towards irreversible aggregation particularly critical during refolding steps. Reversible (non-covalent) association of proteins with water-soluble polymers could circumvent this issue. In the present study, we investigated the interactions between model proteins and hydrophobically-modified poly(sodium acrylate) (PAA) chains with experimental techniques including fluorescence correlation spectroscopy, synchrotron-radiation circular dichroism, light scattering, capillary zone electrophoresis and differential scanning calorimetry. As a proof of concept, we demonstrated that PAA derivatives enhanced the renaturation yield of a single-domain model enzyme, bovine carbonic anhydrase, because of protection of partly-folded conformers against aggregation. Colloidal stabilisation during refolding was extended to two-domain artificial antibody fragments, single chains Fv fragments, as important models of aggregation-prone biotherapeutics. On similar basis, efficient protection was also validated with full-length immunoglobulins G under heat-stress. Prevalence of hydrophobic association between polymers and proteins is questioned in this work. Rather, electrostatic binding with PAA chains turns out to be sufficient to minimize in vitro protein aggregation, most-likely because of dynamic association with partly-folded conformers. A major advantage of these polymers is their use at extremely low amount compared to conventional osmolytes and absence of chemical modification of proteins.

Key words: renaturation; artificial chaperone; antibody; aggregation; hydrophobically modified polyelectrolyte; polymer:protein complexes.